Swansea University

Swansea University
Prifysgol Abertawe

Doctoral Thesis

Holography and Composite Higgs

by:
Ali Fatemiabhari

A thesis submitted in fulfillment of the requirements
for the Doctor of Philosophy

of the

Department of Physics,
Faculty of Science and Engineering,
Swansea University

September 20, 2024

Declaration of Authorship

I, Ali Fatemiabhari, declare that this thesis titled, "Holography and Composite Higgs" and the work presented in it are my own. I confirm that:

- This work has not previously been accepted in substance for any degree and is not being concurrently submitted in candidature for any degree.
- This thesis is the result of my own investigations, except where otherwise stated. Other sources are acknowledged by footnotes giving explicit references. A bibliography is appended. Specially, the thesis is based on the following publications:

  D. Chatzis, A. Fatemiabhari, C. Nunez, and P. Weck, *SCFT deformations via uplifted solitons,* [arXiv:2406.01685].

  D. Elander, A. Fatemiabhari, and M. Piai, *On Holographic Vacuum Misalignment,* [arXiv:2405.08714].

  D. Chatzis, A. Fatemiabhari, C. Nunez, and P. Weck, *Conformal to confining SQFTs from holography,* [arXiv:2405.05563].

  A. Fatemiabhari and C. Nunez, *From conformal to confining field theories using holography, JHEP* 03 (2024) 160, [arXiv:2401.04158].

  D. Elander, A. Fatemiabhari, and M. Piai, *Toward minimal composite Higgs models from regular geometries in bottom-up holography, Phys. Rev. D* 107 (2023), no. 11 115021, [arXiv:2303.00541].

  D. Elander, A. Fatemiabhari, and M. Piai, *Phase transitions and light scalars in bottom-up holography, Phys. Rev. D* 108 (2023), no. 1 015021, [arXiv:2212.07954].

  A. Fatemiabhari and C. Nunez, *Wilson loops for 5d and 3d conformal linear quivers, Nucl. Phys. B* 989 (2023) 116125, [arXiv:2209.07536].

  The data generated for this manuscript can be downloaded from:

  D. Elander, A. Fatemiabhari, and M. Piai, *On holographic vacuum misalignment — data release,* Zenodo (2024) doi:10.5281/zenodo.11774202.

  D. Elander, A. Fatemiabhari, and M. Piai, *Towards composite Higgs: minimal coset from a regular bottom-up holographic model — data release,* Zenodo (2023)

  D. Elander, A. Fatemiabhari, and M. Piai, *Phase transitions and light scalars in bottom-up holography — data release,* Zenodo (2022) doi:10.5281/zenodo.7477647.

- I hereby give consent for my thesis, if accepted, to be available for photocopying and for inter-library loan, and for the title and summary to be made available to outside organisations.
- The University's ethical procedures have been followed and, where appropriate, that ethical approval has been granted.

Signed: A. Fatemiabhari

Date: 30/07/2024

بشنو از نی چون حکایت می کند از جدایی ها شکایت می کند

کز نیستان تا مرا ببریده اند از نفیرم مرد و زن نالیده اند

مولانا

Listen to the reed as it tells its tale,
Of love's separations, a sorrowful wail.
Since they cut me from the reed bed so deep,
My cries of lament make both men and women weep.

Rumi

عاشقی را که چنین باده سحرگاهی دهند کافر عشق بود گر نشود باده پرست

خنده جام می و زلف گره‌گیر نگار ای بسا توبه که چون توبه حافظ بشکست

حافظ

To a lover who is given such an early morning wine,
It would be infidelity to love if he did not become a worshiper of the wine.
The laughter of the wine cup and the captivating curls of the beloved,
Oh, how many vows of repentance have been broken like Hafez's.

Hafez

Acknowledgement

I would like to express my deepest gratitude to my advisors, Maurizio Piai and Carlos Núñez, for their invaluable guidance, support, and insightful feedback throughout this journey. Their expertise and encouragement have been influential in the completion of this work.

A special thanks to Daniel Elander for his help, guidance, and insightful contributions throughout our collaboration as well as my other collaborators Peter Weck and Dimitrios Chatzis. I would like to thank Prem Kumar and Daniel Thompson for discussions that have broadened my perspectives

I am grateful to all of my collaborators and friends who contributed significantly to discussions and made our group so vibrant. There are so many people to be named: Amr, Andrea, Ben, Chanju, David, Diaa, Dimitrios, Fabian, Federico, James, Karol, Mohammad, Mohammad Naeem, Neil, Niccolò, Lewis, Lucas, Luke, Paul, Peter, Ricardo, Ryan, Siddharth and Zsolt.

I extend my sincere appreciation to my parents and my whole family for their endless love, patience, and encouragement, which have been a constant source of strength and motivation.

Abstract

In this PhD thesis, we study different supergravity backgrounds which correspond to dual field theories based on Gauge/Gravity correspondences. We calculate different properties and observables in the dual field theory, such as Wilson loops and mass spectra, using holographic methods, to shed light on the nature of the theories. Some of these setups are used in the context of composite Higgs models to address the Naturalness problem in the standard model of particle physics.

First, we focus on holographic models for describing Higgs compositeness, both in the context of Higgs as a dilaton or as a pseudo-Nambu-Goldston boson of SO(5)/SO(4) symmetry-breaking pattern. Next, other supergravity backgrounds with asymptotic AdS_6 or AdS_5 factors in their geometry are studied, which are deformations of previously well-studied solutions. In their field theory duals, we establish that these deformations lead to a transition from conformal behaviour to confining or screening. A variety of observables are calculated in these backgrounds to assess the field theory properties.

Keywords: Gauge/Gravity Duality, Holography, Composite Higgs Models

Contents

Chapter 1

Preface

Quantum field theory (QFT) has provided a successful, self-consistent framework for a description of diverse phenomena in Nature. It has been implemented on a range of different subjects, extending from elementary particle physics to condensed matter systems, cosmological models and quantum gravity. This theory emerged during the 20th century in attempts to merge quantum mechanics with principles of special relativity while respecting the conditions imposed by locality and unitarity. It was shown that any quantum theory respecting relativity at low enough energies would resemble a quantum field theory [1]. A generic QFT is better understood in the regions of its parameter space in which one has access to a small expansion parameter or coupling. In this so-called perturbative regime, one can study the weakly coupled theory by expansions of the observables in this small parameter. There exists a systematic approach using namely the Feynman diagrams to capture this expansion, which was developed and extensively used during the 20th century. The strongly coupled regime of the theory is cumbersome to deal with, and a unique framework for understanding it does not exist.

One of the approaches to understanding the strongly coupled regime of field theories is making use of dualities. Dualities, in their strong form, provide an equivalence relation between observables of different QFTs, which results in them being the same theory formulated in different formalisms. For our purposes, it is desired for a duality to provide a relation between the weakly coupled regime of gravity theory and the strongly coupled counterpart of the other party. Then, the dictionary for duality can be implemented to derive the observables that are not easily calculable in the strongly coupled realm.

The AdS/CFT correspondence [2] conjectures a duality between quantum string theory on anti-de Sitter (AdS) spacetime, with a compact internal manifold, M, and a conformal field theory (CFT). The duality is usually between the strongly coupled dynamics of one theory and the weakly coupled dynamics of the dual one, hence being useful to understand the non-perturbative dynamics.

The AdS/CFT correspondence was subsequently refined in Refs. [3, 4]. Later, it was

extended to more generalised settings with less supersymmetry preserved and backgrounds without conformal symmetry. In its final form, *Gauge/Gravity* correspondences provide new tools for the study of both gravity and field theory topics. They make calculations feasible in strongly coupled field theories, some of which are realised in Nature, and also opens new formal methods of classification of gravity backgrounds and their field theory duals.

In this PhD thesis, we focus on two subjects related to this formalism: **holographic composite Higgs models** and investigation of **quiver gauge field theories**. We seek comprehensive methods to study a broad set of quantum field theories with or without conformal symmetry and supersymmetry. Using field-theoretic and holographic methods, we compute observables such as spectra of bound states and Wilson loops. This thesis is based on the papers [5–10].

One of the outstanding problems in the Standard Model (SM) is the so-called hierarchy problem. The mass of the Higgs boson is UV sensitive, and even if one finds a UV completion for SM, this mass will remain a free parameter not derivable from parameters in higher energy theory. We construct a new formal framework for the investigation of certain classes of composite models based on symmetry breaking in strongly coupled theories [5–7]. These theories are difficult to solve without using gauge/gravity dualities.

As the Standard Model possesses an approximate scale invariance (explicitly and spontaneously broken), the Higgs boson itself can be identified as a dilaton, the pseudo-Nambu-Goldstone boson (pNGB) associated with dilatations. The question is the possibility of the Higgs boson originating as a composite dilaton from a more fundamental theory. If this is the case, the underlying dynamics required to yield realistic values for its couplings and mass should be investigated carefully.

The dilaton effective field theory had been under consideration for many decades [11, 12]. More recently, there had been an interpretation of lattice data specially the numerical work on particular $SU(3)$ gauge theories that indicates of a light scalar mode in the spectrum of the theory [13–24].

Another line of thought is the idea based on the fact that Higgs scalar fields would arise as pseudo-Nambu-Goldstone Bosons (pNGBs) in the low-energy description of a more generic fundamental theory [25](see also Refs. [26–31]).

To further study these ideas, we begin the thesis in Chapter 2, with a review of the crucial material used in the development of our work.

In Chapter 3, we consider a class of six-dimensional gravity models and solutions within the bottom-up approach to holography. These can be interpreted as dual five-dimensional CFTs deformed by scalar operators. The scaling dimension of this operator appears as a free parameter. To mimic confinement in the dual four-dimensional theories, one dimension in the geometry is compactified on a shrinking circle [32]. We calculate the mass spectrum of bosonic

states using numerical methods. In a region of parameter space, the lightest scalar can be interpreted as an approximate dilaton with a parametrically suppressed mass, which will be a candidate for Higgs. Unfortunately, the dilatonic region is hidden behind a first-order phase transition, and the approximate dilaton appears in the metastable region of solutions.

In Chapter 4, we show how to repurpose the gravity background in a new context, as a CHM with vacuum misalignment. We add a $SO(5)$ global symmetry to our model and study its spontaneous breaking to a $SO(4)$ subgroup, trying to find a composite state with the right quantum numbers to be a suitable candidate for the Higgs particle [6].

Chapter 5 deals with vacuum misalignment. We weakly gauged another $SO(4)$ subgroup of the $SO(5)$ global symmetry of the field theory living at the boundary. At that stage, we consider the symmetry-breaking boundary terms while retaining the spontaneously broken gauge $SO(5)$ symmetry in the bulk. This will generate a new symmetry-breaking pattern, causing **vacuum misalignment** phenomena and giving a small mass to the NGBs, identified with Higgs mass [7].

At this stage, we pass on to quiver field theories and their deformations. The classification of SUSY Type II and M-theory backgrounds with AdS_{d+1} factors is of crucial importance as they are holographic duals to SCFTs in d dimensions. For the case of half-maximally supersymmetric solutions, major progress in classifying string backgrounds corresponding to families of QFTs has been achieved. We focus on the conformal and supersymmetric linear quiver field theories in different dimensions, dual to backgrounds engineered by branes in type IIB or IIA string theory. These string theory embeddings of various QFTs clarify the diverse properties of their strong coupling dynamics. The field theories under consideration here are of a specific type and are non-trivial interacting theories; on the other hand, good analytic control is available on their dynamics. The deformations of these field theories achieved by the deformations in dual supergravity background are of interest in this work.

In Chapter 6, we investigate a six-dimensional supergravity solution which terminates with a cap, contains nontrivial solitonic background fields and is asymptotic to AdS_6 geometries. This solution can be uplifted to an infinite family of solutions in Type IIB. We calculate observables such as the holographic central charge, entanglement entropy and Wilson loops in dual four-dimensional effective theory to study properties like confinement, screening and symmetry breaking [8].

Later in chapter 7, we perform this process for some 5d supergravity solutions, this time preserving the original supersymmetry partially [9, 10].

Chapter 2

Introduction

In this chapter, we provide some introductory material on gauge/gravity dualities and review the hierarchy problem of the SM. The concepts discussed here will be useful throughout this thesis.

2.1 Review of Gauge/gravity dualities

In this section, we briefly review the concept of gauge/gravity dualities. We will first provide an overview of some aspects of string theory and AdS space before the definition of the duality. These essential ideas are summarised following Ref. [33] while more detailed reviews can be found in Refs. [34–37].

2.1.1 Superstring theory and its supergravity limit

String theory initially emerged as a prospective theory to describe strong interaction, which was later accounted for by quantum chromodynamics. Nonetheless, string theory remained in scientific interest owing to being one of the few examples of self-consistent quantum theories of gravity. The idea of gauge/gravity dualities has its roots in string theory, with both string theory and M-theory offering examples of this duality. In this section, we will provide a brief overview of some concepts related to these topics.

The fundamental constituents of string theory are strings, which are one-dimensional objects having a two-dimensional worldsheet. Fluctuations of these strings are quantised, with the various modes of fluctuation corresponding to different particle fields. Interestingly, the spectrum of fluctuations includes a massless spin-2 field is identified as the graviton. This evidence makes string theory a suitable candidate for a quantum theory of gravity.

One can identify five distinct supersymmetric string theories, denoted as types I, IIA, IIB, and the $SO(32)$ and $E_8 \times \mathrm{E}_8$ heterotic theories. Each of these variants requires a ten-dimensional spacetime to be anomaly-free [38]. These theories have been proposed to be different limits of the parent M-theory [39].

There is only a dimensionful parameter in string theory, which is the Regge slope, denoted as α', and it has a dimension of $[\alpha'] = [M^{-2}]$. The masses of the massive string fluctuations scale inversely with the square root of α'. If one is interested in scales below $1/\sqrt{\alpha'}$, one should consider only the massless sector, as the massive sector effectively decouples. This yields an effective theory at lower energies called the ten-dimensional supergravity (SUGRA), with different supergravity theories related to the low-energy limits of various superstring theories mentioned before. For the type IIA and IIB SUGRA theories, the relevant massless bosonic fields are the metric, an antisymmetric two-form, a scalar known as the dilaton, and n-form gauge fields C_n (where n is odd in type IIA SUGRA and even in type IIB SUGRA), along with their corresponding fermionic counterparts.

String theory, besides fundamental strings, contains dynamical and extended objects known as D-branes. A Dp-brane is a $(p+1)$-dimensional object that carries the electric charge of the C_{p+1} gauge field. Open strings can have their endpoints attached to these D-branes. A $U(1)$ gauge field can be accommodated on the world volume of a D-brane, with the endpoints of open strings carrying charge with respect to the $U(1)$ gauge field. When N D-branes are stacked together, the gauge symmetry will be enhanced to an $U(N)$ symmetry. In this case, the string endpoints furnish the fundamental representation of this gauge group.

For type IIA string theory, only Dp-branes with even values of p are stable, while in type IIB, branes with odd p. In the context of supergravity, Dp-branes emerge as classical solitonic charged solutions to the background equations of motion. As an example, a planar arrangement of N coincident D3-branes within type IIB supergravity is given in Ref. [40] as

$$\begin{aligned} ds^2 &= \frac{1}{\sqrt{1+\frac{l^4}{r^4}}}\eta_{\mu\nu}dx^\mu dx^\nu + \sqrt{1+\frac{l^4}{r^4}}\left(dr^2 + r^2 ds^2_{S^5}\right), \\ F_5 &= d\tilde{C}_4 + *d\tilde{C}_4, \quad \tilde{C}_4 \equiv \left(1+\frac{l^4}{r^4}\right)^{-1} dx^0 \wedge dx^1 \wedge dx^2 \wedge dx^3. \end{aligned} \tag{2.1.1}$$

Here, the C_0 and dilaton fields are constants while other potentials are zero. We denote as $\eta_{\mu\nu}$ the four-dimensional Minkowski metric, $ds^2_{S^5}$ is the metric on a unit radius five sphere, $*$ is the Hodge star in ten-dimensions, and $F_5 \equiv dC_4$. The parameter l is given as $l^4 = 4\pi\alpha'^2 g_s N$, with g_s representing the string coupling constant.

The near-horizon limit of stacks of branes leads to an AdS space in supergravity. For example, for the $(r \ll l)$ limit of the solution in Eq. (2.1.1) corresponding to the D3-brane,

the solution would read

$$ds^2 = \frac{r^2}{l^2}\eta_{\mu\nu}dx^\mu dx^\nu + \frac{l^2}{r^2}dr^2 + l^2 ds^2_{S^5},$$
$$\tilde{C}_4 = \frac{r^4}{l^4}dx^0 \wedge dx^1 \wedge dx^2 \wedge dx^3. \tag{2.1.2}$$

After performing a coordinate change, $z \equiv l^2/r$, the resulting solution takes the $AdS_5 \times S^5$ form, with AdS_5 and S^5 factors both having the same radius l.

We also need a definition of asymptotically locally AdS spacetime, in which there exists a coordinate choice with the metric taking the Fefferman-Graham form [41]

$$ds^2 = G_{MN}dX^M dX^N = \frac{L^2}{z^2}\left[dz^2 + g_{\mu\nu}(x,z)dx^\mu dx^\nu\right]. \tag{2.1.3}$$

Now, $z = 0$ corresponds to the boundary. One can expand the metric, $g_{\mu\nu}$, near the boundary as

$$g(x,z) = g^{(0)}(x) + z^2 g^{(2)}(x) + \ldots, \tag{2.1.4}$$

The so-called Poincaré AdS solution is achiavable by choosing $g^{(0)} = \eta_{\mu\nu}$ while $g^{(n\geq 2)} = 0$.

2.1.2 Gauge/gravity dualities

Gauge/gravity dualities consist of correspondence between a d-dimensional QFT and a gravitational theory living in an asymptotically AdS_{d+1} spacetime. The QFT living in one dimension less than its gravitational counterpart is the reason for the terminology of "holography" ascribed to this duality. This equivalence provides a correspondence between gauge invariant physical quantities across both theories. Given the intricate nature of quantum gravity, normally, a classical limit on the gravitational side is taken, wherein the generating functional of the quantum gravity is treated within its saddle-point approximation— see also Refs. [3, 4]

$$Z_{\rm QFT}[\phi_{(0)}] = Z_{\rm gr}[\phi_{(0)}] \approx e^{-I_{\rm gr-saddle}[\phi_{(0)}]} \quad . \tag{2.1.5}$$

Here, $Z_{\rm QFT}$ is the generating functional of the QFT, which depends on the sources for the QFT operators. These sources are collectively denoted as $\phi_{(0)}$. For any gauge-invariant operator living on the QFT side, there is a corresponding counterpart in the gravity theory. In the gravity context, $\phi_{(0)}$ act as boundary conditions for the fields in the gravitational theory. The final equality in Eq. (2.1.5) represents the classical approximation, using the saddle-point method, to the generating functional of the gravitational theory, $Z_{\rm gr}[\phi_{(0)}]$, where $I_{\rm gr-saddle}[\phi_{(0)}]$ denotes the Euclidean-signature on-shell action.

There can be divergences when the action is evaluated on-shell, which will make the classical variational problem ill-defined [42–45]. In this case, one needs to introduce counterterms

on the gravity boundary to regulate the infinities and eventually renormalise the observables. This is the process of holographic renormalisation, which is the holographic version of the QFT renormalisation.

One of the earliest examples of gauge/gravity correspondences was the proposed equivalence between the type IIB string theory on the $AdS_5 \times S_5$ background and the $\mathcal{N} = 4$ supersymmetric Yang-Mills theory (SYM) with gauge group $SU(N)$ [2]. We use this example to elucidate key facets of the duality.

The examination of the low-energy modes of a stack of N coincident D3-branes in asymptotically flat space was the starting point for the connection between the two theories. In the regime of small closed string coupling constant, g_s, two distinct sets of low-energy modes can be identified, which turn out to be decoupled. The first set consists of low-energy closed strings that propagate away from the branes and are described by type IIB theory. The second set includes massless open strings with their endpoints attached to the branes, whose dynamics are captured by a four-dimensional $\mathcal{N} = 4$ SYM theory. This gauge theory has a gauge group $SU(N)$, and a coupling strength denoted as $g_{\text{YM}} = \sqrt{4\pi g_s}$.

In contrast, in cases where the closed string coupling constant, g_s, is large, the characterisation of the D3-branes can be described using the closed string dynamics. The D3-branes curve the spacetime in the large g_s regime, creating a geometric configuration which possesses a horizon. The geometry near to this horizon has an $AdS_5 \times S^5$ form. Notably, these modes get highly redshifted for an observer at infinity. In the low-energy theory, this requires the inclusion of the whole set of modes of the near-horizon string states.

Consider starting from the weakly coupled regime described by weakly coupled SYM theory, where we disregard the presence of decoupled closed strings. Subsequently, by incrementing g_s (and consequently g_{YM}), we scan through a spectrum of values. Notably, Yang-Mills theory is well defined across all g_{YM} regimes, suggesting the theory should be consistent even as g_s takes large values where the D-barnes are described by string excitations in $AdS_5 \times S^5$. The Maldacena conjecture [2] proposes that both descriptions are valid, thereby asserting the equivalence between $\mathcal{N} = 4$ SYM with gauge group $SU(N)$ and type IIB string theory on $AdS_5 \times S^5$. Importantly, the radii of AdS_5 and S_5 are related to the gauge group rank,

$$l = (4\pi\alpha'^2 g_s N)^{1/4}. \tag{2.1.6}$$

As mentioned earlier, to facilitate computations within the framework of string theory, it is more practical to adopt a classical limit. Moreover, as a result of the inherent complexity of string theory on curved backgrounds, it is customary to consider a regime where stringy effects remain marginal, effectively approximating string theory by type IIB supergravity.

This classical limit is achieved by imposing the weak coupling conditions, denoted by

$g_s \ll 1$. Gauge/gravity dualities furnish a relation between the Yang-Mills coupling, denoted as $g_{\rm YM}$, and the string coupling, g_s,

$$g^2_{\rm YM} = 4\pi g_s,$$

thus, the classical limit requires $g_{\rm YM} \ll 1$.

Given that α' governs the characteristic length scale of stringy phenomena, the supergravity regime requires $l \gg \sqrt{\alpha'}$, indicating minimal curvature in string units. Using Eq. (2.1.6), this translates to $g_s N \gg 1$. Satisfying both conditions means $N \gg 1$. In this regime, it is conventional to introduce the 't Hooft coupling, defined as $\lambda \equiv g^2_{\rm YM} N$. This quantity captures a better sense of the coupling among fields in the YM theory. Consequently, the limits are summarised as the first classical limit ($N \to \infty,\ \lambda$) followed by the supergravity limit ($\lambda \to \infty$). Evidently, taking the supergravity limit leads to the strongly coupled regime of the dual YM theory.

It is expected that the symmetries on the two sides of the correspondence should be related, and this is observed. The group $\mathrm{SU}(2,2) \times \mathrm{SU}(4)$ will be the bosonic symmetry group of the $\mathcal{N} = 4$ SYM where the $\mathrm{SU}(4)$ part corresponds to the R-symmetry of N=4 supersymmetry. Meanwhile, $\mathrm{SU}(2,2)$ reflects the theory's invariance under conformal transformations, serving as a double cover of the more familiar 4d conformal group $\mathrm{SO}(4,2)$.

On the gravitational side, $\mathrm{SO}(4,2) \times \mathrm{SO}(6)$ is the isometry group of $\mathrm{AdS}_5 \times \mathrm{S}^5$. Considering that type IIB supergravity contains fermionic fields, it becomes necessary to take the double covers of these groups, resulting in $\mathrm{SU}(2,2) \times \mathrm{SU}(4)$, precisely matching the $\mathcal{N} = 4$ SYM bosonic symmetry. Further examination shows that with the inclusion of fermionic counterparts, the complete superalgebra of both theories is $\mathrm{PSU}(2,2|4)$ [34].

This highlights two key principles of gauge/gravity dualities. First, gravity theory defined on AdS space holistically corresponds to a CFT because the isometries of the AdS space include the full set of conformal transformations. Second, the gauge symmetries present in the gravitational theory correspond to global symmetries in its dual QFT; interestingly, large gauge transformations that act non-trivially on the boundary play the role of global transformations on the boundary, demonstrating a profound interplay between local and global aspects of the theories involved.

A vast range of dual theories has been proposed since the introduction of gauge/gravity dualities. Some of them we will explore in more detail in the following chapters. While definitive proof of gauge/gravity dualities remains elusive, there is overwhelming evidence supporting its existence. Numerous calculations performed on both sides of the correspondence have yielded identical results, providing strong support for this remarkable connection.

2.1.3 The correspondance dictionary

Now, we discuss the holographic dictionary, which is the map between observables in a gravitational theory and its dual QFT.

There is a direct relation between the renormalisation scale, μ, in the corresponding QFT and the z coordinate in Eq. (2.1.3), parametrising the radial direction. Indeed, the μ scale is inversely proportional to z. As we approach the boundary of AdS space (where z approaches zero), the renormalisation scale tends towards infinity, corresponding to the ultraviolet (UV) regime of the QFT. Conversely, as z increases, we move towards the infrared (IR) regime of the QFT. It is a common conceptualisation to imagine the d-dimensional QFT as residing at the boundary of the $d+1$-dimensional asymptotically AdS manifold.

Equation (2.1.5) outlines a method to calculate correlation functions in a QFT using its corresponding gravity theory. For a given set of operators in the QFT, which are related to specific fields in the gravity theory, the correlation function of these operators can be determined by taking functional derivatives of the gravity theory's action evaluated on classical solutions (on-shell action), with respect to the boundary values of the corresponding fields [3, 4]. For the Euclidean signature we have,

$$\langle \mathcal{O}_1(x_1) \dots \mathcal{O}_n(x_n) \rangle = \left(-\frac{\delta}{\delta \phi_{1,(0)}(x_1)} \right) \dots \left(-\frac{\delta}{\delta \phi_{n,(0)}(x_n)} \right) e^{-I_{\text{gr-saddle}}[\phi_0]}, \tag{2.1.7}$$

where x_i is the position that the operator $\mathcal{O}_i$ is inserted and $\phi_{i,(0)}$ is the bouandary value of the corresponding ϕ_i field. $I_{\text{gr-saddle}}$ is the gravity on-shell action.

We examine a bulk field ϕ, considering a scalar field for simplicity, which corresponds dually to an operator $\mathcal{O}$ in the theory at the boundary. The equation governing the dynamics of the ϕ field, derived from the gravitational action, I_{gr}, is a second-order differential equation. Consequently, two boundary conditions are necessary for a complete description. An expansion of ϕ in the neighberhood of $z = 0$ has a general form of:

$$\phi(x, z) = z^{d-\Delta} \phi_{(0)}(x) \left(1 + \dots\right) + z^{\Delta} \phi_{(2\Delta - d)}(x) \left(1 + \dots\right). \tag{2.1.8}$$

The omitted terms within the equation involve higher-order powers of the radial coordinate, z. The coefficients $\phi_{(0)}$ and $\phi_{(2\Delta-d)}$ are determined by the specific boundary conditions imposed on the system. The Δ parameter, related to the scaling dimension of the corresponding operator in the QFT, is fixed by the mass of the scalar field. It is obtained as the largest solution to the following equation:

$$m^2 L^2 = \Delta(\Delta - d). \tag{2.1.9}$$

A derivation for this formula can be found in Ref. [36].

The field $\phi_{(0)}$ is identified with the source for the operator $\mathcal{O}$ with a mass dimension of $[\phi_{(0)}] = d - \Delta$, which aligns with the expected dimension of the source for an operator $\mathcal{O}$ with scaling dimension Δ. The relation $[\phi_{(2\Delta-d)}] = \Delta$ can be checked by dimensional analysis. Through the application of the method outlined in Eq. (2.1.7), it can be demonstrated that this coefficient is related to the VEV of the operator $\mathcal{O}$. One has [42, 43]

$$\langle 0|\mathcal{O}(x)|0\rangle = -(2\Delta - d)\phi_{(2\Delta-d)}(x) + f[\phi_{(0)}(x)]. \tag{2.1.10}$$

Here, f depends on the boundary field $\phi_{(0)}(x)$ and derivatives of it. The general form of f is determined by the I_{gr} action. The condition imposing that Δ must be the largest solution to Eq. (2.1.9) is a condition in the CFT called the unitarity bound. In a CFT which respects unitarity, except for the identity operator, all scalar operators possess a scaling dimension Δ higher than $\frac{d}{2} - 1$.

However, for masses falling within the range $-\frac{d^2}{4} < m^2 l^2 \leq 1 - \frac{d^2}{4}$, there exists an alternative interpretation. In this specific scenario, we can select the smaller root of Eq. (2.1.9) for Δ while still ensuring the theory remains unitary [46]. Notably, scalar fields in AdS space can remain stable even when their mass squared is negative, provided it exceeds a specific lower bound, known as the Breitenlohner-Freedman (BF) bound [47, 48]. This bound, given by $m^2 l^2 \geq -\frac{d^2}{4}$, is essential for maintaining stability in the AdS spacetime.

An important operator within this framework is the stress-energy tensor, $T^{\mu\nu}$, representing the conserved current related to the invariance of the system under translation. Gauge/gravity dualities establish a connection between translational symmetry in the QFT and diffeomorphism invariance in the gravitational theory. As a result, the stress-energy tensor stands as the counterpart to the metric tensor, which defines the geometry of spacetime in the gravity theory.

In the Fefferman-Graham coordinates, as described in Eq. (2.1.3), where the metric has the near-boundary expansion of Eq. (2.1.4), the first coefficient $g_{(0)\mu\nu}$ is identified as the stress-energy tensor source in the dual theory. Correlation functions for the stress-energy tensor can then be calculated by taking functional derivatives respective to the boundary metric $g_{(0)\mu\nu}$ [42],

$$\langle T_{\mu\nu}\rangle = -\frac{2}{\sqrt{\det g_{(0)}}}\frac{\delta \ln Z}{\delta g^{\mu\nu}_{(0)}} = \frac{d}{16\pi G_N} g_{(d)\mu\nu} + \dots\,, \tag{2.1.11}$$

where the omitted terms depend on $g_{(0)}$ and other sources.

2.1.3.1 Gauge/gravity dualities at non-zero temperatures

We will also review systems at finite temperatures and chemical potential. The holographic counterpart to a gravitational solution with the temperature T is a QFT at the same finite temperature [32]. The free energy of the QFT can be obtained from a generating functional related to the gravitational action as $Z = \exp(-F/T)$, with F representing the free energy. Normally, this gravitational solution takes the form of a black hole or black brane, characterised by a Hawking temperature identical to the QFT temperature. To establish a thermodynamic framework for the QFT, we typically employ a Wick rotation to the imaginary time, introducing a time coordinate with a period inverse to the temperature.

Consider the case of a QFT with a $U(1)$ global symmetry, and its associated Noether current J^μ. In bulk, this current corresponds to a $U(1)$ gauge field, here denoted as A_M. Specifically, The temporal element of this gauge field, A_t, corresponds to the density of charge, J^t. In asymptotic boundary of AdS_{d+1}, the near-boundary expansion of A_t takes the form:

$$A_t = \mu + j z^{d-2} + \dots .$$

Employing the holographic dictionary, we recognise μ, the leading coefficient, as the source coupled to the density of charge, representing the chemical potential, by definition. The sub-leading coefficient, j, is directly proportional to the charge density.

2.1.4 Two-point correlation functions

Throughout this thesis, we will make use of holography to study the correlation functions of a QFT at non-zero temperatures and their pole structure. The retarded Green's function in the QFT side can be written as [49]

$$G_{ab}(x_1 - x_2) = \theta(t_1 - t_2)\langle \mathcal{O}_a(x_1)\mathcal{O}_b(x_2)\rangle + \theta(t_2 - t_1)\langle \mathcal{O}_b(x_2)\mathcal{O}_a(x_1)\rangle, \tag{2.1.12}$$

In the given expression, θ denotes the Heaviside step function, while $t_{1,2}$ represents the time component of $x_{1,2}$, and (a, b) labels the operators within the theory. Expressing G_{ab} as a function of the separation $x_1 - x_2$ is a result of assuming the theory's invariance under translations both in space and time.

The significance of the retarded Green's function G_{ab} lies in its role in determining the linear response of the operator, $\mathcal{O}_a$, to a fluctuation in the source of $\mathcal{O}_b$ [50],

$$\delta\langle \mathcal{O}_a(x)\rangle \approx \int d^d y\, G_{ab}(x - y)\delta\phi_{(0),a}(y). \tag{2.1.13}$$

The Fourier transform of the Green's function is

$$G_{ab}(\omega, \mathbf{k}) = \int d^d x \, e^{i\omega t - i\mathbf{k}\cdot\mathbf{x}} G_{ab}(t, \mathbf{x}), \tag{2.1.14}$$

with $x = (t, \mathbf{x})$. For a given momentum, $\mathbf{k}$, the function $G_{ab}(\omega, \mathbf{k})$ has poles in the complex ω plane, located at frequencies denoted as $\omega = \omega_*(\mathbf{k})$. These poles are related to the virtual propagating modes within the field theory, characterised by a frequency $\mathrm{Re}\,(\omega_*)$ and a decay rate $-\mathrm{Im}\,(\omega_*)$. It is worth noting that we assume $\mathrm{Im}\,(\omega_*) < 0$; if instead $\mathrm{Im}\,(\omega_*) > 0$, the mode experiences exponential growth over time, indicating instability in the system.

In the context of gauge/gravity dualities, the poles present in the two-point functions of the boundary theory correspond to the frequencies of the quasinormal modes in the gravitational theory [51, 52].

When considering small fluctuations about a black brane solution in the gravitational theory, which is holographically dual to a thermal state of the boundary QFT, we express the fluctuation of a field ϕ_a, as $\phi_a \to \phi_a + \delta\phi_a(t, \mathbf{x}, z)$. We focus on fluctuations of a single Fourier mode for each field, as different Fourier modes are decoupled owing to the translational invariance of the background solution,

$$\delta\phi_a(t, \mathbf{x}, z) = e^{-i\omega t + i\mathbf{k}\cdot\mathbf{x}} \delta\phi_a(\omega, \mathbf{k}, z), \tag{2.1.15}$$

for a fixed frequency, ω, and momentum, $\mathbf{k}$. We aim to find solutions to the linearised equations of motion for the Fourier modes that meet two criteria: normalizability at the boundary and the regular behaviour at the Horizon.

Each Fourier mode exhibits a near-boundary expansion like Eq. (2.1.8) (with distinct values of Δ). We impose the condition that the leading coefficient at the boundary vanishes. From a holographic perspective, this maintains the sources for all operators fixed.

In the vicinity of the horizon, the equations of motion for the fluctuations have two independent solutions, corresponding to waves propagating into or out of the horizon. We should choose the boundary conditions ensuring that the solution is ingoing. In holographic terms, this fixes that the quasinormal modes correspond to poles of the retarded Green's functions, rather than the advanced counterparts.

Solutions obeying these boundary conditions typically exist only for a discrete set of frequencies for a given momentum. These frequencies represent the quasinormal modes.

To compute the two-point function G_{ab}, the procedure involves the following steps [51, 53, 54].

We analyse fluctuations of the fields ϕ_a, expressing their Fourier-transformed fluctuations

as:

$$\delta\phi_a(t,\mathbf{x},z) = \int \frac{d^dk}{(2\pi)^d} e^{ik\cdot x} F_{ab}(k,z) z^{d-\Delta_b} \delta\phi_{(0),b}(k), \tag{2.1.16}$$

where Δ_b denotes the dimension of the operator dual to ϕ_b, $k = (\omega, \mathbf{k})$, and $F_{ab}(k,0) = \delta_{ab}$. We impose the ingoing boundary conditions on F_{ab} at the horizon. Here, $\delta\phi_{(0),a}(k)$ represents the Fourier transform of the perturbation in the source, $\delta\phi_{(0),a}(x)$.

Upon substituting Eq. (2.1.16) into the linearised action for the fluctuations, and by using the equations of motion, the action can be expressed as:

$$S = \int \frac{d^dk}{(2\pi)^d} \left[\delta\phi_{(0)a}(-k)\mathcal{F}_{ab}(k,z)\delta\phi_{(0)b}(k)\right]_{z=0}^{z=z_H},$$

where z_H denotes the location of the brane horizon, and $\mathcal{F}_{ab}$ depends quadratically on F_{ab}. The specific form of $\mathcal{F}_{ab}$ is dictated by the gravitational theory action.

Finally, the retarded two-point functions, G_{ab}, are derived from:

$$G_{ab} = -2\mathcal{F}_{ab}(k, z = 0).$$

In the next section, we will describe the SM's naturalness issue.

2.2 Naturalness problem

To understand the Naturalness problem mentioned in Chapter 1, we provide a review here, following Ref. [26]. The SM is an effective field theory, implying that its operator coefficients, currently treated as fundamental input parameters, are ideally derived from a more comprehensive beyond-the-Standard-model (BSM) theory in the future. This scenario is similar to the historical development of the Fermi theory of weak interactions, where the Fermi constant, G_F, served as a fundamental input parameter governing the strength of the weak force. It became apparent that the true microscopic framework describing weak interactions is the Electroweak (EW) theory, which enables the prediction of G_F in terms of its underlying parameters g_W and m_W, consistent with experimental observations and lower energy description. The expression for G_F in the standard model, at the tree level, is

$$G_F = \frac{g_W^2}{4\sqrt{2}\, m_W^2}$$

To compute G_F and compare it with low-energy observations, one can measure the microscopic parameters g_W and m_W at high energy. The success of this program allows us to assert that the microscopic origin of the weak interaction is described in terms of the EW theory.

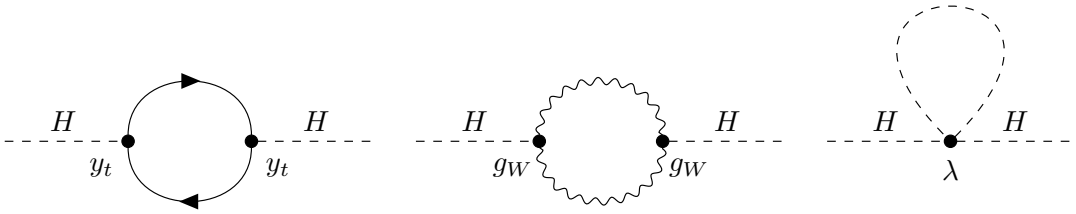

Figure 2.1. Some representative top, gauge and Higgs boson loop diagrams that contribute to the Higgs mass.

Now, we will explore how the Naturalness problem obstructs performing the same procedure for the Higgs mass and, consequently, for the Electroweak Symmetry Breaking (EWSB) scale.

If we know the UV completion of the theory of EWSB, this theory would predict the Higgs mass term, μ^2, or equivalently the physical Higgs mass, $m_H^2 = 2\mu^2$, derived from its intrinsic parameters, p_{true}. This prediction can be expressed as:

$$m_H^2 = \int_0^\infty dE \, \frac{dm_H^2}{dE}(E; p_{\text{true}}), \tag{2.2.1}$$

where the integral over energy covers contributions to m_H^2 from all energy scales, extending potentially up to the high cutoff of the UV completed theory. The integration could get main contributions from a region around a specific scale.

Now, we consider dividing the integral into two regions based on an intermediate scale slightly below the Standard Model cutoff,

$$\begin{aligned} m_H^2 &= \int_0^{\lesssim \Lambda_{\text{SM}}} dE \, \frac{dm_H^2}{dE}(E; p_{\text{true}}) + \int_{\lesssim \Lambda_{\text{SM}}}^\infty dE \, \frac{dm_H^2}{dE}(E; p_{\text{true}}) \\ &= \delta_{\text{SM}} m_H^2 + \delta_{\text{BSM}} m_H^2 \, . \end{aligned} \tag{2.2.2}$$

Here $\delta_{\text{BSM}} m_H^2$ represents an entirely unknown contribution arising from energies equal to or above Λ_{SM}, whereas $\delta_{\text{SM}} m_H^2$ originates from virtual particles below this cutoff, whose behaviour is described by the SM. Before understanding the specifics of the BSM theory, we cannot make any definitive statements about $\delta_{\text{BSM}} m_H^2$. However, we can readily estimate $\delta_{\text{SM}} m_H^2$ using the diagrams illustrated in Figure 2.1 leading to

$$\delta_{\text{SM}} m_H^2 = \frac{3y_t^2}{8\pi^2}\Lambda_{\text{SM}}^2 - \frac{3g_W^2}{8\pi^2}\left(\frac{1}{4} + \frac{1}{8\cos^2\theta_W}\right)\Lambda_{\text{SM}}^2 - \frac{3\lambda}{8\pi^2}\Lambda_{\text{SM}}^2 \, , \tag{2.2.3}$$

obtained from the top quark contributions, EW bosons, and Higgs boson loop, respectively.

Irrespective of the physics at $\Lambda_{\rm SM}$, the SM dictates the above-mentioned terms in Eq. (2.2.3) for m_H^2. Now, one can realise the problem of Naturalness. In the finite formula for m_H^2 derived from the full theory, there are two contributions that are entirely independent because they originate from distinct energy scales. One of these contributions, $\delta_{\rm SM} m_H^2$, is expected to be significantly large especially if $\Lambda_{\rm SM}$ is large. Consequently, the other contribution must be similarly large in magnitude but opposite in sign to $\delta_{\rm SM} m_H^2$ in order to account for the observed lightness of the Higgs mass. This cancellation between the two contributions is quantified by a parameter called fine-tuning,

$$\Delta \geq \frac{\delta_{\rm SM} m_H^2}{m_H^2} = \frac{3\, y_t^2}{8\pi^2} \left(\frac{\Lambda_{\rm SM}}{m_H} \right)^2 \simeq \left(\frac{\Lambda_{\rm SM}}{450\,\text{GeV}} \right)^2 . \tag{2.2.4}$$

This is a lower bound on fine-tuning as only the top particle contribution in Eq. (2.2.3) has been kept for the estimation. This is because of the domination of the top as a result of its considerable Yukawa coupling and also its colour multiplicity.

2.2.1 Dimensional transmutation

The composite Higgs scenario provides a straightforward resolution to the Naturalness problem. Instead of the Higgs being a point-like particle, as in the SM, it is assumed as an extended object with a finite size, l_H. This revision occurs by postulating that it is the composite state of a new strong force, characterised by a confinement scale $m_* = 1/l_H$ on the order of a few TeV.

In this revised framework, the behaviour of the integrand $\frac{dm_H^2}{dE}$ in the Higgs mass formula in Eq. (2.2.1), which carries the influence of virtual quanta at different energies, is peculiar. At lower energies, the wavelength of quanta exceeds l_H, and the Higgs manifests itself as an elementary particle. Consequently, the integral increases linearly with E, showing the same behaviour seen in the SM, leading to quadratic growth with the upper limit of integration.

However, this trend is changed by the introduction of the finite-size effects that emerge as E become closer and surpasses m_*. Similar to how a proton becomes transparent to high-energy photons with wavelengths smaller than its radius, the composite Higgs also exhibits reduced interaction with high-energy quanta. This alters the linear SM behaviour to feature a peak around $E \sim m_*$, followed by a rapid decline in the integrand. The generation of the Higgs mass is thereby localised around $m_* = 1/l_H$, with m_H being insensitivity to higher energies. This is evident from the absence of any Higgs particle at energies much beyond m_*, ensuring no corresponding Higgs field or problematic dimension-two Higgs mass terms emerge to create concerns.

It is noteworthy that this scenario is useful if the Higgs size or the associated confinement scale of the new sector is Natural itself.

At the UV scale $\Lambda_{\rm UV}$ (for instance $\Lambda_{\rm UV} \sim M_{\rm GUT}$), the composite sector of the theory will be close to a fixed point in its Renormalization Group (RG) flow, assuming that there are no strongly relevant deformations around this fixed point. This characteristic ensures that the RG flow towards the infrared IR regime progresses 'slowly'. The rate of departure from the fixed point is governed by the RG 'time' parameter $t = \log[\Lambda_{\rm UV}/E]$, where E is the energy scale. This parameter t indicates how far the theory deviates from the fixed point before confining and ultimately forming the composite Higgs bound state. This confinement occurs at an scale m_* which is exponentially suppressed and it is defined by $\bar{t} = \log[\Lambda_{\rm UV}/m_*]$.

The RG running can be arbitrarily long depending on how close the theory parameters are to the fixed point at $\Lambda_{\rm UV}$ initially. This expectation behaviour for a prolonged RG evolution allows for a naturally large hierarchy between $\Lambda_{\rm UV}$ and m_*. For instance, $\bar{t}$ could be small, of the order of 10, establishing a significant hierarchy between the UV scale and the confinement scale m_*.

Drawing an analogy to QCD is illuminating in this context. In QCD with 3 light quark flavours and starting the running at $m_Z = \Lambda_{\rm UV}$, the familiar relation for QCD confinement scale $\Lambda_{\rm QCD} = m_*$ can be expressed as:

$$\log[\Lambda_{\rm UV}/m_*] = \frac{1}{18}\left(\frac{4\pi}{g_S}\right)^2,$$

The departure from the free fixed point is controlled by the loop expansion parameter, $\frac{g_S^2}{16\pi^2}$, where g_S is the strong coupling constant evaluated at $\Lambda_{\rm UV} = m_Z$. This parameter's inverse determines the total RG running time, thereby establishing the hierarchy in $\Lambda_{\rm UV}$ and m_*. The process by which the scale m_* is generated solely through RG running, without the need for dimensionful parameters but instead relying on $d = 0$ (dimensionless) couplings in the UV theory, is the so-called "dimensional transmutation." This concept is well-known in QCD and is applicable in the broader context considered here. In the composite Higgs scenario, compatibility with the SM gauge symmetry is essential, particularly in how the composite sector interacts with the elementary gauge fields that represent the SM vector bosons.

The composite sector is governed by an exact symmetry group $\mathcal{G}$, which includes an $\mathrm{SU}(2)_L \times \mathrm{U}(1)_Y$ subgroup. This subgroup corresponds to the electroweak gauge symmetry of the SM. The elementary W_μ and B_μ fields are associated with this subgroup through the usual gauging procedure, thereby making $\mathrm{SU}(2)_L \times \mathrm{U}(1)_Y$ a local symmetry. These elementary gauge fields are coupled to the global conserved currents of $\mathrm{SU}(2)_L \times \mathrm{U}(1)_Y$ within the composite sector. This coupling establishes an interaction channel between the two sectors.

Drawing an analogy with QCD, where the elementary sector contains the light leptons and photons, the global symmetry group, $\mathcal{G}$ is $\mathrm{SU}(3)_L \times \mathrm{SU}(3)_R$ (chiral symmetry), with the

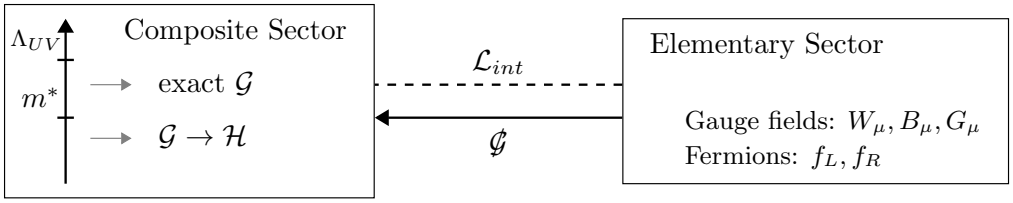

Figure 2.2. The schematic structure of the composite Higgs scenario.

photon gauging the $\mathrm{U}(1)_{\mathrm{e.m.}}$ subgroup. In QCD, the chiral symmetry, $\mathrm{SU}(3)_L \times \mathrm{SU}(3)_R$, is also explicitly broken by the masses of quarks.

The breaking of the global symmetry group, $\mathcal{G}$, is implemented in the composite sector through interactions with the elementary sector, characterised by $\mathcal{L}_{\mathrm{int}}$. This process is analogous to what would happen in QCD if quark masses were set to zero, where the breaking of the chiral symmetry would then primarily stem from the coupling to the elementary photon field.

Similarly, in both QCD and the composite Higgs scenario, at the confinement scale m_*, the global symmetry group $\mathcal{G}$ spontaneously breaks to a subgroup $\mathcal{H}$. This breaking mechanism generates a spectrum of exactly massless Nambu-Goldstone bosons (NGBs) corresponding to the coset space $\mathcal{G}/\mathcal{H}$. The Higgs boson in our scenario emerges as one of these Nambu-Goldstone bosons. However, unlike in traditional composite Higgs models (such as those proposed in [55–57]), where the Higgs was considered a generic bound state of some composite sector, here it retains a crucial property: it is a pseudo-NGB. This designation arises because the Goldstone symmetry $\mathcal{G}$ is explicitly broken by interactions with the elementary sector. The explicit breaking of $\mathcal{G}$ causes the Higgs boson to acquire a small mass and a potential, leading to EWSB.

To sum up, the composite Higgs framework consists of three foundational components, illustrated in Figure 2.2: a composite sector, an elementary sector, and an interaction term $\mathcal{L}_{\mathrm{int}}$ that mediates the explicit breaking of the global symmetry $\mathcal{G}$ from the elementary to the composite sector. The main objective of this work is to investigate the essential characteristics these elements must exhibit and formulate a viable and realistic theoretical framework to study it using holographic.

Chapter 3

Phase transitions and light scalars in bottom-up holography

The Standard Model possesses an approximate scale invariance which is explicitly and spontaneously broken. The Higgs boson in this context can be identified as a dilaton, the pNGB of the dilatations. It is important to ask if this symmetry is accidental, without resulting from a more fundamental and original property of the SM or not [58]. Especially if the Higgs boson originates from a more fundamental theory as a composite dilatonic state. If it is composite, it is crucial to understand what underlying dynamics are required to achieve realistic values for its couplings and mass.

The dilaton EFT had been studied for many decades [11, 12], and its applications in the context of dynamical electroweak symmetry breaking [59–61], extensions of the SM [62–72], and, the interpretation of lattice data [73–89], has been discussed extensively.

Lately, numerical lattice calculations in certain $SU(3)$ gauge theories have detected a light scalar bound state within the spectrum performed by numerical calculations [13–24].

To further investigate the mentioned ideas, gauge/gravity dualities [2–4, 37] have been useful for describing both the appearance of the dilaton and its dynamical origin, either in bottom-up [90–106] or top-down [107–111] approaches.

We aim to study a bottom-up holographic model capturing features related to dilatonic Higgs. In the following, we focus on holographic duals where the geometry of a smooth classical background in a higher-dimensional gravity theory includes a shrinking circle. This shrinking circle is utilised to mimic confinement in the dual field theory, as proposed in Ref. [32] and further explored in Refs. [112–118]. In the strongly coupled theory, the spectra of bound states can be computed perturbatively within its gravity dual. This is achieved by employing the holographic gauge-invariant formalism developed in Refs. [119–123], and also discussed in Refs. [109–111, 118, 124]. See also [125] for earlier studies.

In order to identify (approximate) dilatons in the spectra we use the probe approximation, as discussed in Ref. [124] and Appendix B.

Among different scenarios for the realisations of the dilaton in EFTs, we focus on the ideas presented in Refs. [126–129]—see also Ref. [130] and references therein. The idea is described in more detail in Section 3.1 that proposes the emergence of a light dilatonic state in strongly-coupled theories when their renormalisation group (RG) flow approaches the vicinity of a tachyonic instability.

In this chapter, following the references [131–133], we construct a set of bottom-up models that merge the quadratic superpotential framework from [91] with the confinement mechanism outlined in [32]. Our approach assumes a holographic description of the dynamics, encapsulated within a model featuring a single real scalar field coupled to gravity in a six-dimensional spacetime, with one dimension compactified on a circle.

In the physically relevant branch of solutions, the circle contracts to a point at a finite position along the holographic dimension, introducing a dynamic scale. Importantly, the resulting geometry remains smooth and regular throughout. This setup proposes a dual representation of the hypothetical class of four-dimensional confining theories. At short distances, these theories are most effectively characterised by the circle compactification of a five-dimensional conformal field theory (CFT), incorporating an operator with a non-trivial dimension determined by $\max(\Delta, 5-\Delta)$, where Δ represents a free parameter in the scalar potential of the gravity theory.

The generic model behaviour for each value of Δ closely resembles that presented in Refs. [131–133], as we shall discuss. The bottom-up approach, besides featuring a significantly simpler bosonic action, enables us to flexibly adjust Δ. Our focus will be on revealing the relationship between Δ and the mass spectrum, particularly concerning the lightest scalar, in the vicinity of the phase transition.

The structure of the chapter is as follows: We begin with the gravity theory in $D = 6$ dimensions in Section 3.2. Following this, in Section 3.3, we present various classes of classical background solutions. Then, in Section 3.4, we study the spectrum of fluctuations, concentrating on the regular (confining) branch of solutions. In Section 3.5, we compute the free energy for different branches of solution to detect the stable branch, depending on various parameters in the theory. The key numerical findings are summarised in Section 3.6. Technical details are relegated to the appendices.

3.1 Conformal transition by fixed-point merging

Theories that are nearly conformally invariant are of significant interest because they can produce large hierarchies of scales [90, 95, 134–136]. This interest motivates us to understand how theories behave at the critical point where varying some parameters initiates a transition from a conformal to a non-conformal regime. We follow [129] to review this phenomenon here.

This behaviour is particularly compelling in strongly-coupled theories. A prime example is QCD, where the theory is expected to become conformal at a critical value for the number of flavours $N_F = N_F^{\text{crit}}$. Although the precise value of N_F^{crit} is uncertain, lattice simulations suggest values near $N_F^{\text{crit}} \sim 10$. For $N_F \geq N_F^{\text{crit}}$, the long-distance behaviour of QCD transitions into a CFT up to $N_F = \frac{11}{2}N_c$, where N_c is the number of colour degrees of freedom. At this point, the theory reaches the Banks-Zaks fixed point and becomes IR free for the reange $N_F > \frac{11}{2}N_c$. The range $N_F^{\text{crit}} \leq N_F \leq \frac{11}{2}N_c$ is referred to as the conformal window.

Recent lattice simulations indicate that, unlike real QCD, theories close to the conformal transition contain a 0^{++} state as the lightest resonance, aside from the pions as Goldstone bosons [15, 137]. The reason for the lightness of this state remains unclear. Some conjectures propose it to be a dilaton associated with scale invariance breaking. If so, in the large-N_c limit in which $N_F^{crit}/N_c \equiv x_{crit}$ becomes a continuous parameter, it would be intriguing to check if the dilaton mass reduces as $N_F/N_c \to x_{crit}$ from below.

Here, we review the physics of conformal transitions and related ideas concerning the holographic approach. We proceed the review to build upon the framework presented in Ref. [126], which postulates that the departure from the conformal window in large-N_c QCD occurs when the IR fixed point merges with a UV fixed point. Near the conformal window, the theory incorporates a marginal operator $\mathcal{O}_g$, whose dimension acquires a small imaginary part when we lose the conformal invariance (further details in the subsequent section). Assuming this scenario, the AdS/CFT correspondence can offer a straightforward realisation, where a complex dimension for an operator corresponds to a scalar field with mass below the Breitenlohner-Freedman (BF) bound with $M_\Phi^2 = -4/L^2$. At this point, the scalar becomes tachyonic, inducing a departure from the AdS geometry [126].

The potential existence of a light dilaton could be suggested by the appearance of a marginal operator $\mathcal{O}_g$ in the model, as discussed in works such as [69, 103, 138]. The argument revolves around the effective dilaton potential, typically written as

$$V_{\text{eff}}(\phi_d) = \lambda_{\text{eff}}(\phi_d)\,\phi_d^4,$$

where the dilaton mass is determined by the minimum of the potential

$$\frac{m_{\phi_d}^2}{\langle\phi_d\rangle^2} = \beta_{\lambda_{\text{eff}}}(4 + \beta'_{\lambda_{\text{eff}}}),$$

with $\beta_{\lambda_{\text{eff}}} = \frac{d\lambda_{\text{eff}}}{d\ln\phi_d}$ and $\beta'_{\lambda_{\text{eff}}} = \frac{d\beta_{\lambda_{\text{eff}}}}{d\lambda_{\text{eff}}}$. Here, $\beta_{\lambda_{\text{eff}}}$ arises from an explicit breaking of scale invariance, proportional to β_g if the breaking originates from a term like $g\,\mathcal{O}_g$ in the Lagrangian.

According to this framework, if the dimension of $\mathcal{O}_g$ is close to 4 (denoted as $4+\delta$ with $\delta \ll 1$), the dilaton can be parametrically light, characterised by $m_{\phi_d}^2 \propto \beta_g$. It is important

that $\delta \ll 1$ (or $\beta_g \ll 1$) must be a small and controllable parameter along the RG-flow.

This scenario aligns with the Goldberger-Wise mechanism [90], where $\mathcal{O}_g$ corresponds to an almost massless scalar in a 5-dimensional setup, protected by a shift symmetry [69, 103, 138].

3.1.1 Fixed-point merging and conformal transition

As an example let us consider a 4 dimensional QFT. As we adjust the parameters of the theory, an IR fixed point can be lost in several ways: it can approach zero, diverge to infinity, or merge with a UV fixed point. Following Ref. [126], we discuss conformal transitions characterised by the merging of the IR fixed point with a UV fixed point, as illustrated in Fig. 3.1.

The beta function governing the coupling, g, of the theory, not necessarily the gauge coupling in gauge theories, can be approximated as:

$$\beta_g \simeq -\epsilon - (g - g_*)^2, \tag{3.1.1}$$

where g_* represents the fixed point value of g, and ϵ depends on the theory parameters, such as N_F. The IR and UV fixed points are respectively located at:

$$g = g_* \mp \sqrt{-\epsilon}.$$

By variation of ϵ from negative to positive values, the IR and UV fixed points merge when $\epsilon = 0$. For $\epsilon > 0$, the theory leaves conformality, with the IR fixed point at a complex coupling.

According to Ref. [127], in the vicinity where ϵ is negative and close to zero, the operator $\mathcal{O}_g$ associated with the coupling g has a dimension given by:

$$\mathrm{Dim}[\mathcal{O}_g] = 4 + \frac{d\beta_g}{dg} \simeq 4 + 2\sqrt{-\epsilon}. \tag{3.1.2}$$

This operator $\mathcal{O}_g$ drives the renormalisation group flow towards the IR fixed point. At the point where $\epsilon = 0$, $\mathcal{O}_g$ becomes marginal. As ϵ turns positive, $\mathcal{O}_g$ acquires a complex dimension, thereby indicating the end of conformal behaviour.

One can provide a dual description for the mentioned phenomenon in the holographic context. Operators $\mathcal{O}$ in the CFT_4 correspond to scalar fields Φ in AdS_5, where their dimensions and masses are related through the AdS/CFT correspondence by:

$$\mathrm{Dim}[\mathcal{O}] = 2 + \sqrt{4 + M_\Phi^2 l^2},$$

where M_Φ is the mass of the scalar field Φ and l is the AdS_5 curvature radius.

Equation (3.1.1) indicates that the dual of a CFT_4 operator with a complex dimension

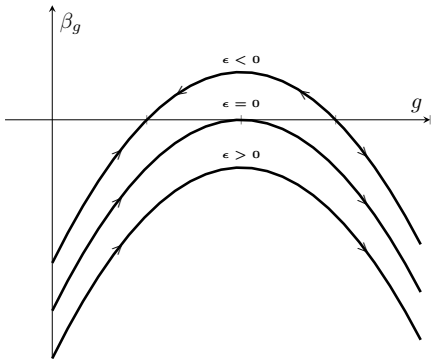

Figure 3.1. The approximated beta function in Eq. (3.1.1) for the coupling g for different values of ϵ.

is a scalar Φ in AdS_5 with a mass slightly below the BF bound, specifically $M_\Phi^2 = -(4+\epsilon)/l^2$. As $\epsilon \to 0$, the operator $\mathcal{O}_*$ with complex dimension approaches dimension 2 instead of 4, as described in Eq. (3.1.1). Hence, $\mathcal{O}_g$, can be identified as $\mathcal{O}_g = |\mathcal{O}_*|^2$, and in the large N_c limit, $\mathrm{Dim}[\mathcal{O}_g] = 2\mathrm{Dim}[\mathcal{O}_*]$, consistent with the dimension given in Eq. (3.1.2).

The existence and properties of $\mathcal{O}_*$ during a conformal transition are not universally true but rather specific to large-N_c limits or particular scenarios. As discussed in Ref. [126], in QCD $\mathcal{O}_*$ is expected to correspond to the $q\bar{q}$ operator, whose dimension transitions from approximately 3 when entering the conformal window to 2 when leaving it and becoming complex [139–141].

When the theory is near the conformal window with $0 < \epsilon \ll 1$ the RG flow "time" required to traverse the region where $g \sim g_*$ and $|\beta_g| \ll 1$ is calculable. This provides us with the infrared scale Λ_{IR} at which the theory is anticipated to confine, corresponding to when g is large. From Eq. (3.1.1) one have

$$\Lambda_{\mathrm{IR}} \sim e^{-\pi/\sqrt{\epsilon}} \Lambda_{\mathrm{UV}} \,, \tag{3.1.3}$$

with Λ_{UV} the scale at which $g \lesssim g_*$. The Eq. (3.1.3) is referred to as Miransky scaling or walking.

In the following section, we will describe our model for realising a system analogous to the conformal transition behaviour described here.

3.2 The model

This section presents a model formulated within the framework of bottom-up holography, containing a real scalar field, ϕ, coupled to gravity in $D = 6$ dimensions, featuring a simple quartic scalar potential as detailed in Ref. [91]. The scalar field ϕ, within the gravitational

context, encapsulates the effects of deforming the dual five-dimensional CFT by a scalar operator, and the formation of its corresponding condensate. Additionally, one spatial dimension is compactified on a circle, both in the field theory and gravitational perspectives.

As discussed in Section 3.3, this system exhibits solutions where the circle smoothly shrinks towards the IR end of space which introduces a physical low-energy scale. This behaviour mimics the confinement effects observed in top-down models of the dual four-dimensional field theory [32]. Moreover, we provide a description of the resulting gravity theory in $D = 5$ dimensions following the dimensional reduction over the compact circle.

3.2.1 Action in six dimensions

Following the conventions in Ref. [124], summarised in Appendix A, for the model to resemble the dual of a confining four-dimensional theory, we opt for working in $D = 6$ dimensions. The action is

$$\mathcal{S}_6 = \mathcal{S}_6^{(bulk)} + \sum_{i=1,2} \mathcal{S}_{5,i}\,, \tag{3.2.1}$$

$$\mathcal{S}_6^{(bulk)} = \int \mathrm{d}^6x\sqrt{-\hat{g}_6}\left\{\frac{\mathcal{R}_6}{4} - \frac{1}{2}\hat{g}^{\hat{M}\hat{N}}\partial_{\hat{M}}\phi\partial_{\hat{N}}\phi - \mathcal{V}_6(\phi)\right\}, \tag{3.2.2}$$

$$\mathcal{S}_{5,i} = (-)^i \int \mathrm{d}^5x\sqrt{-\tilde{\hat{g}}}\left\{\frac{\mathcal{K}}{2} + \lambda_i(\phi) + f_i\left(\tilde{\hat{g}}_{\hat{M}\hat{N}}\right)\right\}\Bigg|_{\rho=\rho_i}, \tag{3.2.3}$$

which contains a bulk part, $\mathcal{S}_6^{(bulk)}$, and two boundary actions, $\mathcal{S}_{5,i}$, chosen to be localised at the two boundaries of the radial coordinate, $\rho_1 < \rho < \rho_2$. The index $\hat{M} = 0,1,2,3,5,6$ is our space-time index. The extrinsic curvature $\mathcal{K}$ depends on the induced metric on the boundaries, $\tilde{\hat{g}}_{\hat{M}\hat{N}}$, and appears in the Gibbons-Hawking-York (GHY) term for the boundary actions.

The bulk potential, $\mathcal{V}_6$, is chosen as the following

$$\begin{aligned}\mathcal{V}_6(\phi) &= \frac{1}{2}\left(\frac{\partial\mathcal{W}_6(\phi)}{\partial\phi}\right)^2 - \frac{5}{4}\mathcal{W}_6(\phi)^2 \\ &= -5 - \frac{\Delta(5-\Delta)}{2}\phi^2 - \frac{5\Delta^2}{16}\phi^4\,,\end{aligned} \tag{3.2.4}$$

with the 'superpotential' given by [91]

$$\mathcal{W}_6(\phi) \equiv -2 - \frac{\Delta}{2}\phi^2\,. \tag{3.2.5}$$

The adoption of a simple quadratic superpotential offers a clear interpretation within field theory for configurations where the background value for ϕ is non-zero. In the asymptotic UV

regime, the dual field theory undergoes a flow towards a CFT in $D-1=5$ dimensions. This flow is deformed by the insertion of an operator, $\mathcal{O}$, with a scaling dimension determined by $\max(\Delta, 5-\Delta)$. In the context of field theory, the two parameters emerging from the solutions of the corresponding second-order classical equations correspond to the coupling strength and the condensate related to $\mathcal{O}$.

In contrary to the top-down models in which the counterparts of the Δ parameter descend from first principles, Δ is kept as a free parameter here. In the examples discussed in the literature [131–133], the choice of $\Delta > (D-1)/2$ has been made for the first-order background equations. Later in the chapter, the differences emerging for cases with $0 < \Delta < (D-1)/2 = 5/2$ are discussed.

The counter-term necessary for holographic renormalisation matches with $\mathcal{W}_6$ for $\Delta < 5/2$, but for $\Delta > 5/2$ one needs the following superpotential

$$\overline{\mathcal{W}}_6 = -2 - \frac{1}{2}(5-\Delta)\phi^2 - \frac{25(2\Delta-5)}{16(4\Delta-15)}\phi^4 - \frac{125(2\Delta-5)\left(4\Delta^2-15\Delta+25\right)}{64(4\Delta-15)^2(6\Delta-25)}\phi^6 + \cdots, \tag{3.2.6}$$

that is only known perturbatively in ϕ. Nevertheless, this potential solves Eq. (3.2.4). There are some pathological values for Δ at $\Delta = \frac{15}{4}, \frac{25}{6}, \cdots$, that appear at higher orders in ϕ. In what follows, we will not use these special values. The case of $\Delta = 5/2$ is also a special case, and it is treated separately later in the chapter.

The boundary terms described in Eq. (3.2.3) contribute to establishing the boundary conditions for the classical background solutions, ensuring the consistency of the variational principle. These terms are also instrumental in computing the spectrum of fluctuations around these background solutions.

Moreover, these boundary terms are essential in the calculation of the free energy. It is important to note that adjustments to the UV-boundary terms are necessary for this calculation. Specifically, λ_2 (and f_2) must be altered by appropriate counter-terms necessary for the holographic renormalisation. These counter-terms guarantee that the free energy calculation is properly regularised and finite, particularly in the ultraviolet region where divergences may arise.

3.2.2 Dimensional reduction to five dimensions

The coordinate $0 \leq \eta < 2\pi$ is chosen to parametrise our compact circle in the background. The metric, after reduction to five dimensions, is written as

$$\mathrm{d}s_6^2 = e^{-2\chi}\mathrm{d}x_5^2 + e^{6\chi}\left(\mathrm{d}\eta + \chi_M \mathrm{d}x^M\right)^2, \tag{3.2.7}$$

where the space-time index is chosen as $M = 0, 1, 2, 3, 5$. Thus, the reduced action reads

$$\mathcal{S}_5 = \mathcal{S}_5^{(bulk)} + \sum_{i=1,2} \mathcal{S}_{4,i}\,, \tag{3.2.8}$$

$$\mathcal{S}_5^{(bulk)} = \int \mathrm{d}^5x\sqrt{-g_5}\left\{\frac{R}{4} - \frac{1}{2}g^{MN}\left[6\partial_M\chi\partial_N\chi + \partial_M\phi\partial_N\phi\right] - e^{-2\chi}\mathcal{V}_6(|\phi|)\right.$$
$$\left. -\frac{1}{16}e^{8\chi}g^{MP}g^{NQ}F^{(\chi)}_{MN}F^{(\chi)}_{PQ}\right\}, \tag{3.2.9}$$

$$\mathcal{S}_{4,i} = (-)^i\int \mathrm{d}^4x\sqrt{-\tilde{g}}\left\{\frac{K}{2} + e^{-\chi}\lambda_i(\phi) + e^{-\chi}f_i(\chi)\right\}\Big|_{\rho=\rho_i}. \tag{3.2.10}$$

The five-dimensional metric g_{MN} has determinant g_5, with the induced metric on the boundaries $\tilde{g}_{MN}$. The five-dimensional Ricci scalar is represented by R, alongside K, the extrinsic curvature. The form $F^{(\chi)}_{MN} = \partial_M\chi_N - \partial_N\chi_M$ is the field strength for the vector χ_M. Since we want to produce solutions that lift to geometries in six dimensions with a circle shrinking smoothly, the functions f_i in the six-dimensional theory must depend explicitly on the χ field.

Two scalars $\Phi^a = \{\phi, \chi\}$ can be considered as a sigma-model coupled to gravity with the action being the same as Eq. (A.1.1) where $D = 5$ and sigma-model metric is $G_{ab} = \mathrm{diag}(1, 6)$. We concentrate on the background solutions that χ_M is zero, although g_{MN}, ϕ, and χ have a non-trivial profile that depends only on the radial coordinate. In five dimensions, The metric is chosen to be of the domain-wall (DW) form

$$\mathrm{d}s_5^2 = \mathrm{d}r^2 + e^{2A(r)}\mathrm{d}x_{1,3}^2 = e^{2\chi(\rho)}\mathrm{d}\rho^2 + e^{2A(\rho)}\mathrm{d}x_{1,3}^2\,. \tag{3.2.11}$$

Here, the change of radial coordinate $\mathrm{d}\rho = e^{-\chi}\mathrm{d}r$ is introduced, which will be used extensively later. The equations of motion (EOM) for the background fields are

$$\partial_\rho^2\phi + (4\partial_\rho A - \partial_\rho\chi)\partial_\rho\phi = \frac{\partial\mathcal{V}_6}{\partial\phi}\,, \tag{3.2.12}$$

$$\partial_\rho^2\chi + (4\partial_\rho A - \partial_\rho\chi)\partial_\rho\chi = -\frac{\mathcal{V}_6}{3}\,, \tag{3.2.13}$$

$$3(\partial_\rho A)^2 - \frac{1}{2}(\partial_\rho\phi)^2 - 3(\partial_\rho\chi)^2 = -\mathcal{V}_6\,, \tag{3.2.14}$$

with the following boundary conditions

$$\left(\partial_\rho\phi - \frac{\partial\lambda_i}{\partial\phi}\right)\Big|_{\rho_i} = 0\,, \qquad \left(6\partial_\rho\chi + \lambda_i + f_i - \frac{\partial f_i}{\partial\chi}\right)\Big|_{\rho_i} = 0\,, \qquad \left(\frac{3}{2}\partial_\rho A + \lambda_i + f_i\right)\Big|_{\rho_i} = 0\,. \tag{3.2.15}$$

If $f_i = 0$, one has the solutions that can be lifted to the domain walls in 6D.

It is noteworthy that the solutions also satisfy the following equation:

$$0 = 12(\partial_\rho A)^2 + 3\partial_\rho^2 A - 3\partial_\rho\chi\partial_\rho A + 4\mathcal{V}_6\,, \tag{3.2.16}$$

which in combination with Eq. (3.2.13) yields the conservation law (see also Ref. [131])

$$\partial_\rho\Big[\, e^{4A-\chi}\,(\partial_\rho A - 4\partial_\rho\chi)\Big] = 0\,. \tag{3.2.17}$$

This introduces a conserved quantity that vanishes for DW solutions in 6D. In this case the metric $\mathrm{d}s_6^2$ in Eq. (3.2.7) has the warp factor $\mathcal{A} \equiv A - \chi = 3\chi$ (or $A = 4\chi$).

3.3 Classes of solutions

This chapter uses three primary classes of solutions, which are investigated subsequently. First, we clarify our naming conventions for the solutions.

The first class of solutions that are interesting to us is solutions derived from the first-order equations from the superpotential formalism. In the direction of the fake supergravity [142], we term them supersymmetric solutions. Despite the absence of actual supersymmetry in this bosonic theory, we adopt this name in analogy to top-down models where first-order equations align with the Bogomol'nyi-Prasad-Sommerfield (BPS) constraints found in supersymmetric theories.

The most important class of solutions is labelled as confining solutions. This solution is used for our subsequent analysis of fluctuation spectra. The naming convention is borrowed from contexts involving higher-dimensional supergravity derived from string theories. Such models permit the computation of Wilson loops, analogous to other holographic models discussed in [143–148], revealing the anticipated area-law behaviour characteristic of confinement. However, in our bottom-up approach, such detailed calculations are not feasible. Nonetheless, our solutions exhibit smooth behaviour and introduce a mass gap in the spectrum of fluctuations, fulfilling some of the expected criteria for a gravity dual of a confining theory.

Lastly, we introduce another set of backgrounds termed domain-wall solutions, named after their resemblance to Poincaré domain walls in six dimensions. It is noteworthy that these solutions exhibit singularities, which, strictly speaking, disqualify them as proper background solutions. This caveat requires cautious interpretation, as discussed in Ref. [149].

Despite their singular nature, domain-wall solutions are included in our study because they provide insights into the properties and stability of the other classes of solutions we examine.

3.3.1 UV expansions

For $\rho \to \infty$, all of the solutions under study approach to the critical point $\phi = 0$ of $\mathcal{V}_6$, where $\chi \approx \frac{1}{3}\rho$ and $A \approx \frac{4}{3}\rho$ (equivalent to $\mathcal{A} \approx \rho$). This behaviour shows that asymptotically, in the UV, the gravity duals can be interpreted uniformly as relevant or marginal deformations of the same five-dimensional CFT.

To classify these solutions systematically, we utilise a power expansion in the small parameter $z \equiv e^{-\rho}$. These expansions are parameterised by five free parameters: Two of them, χ_U and A_U, represent additive contributions to χ and A, respectively. Another one is χ_5 that appears in the coefficient of the z^5 term in χ expansion. To ensure consistency with the DW solutions, which satisfy $A = 4\chi$, a constraint is imposed: χ_5 is fixed such that $\chi_5 = 0$ corresponds to the DW solutions.

Two remaining free parameters, for generic values of Δ, emerge in the asymptotic expansion of ϕ at orders z^{Δ} and $z^{5-\Delta}$. We name the coefficient of the term with the smaller (larger) exponent Δ_J (Δ_V) as ϕ_J (ϕ_V). The expansions have the following generic form:

$$\phi(z) = \phi_J z^{\Delta_J} + \cdots + \phi_V z^{\Delta_V} + \cdots, \tag{3.3.1}$$

$$\chi(z) = \chi_U - \frac{1}{3}\log(z) + \cdots + (\chi_5 + \cdots) z^5 + \cdots, \tag{3.3.2}$$

$$A(z) = A_U - \frac{4}{3}\log(z) + \cdots. \tag{3.3.3}$$

The case of $\Delta = 5/2$ is special as the two independent parameters mentioned above appear as coefficients of the $z^{5/2}$ and $z^{5/2}\log(z)$ terms in the expansion of ϕ. They are indicated as ϕ_V and ϕ_J, respectively.

As we will explore in detail, these coefficients χ_U, A_U, and χ_5 determine the physical characteristics of the solutions and their corresponding field-theory duals. Each parameter plays a crucial role in shaping different aspects of the field-theoretical descriptions. It is noteworthy that for simplicity and without loss of generality, one can focus on solutions where $A_U = 0$ and $\chi_U = 0$.

The UV expansion of the fields depends on Δ in a non-trivial manner. We mention the case of $\Delta = 3$ here while more cases can be found in Appendix C of Ref. [5]:

$$\phi(z) = \phi_J z^2 + \phi_V z^3 - \frac{25}{48}\phi_J^3 z^6 - \frac{57}{80}\phi_J^2 \phi_V z^7 + \mathcal{O}\left(z^8\right), \tag{3.3.4}$$

$$\chi(z) = \chi_U - \frac{1}{3}\log(z) - \frac{1}{24}\phi_J^2 z^4 + \left(\chi_5 - \frac{2}{25}\phi_J \phi_V\right) z^5 - \frac{1}{24}\phi_V^2 z^6 + \mathcal{O}\left(z^8\right), \tag{3.3.5}$$

$$A(z) = A_U - \frac{4}{3}\log(z) - \frac{1}{6}\phi_J^2 z^4 + \left(\frac{1}{4}\chi_5 - \frac{8}{25}\phi_J \phi_V\right) z^5 - \frac{1}{6}\phi_V^2 z^6 + \mathcal{O}\left(z^8\right). \tag{3.3.6}$$

3.3.2 Supersymmetric solutions

The fact that the scalar potential, $\mathcal{V}_6$, is obtained from a superpotential $\mathcal{W}_6$, enables us to find a class of six-dimensional DW solutions by solving the first-order equations

$$\partial_\rho \mathcal{A} = -\frac{1}{2}\mathcal{W}_6 = 1 + \frac{\Delta}{4}\phi^2\,, \tag{3.3.7}$$

$$\partial_\rho \phi = \frac{\partial \mathcal{W}_6}{\partial \phi} = -\Delta\phi\,. \tag{3.3.8}$$

In this solutions $A(\rho) = 4\chi(\rho) = \frac{4}{3}\mathcal{A}(\rho)$ and we call them supersymmetric solutions:

$$\phi(\rho) = \phi_c\, e^{-\Delta\rho} = \phi_c\, z^{\Delta}\,, \tag{3.3.9}$$

$$\mathcal{A}(\rho) = \rho - \frac{1}{8}\phi_c^2\, e^{-2\Delta\rho} = -\log(z) - \frac{1}{8}\phi_c^2\, z^{2\Delta}\,. \tag{3.3.10}$$

Alongside ϕ_c, another additive integration constant has been absorbed in $\mathcal{A}$. For $\phi_c = 0$ one recovers the AdS_6 background.

3.3.3 Confining solutions

In this section, we describe the properties of the confining solutions. For this case, the circle parametrised by η coordinate shrinks to zero radius at a finite point, ρ_o, of the radial direction, ρ. Hence, the range of the ρ coordinate is bounded as $\rho_o < \rho_1 \le \rho < \rho_2 \to +\infty$. Since there is no conical singularity and the metric in 6D has finite curvature invariants, the background is regular and smooth all along the range of ρ. Near the end of space, by expanding the solution for small $(\rho - \rho_o)$, one finds

$$\phi(\rho) = \phi_I - \frac{1}{16}\Delta\phi_I\left(20 + \Delta\left(5\phi_I^2 - 4\right)\right)(\rho-\rho_o)^2 + \mathcal{O}\left((\rho-\rho_o)^4\right)\,, \tag{3.3.11}$$

$$\chi(\rho) = \chi_I + \frac{1}{3}\log(\rho-\rho_o) + \frac{1}{288}\left(-80 + 8\left(\Delta-5\right)\Delta\phi_I^2 - 5\Delta^2\phi_I^4\right)(\rho-\rho_o)^2 + O\left((\rho-\rho_o)^4\right)\,, \tag{3.3.12}$$

$$A(\rho) = A_I + \frac{1}{3}\log(\rho-\rho_o) + \frac{7}{576}\left(80 + \Delta\phi_I^2\left(40 + \Delta\left(5\phi_I^2 - 8\right)\right)\right)(\rho-\rho_o)^2 + \mathcal{O}\left((\rho-\rho_o)^4\right)\,. \tag{3.3.13}$$

Here ρ_o, ϕ_I, χ_I, and A_I are constants of integration.

To check the regularity of the metric near the end of space, we calculate the induced metric on the sub-manifold spanned by (ρ, η),

$$\mathrm{d}s_2^2 = \mathrm{d}\rho^2 + e^{6\chi}\mathrm{d}\eta^2 \simeq \mathrm{d}\rho^2 + e^{6\chi_I}(\rho-\rho_o)^2\mathrm{d}\eta^2 + \cdots\,, \tag{3.3.14}$$

To evade the conical singularity, we fix $\chi_I = 0$. With this choice, the metric is of the two-dimensional real plane, in case η has the periodicity 2π.

Different curvature invariants in six dimensions can be defined. We calculate the Ricci scalar $\mathcal{R} \equiv \mathcal{R}_6$, the squared Ricci tensor $\mathcal{R}_2^2 \equiv \mathcal{R}_{6\hat{M}\hat{N}}\mathcal{R}_6{}^{\hat{M}\hat{N}}$, and the squared Riemann tensor $\mathcal{R}_4^2 \equiv \mathcal{R}_{6\hat{M}\hat{N}\hat{R}\hat{S}}\mathcal{R}_6{}^{\hat{M}\hat{N}\hat{R}\hat{S}}$. They can be simplified and re-written in terms of a quantity defined here as

$$d \equiv A - 4\chi\,. \tag{3.3.15}$$

This non-trivial quantity vanishes for the DW solutions. By using the equations of motion, one has [131]:

$$\mathcal{R} = 6\mathcal{V}_6 + 2\big(\partial_\rho\phi\big)^2\,, \tag{3.3.16}$$

$$\mathcal{R}_2^2 = 6\mathcal{V}_6^2 + 4\mathcal{V}_6\big(\partial_\rho\phi\big)^2 + 4\big(\partial_\rho\phi\big)^4\,, \tag{3.3.17}$$

$$\mathcal{R}_4^2 = \frac{1}{250}\Bigg(32(\partial_\rho d)^2\Big(4\partial_\rho d\sqrt{36(\partial_\rho d)^2 + 15\sqrt{5}\sqrt{6\mathcal{R}_2^2 - \mathcal{R}^2} - 30\mathcal{R}} + 24(\partial_\rho d)^2 + 5\sqrt{5}\sqrt{6\mathcal{R}_2^2 - \mathcal{R}^2} - 10\mathcal{R}\Big) - 25\left(\mathcal{R}^2 - 10\mathcal{R}_2^2\right)\Bigg)\,. \tag{3.3.18}$$

By making use of the IR expansions, it can be checked that all of these quantities are finite in the limit of $\rho \to \rho_o$,

$$\lim_{\rho\to\rho_o}\mathcal{R} = -30 - 3\Delta(5-\Delta){\phi_I}^2 - \frac{15\Delta^2}{8}{\phi_I}^4\,, \tag{3.3.19}$$

$$\lim_{\rho\to\rho_o}\mathcal{R}_2^2 = \frac{1}{6}\left(\lim_{\rho\to\rho_o}\mathcal{R}\right)^2\,, \tag{3.3.20}$$

$$\lim_{\rho\to\rho_o}\mathcal{R}_4^2 = \frac{1}{3}\left(\lim_{\rho\to\rho_o}\mathcal{R}\right)^2\,. \tag{3.3.21}$$

However, for $\Delta \neq 0$, and for $\phi_I \to \infty$ all of the invariants diverge. The divergences suggest a constraint on the allowable values for ϕ_I, namely, that ϕ_I should not be taken arbitrarily large.

3.3.4 Singular domain-wall solutions

The final set of solutions considered here is the singular DW solutions. They satisfy the relation $A = 4\chi = \frac{4}{3}\mathcal{A}$ and they have Δ dependent IR expansions. One has the following,

$$\begin{aligned}
\phi(\rho) \;=\; & \phi_I - \sqrt{\frac{2}{5}}\log(\rho-\rho_o) \\
& + \frac{(\rho-\rho_o)^2}{25920}\Big(2\sqrt{10}(6\Delta\log(\rho-\rho_o)(3\log(\rho-\rho_o)(\Delta\log(\rho-\rho_o)(3\log(\rho-\rho_o)+2) \\
& -23\Delta+60)+37\Delta+60)-\Delta(47\Delta+660)+5400) \\
& +15\Delta\phi_I\Big(-60\phi_I^2(6\Delta\log(\rho-\rho_o)+\Delta)+6\sqrt{10}\phi_I(6\Delta\log(\rho-\rho_o)(3\log(\rho-\rho_o)+1) \\
& -23\Delta+60)-4(6\log(\rho-\rho_o)(3\Delta\log(\rho-\rho_o)(2\log(\rho-\rho_o)+1) \\
& -23\Delta+60)+37\Delta+60)+45\sqrt{10}\Delta\phi_I^3\Big)\Big) \;+\; \mathcal{O}((\rho-\rho_o)^4)\,, \qquad (3.3.22)\\
\mathcal{A}(\rho) \;=\; & \frac{1}{5}\log(\rho-\rho_o) \\
& + \frac{(\rho-\rho_o)^2}{12960}\,(2(6\Delta\log(\rho-\rho_o)(3\log(\rho-\rho_o)(\Delta\log(\rho-\rho_o)(3\log(\rho-\rho_o)-10) \\
& +7\Delta+60)-5(\Delta+60))+(1140-17\Delta)\Delta+5400) \\
& +3\Delta\phi_I\Big(2\sqrt{10}(5(\Delta+60)-6\log(\rho-\rho_o)(3\Delta\log(\rho-\rho_o)(2\log(\rho-\rho_o)-5)+7\Delta+60)) \\
& +15\phi_I\,(2(6\Delta\log(\rho-\rho_o)(3\log(\rho-\rho_o)-5)+7\Delta+60) \\
& +\Delta\phi_I\Big(2\sqrt{10}(5-6\log(\rho-\rho_o))+15\phi_I\Big)\Big)\Big) \;+\; \mathcal{O}((\rho-\rho_o)^4)\,. \qquad (3.3.23)
\end{aligned}$$

Here, ϕ_I is an integration constant, and an additive integration constant is omitted in $\mathcal{A}$ without loss of generality.

We note that the system of equations has a symmetry under the transformation $\phi \to -\phi$. Consequently, a new branch of solutions can be derived simply by changing the sign of ϕ.

These solutions are characterised by singular behaviour at the end of space. Their interpretation within the gravity theory remains unclear, and they lack a straightforward field theory counterpart. In particular, we refrain from computing the spectrum of their fluctuations, which would otherwise correspond to bound states in a putative dual theory, as such an analysis may not yield meaningful information about observable quantities.

However, we will compute their free energy later. This computation reveals that for certain parameter configurations, solutions from this class are energetically preferred over the confining solutions. This finding anticipates a more detailed discussion later, where we will need to restrict our physical interpretations of the confining solutions to a subset of the parameter space.

3.4 Mass spectrum of fluctuations

In this section, to study the fluctuations over the background, we focus on confining solutions. For a given background solution in the gravity theory, we linearise the equations of motion for small fluctuations around it. According to the gauge/gravity duality dictionary, as discussed in Section 2.1.4, the mass spectra resulting from the fluctuations of the bosonic fields correspond to composite particles with spin-0, 1, and 2 in the dual confining field theory.

To carry out these calculations, we employ the gauge-invariant formalism that has been developed and refined in several works, including Refs. [119–123]. This formalism is essential for accurately capturing the spectrum of fluctuations and interpreting them in terms of physical particles and their properties within the context of the dual field theory. By focusing on confining solutions and utilising this formalism, we aim to get insights into the nature of the mesonic particles that would exist in the corresponding four-dimensional field theory.

The scalar fluctuations, $\mathfrak{a}^a = \mathfrak{a}^a(q,\rho)$, are the starting point where q^μ is the four-momentum. The equations of motion for these fluctuations are (see also Appendix A.2):

$$\left[\partial_\rho^2 + (4\partial_\rho A - \partial_\rho\chi)\partial_\rho - e^{2\chi-2A}q^2\right]\mathfrak{a}^a - e^{2\chi}\mathcal{X}^a{}_c\mathfrak{a}^c = 0\,. \tag{3.4.1}$$

As a result of having a simple sigma-model metric $G_{ab} = \mathrm{diag}(1,6)$, in the $\Phi^a = \{\phi,\chi\}$ basis, the sigma-model connection is zero. This simplifies the equations of motion drastically, leading to the expression for $\mathcal{X}^a{}_c$,

$$\begin{aligned}\mathcal{X}^a{}_c \equiv{}& \frac{\partial}{\partial\Phi^c}\left(G^{ab}\frac{\partial(e^{-2\chi}\mathcal{V}_6)}{\partial\Phi^b}\right) + \frac{4}{3\partial_\rho A}\left[\partial_\rho\Phi^a\frac{\partial(e^{-2\chi}\mathcal{V}_6)}{\partial\Phi^c} + G^{ab}\frac{\partial(e^{-2\chi}\mathcal{V}_6)}{\partial\Phi^b}\partial_\rho\Phi^d G_{dc}\right]\\ &+\frac{16(e^{-2\chi}\mathcal{V}_6)}{9(\partial_\rho A)^2}\partial_\rho\Phi^a\partial_\rho\Phi^b G_{bc}\,.\end{aligned} \tag{3.4.2}$$

The functions A, $\Phi^a = \{\phi,\chi\}$, and $\mathcal{V}_6$ appearing in this equation are taking their background value.

By implementing the following boundary conditions, a discrete spectrum is obtainable:[1]

$$e^{-2\chi}\partial_\rho\Phi^c\partial_\rho\Phi^d G_{db}\partial_\rho\mathfrak{a}^b\Big|_{\rho_i} = \left[\frac{3\partial_\rho A}{2}e^{-2A}q^2\delta^c{}_b + \partial_\rho\Phi^c\left(\frac{4\mathcal{V}_6}{3\partial_\rho A}\partial_\rho\Phi^d G_{db} + \frac{\partial\mathcal{V}_6}{\partial\Phi^b}\right)\right]\mathfrak{a}^b\Big|_{\rho_i}\,, \tag{3.4.3}$$

One can satisfy the boundary conditions at the two boundaries simultaneously for just a discrete set of choices for q^2. Thus, the physical composite states in the dual field theory will have a mass with $M^2 = -q^2$.

[1] There is an equivalent form for the boundary conditions of the scalars derived in Eq. (14) of Ref. [109] and is more convenient for numerical methods.

Now we move to the transverse and traceless tensor fluctuations, $\mathfrak{e}^{\mu}{}_{\nu}$, and the gauge-invariant transverse polarisations of vector, χ_M, which obey the following equations of motion [118]:

$$0 = \left[\partial_\rho^2 + (4\partial_\rho A - \partial_\rho \chi)\partial_\rho - e^{2\chi-2A}q^2\right]\mathfrak{e}^{\mu}{}_{\nu}\,, \tag{3.4.4}$$

$$0 = P^{\mu\nu}\left[\partial_\rho^2 + (2\partial_\rho A + 7\partial_\rho \chi)\partial_\rho - e^{2\chi-2A}q^2\right]\chi_\nu\,. \tag{3.4.5}$$

Here the projector is defined as $P^{\mu\nu} \equiv \eta^{\mu\nu} - \frac{q^\mu q^\nu}{q^2}$. Neumann boundary conditions are imposed on the fluctuations of interest in the boundaries. This condition will enable us to compute the spectrum of masses with $M > 0$ for the mesonic bound states in the dual field theory.

The spectrum is first calculated for finite values of ρ_1 and ρ_2, and then extrapolated towards the limits $\rho_1 \to \rho_o$ and $\rho_2 \to +\infty$. More details for this method are provided in works such as [117, 118, 123]. Another numerical strategy is also implemented, helping us by improving convergence, by using UV and IR expansions of the fluctuations. In this method, one decomposes fluctuations into subdominant and dominant modes. Utilising boundary conditions to suppress the dominant modes, one matches the solutions to their asymptotic expansions evaluated at finite positions of the boundary at $\rho_{1,2}$.

This method requires higher order expansions in z, in the UV boundary, and $\rho - \rho_o$, in the IR. Nevertheless, it overcomes the necessity to solve the nonlinear equations for the background in the regions at large or small $\rho - \rho_o$ that are numerically challenging. This numerical strategy adopted here has proven successful in studies like the Klebanov-Strassler system [121] and its baryonic branch [110, 111]. Details of IR and an example of UV expansions for fluctuations are provided in Appendix E.

As detailed in Ref. [124] and further discussed in Appendix B, the probe approximation neglects the coupling of states to the trace of the energy-momentum tensor. This results in the exclusion of the mixing effect among the dilaton field with other physical states. However, this approximation fails to accurately predict the masses of states that strongly interact with the dilaton field. When such states have low masses, they can be interpreted as approximate dilatons. Thus, this approximation serves as a diagnostic tool for identifying approximate dilatons within the spectrum. In this chapter, we specifically analyse the mass spectrum in the probe approximation for the case where $\Delta = 5/2$. This choice turns out to be particularly interesting within the context of our study.

We compute the mass spectra of fluctuations numerically, and the results are reported in Figs. 3.2, 3.3, 3.4, and 3.5, for some choices of Δ. For each Δ, states with spin-0, spin-1 and spin-2 are presented. The spectra are normalised to the mass of the lightest tensor state. For

each value of Δ, it is crucial to assess the convergence of the mass spectrum with respect to the parameters ρ_1 and ρ_2 independently. This evaluation ensures that the results are reliable and accurate, meeting a numerical accuracy goal.

In our numerical computations, we chose values of ρ_1 and ρ_2, where the dependence on these cutoffs can be safely neglected within the desired accuracy threshold of 0.5%. Additionally, in our plots, we include the position of critical value $\phi_I(c)$ obtained from the study of the free energy, which will be explained in the subsequent section.

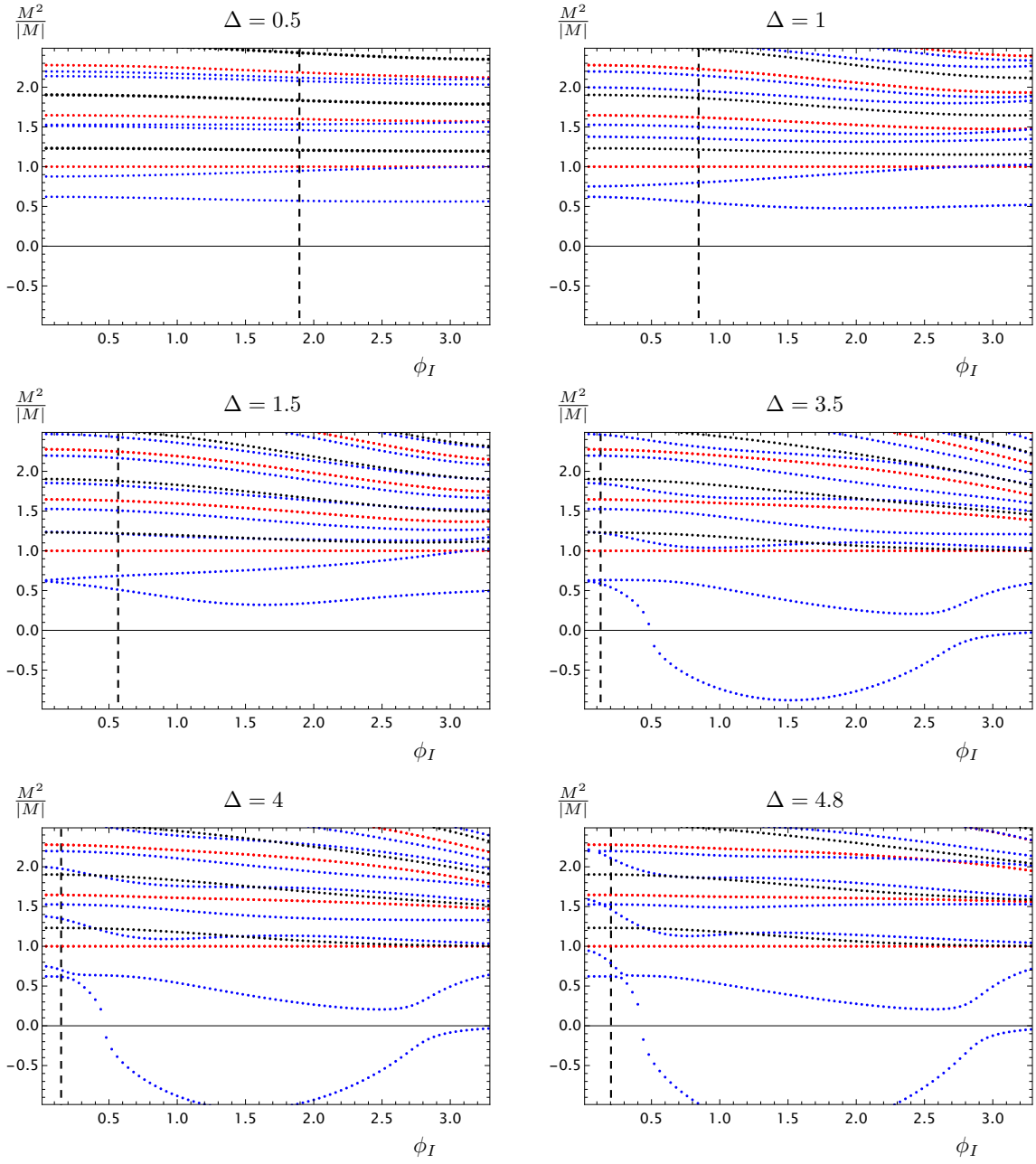

Figure 3.2. Mass spectrum of fluctuations on the background solution as a function of the IR parameter ϕ_I, calculated for confining backgrounds, with different Δ. For each Δ, states with spin-0, spin-1 and spin-2 are shown in blue, black and red, respectively. The IR and UV cutoffs are chosen respectively as $\rho_1 - \rho_o = 10^{-9}$ and $\rho_2 - \rho_o = 5$. The masses are normalised to the mass of the lightest tensor (spin-2) state. The critical value $\phi_I(c)$ is denoted by vertical dashed lines.

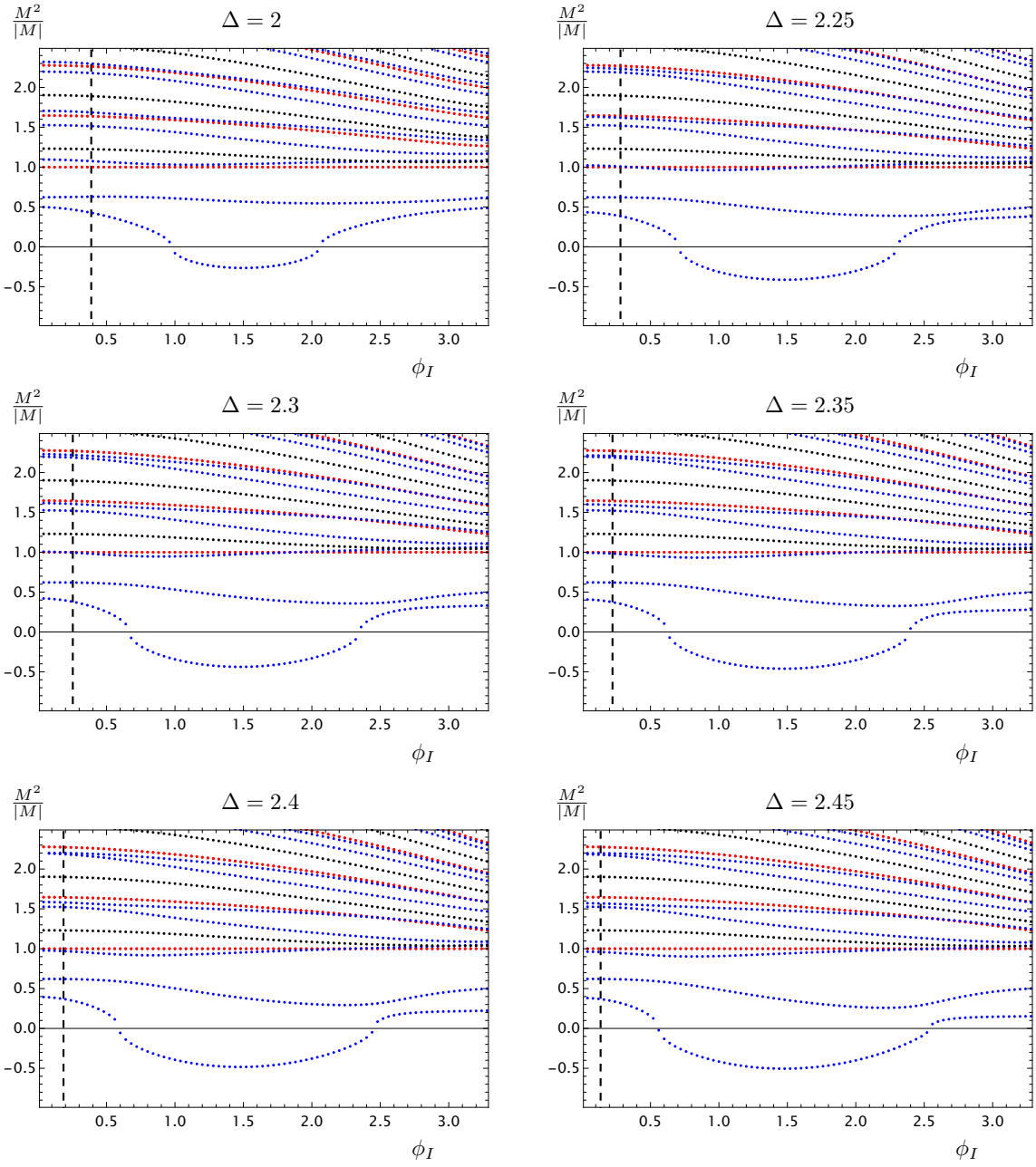

Figure 3.3. Mass spectrum of fluctuations on the background solution as a function of the IR parameter ϕ_I, calculated for confining backgrounds, with different Δ. For each Δ, states with spin-0, spin-1 and spin-2 are shown in blue, black and red, respectively. The IR and UV cutoffs are chosen respectively as $\rho_1 - \rho_o = 10^{-9}$ and $\rho_2 - \rho_o = 5$. The masses are normalised to the mass of the lightest tensor (spin-2) state. The critical value $\phi_I(c)$ is denoted by vertical dashed lines.

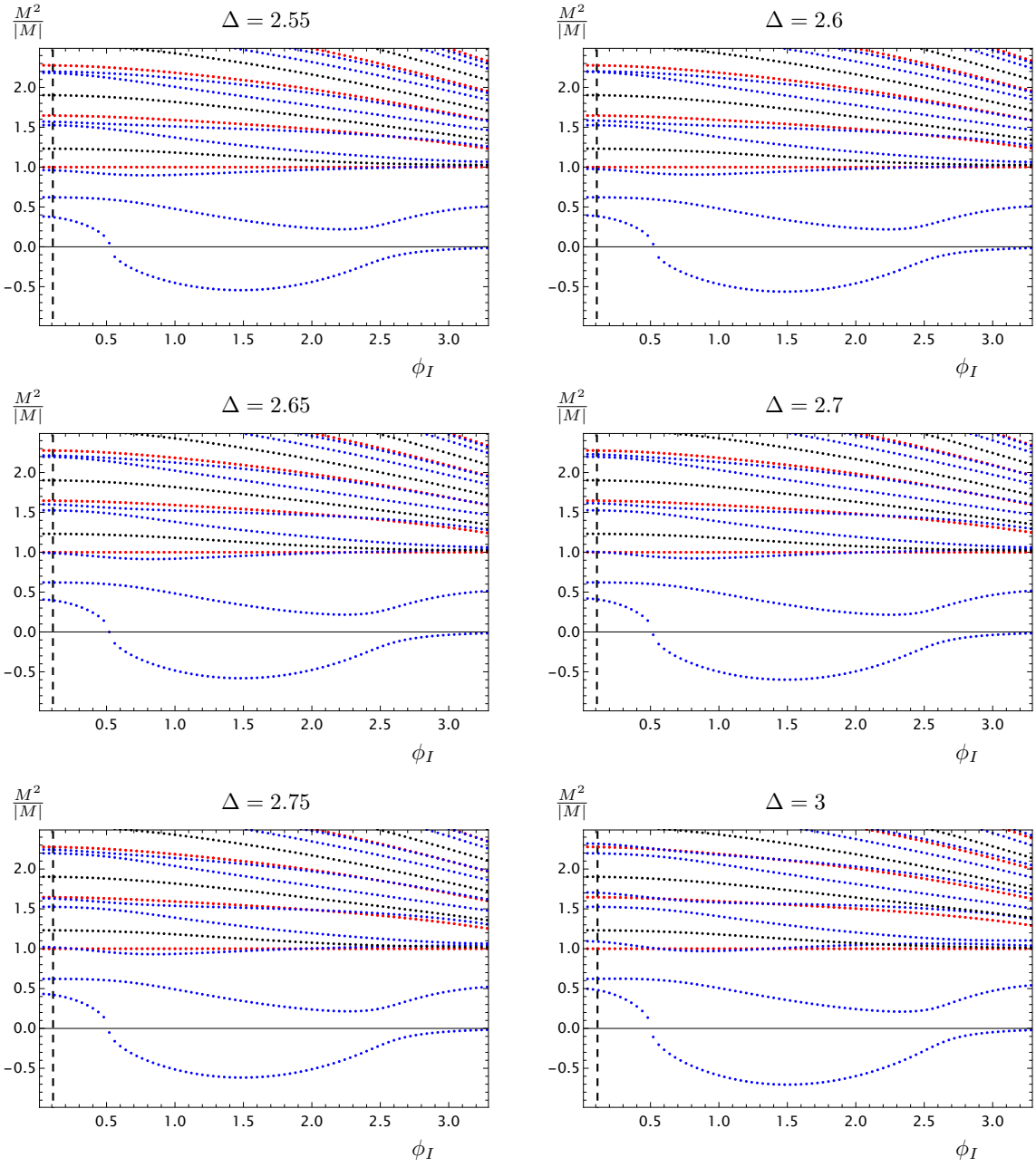

Figure 3.4. Mass spectrum of fluctuations on the background solution as a function of the IR parameter ϕ_I, calculated for confining backgrounds, with different Δ. For each Δ, states with spin-0, spin-1 and spin-2 are shown in blue, black and red, respectively. The IR and UV cutoffs are chosen respectively as $\rho_1 - \rho_o = 10^{-9}$ and $\rho_2 - \rho_o = 5$. The masses are normalised to the mass of the lightest tensor (spin-2) state. The critical value $\phi_I(c)$ is denoted by vertical dashed lines.

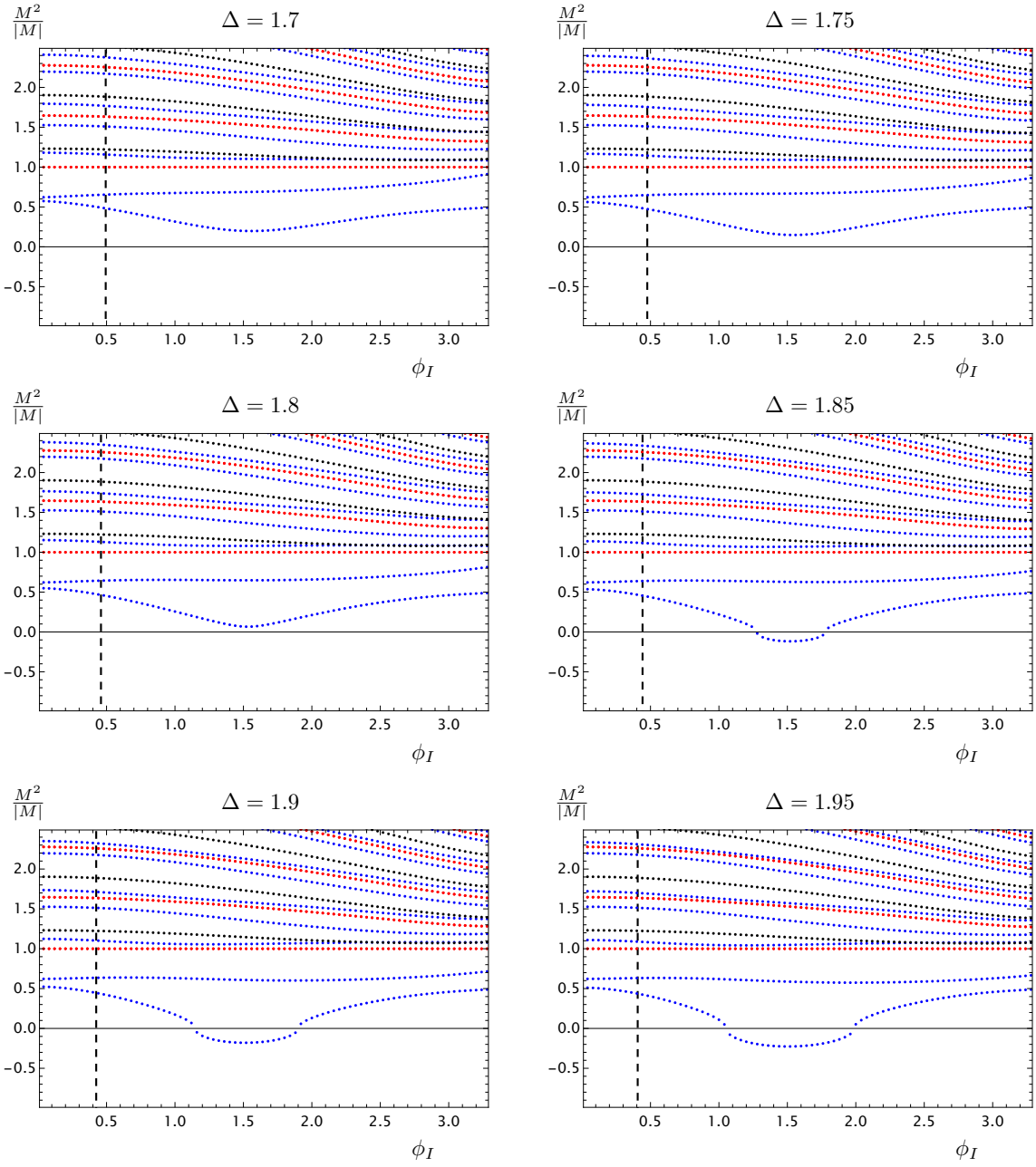

Figure 3.5. Mass spectrum of fluctuations on the background solution as a function of the IR parameter ϕ_I, calculated for confining backgrounds, with different Δ. For each Δ, states with spin-0, spin-1 and spin-2 are shown in blue, black and red, respectively. The IR and UV cutoffs are chosen respectively as $\rho_1 - \rho_o = 10^{-9}$ and $\rho_2 - \rho_o = 5$. The masses are normalised to the mass of the lightest tensor (spin-2) state. The critical value $\phi_I(c)$ is denoted by vertical dashed lines.

3.5 Free energy

The free energy density in our backgrounds can be calculated as:

$$\mathcal{F} = -\lim_{\rho_2 \to +\infty} e^{4A-\chi}\Big(\frac{3}{2}\partial_\rho A + \mathcal{W}_2\Big)\Big|_{\rho_2}, \tag{3.5.1}$$

where $\mathcal{W}_2 = \mathcal{W}_6$ for $\Delta < 5/2$, and $\mathcal{W}_2 = \overline{\mathcal{W}}_6$ for $\Delta > 5/2$. This expression can be obtained by using the results in Ref. [131]. The contributions from the bulk action after evaluation of the equations of motion, and the contribution from the boundary terms are included in the calculation. It is also essential to include the suitable UV-localised counter-term, $\mathcal{W}_2$, to remove the UV divergences and is required in the procedure of holographic renormalisation [43, 44, 150]. In order to evaluate a term defined at the IR boundary, ρ_1, the conservation law of Eq. (3.2.17) is used and enables us to evaluate the expression at ρ_2 (the UV boundary) only.

For each choice of the parameter Δ, $\mathcal{F}$ is expressed in terms of the coefficients that appear in the UV expansion of the background. These coefficients are extracted by matching the expansions to numerical solutions. It is essential to ensure that the results converge as $\rho_2 \to +\infty$.

Empirically, we find that for $\Delta < 5/2$, the free energy density is given by:

$$\mathcal{F} = -\frac{1}{40}e^{4A_U-\chi_U}\left(16\Delta\left(\frac{5}{2}-\Delta\right)\phi_J\phi_V - 75\chi_5\right), \tag{3.5.2}$$

whereas for $\Delta > 5/2$, retaining a sufficient number of terms in $\overline{\mathcal{W}}_6$ to ensure the absorption of all divergences, the free energy density is given by:

$$\mathcal{F} = -\frac{1}{40}e^{4A_U-\chi_U}\left(16(\Delta-5)\left(\frac{5}{2}-\Delta\right)\phi_J\phi_V - 75\chi_5\right). \tag{3.5.3}$$

We have explicitly verified that this expression accurately describes the free energy density for all values of Δ examined in this work. For the special case of $\Delta = 5/2$, we have

$$\mathcal{W}_2 = -2 - \frac{5}{4}\phi^2\left(1 + \frac{2}{5\log(k\,z)}\right), \tag{3.5.4}$$

and the free energy density is given by

$$\mathcal{F} = \frac{1}{40}e^{4A_U-\chi_U}\Big(20\phi_J\phi_V - 4\phi_J^2 + 75\chi_5 - 20\phi_J^2\log(k)\Big). \tag{3.5.5}$$

A residual scheme dependence is introduced by the logarithmic term, which is encapsulated in the parameter k. In our subsequent analysis, we adopt $k = \Lambda$.

Building on the framework established in Refs. [131–133], we find it advantageous to define a scale Λ using the approach outlined in [151]:

$$\Lambda^{-1} \equiv \int_{\rho_o}^{\infty} \mathrm{d}\rho\, e^{\chi(\rho)-A(\rho)}\,, \tag{3.5.6}$$

where ρ_o is the end of space. While other choices for k are possible, selecting $k = \Lambda$ aligns with previous studies. This choice is particularly useful because it enables direct comparisons between the confining and DW classes of solutions.

Consequently, we proceed by expressing all relevant quantities in units of this scale Λ. Specifically, we define the rescaled free energy density

$$\hat{\mathcal{F}} \equiv \frac{\mathcal{F}}{\Lambda^5}\,, \tag{3.5.7}$$

and the rescaled source takes the form

$$\hat{\phi}_J \equiv \frac{\phi_J}{\Lambda^{\Delta_J}}\,. \tag{3.5.8}$$

Here, the dimension, Δ_J, represents the scaling dimension of the source related to the dual operator with dimension $\Delta_V \equiv 5 - \Delta_J$. Therefore, we also define the rescaled condensates as

$$\hat{\phi}_V \equiv \frac{\phi_V}{\Lambda^{\Delta_V}}\,, \tag{3.5.9}$$

$$\hat{\chi}_5 \equiv \frac{\chi_5}{\Lambda^5}\,. \tag{3.5.10}$$

For a background solution, the computation of the free energy proceeds as follows.

Initially, the background solution is matched to its UV expansions. This process determines coefficients such as A_U, χ_U, ϕ_J, ϕ_V, and χ_5. To impose constraints $A_U = 0 = \chi_U$, both the radial coordinate, ρ, and the definition of the function $A(\rho)$, are additively shifted. This adjustment ensures that the background solution meets these specific conditions. After applying the shifts, all of the coefficients are recalculated to reflect the new configuration of the background solution and implemented in the free energy expression.

Then, the scale Λ is computed for each background solution after the shifts in ρ and $A(\rho)$. Finally, the quantities of interest, including the rescaled free energy density and other relevant parameters, are plotted. This allows for comparative analysis between confining and singular DW solutions, and these are shown together for each value of Δ in the provided plots. Examples of such plots are depicted in Figures 3.6, 3.7, 3.8, and 3.9.

By examining the figures, a consistent pattern emerges: For small values of the source,

$|\hat{\phi}_J|$, the confining solutions minimise the free energy, $\hat{\mathcal{F}}$, in all cases. In contrast, the singular domain-wall (DW) solutions are the solutions with the lowest $\hat{\mathcal{F}}$ for larger values of the source.

A critical value $|\hat{\phi}_J(c)|$ emerges, which corresponds to a critical point in the IR parameter $|\phi_I(c)|$, marking a first-order phase transition. For $|\phi_I| \leq |\phi_I(c)|$, the confining solutions are physically viable. However, for $|\phi_I| > |\phi_I(c)|$, the physical interpretation of the solutions becomes uncertain, leading us to discard these regions of the parameter space. It is noteworthy that we do not assert the physical realisation of the singular solutions themselves. Instead, we acknowledge the possibility that another branch of solutions not explored in this study could exist and dominate the long-distance dynamics.

Upon closer inspection of the figures, additional features become apparent. For $\Delta \geq 5/2$, above a certain threshold value $|\hat{\phi}_J(\text{max})| > |\hat{\phi}_J(c)|$, no singular and confining solutions exist. This observation aligns with our earlier understanding that for large $|\hat{\phi}_J| > |\hat{\phi}_J(c)|$, another branch of solutions must exist, potentially in a more complete theory. Therefore, this outcome is not unexpected and is consistent with similar findings in the analysis of top-down holographic models as reported in Refs. [131–133]. Interestingly, this feature is absent for $\Delta < 5/2$, where confining and singular solutions persist across all ranges of $|\hat{\phi}_J|$.

In thermodynamics, stability considerations often rely on concavity theorems applied to the free energy functional dependence on specific parameters of the theory. However, applying such arguments directly to our current context is challenging due to divergences and scheme dependencies present in holographic models (see also Ref. [152] for related discussions). Therefore, one should be cautious in interpreting stability solely based on thermodynamic analogies.

Nevertheless, upon comparing Figs. 3.6, 3.7, 3.8, and 3.9 with Figs. 3.2, 3.3, 3.4, and 3.5, several observations can be made:

- A tachyonic mode appears in the spectra of confining theories for values of $\Delta \gtrsim 1.8$, but this occurs only within a specific range of the parameter ϕ_I.
- The region of parameter space where the tachyon appears consistently lies beyond the phase transition point.
- There exists a parameter space region where the mass of the lightest scalar is significantly small, particularly near the point where it becomes tachyonic. Importantly, this phenomenon occurs exclusively beyond the phase transition, where confining solutions are probably metastable.

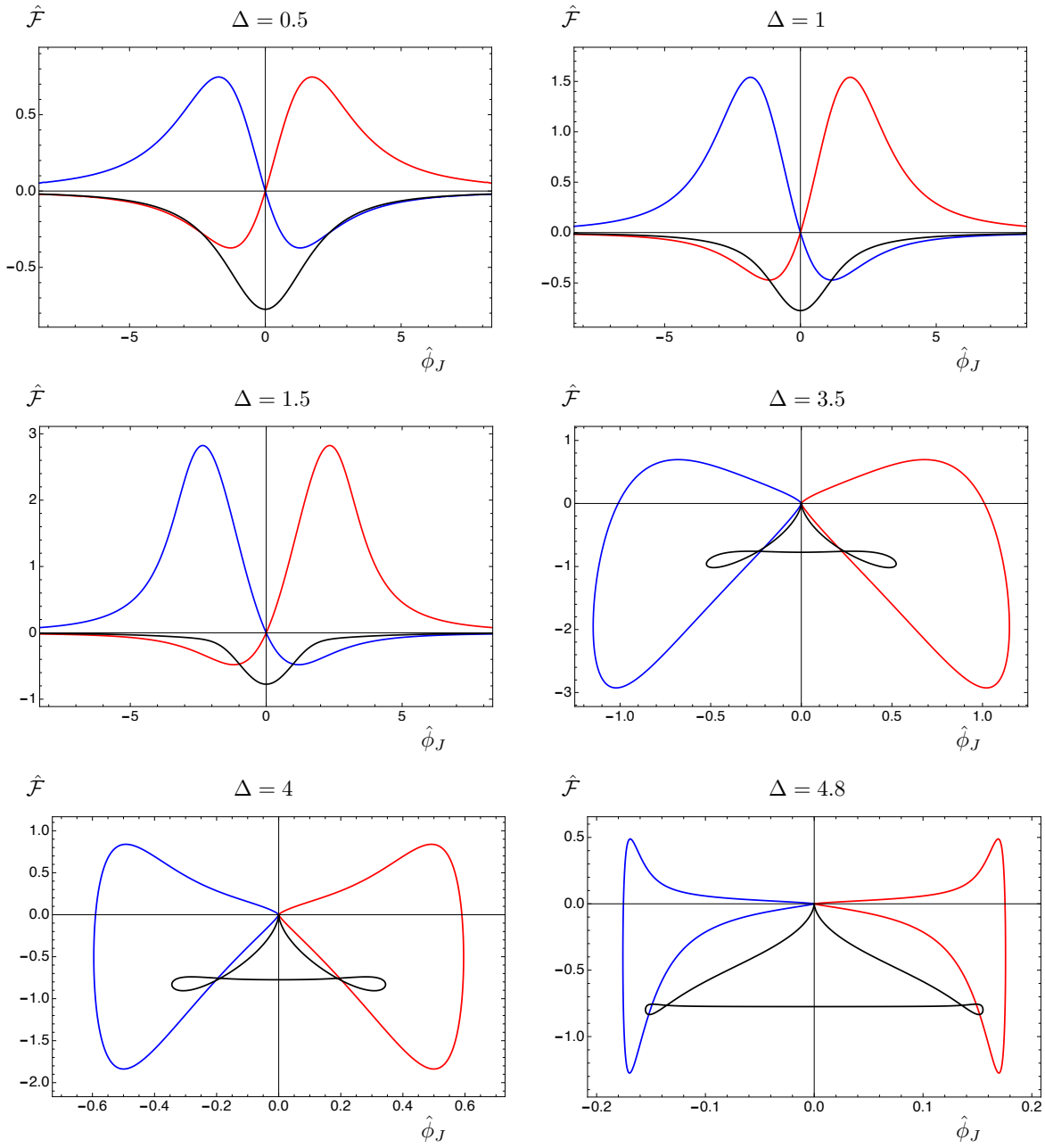

Figure 3.6. The free energy density $\hat{\mathcal{F}}$ for different choices of Δ as a function of the source parameter $\hat{\phi}_J$. Quantities are reported in units of the scale Λ. The plots feature confining solutions represented by the black curve, alongside singular domain-wall solutions plotted in red and blue.

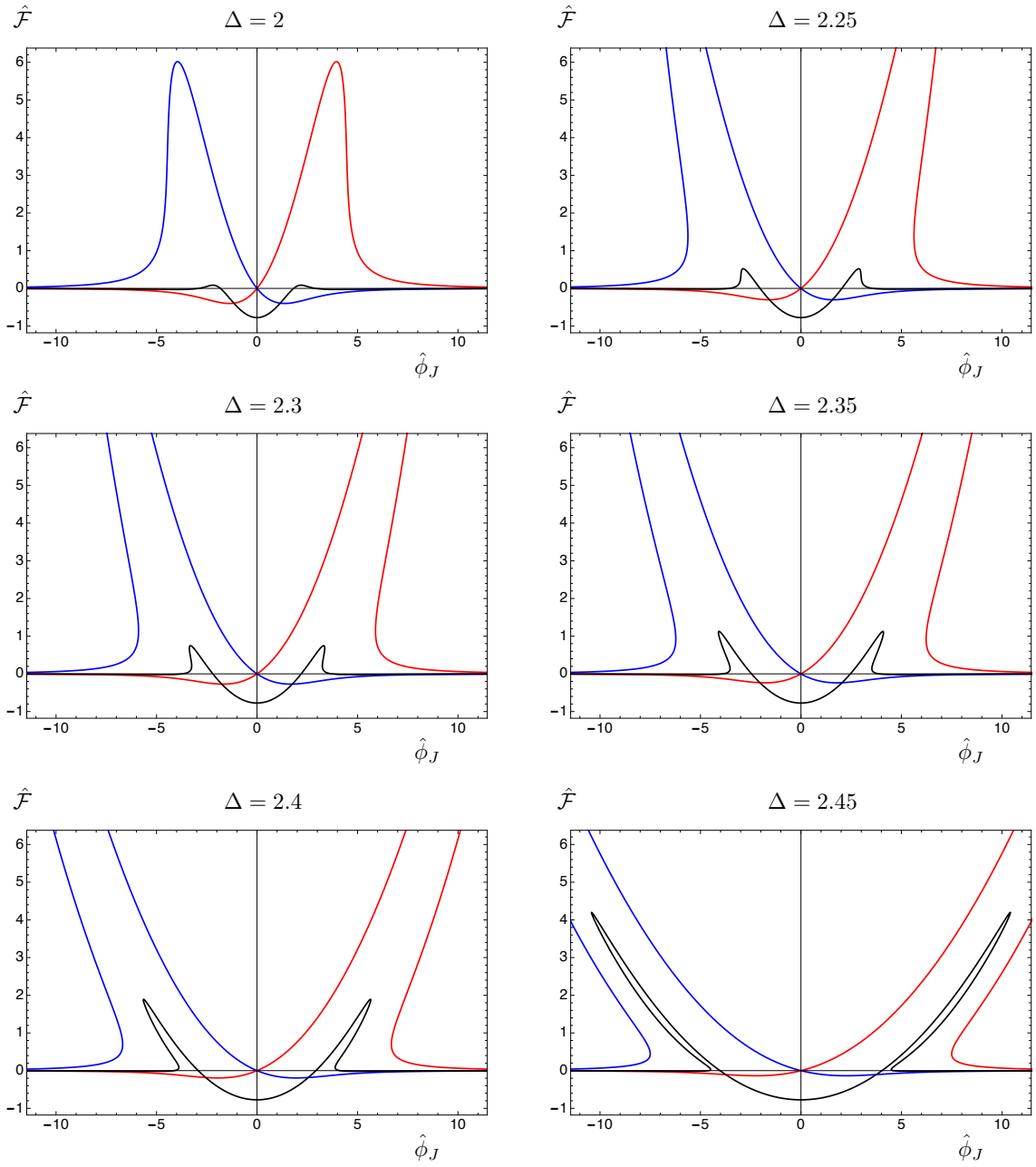

Figure 3.7. The free energy density $\hat{\mathcal{F}}$ for different choices of Δ as a function of the source parameter $\hat{\phi}_J$. Quantities are reported in units of the scale Λ. The plots feature confining solutions represented by the black curve, alongside singular domain-wall solutions plotted in red and blue.

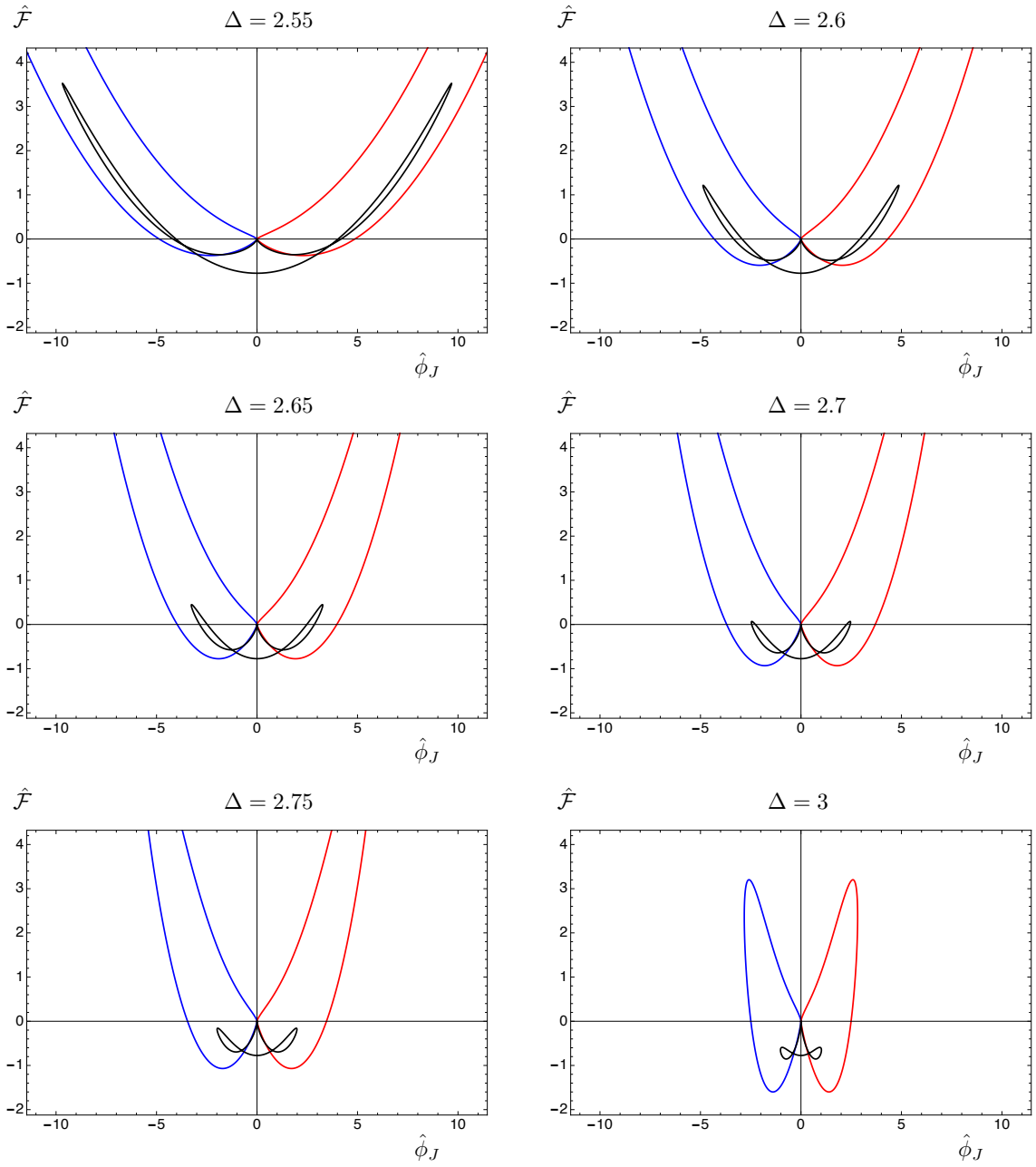

Figure 3.8. The free energy density $\hat{\mathcal{F}}$ for different choices of Δ as a function of the source parameter $\hat{\phi}_J$. Quantities are reported in units of the scale Λ. The plots feature confining solutions represented by the black curve, alongside singular domain-wall solutions plotted in red and blue.

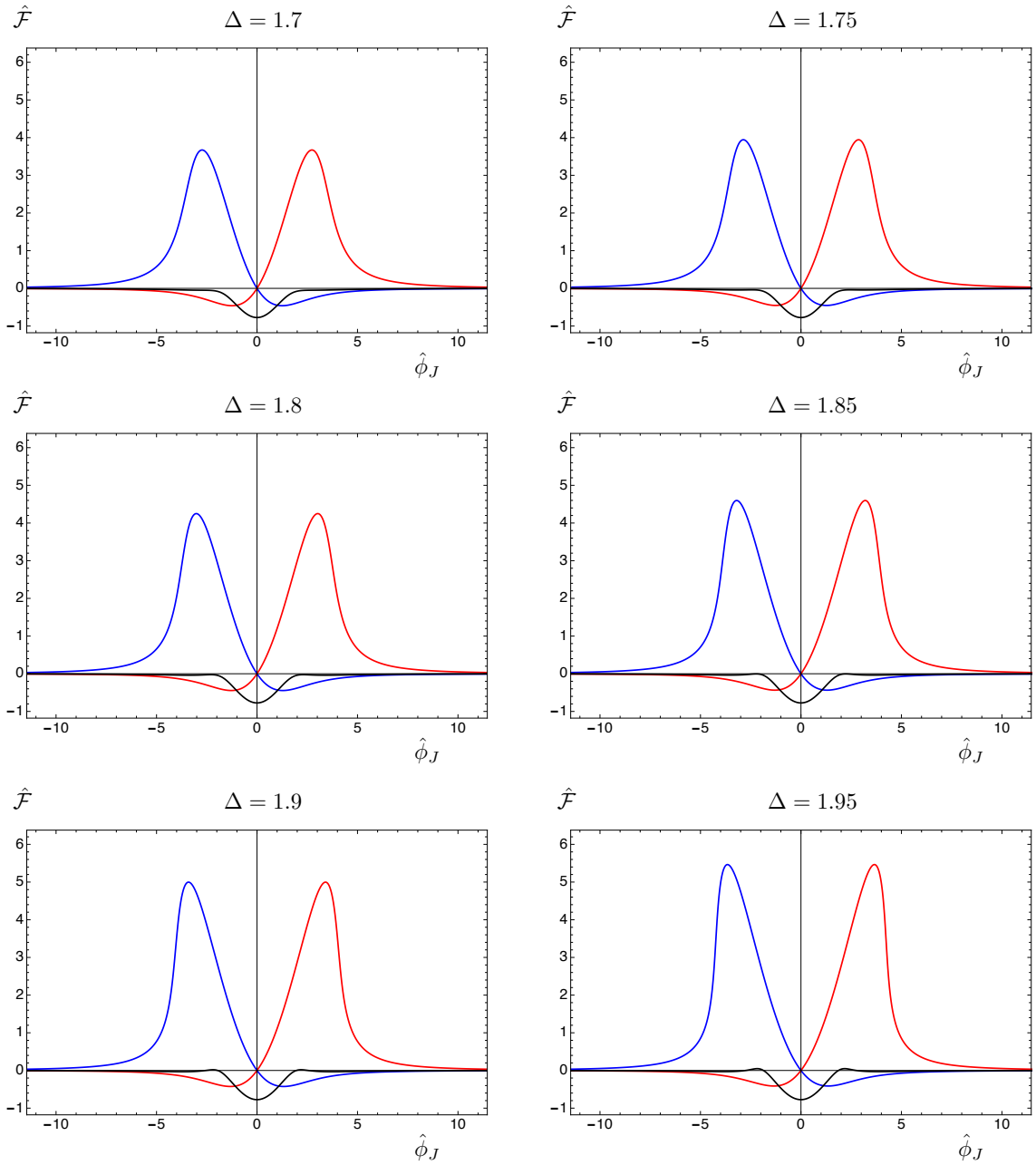

Figure 3.9. The free energy density $\hat{\mathcal{F}}$ for different choices of Δ as a function of the source parameter $\hat{\phi}_J$. Quantities are reported in units of the scale Λ. The plots feature confining solutions represented by the black curve, alongside singular domain-wall solutions plotted in red and blue.

3.6 Summary

Our numerical results are summarised in Table 3.1. For selected values of Δ, we present critical parameters such as $\hat{\phi}_J(c)$ (source) and $\phi_I(c)$ (IR asymptotic value of ϕ), along with the mass of the lightest scalar, $M(c)$, near the phase transition which is normalised by the mass of the lightest tensor. Additionally, we include values of the condensates in the dual field theory: $\hat{\phi}_V(c)$ and $\hat{\chi}_5(c)$. Fig. 3.10 displays the mass spectrum and free energy for the $\Delta = 5/2$ case, while Fig. 3.11 shows the mass spectrum computed at $\phi_I(c)$ for various Δ.

In summary, our model allows for a comprehensive study of the spectrum and free energy across different values of the parameter Δ, which corresponds either to the dimension of the coupling deforming the dual CFT or to the related condensate. We focus on non-singular backgrounds for each Δ, ensuring the dual field theory features a mass gap and discrete spectrum of bound states. These regular solutions in five-dimensional gravity lift smoothly to six dimensions with a finite radial endpoint $\rho > \rho_o$. Termed "confining" solutions for their behaviour, they undergo a first-order phase transition for $0 < \Delta < 5$, imposing an upper bound on the source $\hat{\phi}_J$ associated with the scalar field ϕ. At large deforming parameters, singular domain-wall solutions in six dimensions become energetically favoured over the regular ones despite their singularity. For $\Delta \gtrsim 1.8$, the mass spectrum exhibits a tachyon, yet this only occurs in an unphysical region far beyond the phase transition. In the physically meaningful parameter space, all fluctuations have positive $M^2 > 0$ and are not parametrically light.

Examining Figs. 3.2, 3.3, 3.4, and 3.5, we observe that the mass of the lightest scalar state decreases as the source, $\hat{\phi}_J$, approaches its critical value. Thus, the minimum mass $M(c)$ of the lightest scalar is found in close proximity to the transition point. For each Δ, we precisely compute the mass spectrum of bound states at the phase transition, detailed in Fig. 3.11.

An interesting finding is that the mass of the lightest state exhibits a minimum near $\Delta = 5/2$, where its mass is approximately one-third of the lightest tensor mass. The top panel of Fig. 3.10 illustrates the mass spectrum computed in the probe approximation, highlighting significant deviation from the actual mass of the lightest scalar for large $|\phi_I|$. In such cases, the lightest scalar particle exhibits overlap with the dilaton [124], albeit this occurs only within metastable or tachyonic regions of parameter space. Conversely, the probe approximation accurately reflects the mass of the lightest scalar in the physical region where $|\phi_I| \leq |\phi_I(c)|$.

Additionally, the summary plot reveals a discontinuity precisely at $\Delta = 5/2$ (as is visible in the inset of Fig. 3.11). The mass of the scalar at $\Delta = 5/2$ closely matches those obtained for $\Delta > 5/2$ and represents the absolute minimum of this mass across all studied values of Δ. However, the series of masses for $\Delta < 5/2$ converges to a slightly higher value. The reason behind this second feature remains unclear, underscoring the inherent numerical challenges in

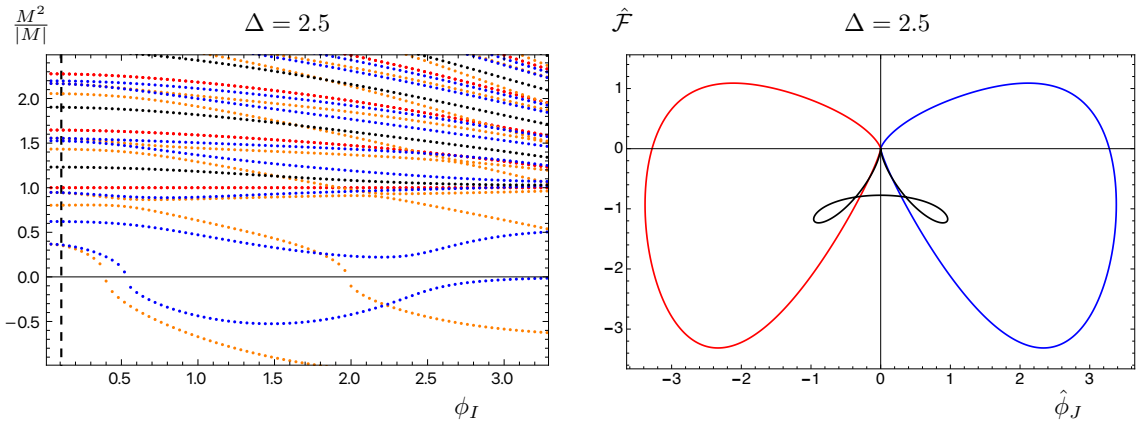

Figure 3.10. Mass spectrum of fluctuations on the background solution as a function of the IR parameter ϕ_I, calculated for confining background, with $\Delta = 5/2$. States with spin-0, spin-1 and spin-2 are shown in blue, black and red, respectively (left panel). The plot also includes the scalar states in the probe approximation shown in orange. The IR and UV cutoffs are chosen respectively as $\rho_1 - \rho_o = 10^{-9}$ and $\rho_2 - \rho_o = 5$. Every mass is normalised to the mass of the lightest tensor (spin-2) state. The free energy density $\hat{\mathcal{F}}$ for $\Delta = 2.5$ as a function of the source parameter $\hat{\phi}_J$ (right panel). Quantities are reported in units of the scale Λ. The plot features the confining solution represented by the black curve, alongside singular domain-wall solutions plotted in red and blue. The critical value $\phi_I(c)$ is denoted by vertical dashed lines in the left panel, derivable from the right panel.

our analysis. Nonetheless, this discontinuity is a minor effect compared to the more significant finding that the mass of the lightest scalar is minimised at $\Delta = 5/2$.

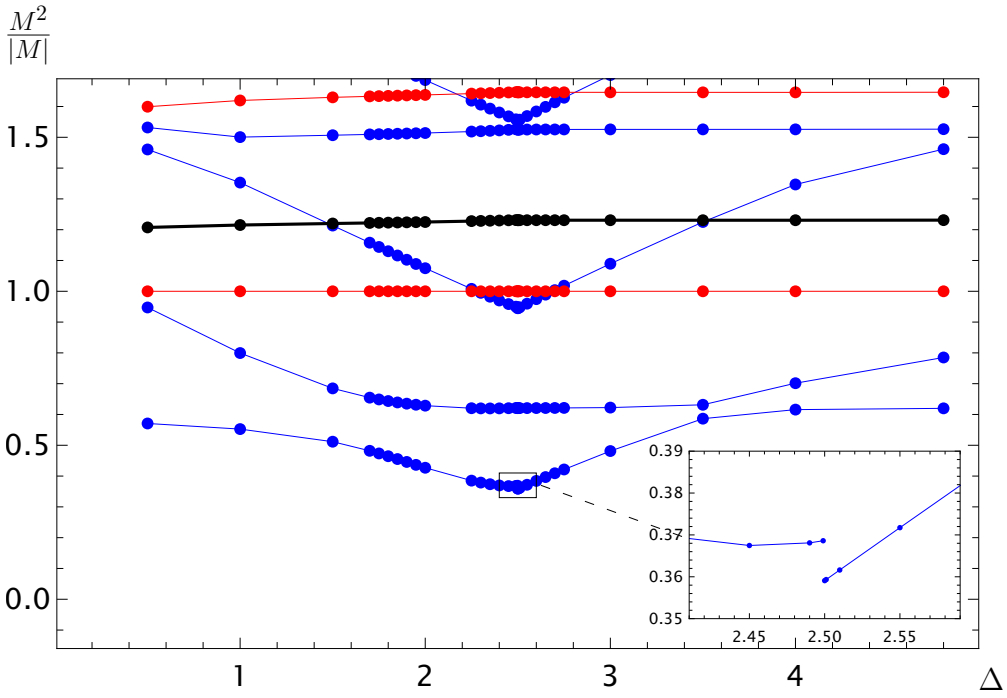

Figure 3.11. Mass spectrum of fluctuations on the confining background solution calculated at the critical $\phi_I(c)$ as a function of Δ, calculated for confining backgrounds. States with spin-0, spin-1 and spin-2 are shown in blue, black and red, respectively. The IR and UV cutoffs are chosen respectively as $\rho_1 - \rho_o = 10^{-9}$ and $\rho_2 - \rho_o = 5$. The masses are normalised to the mass of the lightest tensor (spin-2) state.

Table 3.1. Summary table. For each Δ, the critical value of the normalised source $\hat{\phi}_J(\mathrm{c})$ is reported at the phase transition point. The critical value for $\phi_I(\mathrm{c})$, and the mass $M(\mathrm{c})$ of the lightest scalar state at the transition (all normalised in terms of the mass of the lightest tensor state for the same set of parameters) is also stated. We present the value of the $\hat{\phi}_V(c)$ and $\hat{\chi}_5(c)$, in addition.

Δ	$\hat{\phi}_J(\mathrm{c})$	$\phi_I(\mathrm{c})$	$M(\mathrm{c})$	$\hat{\phi}_V(\mathrm{c})$	$\hat{\chi}_5(\mathrm{c})$
0.50	2.373	1.89	0.571	−0.063	−0.176
1.00	1.149	0.845	0.553	−0.208	−0.328
1.50	0.990	0.567	0.512	−0.369	−0.368
1.70	1.010	0.494	0.482	−0.471	−0.377
1.75	1.022	0.477	0.473	−0.504	−0.380
1.80	1.038	0.459	0.464	−0.539	−0.382
1.85	1.059	0.442	0.455	−0.579	−0.384
1.90	1.084	0.424	0.446	−0.625	−0.386
1.95	1.115	0.407	0.436	−0.677	−0.388
2.00	1.153	0.388	0.427	−0.736	−0.390
2.25	1.567	0.281	0.385	−1.276	−0.401
2.30	1.756	0.254	0.379	−1.496	−0.403
2.35	2.045	0.223	0.374	−1.821	−0.405
2.40	2.554	0.186	0.370	−2.371	−0.408
2.45	3.748	0.136	0.367	−3.618	−0.410
2.49	8.750	0.063	0.368	−8.691	−0.412
2.499	27.82	0.020	0.369	−27.80	−0.413
2.50	−0.295	0.107	0.359	0.439	−0.411
2.501	147.3	0.107	0.359	−147.2	−0.411
2.51	14.79	0.107	0.362	−14.69	−0.411
2.55	3.001	0.108	0.372	−2.899	−0.411
2.60	1.528	0.108	0.384	−1.426	−0.411
2.65	1.038	0.108	0.397	−0.935	−0.411
2.70	0.793	0.109	0.409	−0.689	−0.411
2.75	0.647	0.109	0.421	−0.542	−0.411
3.00	0.358	0.113	0.481	−0.246	−0.411
3.50	0.225	0.127	0.586	−0.068	−0.411
4.00	0.189	0.150	0.616	−0.102	−0.410
4.80	0.136	0.204	0.620	−0.179	−0.410

Chapter 4

Toward minimal composite Higgs models from regular geometries in bottom-up holography

In this chapter, we introduce a new bottom-up holographic model of the $SO(5)/SO(4)$ symmetry-breaking pattern essential for minimal CHMs. This model extends the simpler version in Chapter 3, previously studied in Ref. [5], employing similar background geometries. While the previous chapter primarily identifies parameter space regions crucial for understanding the physics of the dilaton following the programmatic approach outlined in Refs. [126–128, 131–133], our focus in this chapter and the subsequent one is to explore the potential of PNGB states obtained from the $SO(5)/SO(4)$ coset for constructing CHMs.

We will make use of holography to study our model. Earlier applications of similar holographic methods are the holographic description of confinement phenomena [32, 153–155], the glueball (composite) mass spectra calculations [109–111, 114–117, 119–123], masses of mesons [112, 113, 156–158], and the study of chiral symmetry breaking [159–161]. Embedding realistic models to achieve the low-energy theories usable for CHMs in string theory and supergravity is very challenging. A top-down study towards a CHMs within $SO(5)/SO(4)$ coset has been done in [162]. Other bottom-up approaches to holography for the minimal $SO(5)/SO(4)$ coset has been developed in Refs. [163–170]. Other CHMs have been investigated that are also suitable for lattice explorations [171–174].

Here, we first review the key aspects of the model discussed in Chapter 3. The model involves a single scalar field coupled to gravity in six dimensions, where the scalar dynamics are governed by a polynomial potential. A free parameter within the potential determines the dimensionality of the operator or deformation in the dual interpretation of the model in five-dimensional field theory. Additionally, one of the spatial dimensions in this six-dimensional spacetime is compactified into a circle, with its size decreasing along the holographic direction. This geometric configuration leads to a smooth termination of space in the regular geometry.

In the dual field theory interpretation, this compactification effectively introduces a mass gap akin to what is observed in confining theories.

In this chapter, we promote the scalar field to an $SO(5)$ vector multiplet. This $SO(5)$ is gauged within the framework of six-dimensional gravity compactified on a circle. We pick the R_ξ gauge, following the approach in Ref. [118], and calculate the mass spectrum for the new states with $SO(4)$ quantum numbers. Central to our approach is the identification of the single scalar field from Section 4.1.1 with the modulus of the $SO(5)$ vector multiplet. This identification ensures that both fields obey the same equations of motion and enables us to consider the previous classical background solutions. As a result, in the dual field theory, a global symmetry breaking pattern $SO(5) \to SO(4)$ emerges.

While our primary interest lies in CHMs, we describe the theory in isolation in this chapter. We refrain from coupling it to external weakly-coupled elementary fields, deferring this mission to the next chapter. Remarkably, we find that within certain parameter regimes, in a metastable region, the spectrum includes parametrically light PNGBs alongside a light pseudo-dilaton, though not parametrically light. This observation suggests the necessity of incorporating a dilaton into the low-energy description of the theory [11, 12, 58]. Even when considered independently, the appearance of a dilaton field carries important phenomenological applications, explored extensively in the literature such as Refs. [62–72, 130], and references therein.

The chapter is structured as follows. We introduce the model in Section 4.1 and discuss the relevant classical solutions making use of key findings from Chapter 3. Subsequently, in Section 4.2, we analyse the mass spectrum of the states, especially states with $SO(4)$ quantum numbers. We investigate these findings compared with the singlet states, exploring the three-dimensional space of parameters in the model. Technical details necessary for replicating our primary results are transferred to appendices.

4.1 The model

In this section, we outline the gravity description of the model under analysis, which is related to the one studied in the previous chapter. The gravitational dynamics in $D = 6$ dimensions are governed by a two-derivative bulk action, where gravity is coupled to a real scalar field $\mathcal{X}$ charged under a gauged $SO(5)$ symmetry.

To regulate the system, we introduce two boundaries positioned at $\rho = \rho_1$ and $\rho = \rho_2$ along the radial direction. Consequently, the action needs appropriate boundary-localized terms. It is important to note that these boundaries serve solely as regulators; physical predictions are obtained by going to the limit where the boundaries are removed.

In the bulk description, the gauged $SO(5)$ symmetry faces a spontaneous breaking to $SO(4)$ due to the non-zero VEV of the field $\phi \equiv \sqrt{\mathcal{X}^T \mathcal{X}}$. This field ϕ corresponds to the

scalar field discussed in Chapter 3. The assumed dual field theory possesses a global $SO(5)$ symmetry, which corresponds to the $SO(5)$ in the bulk. The breaking of this symmetry is normally understood as a combination of spontaneous and explicit breaking, influenced by the coupling and VEV of the operator dual to the ϕ field. In our study of the bulk section, we choose the R_ξ gauge, following the methods and notation outlined in Ref. [118]. This gauge choice necessitates the inclusion of both bulk and boundary terms, although specific details are omitted in this section.

4.1.1 The six-dimensional action

The model $D = 6$ dimensions is an extension to the Eqs. (3.2.1–3.2.3). The field content is the metric, scalar fields, $\mathcal{X}_\alpha$, furnishing the 5 of the gauged group $SO(5)$, and $\mathcal{A}_{\hat{M}\,\alpha}{}^{\beta}$ which are the $SO(5)$ gauge fields. The index $\hat{M} = 0, 1, 2, 3, 5, 6$ is our space-time index while the Greek indexes $\alpha = 1, \cdots, 5$ mark the components of the 5 of $SO(5)$. The matrices t^A $(A = 1, \cdots, 10)$ are the generators of $SO(5)$ and normalised as $\mathrm{Tr}\left(t^A t^B\right) = \frac{1}{2}\delta^{AB}$. Hence, the action reads

$$\mathcal{S}_6 = \mathcal{S}_6^{(bulk)} + \sum_{i=1,2} \mathcal{S}_{5,i}\,, \tag{4.1.1}$$

$$\mathcal{S}_6^{(bulk)} = \int \mathrm{d}^6x\sqrt{-\hat{g}_6}\left\{\frac{\mathcal{R}_6}{4} - \frac{1}{2}\hat{g}^{\hat{M}\hat{N}}\left(D_{\hat{M}}\mathcal{X}\right)^T D_{\hat{N}}\mathcal{X} - \mathcal{V}_6(\mathcal{X}) - \frac{1}{2}\,\mathrm{Tr}\left[\hat{g}^{\hat{M}\hat{P}}\hat{g}^{\hat{N}\hat{Q}}\mathcal{F}_{\hat{M}\hat{N}}\mathcal{F}_{\hat{P}\hat{Q}}\right]\right\}, \tag{4.1.2}$$

$$\mathcal{S}_{5,i} = (-)^i \int \mathrm{d}^5x\sqrt{-\tilde{\hat{g}}}\left\{\frac{\mathcal{K}}{2} + \lambda_i(\mathcal{X}) + f_i\left(\tilde{\hat{g}}_{\hat{M}\hat{N}}\right)\right\}\Bigg|_{\rho=\rho_i}, \tag{4.1.3}$$

which contains a bulk part, $\mathcal{S}_6^{(bulk)}$, and two boundary actions, $\mathcal{S}_{5,i}$, chosen to be localised at the two boundaries of the radial coordinate $\rho_1 < \rho < \rho_2$. The quantity $\hat{g}_6$ is the determinant of the six-dimensional metric, $\hat{g}_{\hat{M}\hat{N}}$, with mostly plus signature. The Ricci scalar in 6D is $\mathcal{R}_6$. The extrinsic curvature, $\mathcal{K}$, depends on the induced metric on the boundaries, $\tilde{\hat{g}}_{\hat{M}\hat{N}}$, and appears in the GHY term for the boundary actions.

The convention for the covariant derivatives is

$$\left(D_{\hat{M}}\mathcal{X}\right)_\alpha \equiv \partial_{\hat{M}}\mathcal{X}_\alpha + ig\mathcal{A}_{\hat{M}\,\alpha}{}^{\beta}\mathcal{X}_\beta\,, \tag{4.1.4}$$

with the field-strength

$$\mathcal{F}_{\hat{M}\hat{N}\,\alpha}{}^{\beta} \equiv 2\left(\partial_{[\hat{M}}\mathcal{A}_{\hat{N}]\,\alpha}{}^{\beta} + ig\mathcal{A}_{[\hat{M}\,\alpha}{}^{\gamma}\mathcal{A}_{\hat{N}]\,\gamma}{}^{\beta}\right). \tag{4.1.5}$$

Here the comutator is defined as $[n_1 n_2] \equiv \frac{1}{2}\left(n_1 n_2 - n_2 n_1\right)$ with the coupling g as a free parameter.

The bulk potential, $\mathcal{V}_6(\mathcal{X})$, and the the boundary potentials, $\lambda_i(\mathcal{X})$, are assumed to be invariant under $SO(5)$, and thus depend only on the single variable $\phi \equiv \sqrt{\mathcal{X}^T\mathcal{X}}$. Following the approach in Ref. [5], we adopt the specific form of $\mathcal{V}_6(\phi)$, which is expressed in terms of $\mathcal{W}_6$ superpotential (this is chosen for convenience though the model is not supersymmetric). The potential is given by

$$\mathcal{V}_6 = \frac{1}{2}\sum_\alpha \left(\frac{\partial \mathcal{W}_6}{\partial \mathcal{X}_\alpha}\right)^2 - \frac{5}{4}\mathcal{W}_6^2\,, \tag{4.1.6}$$

with the superpotential defined as

$$\mathcal{W}_6 \equiv -2 - \frac{\Delta}{2}\mathcal{X}^T\mathcal{X} = -2 - \frac{\Delta}{2}\phi^2\,. \tag{4.1.7}$$

Hence

$$\mathcal{V}_6 = -5 - \frac{\Delta(5-\Delta)}{2}\phi^2 - \frac{5\Delta^2}{16}\phi^4\,. \tag{4.1.8}$$

4.1.2 Dimensional reduction

The coordinate $0 \le \eta < 2\pi$ is chosen to parametrise the compact circle. The metric, after reduction to five dimensions, is written as

$$\mathrm{d}s_6^2 = e^{-2\chi}\mathrm{d}x_5^2 + e^{6\chi}\left(\mathrm{d}\eta + \chi_M \mathrm{d}x^M\right)^2\,, \tag{4.1.9}$$

where the space-time index is chosen as $M = 0,1,2,3,5$. The five-dimensional metric is assumed to be of the domain-wall form

$$\mathrm{d}s_5^2 = \mathrm{d}r^2 + e^{2A(r)}\mathrm{d}x_{1,3}^2 = e^{2\chi(\rho)}\mathrm{d}\rho^2 + e^{2A(\rho)}\mathrm{d}x_{1,3}^2\,. \tag{4.1.10}$$

Thus, the reduced action reads

$$\mathcal{S}_5 = \mathcal{S}_5^{(bulk)} + \sum_{i=1,2} \mathcal{S}_{4,i}\,, \tag{4.1.11}$$

$$\begin{aligned}
\mathcal{S}_5^{(bulk)} = \int \mathrm{d}^5x\sqrt{-g_5}\Bigg\{ & \frac{R}{4} \\
& - \frac{1}{2}g^{MN}\left[6\partial_M\chi\partial_N\chi + \sum_{\alpha=1}^{5}\left(D_M\mathcal{X}\right)_\alpha\left(D_N\mathcal{X}\right)_\alpha + e^{-6\chi}\sum_{A=1}^{10}\left(D_M\mathcal{A}_6\right)^A\left(D_N\mathcal{A}_6\right)^A\right] \\
& - e^{-2\chi}\mathcal{V}_6 - \frac{1}{2}g^2e^{-8\chi}\mathcal{X}^T\mathcal{A}_6^2\mathcal{X} - \frac{1}{16}e^{8\chi}g^{MP}g^{NQ}F^{(\chi)}_{MN}F^{(\chi)}_{PQ} \\
& - \frac{1}{2}e^{2\chi}\,\mathrm{Tr}\left[g^{MP}g^{NQ}\mathcal{F}_{MN}\mathcal{F}_{PQ}\right] \\
& - g^{MN}(ig)\chi_M\mathcal{X}^T\mathcal{A}_6D_N\mathcal{X} - 2e^{2\chi}g^{MN}g^{OP}\chi_M\,\mathrm{Tr}\left(\mathcal{F}_{NO}D_P\mathcal{A}_6\right) \\
& - \frac{1}{2}g^2g^{MN}\chi_M\chi_N\mathcal{X}^T\mathcal{A}_6^2\mathcal{X} + e^{2\chi}g^{MP}g^{NQ}\chi_M\chi_N\,\mathrm{Tr}\left(D_P\mathcal{A}_6D_Q\mathcal{A}_6\right) \\
& - e^{2\chi}g^{MN}g^{PQ}\chi_M\chi_N\,\mathrm{Tr}\left(D_P\mathcal{A}_6D_Q\mathcal{A}_6\right)\Bigg\}\,,
\end{aligned} \tag{4.1.12}$$

$$\mathcal{S}_{4,i} = (-)^i\int \mathrm{d}^4x\sqrt{-\tilde{g}}\left\{\frac{K}{2} + e^{-\chi}\lambda_i(\mathcal{X}) + e^{-\chi}f_i(\chi)\right\}\Bigg|_{\rho=\rho_i}\,. \tag{4.1.13}$$

Here, g_5 is the determinant of the five-dimensional metric, g_{MN}, with the induced metric on the boundaries $\tilde{g}_{MN}$. Also, R is the five-dimensional Ricci scalar, alongside K, the extrinsic curvature. The form $F^{(\chi)}_{MN} = \partial_M\chi_N - \partial_N\chi_M$ is the field strength for the vector χ_M. Since we want to produce solutions that lift to geometries in six dimensions with a circle shrinking smoothly, the functions f_i in the six-dimensional theory must depend explicitly on the χ field. The notation $\mathcal{A}_6 \equiv \mathcal{A}_6^A t^A$ is defined, where $\mathcal{A}_6^A$ is a scalar in the adjoint of $SO(5)$. This scalar is obtained from the sixth component of the gauge field in the six-dimensional theory.

We concentrate on the background solutions that $\mathcal{A}_6 = 0$, $\mathcal{A}_M = 0$, $\chi_M = 0$, although g_{MN}, $\mathcal{X}_\alpha$, and χ have a non-trivial profile that depends only on the radial coordinate. The equations of motion for background fields are

$$\partial_\rho^2\mathcal{X}_\alpha + (4\partial_\rho A - \partial_\rho\chi)\partial_\rho\mathcal{X}_\alpha = \frac{\partial\mathcal{V}_6}{\partial\mathcal{X}_\alpha}\,, \tag{4.1.14}$$

$$\partial_\rho^2\chi + (4\partial_\rho A - \partial_\rho\chi)\partial_\rho\chi = -\frac{\mathcal{V}_6}{3}\,, \tag{4.1.15}$$

$$3(\partial_\rho A)^2 - \frac{1}{2}\partial_\rho\mathcal{X}_\alpha\partial_\rho\mathcal{X}_\alpha - 3(\partial_\rho\chi)^2 = -\mathcal{V}_6\,, \tag{4.1.16}$$

and boundary conditions

$$\left(\partial_\rho \mathcal{X}_\alpha - \frac{\partial \lambda_i}{\partial \mathcal{X}_\alpha}\right)\Big|_{\rho_i} = 0\,, \qquad \left(6\partial_\rho \chi + \lambda_i + f_i - \frac{\partial f_i}{\partial \chi}\right)\Big|_{\rho_i} = 0\,, \qquad \left(\frac{3}{2}\partial_\rho A + \lambda_i + f_i\right)\Big|_{\rho_i} = 0\,. \tag{4.1.17}$$

If $f_i = 0$, the solutions lift to domain walls in six dimensions, with

$$\mathcal{A} = A - \chi = 3\chi. \tag{4.1.18}$$

The solutions of our interest introduce a non-trivial background profile for the $\phi(\rho)$ field, hence breaking the $SO(5)$ symmetry to $SO(4)$. We decompose $\mathcal{X}_\alpha$ in accordance with irreducible representations of $SO(4)$ as $5 = 1 \oplus 4$. This defines ϕ and $\pi^{\hat{A}}$ fields respectively. One has

$$\mathcal{X} = \exp\left[2i\pi^{\hat{A}} t^{\hat{A}}\right] \phi\, \mathcal{X}_0\,, \qquad \mathcal{X}_0 = (0,0,0,0,1)^T\,, \tag{4.1.19}$$

with the chosen decomposition

$$\mathcal{A}_{\hat{M}\,\alpha}{}^{\beta} = \mathcal{A}_{\hat{M}}{}^{\bar{A}} \left(t^{\bar{A}}\right)_\alpha{}^{\beta} + \mathcal{A}_{\hat{M}}{}^{\hat{A}} \left(t^{\hat{A}}\right)_\alpha{}^{\beta}\,. \tag{4.1.20}$$

Here the broken as well as unbroken generators of $SO(5)$ with respect to $\mathcal{X}_0$ are denoted by $t^{\hat{A}}$ ($\hat{A} = 1, \cdots, 4$) and $t^{\bar{A}}$ ($\bar{A} = 5, \cdots, 10$) respectively. A representation for the basis of generators is provided in Appendix C with the normalisation conditions $\mathrm{Tr}\left(t^{\bar{A}} t^{\hat{B}}\right) = 0$, $\mathrm{Tr}\left(t^{\hat{A}} t^{\hat{B}}\right) = \frac{1}{2}\delta^{\hat{A}\hat{B}}$, and $\mathrm{Tr}\left(t^{\bar{A}} t^{\bar{B}}\right) = \frac{1}{2}\delta^{\bar{A}\bar{B}}$.

Since potentials $\lambda_i(\phi)$ in the boundary are $SO(5)$ invariant, the $\mathcal{X}_\alpha$ boundary conditions in Eq. (5.5.12) simplify as

$$0 = \left(\left[\partial_\rho \phi - \frac{\partial \lambda_i}{\partial \phi}\right]\frac{\mathcal{X}_\alpha}{\phi} + 2i\partial_\rho \pi^{\hat{A}} (t^{\hat{A}})_\alpha{}^{\beta} \mathcal{X}_\beta\right)\Big|_{\rho_i}\,, \tag{4.1.21}$$

and solved by requiring

$$\partial_\rho \phi|_{\rho_i} = \frac{\partial \lambda_i}{\partial \phi}\Big|_{\rho_i}\,, \qquad \partial_\rho \pi^{\hat{A}}|_{\rho_i} = 0\,. \tag{4.1.22}$$

With these boundary conditions, one can choose background solutions with $\pi^{\hat{A}} = 0$, without loss of generality. The only non-trivial background functions will be A, ϕ and χ.

4.1.3 Truncation to quadratic order

As ϕ, A, and χ are the primary non-trivial functions in the background, we can simplify the reduced action further by expanding the other scalar and gauge fields and keeping the expansion at quadratic order. This approach respects the same classical solutions while retaining sufficient information to compute the linearised equations of motion for the fluctuations in all fields.

Besides ϕ, χ, and g_{MN}, the other degrees of freedom are kept as perturbative degrees of freedom; hence the 5D action truncated at the quadratic order is

$$\mathcal{S}_5^{(2)} = \mathcal{S}_5^{(bulk,2)} + \sum_{i=1,2} \mathcal{S}_{4,i}\,, \tag{4.1.23}$$

where the bulk action reads as

$$\begin{aligned}\mathcal{S}_5^{(bulk,2)} = \int \mathrm{d}^5x\sqrt{-g_5}\Big\{&\frac{R}{4} - \frac{1}{2}g^{MN}G_{ab}\partial_M\Phi^a\partial_N\Phi^b - \mathcal{V}_5(\Phi^a)\\ &- \frac{1}{2}g^{MN}G^{(0)}_{ab}\partial_M\Phi^{(0)a}\partial_N\Phi^{(0)b} - \frac{1}{2}m^{(0)2}_{ab}\Phi^{(0)a}\Phi^{(0)b}\\ &- \frac{1}{2}g^{MN}G^{(1)}_{AB}\mathcal{H}^{(1)A}_M\mathcal{H}^{(1)B}_N - \frac{1}{4}g^{MO}g^{NP}H^{(1)}_{AB}F_{MN}{}^AF_{OP}{}^B\Big\},\end{aligned} \tag{4.1.24}$$

while the boundary terms are

$$\mathcal{S}_{4,i} = (-)^i\int \mathrm{d}^4x\sqrt{-\tilde{g}}\left\{\frac{K}{2} + e^{-\chi}\lambda_i(\phi) + e^{-\chi}f_i(\chi)\right\}\Big|_{\rho=\rho_i}. \tag{4.1.25}$$

Two scalars $\Phi^a = \{\phi, \chi\}$ can be considered as a sigma-model coupled to gravity where $D = 5$ and sigma-model metric is $G_{ab} = \mathrm{diag}(1, 6)$, with the potential $\mathcal{V}_5(\phi, \chi) = e^{-2\chi}\mathcal{V}_6(\phi)$. The non active scalars $\Phi^{(0)a} = \{\mathcal{A}_6^{\bar{A}}, \mathcal{A}_6^{\hat{A}}\}$ have their sigma-model metric as

$$G^{(0)} = \left(\begin{array}{c|c} e^{-6\chi}\mathbb{1}_{6\times6} & \\ \hline & e^{-6\chi}\mathbb{1}_{4\times4}\end{array}\right). \tag{4.1.26}$$

and mass matrix

$$\frac{m^{(0)2}}{g^2} = \left(\begin{array}{c|c} \mathbb{0}_{6\times6} & \\ \hline & \frac{1}{4}\phi^2e^{-8\chi}\mathbb{1}_{4\times4}\end{array}\right). \tag{4.1.27}$$

The field strengths for the 1-forms $V_M{}^A = \{\chi_M, \mathcal{A}_M{}^{\bar{A}}, \mathcal{A}_M{}^{\hat{A}}\}$ are $F_{MN}{}^A = 2\partial_{[M}V_{N]}{}^A$, and

$$H^{(1)} = \left(\begin{array}{c|c|c} \frac{1}{4}e^{8\chi} & & \\ \hline & e^{2\chi}\,\mathbb{1}_{6\times 6} & \\ \hline & & e^{2\chi}\,\mathbb{1}_{4\times 4} \end{array}\right), \tag{4.1.28}$$

while $\mathcal{H}_M^{(1)A} = \left\{0, 0, \partial_M \pi^{\hat{A}} + \frac{g}{2}\mathcal{A}_M{}^{\hat{A}}\right\}$ which are a combinations of derivatives of the vectors and pseudo-scalars chosen to be gauge-invariant. Finally we have

$$G^{(1)} = \left(\begin{array}{c|c|c} 0 & & \\ \hline & \mathbb{0}_{6\times 6} & \\ \hline & & \phi^2\,\mathbb{1}_{4\times 4} \end{array}\right). \tag{4.1.29}$$

By the choices made here, the details of the background solutions are the same as solutions discussed in Section 3.3; hence, we avoid repeating the details and use the same parametrisation mentioned there.

4.2 Mass spectrum of fluctuations

Chapter 3, based on Ref. [5], presented the spectrum of fluctuations for the $SO(5)$ singlet sector. The fluctuating variables for the fields ϕ, χ and metric are represented, respectively, by $\mathfrak{a}^\phi$, $\mathfrak{a}^\chi$, and $\mathfrak{e}$. The fluctuations associated with χ_M are denoted by $\mathfrak{v}$. Building on the same background solutions, we investigate the additional fields that transform under $SO(5)$ multiplets: $\mathcal{A}_6^{\bar{A}}$, $\mathcal{A}_6^{\hat{A}}$, $\mathcal{A}_M^{\bar{A}}$, $\mathcal{A}_M^{\hat{A}}$, and $\pi^{\hat{A}}$. These additional fields do not acquire VEVs, ensuring they do not mix with components of the metric. However, due to the presence of $SO(5)$ gauge symmetry in the bulk, we adopt the R_ξ gauge to compute the spectrum of their fluctuations. To ensure gauge invariance and identify physical combinations, we follow the formalism developed in Ref. [118] (also see Ref. [162]). The gauge-invariant combinations of fluctuating fields are named as $\mathfrak{a}^{\hat{A}}$, $\mathfrak{a}^{\bar{A}}$, $\mathfrak{v}^{\hat{A}}$, $\mathfrak{v}^{\bar{A}}$, and $\mathfrak{p}^{\hat{A}}$, respectively.

We focus on the $SO(5)$ multiplets and their corresponding equations of motion, avoiding a repetition of details discussed in Chapter 3. The equations can be summarised as follows:

$$0 = \left[\partial_\rho^2 + (4\partial_\rho A - 7\partial_\rho \chi)\,\partial_\rho - e^{2\chi-2A}q^2\right]\mathfrak{a}^\phi\,, \tag{4.2.1}$$

$$0 = \left[\partial_\rho^2 + (4\partial_\rho A - 7\partial_\rho \chi)\,\partial_\rho - \frac{g^2\phi^2}{4} - e^{2\chi-2A}q^2\right]\mathfrak{a}^\chi\,, \tag{4.2.2}$$

$$0 = \left[\partial_\rho^2 + (2\partial_\rho A + \partial_\rho \chi)\partial_\rho - e^{2\chi-2A}q^2\right]\mathfrak{v}^{\bar{A}}\,, \tag{4.2.3}$$

$$0 = \left[\partial_\rho^2 + (2\partial_\rho A + \partial_\rho \chi)\partial_\rho - \frac{g^2\phi^2}{4} - e^{2\chi-2A}q^2\right]\mathfrak{v}^{\hat{A}}\,, \tag{4.2.4}$$

$$0 = \left[\partial_\rho^2 - \left(2\partial_\rho A + \partial_\rho \chi + \frac{2\partial_\rho \phi}{\phi}\right)\partial_\rho - \frac{g^2\phi^2}{4} - e^{2\chi-2A}q^2\right]\mathfrak{p}^{\hat{A}}\,, \tag{4.2.5}$$

where q^μ is the four-momentum and $q^2 \equiv \eta_{\mu\nu}q^\mu q^\nu$.

The solutions of the linearised equations are studied numerically for $\rho_1 \le \rho \le \rho_2$, with $\rho_1 > \rho_o$. The process is performed using the IR and UV expansions described in Section 3.4. The boundary conditions for the scalars $\mathfrak{a}^\phi$ and $\mathfrak{a}^\chi$ are Dirichlet at both boundaries, $\rho = \rho_1$ and, $\rho = \rho_2$ namely, $\mathfrak{a}^{\phi,\chi}|_{\rho_i} = 0$. The vectors $\mathfrak{v}^{\bar{A}}$ and $\mathfrak{v}^{\hat{A}}$ obey Neumann boundary conditions, $\partial_\rho \mathfrak{v}^{\bar{A},\hat{A}}|_{\rho_i} = 0$. The pseudoscalar $\mathfrak{p}^{\hat{A}}$ is chosen to have Dirichle boundary conditions at $\rho = \rho_1$ but Neumann for $\rho = \rho_2$ [162, 173]. See Appendix E for the relevant IR and UV expansions. In Chapter 5, we will discuss how the conditions are altered by the introduction of other non-trivial boundary terms in the action which will generate the coupling of the theory to other external fields.

To discuss our new findings and interpret them properly, it is essential to clarify the physical significance of the parameters ϕ_I and g. The parameter ϕ_I governs the magnitude of $SO(5)$ symmetry-breaking effects. Interestingly, in spite of ϕ satisfying a second-order nonlinear differential equation, the requirement for geometric regularity at the end of space imposes a non-trivial relationship between the two free parameters typically found in a confining solution. Specifically, these parameters can be associated with coefficients like ϕ_J and ϕ_V in UV expansions, which relate to explicit and spontaneous symmetry breaking in the corresponding field theory.

Numerical investigations in Section 3.5 illustrate that for $0 < \Delta < 5$, there exists a critical value $\phi_I(c)$. When $\phi_I > \phi_I(c)$, an alternative classical solution should emerge with a lower free energy for the same source value. This observation indicates the presence of a phase transition. In our presentation, we choose $\phi_I = \phi_I(c)$ in the plots as this case minimises the mass of the lightest scalar state.

Self-coupling strength of the bulk gauge fields is the g parameter. It plays a role in determining how composite vector mesons couple and decay into two PNGBs within the

effective description of the dual field theory. However, it is useful to clarify these statements within the notational conventions adopted. A multiplicative factor of $2/\kappa^2$ is omitted in the action $\mathcal{S}_6$. For our purposes in this paper, where we focus on solving classical background equations and linearised fluctuations around these backgrounds, the factor $2/\kappa^2$ acts as an overall scaling factor that does not affect the final results. These classical results remain exact in the limit where $\kappa \to 0$, with g and ϕ_I held fixed. Approaching the classical regime can be calculated by perturbative corrections in terms of loop diagrams, assuming g is not large. A rough upper bound estimation suggests $\frac{3g^2\kappa^2}{256\pi^3} \ll 1$ [175].[1]

We present examples of mass spectra in Figs. 4.1 and 4.2 for different choices of Δ where $\Delta < \frac{5}{2}$ and $\Delta \geq \frac{5}{2}$, respectively. For each selected value of Δ, we provide two plots: one with fixing $g = 5$ and varying ϕ_I and second with fixing $\phi_I = \phi_I(c)$ and varying g. In these plots, all states of the system are depicted, differentiated by colour and marker shape corresponding to different $SO(4)$ representations. Additionally, we include results for $SO(5)$ singlets for completeness and to highlight their physical role. Further numerical results can be found in Appendix C of [6].

For any given values of Δ, we observe that the masses of the axial vectors, which transform as 4 under $SO(4)$, are consistently larger than those of the vector states, and this difference increases with g. Additionally, the mass of the lightest PNGBs also increases with g. For ϕ_I variation with $\Delta \lesssim 2$ and with fixed g, we find that the mass of the spin-0 states, which transform as 4 under $SO(4)$, increases with ϕ_I. In field-theory dual, in this region of parameter space, the explicit symmetry breaking effect dominates over the spontaneous breaking effect, and these states cannot be considered as genuine PNGBs contrary to their quantum numbers. Conversely, for $\Delta \geq 2.5$, we observe that the mass of the lightest spin-0 states transforming in 4 of $SO(4)$ can be made arbitrarily light by going to the larger values of ϕ_I. However, the critical values of ϕ_I where this occurs are very small, often leading to tachyonic regions in the spectrum. In conclusion, across all values of Δ and g, if we confine our analysis to the stable region of parameter space where $\phi_I \leq \phi_I(c)$, we find no evidence that the masses of PNGBs are suppressed.

A novel observation arises when we focus on the regime where $2 \lesssim \Delta < 2.5$. Previous work in Ref. [5], described in Section 3.4, identified a metastable region of parameter space characterised by large values of ϕ_I, where the lightest scalar state is identified as a dilaton. In our study, we additionally find that the PNGBs transforming as 4 under $SO(4)$ are also light in this parameter region, having suppressed masses compared to other bound states. This is observable in the bottom-left panel of Fig. 4.1.

To further illustrate the capability to tune the masses of these states to be arbitrarily

[1] The second Casimir of the adjoint representation $C_2(\text{Adj}) = 3$ for $SO(5)$ determines the factor of 3 in this expression; for $SU(N_c)$, it is $C_2(\text{Adj}) = N_c$.

small relative to the typical mass scale of other bound states, represented by the mass of spin-2 particles, Fig. 4.3 provides detailed information for $\Delta = 2.35$, $\Delta = 2.40$, and $\Delta = 2.45$. The left panels of the figure illustrate the dependence on g of the spectrum for a fixed choice of $\phi_I = 3$, which falls within the parameter space region where both a light dilaton and a set of light PNGBs in the 4 representation of $SO(4)$ coexist.

While we previously identified metastable confining background solutions for large values of ϕ_I, we present here three expanded and detailed plots that demonstrate the near-degeneracy of the free energy with another branch of solutions. The right panels of Fig. 4.3 display the holographically renormalised free energy, $\hat{\mathcal{F}}$, as a function of the source, $\hat{\phi}_J$, appropriately normalised. These plots expand upon those presented in Section 3.5, derived from the following relations:

$$\mathcal{F} = -\frac{1}{40} e^{4A_U - \chi_U} \left(16\Delta \left(\frac{5}{2} - \Delta \right) \phi_J \phi_V - 75\chi_5 \right), \tag{4.2.6}$$

$$\Lambda^{-1} \equiv \int_{\rho_o}^{\infty} \mathrm{d}\rho \, e^{\chi(\rho) - A(\rho)}, \tag{4.2.7}$$

with the rescaled $\hat{\mathcal{F}} \equiv \mathcal{F}/\Lambda^5$ and $\hat{\phi}_J \equiv \phi_J/\Lambda^\Delta$. In the plots, choosing $\phi_I = 3$ lead to confining solutions with parameter $\hat{\phi}_J = 6.78$ for $\Delta = 2.35$, $\hat{\phi}_J = 6.83$ for $\Delta = 2.40$, and $\hat{\phi}_J = 6.88$ for $\Delta = 2.45$. The plots illustrate not only the confining solutions but also the analysis of free energy for (singular) solutions that respect five-dimensional Poincaré invariance, providing a graphical comparison. Specifically, they demonstrate that for $\phi_I = 3$, as shown in all three examples here, the confining solutions do not have minimal free energy. As ϕ_I becomes large, these metastable solutions could potentially have a long lifetime. The question of whether regions of parameter space exist that could support the construction of a viable CHM that relies on the presence of a long-lived metastable vacuum is important and needs further dedicated investigation. The model may also have other interesting phenomenological implications, that are valuable for improving in the future.

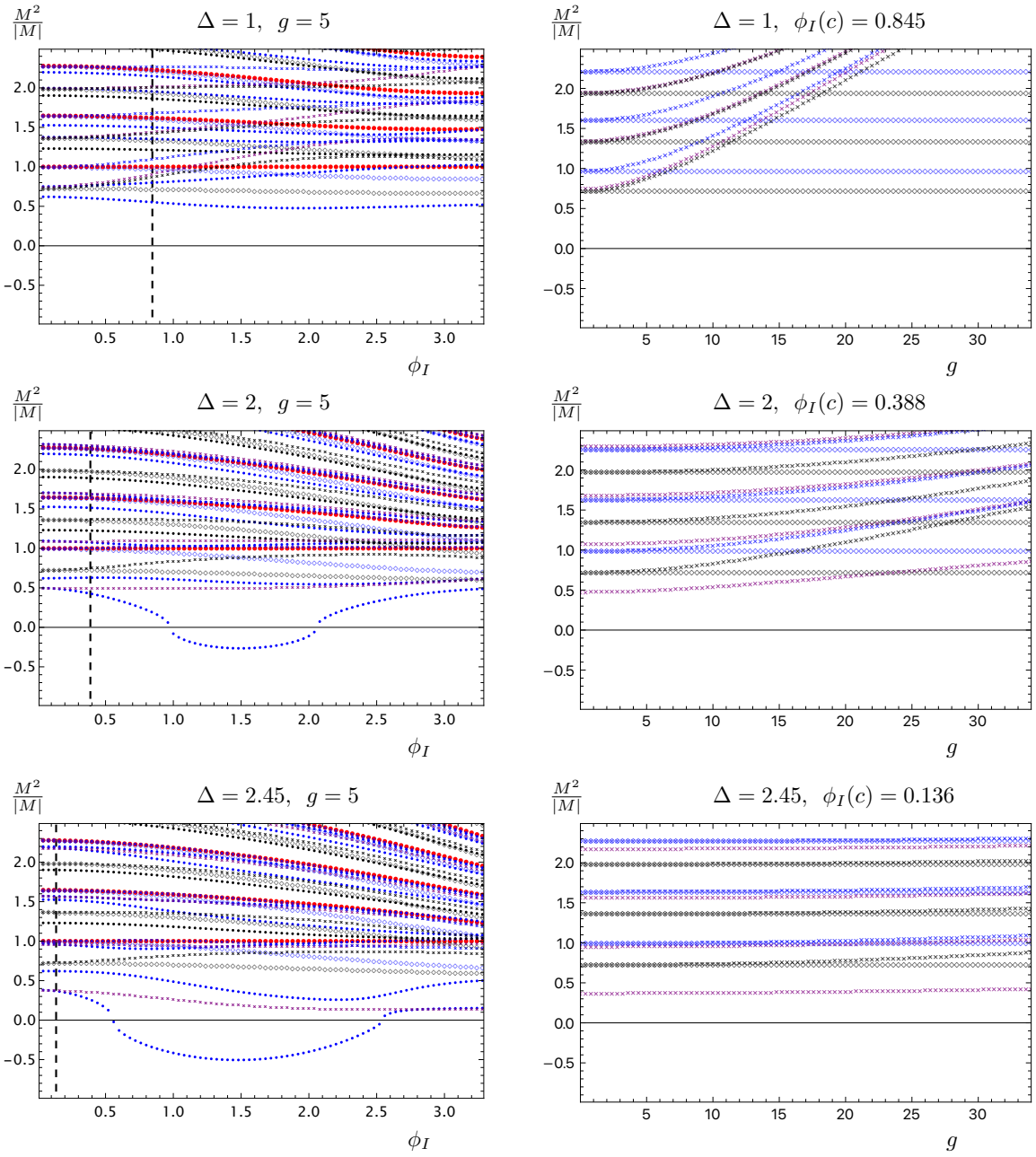

Figure 4.1. Mass spectrum of fluctuations as a function of the IR parameter ϕ_I with $g = 5$ (left), and as a function of parameter g for $\phi_I = \phi_I(c)$ (right), calculated for confining backgrounds, for different Δ choices. For each Δ, states with spin-0 scalar, spin-0 pseudo-scalar, spin-1 and spin-2 are shown in blue, purple, black and red, respectively. The IR and UV cutoffs are chosen respectively as $\rho_1 - \rho_o = 10^{-9}$ and $\rho_2 - \rho_o = 5$. Disks represent singlets of the unbroken $SO(4)$, reported in Section 3.4, diamonds are the 6 of $SO(4)$, and crosses represent the 4 of $SO(4)$. Every mass is normalised to the mass of the lightest tensor (spin-2) state. As the singlets masses are independent of g, we do not show them in the right panels that contain only the non-trivial multiplets charged under $SO(5)$. The critical value $\phi_I(c)$ is denoted by vertical dashed lines.

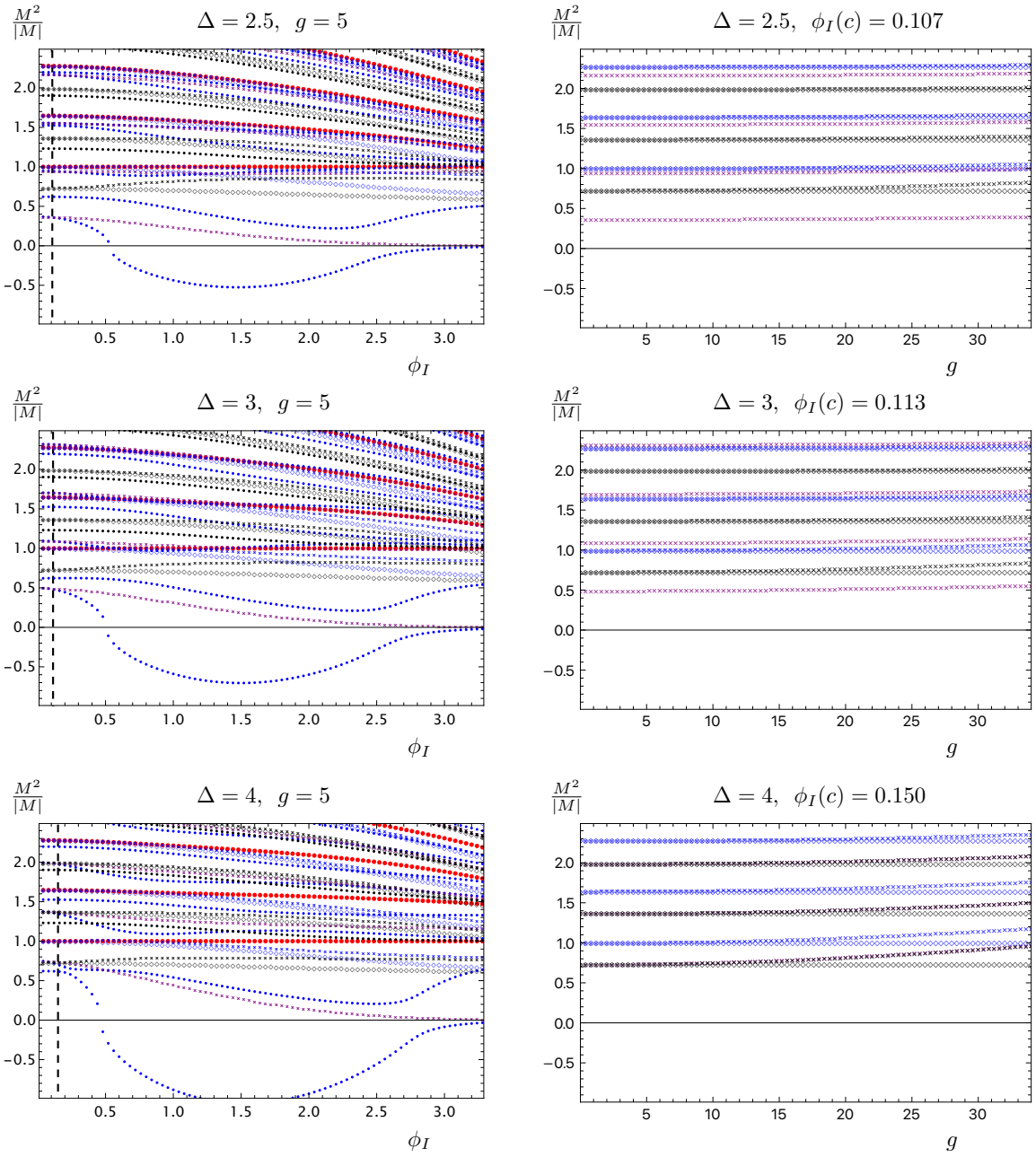

Figure 4.2. Mass spectrum of fluctuations as a function of the IR parameter ϕ_I with $g = 5$ (left), and as a function of parameter g for $\phi_I = \phi_I(c)$ (right), calculated for confining backgrounds, for different Δ choices. For each Δ, states with spin-0 scalar, spin-0 pseudo-scalar, spin-1 and spin-2 are shown in blue, purple, black and red, respectively. The IR and UV cutoffs are chosen respectively as $\rho_1 - \rho_o = 10^{-9}$ and $\rho_2 - \rho_o = 5$. Disks represent singlets of the unbroken $SO(4)$, reported in Section 3.4, diamonds are the 6 of $SO(4)$, and crosses represent the 4 of $SO(4)$. Every mass is normalised to the mass of the lightest tensor (spin-2) state. As the singlets masses are independent of g, we do not show them in the right panels that contain only the non-trivial multiplets charged under $SO(5)$. The critical value $\phi_I(c)$ is denoted by vertical dashed lines.

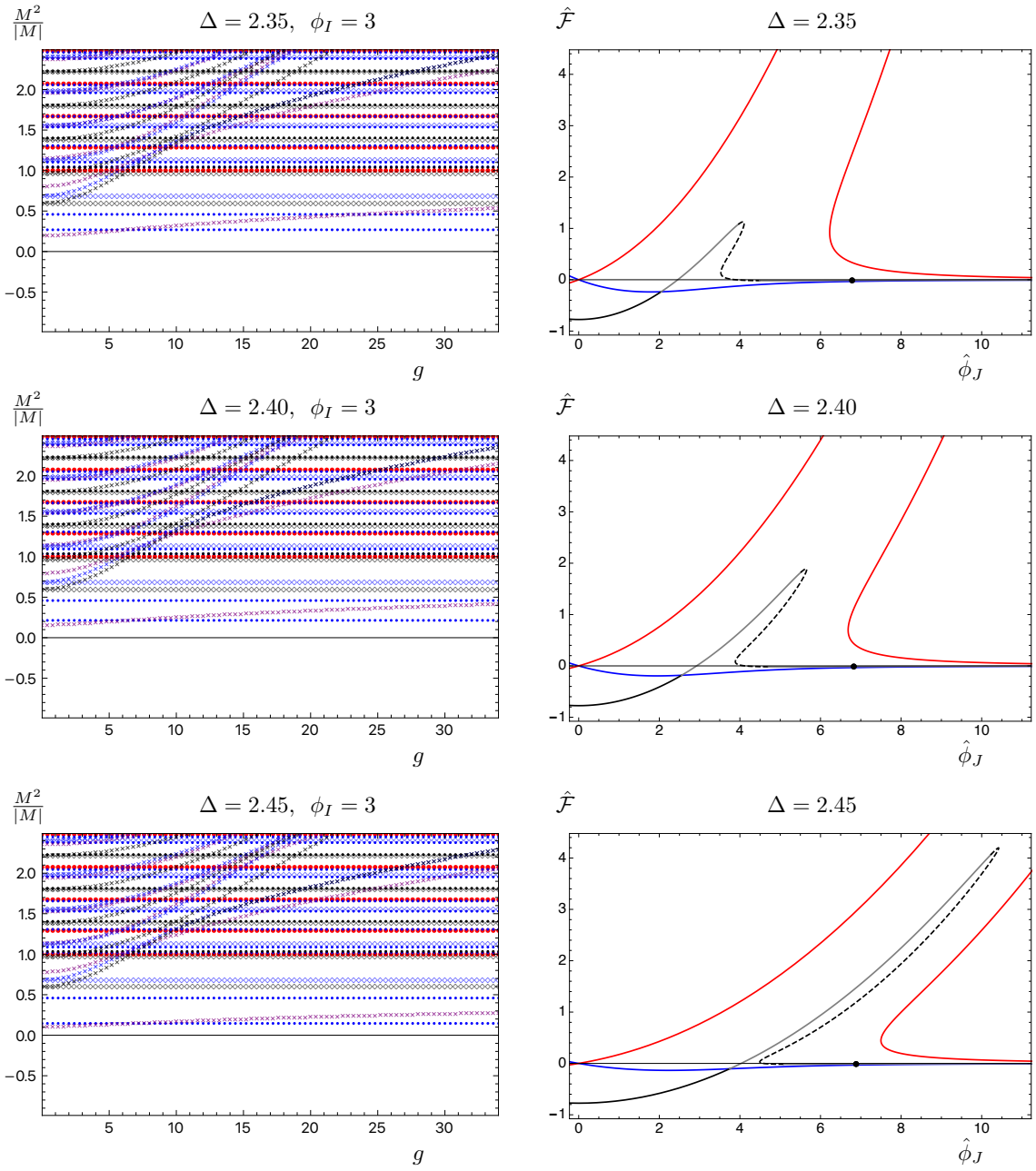

Figure 4.3. Mass spectrum of fluctuations on the confining background solution for $\Delta = 2.35$ (top), $\Delta = 2.40$ (middle), and $\Delta = 2.45$ (bottom), with $\phi_I = 3$ as a function of g (left), and free energy, $\hat{\mathcal{F}}$, as a function of the normalised source parameter $\hat{\phi}_J$ (right). For each Δ, states with spin-0 scalar, spin-0 pseudo-scalar, spin-1 and spin-2 are shown in blue, purple, black and red, respectively. The IR and UV cutoffs are chosen respectively as $\rho_1 - \rho_o = 10^{-9}$ and $\rho_2 - \rho_o = 5$. Disks represent singlets of the unbroken $SO(4)$, reported in Section 3.4, diamonds are the 6 of $SO(4)$, and crosses represent the 4 of $SO(4)$. Every mass is normalised to the mass of the lightest tensor (spin-2) state. The critical value $\phi_I(c)$ is denoted by vertical dashed lines. Normalised free energy, $\hat{\mathcal{F}}$, and normalised source, $\hat{\phi}_J$, are discussed in Section 3.5. For the confining branch, we mark the regions of the curve with black for stable, grey for metastable, and dashed black for tachyonic parts; singular solutions are plotted in red and blue. The solutions with $\phi_I = 3$ are denoted by the black dots on the right panels.

Chapter 5

Holographic Vacuum Misalignment

In this chapter, we will take our final step towards a holographic composite Higgs model. One of the important goals of the composite Higgs models is keeping the scale of new physics, denoted as f, considerably higher than the electroweak scale v. The dynamics of strong coupling should lead to this little hierarchy, where small destabilising perturbations of the vacuum arise due to perturbative weak interactions with an external sector. As we will describe in more detail, and as mentioned in the Ref. [176], the electroweak scale is suppressed by the so-called vacuum misalignment angle, $\theta \sim v/f \ll 1$ — see Section 5.1 and also Section 2.2.1 of Ref. [28] and related references. In this case, the constraints imposed by phenomenology can be met with a relatively modest suppression of θ, requiring only mild parameter tuning. However, calculating θ based on first principles needs non-perturbative treatment.

In this chapter, we advance the development of a minimal holographic CHM. Our motivation stems from the requirement of building a foundational groundwork in formalism before undertaking the ambitious task of embedding holographic CHMs within a rigorous top-down holographic context. This simpler work is essential to ensure that subsequent model-building and phenomenological studies are based on a firmer theoretical framework. In the following subsections, we discuss the basics of vacuum misalignment and also why this preparatory work is necessary. Our focus here is on refining and testing the formalism using a bottom-up model. The simpler model we develop encapsulates many of the important aspects of the CHM scenario and stands independently as a valuable model in its own right.

5.1 Vacuum misalignement

To review the vacuum misalignment phenomenon, following Ref. [26], we assume a new sector alongside the SM gauge fields and fermions, characterised by a global Lie group symmetry denoted as $\mathcal{G}$. This sector, referred to as the "composite sector," aims to tackle the naturalness problem through the mechanism of dimensional transmutation (see Section 2.2.1), which is similar to QCD-like confining theories. In this scenario, we consider a strongly interacting composite sector where the vacuum state, in case of no explicit breaking, has an invariance

only under a subgroup $\mathcal{H} \subset \mathcal{G}$. This leads to a spontaneous breaking $\mathcal{G} \to \mathcal{H}$, resulting in a set of massless NGBs living in the coset $\mathcal{G}/\mathcal{H}$. The subgroup $\mathcal{H}$ is normally assumed to include the electroweak group $G_{\rm EW} = \mathrm{SU}(2)_L \times \mathrm{U}(1)_Y$. In the case of our work, for simplicity, it will contain a larger SO(4) group, which will be gauged at a later stage. Yet, the process is extendable to the desired EW group. The group $\mathcal{G}$ should be sufficiently large to accommodate at least one Higgs doublet within the coset $\mathcal{G}/\mathcal{H}$, crucial for generating masses of SM fermions and gauge bosons via the Higgs mechanism.

To analyse this system rigorously, we begin by establishing a reference coordinate in the Lie algebra of $\mathcal{G}$. This involves selecting a basis of linearly independent generators T^A and dividing them into "unbroken" and "broken" sets denoted by $A = a = 1, \ldots, \dim[\mathcal{H}]$ and $A = \hat{a} = \hat{1}, \ldots, \dim[\mathcal{G}/\mathcal{H}]$ indices, as expressed by the decomposition:

$$\{T^A\} = \{T^a, \Theta^{\hat{a}}\}\,. \tag{5.1.1}$$

The $\{T^a\}$s are the generators of the subgroup $\mathcal{H}$ algebra. The $\vec{F}$ vector is chosen as a reference vacuum configuration for the composite sector that represents one of the degenerate vacua, among other choices. It is defined by

$$T^a \vec{F} = 0\,, \qquad \Theta^{\hat{a}} \vec{F} \neq 0\,. \tag{5.1.2}$$

Here $\{\Theta^{\hat{a}} \vec{F}\}$ are linearly independent vectors over the reals.

Note that Eq. (5.1.1), and hence Eq. (5.1.2), represents a conventional selection of the reference framework within the $\mathcal{G}$ algebra. For the isolated composite sector exclusively, where $\mathcal{G}$ manifests as an exact symmetry, no specific direction holds preference. Normally, different embeddings of $\mathcal{H}$ subgroup into $\mathcal{G}$, achieved by applying $\mathcal{G}$ elements to Eq. (5.1.1), are equivalent. Yet, in our construction, $\mathcal{G}$ will finally be broken by relating some of its generators with the generators of the EW group. It is advantageous to select the reference direction so that $\mathcal{H}$ includes all generators of the EW group. Indeed, the $W_\mu^{1,2,3}$ and B_μ fields from SM, which gauge the $G_{\rm EW}$ group, will couple to certain global currents associated with $\{T^a\}$ and not the broken $\{\Theta^{\hat{a}}\}$. This defines our choice of the $\{T^a\}$ set and the reference vacuum $\vec{F}$.

The NGB fields manifold is parametrised by $\{\Theta^{\hat{a}}\}$ generators and we do a field definition as

$$\vec{\Phi}(x) = e^{i\,\theta^{\hat{a}}(x)\Theta^{\hat{a}}}\,\vec{F}\,, \tag{5.1.3}$$

The four real components of one Higgs doublet, along with potentially other scalars from an expanded Higgs sector, can be extracted from the $\theta_{\hat{a}}$ fields. When a Higgs field acquires a VEV, it ultimately breaks $G_{\rm EW}$ down to the EW group, analogous to the SM. To study this

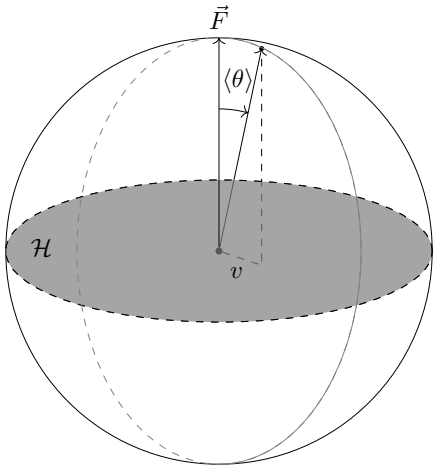

Figure 5.1. A diagram presenting the vacuum misalignment concept, in the example for $\mathcal{G} = \mathrm{SO}(3)$ to $\mathcal{H} = \mathrm{SO}(2)$ breaking. $v = f \sin\langle\theta\rangle$ is the projection of $\vec{F}$ to the SO(2) subgroup plane and proportionally determines the SO(2) breaking as a result of vacuum misalignment.

mechanism, we focus on the composite sector alone, disregarding $\mathcal{G}$-breaking effects coming from interactions with SM fields. In this isolated scenario, the θ fields act as exact NGBs and thus have no potential with a non-constrained VEV $\langle\theta_{\hat{a}}\rangle$. As any constant configuration of θ corresponds to an equivalent vacuum obtained by applying a $\mathcal{G}$ transformation to $\vec{F}$, specifically $\exp\left[-i\langle\theta_{\hat{a}}\rangle\Theta^{\hat{a}}\right]$, the VEVs are unobservable.

When considering $\mathcal{G}$-breaking effects and θ becoming a pNGB, the dynamics change. Now, θ gets a potential, losing the arbitrariness in its VEV. This VEV, denoted as $\langle\theta\rangle$, becomes observable because it is not possible to remove it by a symmetry transformation. Its physical role will be in breaking G_{EW}, in $\mathcal{H}$, by initiating EWSB.

From a geometric perspective, as illustrated in Fig. 5.1, $\langle\theta\rangle$ quantifies the angle by which the vacuum state deviates from the chosen reference vector $\vec{F}$, which is set orthogonal to the plane spanned by $\mathcal{H} \supseteq G_{\mathrm{EW}}$. The θ field behaves analogously to the SM Higgs field: EWSB is trigeered by its non-zero VEV. Specifically, we anticipate that different EWSB-related observables, such as the masses of SM particles, are governed by the projection of $\vec{F}$ onto the G_{EW} subgroup plane, $v = f \sin\langle\theta\rangle$, where $f = |\vec{F}|$ represents the scale of spontaneous breaking from $\mathcal{G}$ to $\mathcal{H}$.

The specific value of $\langle\theta\rangle$ is determined by the details of the new sector and the symmetry-breaking interactions within each explicit model. It can be found by minimising the potential of the pNGB. Unless there exists a special mechanism or a cancellation, on general grounds, one expects $\langle\theta\rangle$ to be around 1 in magnitude. This indicates that the vacuum state does not align closely with $\vec{F}$, leading to maximal EWSB, where $v \sim f$. In such scenarios, our framework

resembles a non-minimal technicolour model where $\mathcal{H}$ is extended to include not only the electromagnetic U(1) but also the broken SM generators. The CHM becomes particularly distinct from standard technicolour when the misalignment angle $\langle\theta\rangle$ is small, namely $\langle\theta\rangle \ll 1$. In such cases, a hierarchy develops between f and the EWSB scale v, creating a gap. This is the virtue of the so-called "vacuum misalignment" mechanism, [25, 177, 178],

$$\xi \equiv \frac{v^2}{f^2} = \sin^2\langle\theta\rangle \ll 1\,. \tag{5.1.4}$$

To obtain a small ξ in the model, cancellations of the order of one part in ten might be acceptable from the point of view of the Naturalness issue discussed in the introduction.

In the next section, we will draw the mainlines to follow to obtain a holographic model for our study of CHMs.

5.2 A roadmap towards top-down holographic composite Higgs

A path to construct a top-down holographic CHM may pass through the following stages:

1) Find a theory of gravity, which may also have a low energy supergravity description, that provides a dual for a field theory. This field theory undergoes spontaneous symmetry breaking involving the G/H coset relevant to the specific CHM under consideration.

2) Solve for gravity solutions that holographically correspond to confinement within the dual four-dimensional field theory.

3) Calculate the free energy and spectrum of fluctuations, corresponding to bound states of the field theory. Ensure there are no tachyons or other signs of instability.

4) Extend the gravity theory to incorporate the gauging of a subgroup of the field theory global symmetry. The coupling strength should be sufficiently weak to allow for a perturbative study.

5) Expand the gravity theory to include the explicit breaking of the field theory global symmetry, respecting gauged symmetries principles and unitarity. This may require additional auxiliary fields called spurions.

6) Conduct a vacuum alignment study on the gravity side to ascertain the structure of field-theory vacua.

7) Check the absence of mass spectrum pathologies like tachyons after the introduction of symmetry-breaking terms.

8) Introduce SM fields to the theory and relevant couplings alongside identifying suitable ranges of parameter space. This step may require incorporating other concepts like top partial compositeness [179] (also discussed in Refs. [67, 180–183]).

Points 1)-3) are investigated in Ref. [162]. The relevant CHM coset for us, being the minimal $SO(5)/SO(4)$ coset, arises within $D = 7$ maximal supergravity, with uplifts to type-IIA supergravity in $D = 10$ dimensions. The spectrum of bosonic fluctuations is computed in Ref. [162] after compactification on a 2-torus. These computations are carried out for backgrounds that are dual to a confining four-dimensional field theory, utilising the formalism established in previous works [119–123]— also Refs. [109–111, 118, 124, 132, 184].

The bottom-up $D = 6$ dimensional model, described in Refs. [5, 6] and Chapters 3–4, revisits points 1), 2), and 3) with some technical advantages. This model features a simpler spectrum and an action that includes only minimally required fields with canonical normalisations and limited set of interactions. Unlike constructions in higher-dimensional supergravity, this model avoids the complexities associated with supersymmetry while preserving key aspects such as confinement and symmetry breaking.

The model presented in these works builds upon earlier work in Ref. [5] and represents a bottom-up holographic model for mechanisms similar to those found in top-down constructions like Refs. [131–133]. However, it is tailored specifically for the context of CHMs, focusing on parameter ranges relevant to our considerations.

To clarify further, unlike the approach taken in Chapter 3, the present study does not dive into exploring relationships involving classical instabilities within certain parameter spaces, as discussed in Ref. [126], nor does it engage with topics like scale invariance spontaneous breaking, unitarity bounds, walking dynamics, etc. which have been extensively discussed in the literature (Refs. [127–129, 139, 185–190]). Instead, the examples presented in later sections of the chapter focus on parameter regions where the background solutions remain stable. Particularly, in the regions of parameter space under consideration, there is no presence of a light dilaton within the spectrum.

In this chapter, we tackle points 4), 5), 6), and 7) concerning the bottom-up model introduced in previous chapters, extending our approach to also add the ability to accommodate more complex cosets and geometries. We weakly gauge the $SO(4)$ subgroup of the global symmetry within the field theory framework. This gauging is facilitated by introducing a spurion field that explicitly breaks $SO(5)$ down to $SO(4)$. Then, we explore the implementation of gauge-fixing procedures within this context, ensuring consistency with the dynamics of the background. Both the gauging of $SO(4)$ and the explicit breaking of $SO(5)$ to $SO(4)$ are governed by actions localised on the boundaries in the gravity theory. The interaction between these newly introduced features and the background dynamics, particularly vacuum (mis)alignment, plays a pivotal role. It determines whether the mass spectra exhibit

$SO(5) \to SO(4)$ breaking, where the gauged $SO(4)$ remains unbroken, or $SO(5) \to SO(3)$ breaking, with the gauged $SO(4)$ subgroup being Higgsed to $SO(3)$.

Compared to the other bottom-up models [169], our model with smooth geometry features a considerable deviation from AdS. Here, the mass gap arises from the appearance of an endpoint in the radial direction, as discussed in Ref. [32]. Symmetry breaking in our setup is initiated by bulk fields, resembling the soft-wall models previously explored in the literature [168, 191, 192]. Due to these distinctive features, certain formal developments deserve special attention and constitute the primary focus of this chapter.

The implications of holographic vacuum misalignment are developed within this simplified model to underscore general outcomes applicable across a broad spectrum of holographic realisations of CHMs. We provide an in-depth discussion of necessary and yet rigorous aspects of the formalism, as well as nuances involved in the weak gauging of symmetry that extends concepts of holographic renormalization [43, 44, 150]. Our aim is to defer the construction of a realistic bottom-up holographic CHM, which involves gauging the standard-model $SU(2)_L \times U(1)_Y \subset SO(4) \times U(1)_{B-L}$ and incorporating fermions either in bulk or at the boundary to a later work.

The remaining parts of the chapter are structured as follows. In Section 5.3, we complete our six-dimensional bottom-up gravity model featuring an $SO(5)$ gauge symmetry discussed in Section 4.1.1. In Section 5.4, we take a detour to discuss a generic description, in effective field theory terms, of non-linear sigma models with the $SO(5)/SO(4)$ coset. This discussion helps clarify the distinctions between the notion of gauge and global symmetries, as well as explicit versus spontaneous symmetry-breaking mechanisms.

Returning to the gravity theory in Section 5.5, we address the incorporation of boundary terms necessary to weakly gauge an $SO(4)$ subgroup of the global $SO(5)$ in the dual field theory. We explore the implications for the vacuum structure of the theory and analyse the resulting pattern of symmetry breaking. Section 5.6 focuses on detailing the vacuum structure, while in Section 5.7, we present the mass spectrum of fluctuations within the gravity theory. Additionally, we provide many technical details in the appendices to complement the main text.

5.3 The gravity model

The bottom-up holographic model is based on the model in Section 4.1.1 in $D = 6$ dimensions with a bulk scalar field, $\mathcal{X}$, transforming in 5 of a gauged $SO(5)$ symmetry, and one dimension is compactified to mimic confinement. We consider background solutions with a non-trivial profile for $\mathcal{X}$, leading to the spontaneous breaking of the $SO(5)$ gauge symmetry on the gravity to its $SO(4)$ subgroup.

5.3.1 Six-dimensional action

The action in $D = 6$ dimensions is rescaled respective to Eq. (4.1.2) by an overall factor of $\frac{1}{2\pi}$ for convenience,

$$\mathcal{S}_6^{(bulk)} = \frac{1}{2\pi}\int \mathrm{d}^6x\sqrt{-\hat{g}_6}\left\{\frac{\mathcal{R}_6}{4} - \frac{1}{2}\hat{g}^{\hat{M}\hat{N}}\left(D_{\hat{M}}\mathcal{X}\right)^T D_{\hat{N}}\mathcal{X} - \mathcal{V}_6(\mathcal{X}) - \frac{1}{2}\,\mathrm{Tr}\left[\hat{g}^{\hat{M}\hat{P}}\hat{g}^{\hat{N}\hat{Q}}\mathcal{F}_{\hat{M}\hat{N}}\mathcal{F}_{\hat{P}\hat{Q}}\right]\right\}. \tag{5.3.1}$$

The convetions and parametrs are described in Section 4.1.1. The detailed field content is summarised in Table 5.1.

For $\langle\phi\rangle \neq 0$, we can write $\mathcal{X}$ explicitly,

$$\mathcal{X} = \phi\left(\sin(|\vec{\pi}|)\frac{\vec{\pi}}{|\vec{\pi}|}, \cos(|\vec{\pi}|)\right)^T, \tag{5.3.2}$$

containing the the four PNGBs, $\vec{\pi} = (\pi^1, \pi^2, \pi^3, \pi^4)$, which span the $SO(5)/SO(4)$ coset.

The dimensional reduction to 5D, Background profiles for the fields and their UV and IR expansions will be followed from Section 4.1.2.

In the previous chapter, we picked $\langle\vec{\pi}\rangle = 0$. However, on this chapter, we will keep the same backgrounds for $\phi(\rho)$, $\chi(\rho)$, and $A(\rho)$, but $\langle\vec{\pi}\rangle \neq 0$ will arise as described in Section 5.5.

Table 5.1. The model field content is categorised based on irreducible representations of symmetries across different dimensions: in $D = 6$ dimensions (as $SO(5)$ multiplets), $D = 5$ dimensions (as $SO(4)$ multiplets, with $\langle \mathcal{X} \rangle \neq 0$), and $D = 4$ dimensions (as $SO(3)$ multiplets, with $\langle \vec{\pi} \rangle \neq 0$). When discussing $D = 4$ dimensions, we describe the field content in terms of representations under the massive representations of the Poincaré group, focusing on gauge-invariant combinations of degrees of freedom. Cases denoted with $N_{\text{dof}} = -$ indicate representations where degrees of freedom are accounted for within propagating degrees of freedom of other fields, forming gauge-invariant states. For the space-time indexes we have, $\hat{M} = 0, 1, 2, 3, 5, 6$, and $M = 0, 1, 2, 3, 5$, while $\mu = 0, 1, 2, 3$. For internal symmetry indices, $\alpha, \beta = 1, \cdots, 5$, with $A = 1, \cdots, 10$, $\hat{A} = 1, \cdots, 4$, and $\bar{A} = 6, \cdots, 10$. After $SO(4)$ to $SO(3)$ breaking, we use the notation $\hat{\mathcal{A}} = 1, 2, 3$, $\tilde{\mathcal{A}} = 5, 6, 7$, and $\bar{\mathcal{A}} = 8, 9, 10$.

$D = 6$, $SO(5)$, massless irreps.			$D = 5$, $SO(4)$, massless irreps.			$D = 4$, $SO(3)$, massive irreps.		
Field	$SO(5)$	N_{dof}	Field	$SO(4)$	N_{dof}	Field	$SO(3)$	N_{dof}
$\hat{g}_{\hat{M}\hat{N}}$	1	9	g_{MN}	1	5	$g_{\mu\nu}$	1	5
						$g_{\mu 5}$	1	–
						g_{55}	1	–
			χ_M	1	3	χ_μ	1	3
						χ_5	1	–
			χ	1	1	χ	1	1
$\mathcal{X}_\alpha$	5	5	ϕ	1	1	ϕ	1	1
			$\pi^{\hat{A}}$	4	4	$\pi^{\hat{\mathcal{A}}}$	3	3
						π^4	1	1
$\mathcal{A}_{\hat{M}\,\alpha}{}^{\beta}$	10	40	$\mathcal{A}_M{}^{\hat{A}}$	4	12	$\mathcal{A}_\mu{}^{\hat{\mathcal{A}}}$	3	9
						$\mathcal{A}_\mu{}^4$	1	3
						$\mathcal{A}_5{}^{\hat{\mathcal{A}}}$	3	–
						$\mathcal{A}_5{}^4$	1	–
			$\mathcal{A}_6{}^{\hat{A}}$	4	4	$\mathcal{A}_6{}^{\hat{\mathcal{A}}}$	3	3
						$\mathcal{A}_6{}^4$	1	1
			$\mathcal{A}_M{}^{\bar{A}}$	6	18	$\mathcal{A}_\mu{}^{\tilde{\mathcal{A}}}$	3	9
						$\mathcal{A}_\mu{}^{\bar{\mathcal{A}}}$	3	9
						$\mathcal{A}_5{}^{\tilde{\mathcal{A}}}$	3	–
						$\mathcal{A}_5{}^{\bar{\mathcal{A}}}$	3	–
			$\mathcal{A}_6{}^{\bar{A}}$	6	6	$\mathcal{A}_6{}^{\tilde{\mathcal{A}}}$	3	3
						$\mathcal{A}_6{}^{\bar{\mathcal{A}}}$	3	3
$P_{5\alpha}$	5	5	$P_{5\,\hat{A}}$	4	4	$P_{5\,\hat{\mathcal{A}}}$	3	3
						P_{54}	1	1
			P_{55}	1	1	P_{55}	1	1

5.4 Effective Field Theory

This section aims to illuminate the role of explicit and spontaneous breaking of internal continuous symmetries within the framework of four-dimensional EFTs. Specifically, we aim to highlight the distinctions and similarities in how global and local symmetries can be treated. It is noteworthy that this section does not present the exact effective field theory description of the main theory discussed elsewhere in this chapter. Our focus here is not on aligning these descriptions, as such an endeavour exceeds the scope of our current objectives.

We begin by formulating the Lagrangian density of a nonlinear sigma model. This captures the long-distance behaviour arising from the spontaneous breaking of a gauged $SO(5)$ symmetry down to its $SO(3)$ subgroup. The field content comprises two real fields, Σ and Ξ, both transforming under 5 of $SO(5)$, such that under a symmetry transformation:

$$(\Sigma, \Xi) \to (U\Sigma, U\Xi),$$

where $U \in SO(5)$ represents a special orthogonal real matrix.

The generators of $SO(5)$, t^A, are normalised as $\mathrm{Tr}\,(t^A t^B) = \frac{1}{2}\delta^{AB}$ and the basis introduced in Appendix C is mostly used in our calculations. The $SO(5)$ symmetry, can be gauged by definition of $A_\mu \equiv \sum_A A_\mu^A t^A$, with the covariant derivatives

$$D_\mu \Sigma \equiv \partial_\mu \Sigma + i\, g\, A_\mu \Sigma\,, \tag{5.4.1}$$

$$D_\mu \Xi \equiv \partial_\mu \Xi + i\, g\, A_\mu \Xi\,, \tag{5.4.2}$$

$$F_{\mu\nu} \equiv \partial_\mu A_\nu - \partial_\nu A_\mu + i\, g\, [A_\mu,\, A_\nu]\ , \tag{5.4.3}$$

with g presenting the (weak) gauge coupling strength. The Lagrangian density respecting

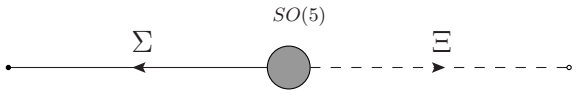

Figure 5.2. Schematic presentation of the $SO(5)/SO(4)$ EFT (figure generated with axodraw2 [193]).

$SO(5)$ is:[1]

$$\begin{aligned}\mathcal{L}_{SO(5)} \equiv & \frac{f^2}{2}\left[(D_\mu\Sigma)^T(D^\mu\Sigma)\right] + \frac{\kappa^2 f^2}{2}\left[(D_\mu\Xi)^T(D^\mu\Xi)\right] \\ & -\frac{1}{2}\mathrm{Tr}\left[F_{\mu\nu}F^{\mu\nu}\right] + (1-\tilde{\kappa}^2)\,\Xi^T F_{\mu\nu}F^{\mu\nu}\Xi \\ & -\lambda_\Sigma f^4\left(\Sigma^T\Sigma-1\right)^2 - \lambda_\Xi f^4\left(\Xi^T\Xi-1\right)^2 - \mathcal{V}_{SO(5)}(\Sigma,\Xi)\,,\end{aligned} \tag{5.4.4}$$

with f parametrising the scale of the theory. Here he couplings are chosen as κ, $\tilde{\kappa}$, λ_Σ, and λ_Ξ. The potential, $\mathcal{V}_{SO(5)}(\Sigma,\Xi)$, and its physical significance will be discussed later here.

We need take a limit on the couplings $\lambda_\Sigma \to +\infty$ and $\lambda_\mathcal{V} \to +\infty$ to impose $\Sigma^T\Sigma = 1 = \Xi^T\Xi$ constraints. These VEVs break $SO(5)$ to potentially two different $SO(4)$ subgroups. In our conventional approach, we select a basis for $SO(5)$ where $t^{\bar{A}}$ (with $\bar{A} = 5,\ldots,10$) are the generators satisfying $t^{\bar{A}}\langle\Xi\rangle = 0$. These generators form an $SO(4)$ subgroup within $SO(5)$. The generators $t^{\hat{A}}$ (with $\hat{A} = 1,\ldots,4$) describe the $SO(5)/SO(4)$ coset.

We then introduce parameterisations for the two scalar fields:

$$\varsigma = \sum_{\hat{A}} \varsigma^{\hat{A}} t^{\hat{A}}, \quad \varrho = \sum_{\hat{A}} \varrho^{\hat{A}} t^{\hat{A}}.$$

as

$$\Sigma = e^{\frac{2i}{f}\varsigma}\begin{pmatrix}0\\0\\0\\0\\1\end{pmatrix}, \qquad \text{and} \qquad \Xi = e^{\frac{2i}{f}\varrho}\begin{pmatrix}0\\0\\0\\0\\1\end{pmatrix}. \tag{5.4.5}$$

In case two VEVs are in the same direction, the $SO(4)$ symmetry is respected. Otherwise, only an $SO(3)$ symmetry is left, by relying on it, one can write the most general vacuum

[1] A term like $\Sigma^T F_{\mu\nu}F^{\mu\nu}\Sigma$ can be added to the Lagrangian. It will change the cubic and quartic interactions; hence, needed to be added to a more complete analysis.

configuration as

$$\langle \Sigma \rangle = \begin{pmatrix} 0 \\ 0 \\ 0 \\ \sin\left(\frac{v}{f}\right) \\ \cos\left(\frac{v}{f}\right) \end{pmatrix}, \qquad \text{and} \qquad \langle \Xi \rangle = \begin{pmatrix} 0 \\ 0 \\ 0 \\ 0 \\ 1 \end{pmatrix}. \tag{5.4.6}$$

A generic value for the $\frac{v}{f}$, the so-called misalignment angle, would lead to the $SO(4)$ to $SO(3)$ breaking. In Eq. (5.4.6), the vacuum is specified by the choices $\langle \varrho \rangle = 0$ and $\langle \varsigma \rangle = v\, t^4$.

Having established the non-linear constraints, the first two lines in Eq. (5.4.4) determine the leading-order, two-derivative terms in the EFT governing all two-point functions, including gauge fields. Higher-derivative terms, which provide minor corrections to observables at low energies, are disregarded. To advance further, we investigate the expected properties of the potential term, $\mathcal{V}_{SO(5)}(\Sigma, \Xi)$, described in Eq. (5.4.4), which governs the vacuum (mis)alignment. The important quantities for current purposes are the position of the potential minimum and its second derivative at this minimum. The first determines the vacuum misalignment angle, while the latter fixes the masses of scalar excitations. Given our omission of interaction terms and higher-order effects, we opt for an illustrative approach for the remainder of this section rather than going into detailed power counting. More realistic and physically motivated choices will be explored in Section 5.4.1. We assume a form for the potential as

$$\mathcal{V}_{SO(5)} = \lambda \frac{f^4}{2} \left(\Xi^T \Sigma - \cos\theta \right)^2 , \tag{5.4.7}$$

with θ and λ, two free parameters related to the mass and VEV. Now, we substitute the configuration of the vacuum given in Eqs. (5.4.6) and study the resulting potential as a function of v:

$$\mathcal{V}_{\text{static}} = -\mathcal{L}_{SO(5)}\Big|_{\varrho=0=A_\mu,\, \varsigma=vt^4} = \frac{\lambda f^4}{2} \left(\cos\left(\frac{v}{f}\right) - \cos\theta \right)^2 . \tag{5.4.8}$$

The minima for the potential will be at $v = \theta f$, along with the second derivative at this point,

$$\frac{\partial^2 \mathcal{V}_{\text{static}}}{\partial v^2}\bigg|_{v=\theta f} = \lambda f^2 \sin^2\theta > 0 \qquad (\text{for } \lambda > 0)\,. \tag{5.4.9}$$

The mass matrix for the spin-0 states, evaluated at $v = \theta f$, reads

$$\mathcal{M}_0^2 = \lambda f^2 \sin^2\theta \begin{pmatrix} 0&0&0&0&0&0&0&0\\ 0&0&0&0&0&0&0&0\\ 0&0&0&0&0&0&0&0\\ 0&0&0&1&0&0&0&-\frac{1}{\kappa}\\ 0&0&0&0&0&0&0&0\\ 0&0&0&0&0&0&0&0\\ 0&0&0&0&0&0&0&0\\ 0&0&0&-\frac{1}{\kappa}&0&0&0&\frac{1}{\kappa^2} \end{pmatrix}, \tag{5.4.10}$$

presented in the basis of $(\varsigma^1, \varsigma^2, \varsigma^3, \varsigma^4, \varrho^1, \varrho^2, \varrho^3, \varrho^4)$. The κ dependence arises due to the normalisation choice in the kinetic terms in $\mathcal{L}_{SO(5)}$. IF $\theta \neq 0$, the seven massless states correspond to NGBs corresponding to the symmetry breaking $SO(5) \to SO(4) \to SO(3)$. Additionally, one scalar field has a mass squared $m_\pi^2 = \frac{1+\kappa^2}{\kappa^2}\lambda f^2 \sin^2(\theta)$.

The matrix $\mathcal{M}_1^2$ containing the mass of the gauge fields, calculated at the minimum of potential, $v = \theta f$, is

$$\frac{4\mathcal{M}_1^2}{g^2 f^2} = \begin{pmatrix} \frac{\cos(2\theta)+2\kappa^2+1}{2\tilde{\kappa}^2} & 0 & 0 & 0 & \frac{\sin(2\theta)}{2\tilde{\kappa}} & 0 & 0 & 0\,0\,0\\ 0 & \frac{\cos(2\theta)+2\kappa^2+1}{2\tilde{\kappa}^2} & 0 & 0 & 0 & \frac{\sin(2\theta)}{2\tilde{\kappa}} & 0 & 0\,0\,0\\ 0 & 0 & \frac{\cos(2\theta)+2\kappa^2+1}{2\tilde{\kappa}^2} & 0 & 0 & 0 & \frac{\sin(2\theta)}{2\tilde{\kappa}} & 0\,0\,0\\ 0 & 0 & 0 & \frac{\kappa^2+1}{\tilde{\kappa}^2} & 0 & 0 & 0 & 0\,0\,0\\ \frac{\sin(2\theta)}{2\tilde{\kappa}} & 0 & 0 & 0 & \sin^2(\theta) & 0 & 0 & 0\,0\,0\\ 0 & \frac{\sin(2\theta)}{2\tilde{\kappa}} & 0 & 0 & 0 & \sin^2(\theta) & 0 & 0\,0\,0\\ 0 & 0 & \frac{\sin(2\theta)}{2\tilde{\kappa}} & 0 & 0 & 0 & \sin^2(\theta) & 0\,0\,0\\ 0 & 0 & 0 & 0 & 0 & 0 & 0 & 0\,0\,0\\ 0 & 0 & 0 & 0 & 0 & 0 & 0 & 0\,0\,0\\ 0 & 0 & 0 & 0 & 0 & 0 & 0 & 0\,0\,0 \end{pmatrix} \tag{5.4.11}$$

provided in the basis $(A_\mu^1, A_\mu^2, A_\mu^3, A_\mu^4, A_\mu^5, A_\mu^6, A_\mu^7, A_\mu^8, A_\mu^9, A_\mu^{10})$. The $\tilde{\kappa}^2$ factors originate from the normalisation of the kinetic terms for the gauge bosons in the case of $\langle \Xi \rangle \neq 0$. Specifically, the kinetic matrix is given by diag $\left(\tilde{\kappa}^2, \tilde{\kappa}^2, \tilde{\kappa}^2, \tilde{\kappa}^2, 1, 1, 1, 1, 1, 1\right)$. In this setup, the three massless states A_μ^8, A_μ^9, and A_μ^{10} correspond to the gauge fields of the unbroken $SO(3)$. In the case of $\theta = 0$, $(A_\mu^1, A_\mu^2, A_\mu^3, A_\mu^4)$ will acquire a mass. When $\theta \neq 0$, with $v = f\theta$,

seven gauge fields find mass, and the seven massless pions are eaten as the longitudinal mode of the gauge field in the Higgs mechanism. Just one real scalar remains massive in the spectrum. Our choice for the unitary gauge is $\varsigma^1 = \varsigma^2 = \varsigma^3 = 0 = \varrho^1 = \varrho^2 = \varrho^3$, and $\varsigma^4 + \kappa\varrho^4 = 0$.

Up to now, all symmetries considered have been local, and only spontaneous symmetry breaking has been implemented. However, this framework is generally applicable and also covers scenarios involving global symmetries and their explicit breaking. In the following, we demonstrate how to systematically take relevant limits and explore more diverse symmetry-breaking patterns. Specifically, we focus on describing a situation where only the $SO(4)$ subgroup of $SO(5)$ is gauged, alongside an additional independent explicit $SO(5)$ breaking to $SO(4)$. Together, these factors induce further spontaneous breaking to $SO(3)$ through vacuum misalignment. Our approach is as follows, building on Eq. (5.4.4).

- the non-linear constraints, $\Sigma^T\Sigma = 1 = \Xi^T\Xi$, are imposed by the limits $\lambda_\Sigma, \lambda_\Xi \to +\infty$. The constant κ, can be rescaled as $\kappa \equiv a\,\tilde{\kappa}$.

- If $\tilde{\kappa} \gg 1$, A^1_μ, A^2_μ, A^3_μ, and A^4_μ have small couplings as their kinetic coefficients are large, and have approximately diagonal mass matrices. Then, one takes another limit, $\tilde{\kappa} \to +\infty$, to get

$$\mathcal{M}_0^2 \to \lambda f^2 \sin^2\theta \,\mathrm{diag}\left(0,0,0,1,0,0,0,0\right), \tag{5.4.12}$$

$$\mathcal{M}_1^2 \to \frac{g^2 f^2}{4}\,\mathrm{diag}\left(a^2,a^2,a^2,a^2,\sin^2(\theta),\sin^2(\theta),\sin^2(\theta),0,0,0\right). \tag{5.4.13}$$

  The unitary gauge is applied by $\varsigma^1 = \varsigma^2 = \varsigma^3 = 0 = \varrho^1 = \varrho^2 = \varrho^3 = \varrho^4 = 0$, where ς^4 still has the role of a physical spin-0 field.

- When $a \gg 1$ and holding g and f (in addition to λ and θ) fixed, the four gauge bosons $A^{\hat{A}}_\mu$ belonging to the $SO(5)/SO(4)$ coset become parametrically heavy and decouple from ς^4. Hence, they can be integrated out. In this limit, $a \to +\infty$, the EFT field content simplifies as follows: Scalar ς^4 with a mass given by $m_\pi^2 = \lambda f^2 \sin^2(\theta)$. There are three massive gauge fields, A^5_μ, A^6_μ, and A^7_μ, emerging from the spontaneous breaking $SO(4) \to SO(3)$. Their masses are $\frac{1}{4}g^2 f^2 \sin^2(\theta)$, and their longitudinal components are ς^1, ς^2, and ς^3 respectively. The remaining gauge bosons A^8_μ, A^9_μ, and A^{10}_μ remain massless. These gauge fields correspond to the unbroken $SO(3)$ subgroup.

As a result, we have the following Lagrangian:

$$\mathcal{L}_{SO(4)} \equiv \frac{f^2}{2}\left[\left(\tilde{D}_\mu\Sigma\right)^T\left(\tilde{D}^\mu\Sigma\right)\right] - \frac{1}{4}\sum_{A=5}^{10} F_{\mu\nu}F^{\mu\nu} - \lambda_\Sigma f^4\left(\Sigma^T\Sigma - 1\right)^2 - \mathcal{V}_{SO(4)}(\Sigma)\,. \tag{5.4.14}$$

Here, the second field, Ξ, is replaced with a spurion, $P_5 = (0, 0, 0, 0, 1)$ with the covariant derivative being restricted to $SO(4)$:

$$\tilde{D}_\mu \Sigma \equiv \partial_\mu \Sigma + i\, g \sum_{A=5}^{10} A_\mu^A t^A \Sigma\,, \tag{5.4.15}$$

similarly for the kinetic terms of the gauge field. By setting $\lambda_\Sigma \to +\infty$, the non-linear constraint $\Sigma^T \Sigma = 1$ is imposed. Based on the choice in Eq. (5.4.7), the potential term is given by $\mathcal{V}_{SO(4)} = \lambda \frac{f^4}{2} \left(P_5^T \Sigma - \cos\theta\right)^2$. This potential induces vacuum misalignment and adds a mass to ς^4. In this case, in the Lagrangian, the global $SO(5)$ is explicitly broken by both the gauging of an $SO(4)$ subgroup as well as by the interaction with the spurion P_5.

To sum up, in the presence of a combination of explicit and spontaneous breaking of continuous global symmetries, it is crucial to only gauge the unbroken subgroups to ensure consistency with the Higgs mechanism. However, there may exist elegant descriptions of the entire system solely in terms of gauge symmetries undergoing spontaneous breaking without reference to the explicit symmetry-breaking terms. If such a formulation can be achieved, the desired physical scenario can be recovered by appropriately taking limits of the parameters.

It is important to exercise caution in the ordering of limits to avoid violations of unitarity, the emergence of ghosts or negative norm states, and to maintain weak coupling throughout the analysis. These considerations ensure the physical consistency and validity of the theory at all stages of investigation.

5.4.1 External fields, Coleman-Weinberg potential, and vacuum misalignment

The potential choice given in Eq. (5.4.7) is convenient due to its simplicity and its ability to induce vacuum misalignment while effectively suppressing the mass of the scalar field ς^4. However, it is acknowledged that this potential is not realistic.

As previously indicated, our interest is primarily in the vacuum misalignment angle and the mass of the scalar field, focusing solely on the two-point functions and not on interaction terms. Therefore, the exact functional form of the potential is not crucial for our current objectives. Nevertheless, it can be insightful to illustrate how a more realistic potential could arise dynamically. In this brief subsection, we will provide a simple example demonstrating such a potential.

To construct an example, we introduce couplings between the EFT and external fermions, taking inspiration from ideas discussed in Eq. (116) of Ref. [169], albeit with significant simplifications. We ensure that the couplings respect an $SO(4) \sim SU(2)_L \times SU(2)_R$ subgroup of $SO(5)$. Instead of implementing a version of top partial compositeness or external fermions that couple to bulk fermions (representing baryons in the dual field theory), we adopt a simpler

mechanism for fermion mass generation. This mechanism is similar to algebraic techniques seen in technicolour theories [56, 61, 194–198]—see also [199–203].

Specifically, we couple fermion bilinears directly to scalar composite operators of the strongly coupled theory, the composite state representing a meson. This approach simplifies our analysis by focusing on the emergence of symmetries and symmetry-breaking patterns rather than the detailed dynamics and precise magnitude of the involved couplings.[2]

We begin with the local identification of $SO(5) \sim Sp(4)$. We choose a useful basis of 4×4 matrices that define the adjoint irreducible representation 10 and the antisymmetric 5 of $Sp(4)$. The basis for the 5 representation is adapted from Refs. [205, 206], with some modifications, as detailed in Appendix C. We express the symplectic matrix Ω as

$$\Omega_{\alpha\beta} \equiv \begin{pmatrix} 0 & 0 & 1 & 0 \\ 0 & 0 & 0 & 1 \\ -1 & 0 & 0 & 0 \\ 0 & -1 & 0 & 0 \end{pmatrix}, \tag{5.4.16}$$

as well as the matrices, T^A, satisfying

$$\Omega T^A + T^{A\,T}\Omega = 0\,, \qquad \text{for} \qquad A = 1, \cdots, 10\,, \tag{5.4.17}$$

for the 10 generators of $Sp(4)$. The Γ^B matrices, which are the Hermitian and traceless matrices are also introduced that satisfy

$$\Omega \Gamma^B - \Gamma^{B\,T}\Omega = 0\,, \qquad \text{for} \qquad B = 1, \cdots, 5\,, \tag{5.4.18}$$

parametrising the 5 of the coset $SU(4)/Sp(4)$, completing the basis of the embedding of $Sp(4)$ in $SU(4)$. The normalisation $\mathrm{Tr}\,(T^A T^B) = \frac{1}{4}\delta^{AB} = \mathrm{Tr}\,(\Gamma^A \Gamma^B)$ is chosen for these matrices.

The elements of Σ, from Eq. (5.4.5), are reorganised to introduce the Hermitian matrix

$$\not{\Sigma}^{\alpha}{}_{\beta} \equiv 4 \sum_{A=1}^{5} \Sigma^A \left(\Gamma^A\right)^{\alpha}{}_{\beta} = \begin{pmatrix} \Sigma^5 & \Sigma^1 - i\Sigma^2 & 0 & -i\Sigma^3 + \Sigma^4 \\ \Sigma^1 + i\Sigma^2 & -\Sigma^5 & i\Sigma^3 - \Sigma^4 & 0 \\ 0 & -i\Sigma^3 - \Sigma^4 & \Sigma^5 & \Sigma^1 + i\Sigma^2 \\ i\Sigma^3 + \Sigma^4 & 0 & \Sigma^1 - i\Sigma^2 & -\Sigma^5 \end{pmatrix}. \tag{5.4.19}$$

[2] In a more realistic construction, one would like to extend to gauging the $SU(2)_L \times U(1)_Y$ subgroup of $SO(4) \times U(1)_{B-L}$ within the standard model context. Additionally, it would involve introducing bulk fermion fields transforming appropriately under these symmetry groups. Such refinements are deferred to future work, particularly in exploring the interplay between fermion partial compositeness and vacuum misalignment [169, 174, 204].

Similarly, for Ξ, we define $\not{\Xi}^{\alpha}{}_{\beta} \equiv 4\sum_{A=1}^{5}\Xi^{A}\left(\Gamma^{A}\right)^{\alpha}{}_{\beta}$. Both these fields are in the adjoint representation

$$(\not{\Sigma}, \not{\Xi}) \to (\tilde{U}\not{\Sigma}\tilde{U}^{\dagger}, \tilde{U}\not{\Xi}\tilde{U}^{\dagger}), \tag{5.4.20}$$

with $\tilde{U} = \exp\left(i\sum_{A=1}^{10}\alpha^{A}T^{A}\right)$, 4×4 unitary matrices that describe the $Sp(4)$ transformations. Now, $\tilde{\Sigma} \equiv \not{\Sigma}\Omega$ will be a 4×4 antisymmetric matrix in 5 of $Sp(4)$. Similarly for $\tilde{\Xi} \equiv \not{\Xi}\Omega$:

$$(\tilde{\Sigma}, \tilde{\Xi}) \to (\tilde{U}\tilde{\Sigma}\tilde{U}^{T}, \tilde{U}\tilde{\Xi}\tilde{U}^{T}). \tag{5.4.21}$$

We introduce $\psi_{L\alpha}$ and $\psi_{R\alpha}$ as the chiral fermions. These furnish 4 of $Sp(4)$, which happens to be the spinorial representation of $SO(5)$. We break the symmetry explicitly by presenting the fermions as incomplete multiplets:

$$\psi_L = \begin{pmatrix} t_L \\ 0 \\ b_L \\ 0 \end{pmatrix}, \qquad \text{and} \qquad \tilde{\psi}_R = \Omega^{-1}\psi_R = \Omega^{T}\begin{pmatrix} t_R \\ 0 \\ b_R \\ 0 \end{pmatrix} = \begin{pmatrix} -b_R \\ 0 \\ t_R \\ 0 \end{pmatrix}. \tag{5.4.22}$$

Each entry of the matrix represents a chiral spinor with 2-component. This notation hints that in an extension of the standard model, these spinors could potentially represent the top and bottom quarks, although they do not carry QCD colour quantum numbers.

To complete the picture, we incorporate into the Lagrangian density, couplings between scalars and fermions as

$$\mathcal{L}_Y = -yf\overline{\psi_L}\left(\tilde{\Sigma} - \tilde{\Xi}\right)\tilde{\psi}_R + \text{h.c.}, \tag{5.4.23}$$

The Yukawa coupling is y in this equation. In case $\langle\tilde{\Sigma}\rangle \neq 0 \neq \langle\tilde{\Xi}\rangle$, one has:

$$\mathcal{L}_Y = -\overline{t_L}\left[y\,f\left(\cos\left(\frac{v}{f}\right)-1\right)\right]t_R - \overline{b_L}\left[y\,f\left(\cos\left(\frac{v}{f}\right)-1\right)\right]b_R + \text{h.c.} + \cdots, \tag{5.4.24}$$

where the interactions with the PNGBs are omited. The Dirac mass matrices obtained here will break $SU(2)_L \times SU(2)_R \sim SO(4)$, while preserving the diagonal $SU(2) \sim SO(3)$ subgroup with the fermion mass $\mathcal{M}_{1/2} = y\,f\left(\cos\left(\frac{v}{f}\right)-1\right)$. If there is a vacuum alignment, the mass vanishes, $\langle\tilde{\Sigma}\rangle = \langle\tilde{\Xi}\rangle$.

At the one-loop perturbative level, the symmetry-breaking terms, induced by the Yukawa coupling and the gauging of $SO(4)$, generate a divergent input of the Coleman-Weinberg form [207] to the effective potential, denoted as $\mathcal{V}_{\text{CW}}$. Introducing the matrix $T \equiv \text{diag}(1,0,1,0)$,

the initial form of $\mathcal{V}_{\rm CW}$ reads

$$\mathcal{V}_{\rm CW} = \frac{\Lambda^2}{32\pi^2}\mathcal{S}\,\mathrm{Tr}\{\mathcal{M}\}^2 \tag{5.4.25}$$

$$= \frac{\Lambda^2}{32\pi^2}\left(3g^2f^2\sum_{A=5}^{10}\Sigma^T t^A t^A \Sigma - 4y^2f^2\,\mathrm{Tr}\left[\left(\tilde{\Sigma} - \tilde{\Xi}\right)T\left(\tilde{\Sigma} - \tilde{\Xi}\right)^\dagger T\right]\right)\Bigg|_{\tilde{\Sigma},\,\tilde{\Xi}=\langle\tilde{\Sigma}\rangle,\langle\tilde{\Xi}\rangle} \tag{5.4.26}$$

This potential has explicit dependence on the Λ, as a divergent cutoff, requiring introducing counter-terms and the adoption of a subtraction scheme. To achieve this, we introduce two free parameters, denoted as C_g and C_t, which control the overall magnitude of terms proportional to g^2 and y^2 respectively. Typically, these parameters are of order $\mathcal{O}(1)$.

Given an estimate $\Lambda \sim \mathcal{O}(4\pi f)$, we complete the Lagrangian density in Eq. (5.4.4) by incorporating to the potential

$$\mathcal{V}_{SO(4)} = \frac{3}{2}g^2f^4C_g\sum_{A=5}^{10}\Sigma^T t^A t^A \Sigma - 2y^2f^4C_t\,\mathrm{Tr}\left[\left(\tilde{\Sigma} - \tilde{\Xi}\right)T\left(\tilde{\Sigma} - \tilde{\Xi}\right)^\dagger T\right]\Bigg|_{\tilde{\Sigma},\,\tilde{\Xi}=\langle\tilde{\Sigma}\rangle,\langle\tilde{\Xi}\rangle} \tag{5.4.27}$$

$$= \frac{9}{8}g^2f^4C_g\sin^2\left(\frac{v}{f}\right) - 4y^2f^4C_t\left(\cos\left(\frac{v}{f}\right)-1\right)^2. \tag{5.4.28}$$

While the potential described in Eq. (5.4.27) differs from Eq. (5.4.7), it is straightforward to recognise that a potential structured as in Eq. (5.4.27) will ultimately induce vacuum misalignment. Moreover, it will exhibit the same long-distance features as those derived from Eq. (5.4.7). Our focus remains on understanding the vacuum structure and the mass of the scalar excitation around the vacuum, rather than on the interactions or the detailed form of the potential away from its minimum. Additionally, there exist various possibilities for the fermion sector that can produce other one-loop potentials. This model can also be extended to incorporate fermion partial compositeness. In such extensions, the divergences in the potential can be less severe or absent altogether, depending on the specific details of the model. Having explored these aspects, we now conclude this discussion and return to considerations related to the gravity theory.

5.5 Boundary terms and action to quadratic order

In this section, we revisit the gravity model and its interpretation through holography, aiming to construct a model whose long-distance behaviour captures the qualitative features of the EFT discussed in Section 5.4.

To achieve this, we gauge an $SO(4)$ subgroup of the global $SO(5)$symmetry in 4D dual theory. The explicit breaking of $SO(5)$ to $SO(4)$ is implemented by adding interactions localised at the boundary of the 5D gravity discussed in Section 5.3. We maintain a general

treatment of these explicit symmetry-breaking terms, without specifying their exact origin in terms of either field theory or higher-dimensional gravity considerations. These details are left for future investigations. We also avoid performing a perturbative effective potential analysis similar to Coleman-Weinberg [207], as discussed in Section 5.4.1. Our focus remains specifically on determining the misalignment angle and the mass of the lightest scalar states. The shape of the effective potential and higher-order corrections are considered beyond the scope of this current study.

On the gravity side, the challenge arises because the $SO(5)$ symmetry is gauged, prohibiting the introduction of explicit terms that break this symmetry directly. As discussed in Section 5.4, this issue can be addressed by reformulating the entire action in a $SO(5)$-invariant manner. This is achieved by introducing a new field, P_5, which transforms under the 5 representation of $SO(5)$ and is localised at the UV boundary. By incorporating P_5, explicit breaking of $SO(5)$ down to $SO(4)$ can be effectively reintroduced into the theory without violating unitarity or introducing other undesirable pathologies. This is achieved through appropriate limits that systematically decouple additional degrees of freedom, preserving the underlying symmetries and ensuring the consistency of the theory.

The terms introduced at the boundary to the gravity model are crucial for gauging a subgroup of the global symmetry in the dual field theory. These terms also add explicit breaking of global symmetries in a manner that induces vacuum misalignment and spontaneous breaking of the $SO(4)$ gauge symmetry in the dual field theory down to its $SO(3)$ subgroup.

The background solutions of interest spontaneously break the $SO(5)$ symmetry to $SO(4)$ due to the radial dependence of the ϕ bulk scalar. Additionally, the boundary conditions imposed on the background fields fix a constant value for $\pi^{\hat{A}}$, further breaking $SO(4)$ to $SO(3)$ spontaneously. The detailed radial profiles of all other background fields were previously discussed in Section 3.2 and remain consistent with those presented in Ref. [6]. To conclude this section, we expand the action of the model to second-order around these background solutions. This expansion is formulated in a way that is appropriate for computing the spectrum of fluctuations, as discussed in Section 5.7. This approach will enable us to analyse the physical spectrum of excitations around the vacuum configuration.

5.5.1 Boundary-localised interactions

In 5D, we add two boundaries at finite radial positions, $\rho = \rho_i$, with $i = 1, 2$, to play the role of regulators; The limits $\rho_1 \to \rho_o$ and $\rho_2 \to \infty$ will be performed at the end of the calculation. Similar to the Table 5.1, space-time indexes at the boundary are $\mu = 0, 1, 2, 3$. Several boundary terms are added the bulk action, $\mathcal{S}_5^{(bulk)}$,—denoted as $\mathcal{S}_{\text{GHY},i}$, $\mathcal{S}_{\lambda,i}$, $\mathcal{S}_{P_5,2}$,

$\mathcal{S}_{\mathcal{V}_4,2}$, $\mathcal{S}_{\mathcal{A},2}$, $\mathcal{S}_{\chi,2}$, and $\mathcal{S}_{\mathcal{X},2}$—to reach to the desired action, $\mathcal{S}_5$:

$$\mathcal{S}_5 = \mathcal{S}_5^{(bulk)} + \sum_{i=1,2} \Big(\mathcal{S}_{\mathrm{GHY},i} + \mathcal{S}_{\lambda,i} \Big) + \mathcal{S}_{P_5,2} + \mathcal{S}_{\mathcal{V}_4,2} + \mathcal{S}_{\mathcal{A},2} + \mathcal{S}_{\chi,2} + \mathcal{S}_{\mathcal{X},2} \,. \tag{5.5.1}$$

Here, actions with subscript $i = 1, 2$ are at positions $\rho = \rho_i$. Each of these terms will be discussed in both gravity and field-theory context.

$\mathcal{S}_{\mathrm{GHY},i}$ (The Gibbons-Hawking-York boundary terms) is written as

$$\mathcal{S}_{\mathrm{GHY},i} = (-)^i \int \mathrm{d}^4x \sqrt{-\tilde{g}}\, \frac{K}{2} \bigg|_{\rho=\rho_i} , \tag{5.5.2}$$

where $\tilde{g}$ is the determinant of $\tilde{g}_{MN}$, the induced metric on the boundaries. The extrinsic curvatureis denoted as K and $\lambda_i(\mathcal{X}, \chi, \mathcal{A}_6)$ are boundary-localised potentials for scalars, that are respecting $SO(5)$ symmetry,

$$\mathcal{S}_{\lambda,i} = (-)^i \int \mathrm{d}^4x \sqrt{-\tilde{g}}\, \lambda_i(\mathcal{X}, \chi, \mathcal{A}_6) \bigg|_{\rho=\rho_i} . \tag{5.5.3}$$

Both types of boundary terms are essential to ensure the variational problem is well-posed in the holographic setup. They play an important role in allowing the background solutions to be consistently truncated at the boundaries located at $\rho = \rho_i$.

The terms $\mathcal{S}_{P_5,2}$ and $\mathcal{S}_{\mathcal{V}_4,2}$ at UV boundary, contain the bulk scalar, $\mathcal{X}$, and introduce a new boundary-localized field, P_5, which transforms as the 5 of $SO(5)$. The P_5 field is referred to as a spurion because its dynamics are effectively frozen in the appropriate limits.

These terms have a qualitative structure and implications analogous to those seen in the second, sixth, and seventh terms of the Lagrangian of Eq. (5.4.4). They are expressed as follows:

$$\mathcal{S}_{P_5,2} = \int \mathrm{d}^4x \sqrt{-\tilde{g}} \bigg\{ -\frac{1}{2} K_5\, \tilde{g}^{\mu\nu} \left(D_\mu P_5\right) D_\nu P_5 - \lambda_5 \left(P_5^T P_5 - v_5^2\right)^2 \bigg\} \bigg|_{\rho=\rho_2} , \tag{5.5.4}$$

$$\mathcal{S}_{\mathcal{V}_4,2} = - \int \mathrm{d}^4x \sqrt{-\tilde{g}}\, \mathcal{V}_4(\mathcal{X}, \chi, P_5) \bigg|_{\rho=\rho_2} . \tag{5.5.5}$$

Here K_5, λ_5, and v_5 are free parameters and the $\mathcal{V}_4(\mathcal{X}, \chi, P_5)$ potential is invariant under $SO(5)$. Besides χ, it also depends on two invariants, $\phi \equiv \sqrt{\mathcal{X}^T \mathcal{X}}$ and $\psi \equiv \mathcal{X}^T P_5$.

For a constant and boundary-localised P_5, the background equation for it reads

$$4\lambda_5 (P_5^T P_5 - v_5^2) P_{5\,\alpha} + \frac{\partial \mathcal{V}_4}{\partial \psi} \mathcal{X}_\alpha = 0 \,. \tag{5.5.6}$$

By taking the limit $\lambda_5 \to \infty$, we freeze one component of the spurion P_5, denoted as

$|P_5| = v_5$. To maintain $SO(5)$ invariance, we fix the background value of P_5 along its fifth component:

$$\overline{P_5} \equiv (0,0,0,0,v_5)^T . \tag{5.5.7}$$

In the next section, we will discuss a limit involving K_5, which decouples the remaining four degrees of freedom of the spurion P_5. There is the assumption that there is a value of ψ for which $\partial_\psi \mathcal{V}_4 = 0$. Since $\mathcal{V}_4$ depends on $SO(5)$ invariants χ, $\mathcal{X}$, and $|\vec{\pi}|$, it respects $SO(4)$ too. Thus, $\mathcal{S}_{\mathcal{V}_4}$ is effectively a boundary-localised potential for $\mathcal{X}$ (and χ) at UV, capturing the explicit breaking of $SO(5)$ to $SO(4)$ induced by an external sector.[3] The mechanism described in Section 5.4 is applied within the framework of five-dimensional gravity with boundaries by the above-mentioned steps. The term, $S_{A,2}$ provides the (weak) gauging of an $SO(4) \subset SO(5)$ subgroup of the global symmetry in the dual field theory side in the gravity theory. One has

$$\mathcal{S}_{\mathcal{A},2} = \int \mathrm{d}^4x\sqrt{-\tilde{g}}\left\{ -\frac{\hat{D}_2}{v_5^2}\,\tilde{g}^{\mu\rho}\tilde{g}^{\nu\sigma}P_5^T\mathcal{F}_{\mu\nu}\mathcal{F}_{\rho\sigma}P_5 - \frac{1}{4}\bar{D}_2\,\tilde{g}^{\mu\rho}\tilde{g}^{\nu\sigma}\left(\mathcal{F}^A_{\mu\nu}\mathcal{F}^A_{\rho\sigma} - \frac{4}{v_5}P_5^T\mathcal{F}_{\mu\nu}\mathcal{F}_{\rho\sigma}P_5\right)\right\}\Bigg|_{\rho=\rho_2} . \tag{5.5.8}$$

By fixing the spurion $P_5 = \overline{P_5}$, we get

$$\mathcal{S}_{\mathcal{A},2}\big|_{P_5=\overline{P_5}} = \int \mathrm{d}^4x\sqrt{-\tilde{g}}\left\{ -\frac{1}{4}\hat{D}_2\,\tilde{g}^{\mu\rho}\tilde{g}^{\nu\sigma}\mathcal{F}^{\hat{A}}_{\mu\nu}\mathcal{F}^{\hat{A}}_{\rho\sigma} - \frac{1}{4}\bar{D}_2\,\tilde{g}^{\mu\rho}\tilde{g}^{\nu\sigma}\mathcal{F}^{\bar{A}}_{\mu\nu}\mathcal{F}^{\bar{A}}_{\rho\sigma}\right\}\Bigg|_{\rho=\rho_2} . \tag{5.5.9}$$

To illustrate how the coefficients $\hat{D}_2$ and $\bar{D}_2$ relate to the gauge coupling of $SO(4)$ in the field theory context, we note that these coefficients are similar to terms that are analogous to the third and fourth terms in the Lagrangian density given by Eq. (5.4.4). Their role will be described later.

During the circle reduction process, an Abelian symmetry is formed in the five-dimensional gravity theory. This symmetry necessitates the inclusion of a boundary action for the $U(1)$ gauge field:

$$\mathcal{S}_{\chi,2} = \int \mathrm{d}^4x\sqrt{-\tilde{g}}\left\{ -\frac{1}{4}D_{\chi,2}\,\tilde{g}^{\mu\rho}\tilde{g}^{\nu\sigma}F^{(\chi)}_{\mu\nu}F^{(\chi)}_{\rho\sigma}\right\}\Bigg|_{\rho=\rho_2} , \tag{5.5.10}$$

where $D_{\chi,2}$ is a constant necessary for the holographic renormalisation and possibly divergent. This term does not play a significant role in our purposes.

On the contrary, the next term is required for holographic renormalisation and carries an

[3] In subsequent discussions, we assume $\mathcal{V}_4$ is written in a way that at $P_5 = \overline{P_5}$, it is v_5 independent.

important role in the work, which is an action for the bulk scalar, $\mathcal{X}$, at the boundary:

$$\mathcal{S}_{\mathcal{X},2} = \int \mathrm{d}^4x\sqrt{-\tilde{g}}\left\{-\frac{1}{2}K_{\mathcal{X},2}\,\tilde{g}^{\mu\nu}(D_\mu\mathcal{X})^T D_\nu\mathcal{X}\right\}\Bigg|_{\rho=\rho_2}. \tag{5.5.11}$$

The final action of the model also incorporates gauge-fixing terms necessary to establish the R_ξ gauge. Details of these terms are provided in the Appendix D, following the formalism outlined in Ref. [118], with adjustments made to accommodate the treatment of the additional boundary-localised spurion.

5.5.2 Boundary conditions for the background solutions

The equations of motion satisfied by the background fields in the bulk, Eqs. (4.1.14)–(4.1.16), are not altered by the addition of the boundary localised terms. The boundary conditions change compared to the previous chapter, as:

$$\begin{aligned}
&\left(\partial_r\mathcal{X}_\alpha - \frac{\partial\lambda_1}{\partial\mathcal{X}_\alpha}\right)\Bigg|_{\rho_1} = 0\,, \qquad \left(\partial_r\mathcal{X}_\alpha - \frac{\partial\lambda_2}{\partial\mathcal{X}_\alpha} + \frac{\partial\mathcal{V}_4}{\partial\mathcal{X}_\alpha}\right)\Bigg|_{\rho_2} = 0\,,\\
&\left(6\partial_r\chi - \frac{\partial\lambda_1}{\partial\chi}\right)\Bigg|_{\rho_1} = 0\,, \qquad \left(6\partial_r\chi - \frac{\partial\lambda_2}{\partial\chi} + \frac{\partial\mathcal{V}_4}{\partial\chi}\right)\Bigg|_{\rho_2} = 0\,,\\
&\left(\frac{3}{2}\partial_r A + \lambda_1\right)\Bigg|_{\rho_1} = 0\,, \qquad \left(\frac{3}{2}\partial_r A + \lambda_2 - \mathcal{V}_4\right)\Bigg|_{\rho_2} = 0\,.
\end{aligned} \tag{5.5.12}$$

Remembering $\psi = \mathcal{X}^T P_5$, and $P_5 = \overline{P_5} = (0,0,0,0,v_5)^T$, one can rewrite the second equation, at $\rho = \rho_2$ (the UV boundary), as follows:

$$0 = \left(\left[\partial_r\phi - \frac{\partial\lambda_2}{\partial\phi} + \frac{\partial\mathcal{V}_4}{\partial\phi}\right]\frac{\mathcal{X}_\alpha}{\phi} + 2i\partial_r\pi^{\hat{A}}(t^{\hat{A}})_\alpha{}^\beta\mathcal{X}_\beta + \frac{\partial\mathcal{V}_4}{\partial\psi}\overline{P_5}_\alpha\right)\Bigg|_{\rho_2}. \tag{5.5.13}$$

By imposing the algebraic constraints of

$$\partial_r\phi|_{\rho_2} = \left(\frac{\partial\lambda_2}{\partial\phi} - \frac{\partial\mathcal{V}_4}{\partial\phi}\right)\Bigg|_{\rho_2}, \qquad \partial_r\pi^{\hat{A}}|_{\rho_2} = 0\,, \qquad \frac{\partial\mathcal{V}_4}{\partial\psi} = 0\,. \tag{5.5.14}$$

the previous equation can be solved.

The boundary conditions of ϕ, χ, and A fields are minimally affected by the presence of $\mathcal{V}_4$. Any modifications induced by $\mathcal{V}_4$ can be absorbed into a redefinition of the λ_i boundary potentials. Therefore, there are no new elements introduced in this regard, and the solutions

remain consistent with those presented in Section 4.1.1.[4]

The primary difference lies in how the third condition in Eq. (5.5.14) is implemented. Specifically, we select $\vec{\pi}$ such that $|\vec{\pi}| = v$, where v characterises the vacuum misalignment angle and controls the spontaneous breaking to $SO(3)$ symmetry. We assume that without loss of generality, only the fourth component of the vector $\vec{\pi}$ is non-vanishing on the background solutions, hence $\pi^4 = v$, which aligns with the discussion in Section 5.4.

5.5.3 Truncation of the action to quadratic order

The primary goal of this paper is computing the mass spectrum of fluctuations around the identified gravity backgrounds, which correspond to the vacuum configurations in the dual field theory. To facilitate this calculation, we simplify the action by expanding it in terms of the fields that deviate from their vacuum values and truncating the resulting action to quadratic order. This approximation captures all necessary information to compute two-point functions, which are crucial for understanding the spectrum of bound states in the field theory.[5] Throughout this process, we maintain the full functional dependence of the action on fields ϕ, χ, and g_{MN} that have non-trivial profiles.

We fix the background value of the spurion P_5 to $\overline{P_5}$ by taking the limit where $\lambda_5 \to \infty$, ensuring that the mass of its fifth component is infinite. Consequently, we consider only the first four components of P_5 as small perturbations.

The resulting truncated five-dimensional action at quadratic order is expressed as:

$$\mathcal{S}_5^{(2)} = \mathcal{S}_5^{(bulk,2)} + \mathcal{S}_{P_5,2}^{(2)} + S_{\mathcal{V}_4,2}^{(2)} + \sum_{i=1,2} \mathcal{S}_{4,i}^{(2)} \,, \tag{5.5.17}$$

with $\mathcal{S}_5^{(\text{bulk},2)}$ representing the bulk part of the action, $\mathcal{S}_{P_5,2}^{(2)}$ and $S_{\mathcal{V}_4,2}^{(2)}$ denote the boundary actions localised at $\rho = \rho_2$, and $\mathcal{S}_{4,i}^{(2)}$ are localised at $\rho = \rho_i$ for $i = 1, 2$. In the following part, we will explicitly outline the forms of these terms.

To analyse the fluctuations around the background where $\pi^4 = v$, breaking $SO(4)$ to $SO(3)$, we adopt indices suited to $SO(3)$ conventions: $\hat{\mathcal{A}} = 1, 2, 3$, $\tilde{\mathcal{A}} = 5, 6, 7$ for the broken

[4] If we consider that we have already obtained background solutions $\phi^{(0)}$, $\chi^{(0)}$, $A^{(0)}$ from the system without $\mathcal{V}_4$, as discussed in Section 3.2, these solutions adhere to the boundary conditions determined by the boundary term $\lambda_2^{(0)}$. Then, after inclusion of $\mathcal{V}_4$, one may write

$$\lambda_2(\phi, \chi, \mathcal{A}_6) = \lambda_2^{(0)}(\phi, \chi, \mathcal{A}_6) + \mathcal{V}_4(\phi^{(0)}, \chi^{(0)}, |\vec{\pi}| = v) \tag{5.5.15}$$

$$+ \left(\phi - \phi^{(0)}\right) \frac{\partial \mathcal{V}_4}{\partial \phi}(\phi^{(0)}, \chi^{(0)}, |\vec{\pi}| = v) + \left(\chi - \chi^{(0)}\right) \frac{\partial \mathcal{V}_4}{\partial \chi}(\phi^{(0)}, \chi^{(0)}, |\vec{\pi}| = v) \,, \tag{5.5.16}$$

In this case, one can choose the potentials in order to have the same background solutions for ϕ, χ, and A again to solve the new boundary conditions. Therefore, the solutions of ϕ, χ, and A fields remain exactly as presented in Section 3.2, regardless of the inclusion of $\mathcal{V}_4$.

[5] It is essential to note that the gauging of $SO(4)$ must be sufficiently weak for this approach to be valid. We will revisit and elaborate on this point later in the chapter and in the appendices.

other generators of $SO(5)$, and $\bar{\mathcal{A}} = 8, 9, 10$ for the remaining unbroken $SO(3)$ generators. The fluctuation of π^4 written as $\pi^4 = v + \Pi^4$. The physical mass eigenstates in the spin-1 sector arise from mixing between the $\hat{\mathcal{A}}$ and $\tilde{\mathcal{A}}$ indices. For clarity and simplicity in the equations, we define the following linear combinations:

$$\mathcal{B}_6^{\hat{\mathcal{A}}} = \cos(v)\mathcal{A}_6^{\hat{\mathcal{A}}} + \sin(v)\mathcal{A}_6^{\hat{\mathcal{A}}+4}\,, \tag{5.5.18}$$

$$\mathcal{B}_6^{\tilde{\mathcal{A}}} = -\sin(v)\mathcal{A}_6^{\tilde{\mathcal{A}}-4} + \cos(v)\mathcal{A}_6^{\tilde{\mathcal{A}}}\,, \tag{5.5.19}$$

$$\mathcal{B}_M{}^{\hat{\mathcal{A}}} = \cos(v)\mathcal{A}_M{}^{\hat{\mathcal{A}}} + \sin(v)\mathcal{A}_M{}^{\hat{\mathcal{A}}+4}\,, \tag{5.5.20}$$

$$\mathcal{B}_M{}^{\tilde{\mathcal{A}}} = -\sin(v)\mathcal{A}_M{}^{\tilde{\mathcal{A}}-4} + \cos(v)\mathcal{A}_M{}^{\tilde{\mathcal{A}}}\,. \tag{5.5.21}$$

Thus, the following set of basis for the fields in the model is adopted, except for the metric, that allows us to fluctuate over the background:[6]

$$\Phi^a = \{\phi, \chi\}\,, \tag{5.5.22}$$

$$\Phi^{(0)a} = \{\mathcal{B}_6^{\hat{\mathcal{A}}}, \mathcal{A}_6^4, \mathcal{B}_6^{\tilde{\mathcal{A}}}, \mathcal{A}_6^{\bar{\mathcal{A}}}\}\,, \tag{5.5.23}$$

$$V_M{}^A = \{\chi_M, \mathcal{B}_M{}^{\hat{\mathcal{A}}}, \mathcal{A}_M{}^4, \mathcal{B}_M{}^{\tilde{\mathcal{A}}}, \mathcal{A}_M{}^{\bar{\mathcal{A}}}\}\,, \tag{5.5.24}$$

$$\mathcal{H}_M^{(1)A} = \left\{0, \frac{\sin(v)}{v}\partial_M\pi^{\hat{\mathcal{A}}} + \frac{g}{2}\mathcal{B}_M{}^{\hat{\mathcal{A}}}, \partial_M\Pi^4 + \frac{g}{2}\mathcal{A}_M{}^4, 0, 0\right\}. \tag{5.5.25}$$

The action is rewritten here, for the bulk part,

$$\begin{aligned}\mathcal{S}_5^{(bulk,2)} = \int \mathrm{d}^5x\sqrt{-g_5}\Big\{&\frac{R}{4} - \frac{1}{2}g^{MN}G_{ab}\partial_M\Phi^a\partial_N\Phi^b - \mathcal{V}_5(\Phi^a)\\ &- \frac{1}{2}g^{MN}G^{(0)}_{ab}\partial_M\Phi^{(0)a}\partial_N\Phi^{(0)b} - \frac{1}{2}m^{(0)2}_{ab}\Phi^{(0)a}\Phi^{(0)b}\\ &- \frac{1}{2}g^{MN}G^{(1)}_{AB}\mathcal{H}_M^{(1)A}\mathcal{H}_N^{(1)B} - \frac{1}{4}g^{MO}g^{NP}H^{(1)}_{AB}F_{MN}{}^AF_{OP}{}^B\Big\}\,,\end{aligned} \tag{5.5.26}$$

with $F_{MN}{}^A \equiv 2\partial_{[M}V_{N]}{}^A$, and the scalar potential as $\mathcal{V}_5(\phi, \chi) = e^{-2\chi}\mathcal{V}_6(\phi)$. All of the entries of the sigma-model matrices which are independent of v are reproduced here, [6]:

$$G_{ab} = \mathrm{diag}\,(1, 6)\,, \qquad G^{(0)} = \left(\begin{array}{c|c} e^{-6\chi}\mathbb{1}_{4\times4} & \\ \hline & e^{-6\chi}\mathbb{1}_{6\times6}\end{array}\right), \qquad \frac{m^{(0)2}}{g^2} = \left(\begin{array}{c|c} \frac{1}{4}\phi^2e^{-8\chi}\mathbb{1}_{4\times4} & \\ \hline & \mathbb{0}_{6\times6}\end{array}\right),$$

$$G^{(1)} = \left(\begin{array}{c|c|c} 0 & & \\ \hline & \phi^2\,\mathbb{1}_{4\times4} & \\ \hline & & \mathbb{0}_{6\times6}\end{array}\right), \qquad H^{(1)} = \left(\begin{array}{c|c|c} \frac{1}{4}e^{8\chi} & & \\ \hline & e^{2\chi}\,\mathbb{1}_{4\times4} & \\ \hline & & e^{2\chi}\,\mathbb{1}_{6\times6}\end{array}\right). \tag{5.5.27}$$

[6] For $v = 0$, this basis, up to a reordering of the fields, matches with Ref. [6] and Chapter 4.

For the boundary-localised actions, $S^{(2)}_{P_5,2}$, $S^{(2)}_{\mathcal{V}_4,2}$, and $\mathcal{S}^{(2)}_{4,i}$, by using the variables

$$\begin{aligned}\mathcal{P}^{(1)\,\hat{A}}_{5\,\mu} &= \left\{\partial_\mu P_5^{\hat{\mathcal{A}}} + \frac{g v_5}{2}\mathcal{A}_\mu{}^{\hat{\mathcal{A}}}, \partial_\mu P_5^4 + \frac{g v_5}{2}\mathcal{A}_\mu{}^4\right\} \\ &= \left\{\partial_\mu P_5^{\hat{\mathcal{A}}} + \frac{g v_5}{2}\left(\cos(v)\mathcal{B}_\mu{}^{\hat{\mathcal{A}}} - \sin(v)\mathcal{B}_\mu{}^{\hat{\mathcal{A}}+4}\right), \partial_\mu P_5^4 + \frac{g v_5}{2}\mathcal{A}_\mu{}^4\right\}, \end{aligned} \tag{5.5.28}$$

one has

$$S^{(2)}_{P_5} = \int \mathrm{d}^4x\sqrt{-\tilde{g}}\left\{-\frac{1}{2}\tilde{g}^{\mu\nu}K_5\delta_{\hat{A}\hat{B}}\mathcal{P}^{(1)\,\hat{A}}_{5\,\mu}\mathcal{P}^{(1)\,\hat{B}}_{5\,\nu}\right\}\Bigg|_{\rho=\rho_2}. \tag{5.5.29}$$

The quadratic order expansion of $\mathcal{V}_4$ can be formally given as

$$S^{(2)}_{\mathcal{V}_4,2} = -\int \mathrm{d}^4x\sqrt{-\tilde{g}}\left\{\mathcal{V}^{(0)}_4(\phi,\chi,v) + \mathcal{V}^{(2)}_4(\phi,\chi,v,P_5^4,\Pi^4)\right\}\Bigg|_{\rho=\rho_2}, \tag{5.5.30}$$

with $\mathcal{V}^{(0)}_4$, the zeroth-order contribution, computed for the background solution and

$$\mathcal{V}^{(2)}_4 = \frac{1}{2}\partial_v^2\mathcal{V}_4\left(\Pi^4 - \frac{P_5^4}{v_5}\right)^2, \qquad \text{with} \qquad \partial_v^2\mathcal{V}_4 = \sin^2(v)\phi^2 v_5^2\frac{\partial^2\mathcal{V}_4}{\partial\psi^2}, \tag{5.5.31}$$

at second order.

The $\mathcal{S}^{(2)}_{4,i}$ term reads

$$\begin{aligned}\mathcal{S}^{(2)}_{4,i} = (-)^i\int \mathrm{d}^4x\sqrt{-\tilde{g}}\Bigg\{&\frac{K}{2} + \lambda_i - \frac{1}{2}\tilde{g}^{\mu\nu}K_{\mathcal{X},i}\partial_\mu\phi\partial_\nu\phi \\ &- \frac{1}{2}\tilde{g}^{\mu\nu}C^{(1)}_{i\,AB}\mathcal{H}^{(1)\,A}_\mu\mathcal{H}^{(1)\,B}_\nu - \frac{1}{4}\tilde{g}^{\mu\sigma}\tilde{g}^{\nu\gamma}D^{(1)}_{i\,AB}F_{\mu\nu}{}^A F_{\sigma\gamma}{}^B\Bigg\}\Bigg|_{\rho=\rho_i}, \end{aligned} \tag{5.5.32}$$

where $C^{(1)}_1 = 0$, $D^{(1)}_1 = 0$, as well as

$$C^{(1)}_2 = K_{\mathcal{X},2}\,\phi^2\begin{pmatrix} 0 & & & & \\ & \mathbb{1}_{3\times3} & & & \\ & & 1 & & \\ & & & \mathbb{0}_{3\times3} & \\ & & & & \mathbb{0}_{3\times3}\end{pmatrix}, \tag{5.5.33}$$

with

$$D_2^{(1)} = \left(\begin{array}{c|c|c|c|c} D_{\chi,2} & & & & \\ \hline & \frac{1}{2}\big[\bar{D}_2 + \hat{D}_2 + \cos(2v)(\hat{D}_2 - \bar{D}_2)\big]\mathbb{1}_3 & & \frac{1}{2}\sin(2v)(\bar{D}_2 - \hat{D}_2)\,\mathbb{1}_3 & \\ \hline & & \hat{D}_2 & & \\ \hline & \frac{1}{2}\sin(2v)(\bar{D}_2 - \hat{D}_2)\,\mathbb{1}_3 & & \frac{1}{2}\big[\bar{D}_2 + \hat{D}_2 + \cos(2v)(\bar{D}_2 - \hat{D}_2)\big]\mathbb{1}_3 & \\ \hline & & & & \bar{D}_2\,\mathbb{1}_3 \end{array}\right). \tag{5.5.34}$$

Here, the notation $\mathbb{1}_3 \equiv \mathbb{1}_{3\times 3}$ is implemented.

5.6 Fluctuation equations and the model parameters

In this part, we explore the fluctuations of the fields around the confining background and outline the key aspects of the gauge-invariant formalism utilised to compute the mass spectrum discussed in Section 5.7. For a comprehensive understanding, including our use of the

Table 5.2. Summary of the field content in 5D theory (left) to their associated fluctuations in the 4D, ADM formalism (right). There is a mixing in the physical fluctuating states marked by the parenthesis: the eigenstates of $(\mathfrak{a}^\phi, \mathfrak{a}^\chi)$ and $\left(\mathfrak{v}_\mu{}^{\bar{A}}, \mathfrak{v}_\mu{}^{\hat{A}}\right)$ are combinations of the originals in the theory. Degeneracies of masses for some of the spin-0 states survive even after $SO(4) \to SO(3)$ spontaneous breaking; thus, the states can be rewritten together in the $SO(4)$ notation.

Field	Fluctuation
g_{MN}	$\mathfrak{e}_{\mu\nu}$
χ_M	$\mathfrak{v}_\mu$
$(\phi,\, \chi)$	$(\mathfrak{a}^\phi, \mathfrak{a}^\chi)$
$\left.\begin{matrix}\mathcal{B}_6^{\hat{A}} \\ \mathcal{A}_6^4\end{matrix}\right\}$ $\left.\begin{matrix}\mathcal{B}_6^{\bar{A}} \\ \mathcal{A}_6^{\bar{A}}\end{matrix}\right\}$	$\mathfrak{a}^{\hat{A}} = \left\{\begin{matrix}\mathfrak{a}^{\hat{A}} \\ \mathfrak{a}^4\end{matrix}\right.$ $\mathfrak{a}^{\bar{A}} = \left\{\begin{matrix}\mathfrak{a}^{\tilde{A}} \\ \mathfrak{a}^{\bar{A}}\end{matrix}\right.$
$\left(\mathcal{B}_M{}^{\hat{A}}, \mathcal{B}_M{}^{\bar{A}}\right)$ $\mathcal{A}_M{}^4$ $\mathcal{A}_M{}^{\bar{A}}$	$\left(\mathfrak{v}_\mu{}^{\hat{A}}, \mathfrak{v}_\mu{}^{\bar{A}}\right)$ $\mathfrak{v}_\mu{}^4$ $\mathfrak{v}_\mu{}^{\bar{A}}$
$\left.\begin{matrix}\pi^{\hat{A}} \\ \Pi^4\end{matrix}\right\}$	$\mathfrak{p}^{\hat{A}} = \left\{\begin{matrix}\mathfrak{p}^{\hat{A}} \\ \mathfrak{p}^4\end{matrix}\right.$

ADM formalism [208] and the choices of gauge-invariant variables from fluctuations, refer to Appendices A and D. The $SO(4)$ language (where indices are $\hat{A} = 1, \cdots, 4$ and $\bar{A} = 5, \cdots, 10$) and the $SO(3)$ language (using indices $\hat{\mathcal{A}} = 1, 2, 3$, $\tilde{\mathcal{A}} = 5, 6, 7$, and $\bar{\mathcal{A}} = 8, 9, 10$) are used based on providing clarity or convenience. We distinguish the original fields in the action and their gauge-invariant fluctuation counterparts using distinct symbols. A summary of these correspondences is provided in Table 5.2.

The gauge-invariant formalism is discussed more in Chapters 3 and 4. Scalar fluctuations $\{\mathcal{B}_6^{\tilde{A}}, \mathcal{A}_6^{\bar{A}}\}$ transform under non-trivial $SO(3)$ irreducible representations, and with $\{\mathcal{B}_6^{\hat{A}}, \mathcal{A}_6^{4}\}$, forming $SO(4)$ multiplets that transform in the adjoint and fundamental representations of $SO(4)$, respectively (see Table 5.2). While these fields are treated similarly to $\mathfrak{a}^{\phi}$ and $\mathfrak{a}^{\chi}$ in terms of the gauge-invariant formalism, they do not mix with components of the metric and do not introduce new elements to the study. For further details, refer to Appendix A.

The vector fluctuations, denoted as $\mathfrak{v}_{\mu}$ (or simply $\mathfrak{v}$), correspond to the $U(1)$ gauge field χ_M and complete the set of $SO(4)$ singlets in the model. Gauge fixing is necessary for their study, but for the study of the mass spectrum, we focus on the gauge-invariant and transverse part of the fluctuations. This transverse part satisfies the differential equation derived in [5]:

$$0 = \left[\partial_{\rho}^2 + (2\partial_{\rho}A + 7\partial_{\rho}\chi)\partial_{\rho} - e^{2\chi-2A}q^2\right]\mathfrak{v}\,, \tag{5.6.1}$$

with the UV boundary condition as

$$0 = \left[e^{7\chi}\partial_{\rho} + D_{\chi,2}e^{-2A}q^2\right]\mathfrak{v}^{\bar{\mathcal{A}}}\Big|_{\rho=\rho_2}\,, \tag{5.6.2}$$

and the Neumann boundary condition $\partial_{\rho}\mathfrak{v}|_{\rho=\rho_1} = 0$ at the IR boundary. The mass spectrum is determined by the values of $M^2 \equiv -q^2$ for which solutions satisfying both the bulk equations of motion and these boundary conditions exist. In this context, we choose $D_{\chi,2} = 0$, reflecting that the $U(1)$ gauge symmetry corresponds to a global symmetry in the dual field theory.

Our focus is primarily on the fluctuations influenced by $SO(5)$ and $SO(4)$ symmetry breaking, which include the vectors $\mathfrak{v}^{\tilde{\mathcal{A}}}$, $\mathfrak{v}^{\bar{\mathcal{A}}}$, $\mathfrak{v}^{\hat{\mathcal{A}}}$, and $\mathfrak{v}^{4}$, related the fields defined in Eq. (5.5.24) (excluding χ_M). Additionally, we consider the pseudoscalars $\mathfrak{p}^{\hat{\mathcal{A}}}$ and $\mathfrak{p}^{4}$, associated with $\mathcal{H}_M^{(1)\hat{\mathcal{A}}}$ and $\mathcal{H}_M^{(1)4}$ as qouted in Eq. (5.5.25). The investigation of these vector and pseudoscalar modes needs the inclusion of relevant gauge-fixing terms. We choose the R_{ξ} gauge for this purpose, and detailed procedures are outlined in Appendix D. The bulk equations of motion for these (gauge-invariant) transverse polarisations of spin-1 fluctuations and for the pseudoscalars

respect the $SO(4)$ symmetry. They can be expressed as follows

$$0 = \left[\partial_\rho^2 + (2\partial_\rho A + \partial_\rho \chi)\partial_\rho - e^{2\chi-2A}q^2\right]\mathfrak{v}^{\bar{A}}\,, \tag{5.6.3}$$

$$0 = \left[\partial_\rho^2 + (2\partial_\rho A + \partial_\rho \chi)\partial_\rho - \frac{g^2\phi^2}{4} - e^{2\chi-2A}q^2\right]\mathfrak{v}^{\hat{A}}\,, \tag{5.6.4}$$

$$0 = \left[\partial_\rho^2 - \left(2\partial_\rho A + \partial_\rho \chi + \frac{2\partial_\rho \phi}{\phi}\right)\partial_\rho - \frac{g^2\phi^2}{4} - e^{2\chi-2A}q^2\right]\mathfrak{p}^{\hat{A}}\,. \tag{5.6.5}$$

The spontaneous symmetry breaking in the pattern of $SO(3) \subset SO(4)$ is induced by the UV boundary conditions, at $\rho = \rho_2$. The fluctuations, $\mathfrak{v}^{\tilde{A}}$ and $\mathfrak{v}^{\hat{A}}$, are the vectors that transform as 3 of $SO(3)$, but are placed in the $SO(5)/SO(3)$ broken directions. They mix due to the boundary conditions and satisfy the equations:

$$\begin{aligned} 0 = &\left[e^{\chi}\partial_\rho + \frac{g^2}{4}\sin(v)^2 K_5 v_5^2 + \frac{1}{2}\Big(\bar{D}_2 + \hat{D}_2 + \cos(2v)(\bar{D}_2 - \hat{D}_2)\Big)e^{-2A}q^2\right]\mathfrak{v}^{\tilde{A}}\Big|_{\rho=\rho_2} \\ &+\frac{\sin(2v)}{2}\left[-\frac{g^2}{4}K_5 v_5^2 + (\bar{D}_2 - \hat{D}_2)e^{-2A}q^2\right]\mathfrak{v}^{\hat{A}}\Big|_{\rho=\rho_2}\,, \end{aligned} \tag{5.6.6}$$

$$\begin{aligned} 0 = &\left[e^{\chi}\partial_\rho + \frac{g^2}{4}\Big(K_{\mathcal{X},2}\phi^2 + \cos(v)^2 K_5 v_5^2\Big) + \frac{1}{2}\Big(\bar{D}_2 + \hat{D}_2 + \cos(2v)(\hat{D}_2 - \bar{D}_2)\Big)e^{-2A}q^2\right]\mathfrak{v}^{\hat{A}}\Big|_{\rho=\rho_2} \\ &+\frac{\sin(2v)}{2}\left[-\frac{g^2}{4}K_5 v_5^2 + (\bar{D}_2 - \hat{D}_2)e^{-2A}q^2\right]\mathfrak{v}^{\tilde{A}}\Big|_{\rho=\rho_2}\,. \end{aligned} \tag{5.6.7}$$

The fluctuations, $\mathfrak{v}^{\bar{A}}$ and $\mathfrak{v}^4$, satisfy the boundary conditions

$$0 = \left[e^{\chi}\partial_\rho + \bar{D}_2 e^{-2A}q^2\right]\mathfrak{v}^{\bar{A}}\Big|_{\rho=\rho_2}\,, \tag{5.6.8}$$

$$0 = \left[e^{\chi}\partial_\rho + \frac{g^2}{4}\Big(K_{\mathcal{X},2}\phi^2 + K_5 v_5^2\Big) + \hat{D}_2 e^{-2A}q^2\right]\mathfrak{v}^{4}\Big|_{\rho=\rho_2}\,. \tag{5.6.9}$$

The boundary conditions for the pseudoscalar triplet, $\mathfrak{p}^{\hat{A}}$, is not affected by the presence of the spurion, P_5,

$$0 = \left[K_{\mathcal{X},2}e^{-\chi}\partial_\rho + 1\right]\mathfrak{p}^{\hat{A}}\Big|_{\rho=\rho_2}\,, \tag{5.6.10}$$

although, there is change for the boundary condition at $\rho = \rho_2$ for $\mathfrak{p}^4$ which is the $SO(3)$ singlet

$$0 = \left[\left(K_{\mathcal{X},2} + \frac{K_5 v_5^2}{\phi^2} + \frac{K_5 v_5^2}{\partial_v^2 \mathcal{V}_4}K_{\mathcal{X},2}e^{-2A}q^2\right)e^{-\chi}\partial_\rho + \left(1 + \frac{K_5 v_5^2}{\partial_v^2 \mathcal{V}_4}e^{-2A}q^2\right)\right]\mathfrak{p}^4\Big|_{\rho=\rho_2}\,. \tag{5.6.11}$$

The boundary conditions at the IR, $\rho = \rho_1$, are considerably simpler. The vectors obey Neumann boundary conditions as $\partial_\rho v^{\bar{A}}(\rho_1) = \partial_\rho v^{\hat{A}}(\rho_1) = \partial_\rho v^{\bar{A}}(\rho_1) = \partial_\rho v^4(\rho_1) = 0$, and pseudoscalars obey Dirichlet boundary conditions as $\mathfrak{p}^{\hat{A}}(\rho_1) = \mathfrak{p}^4(\rho_1) = 0$. They do not introduce any additional symmetry-breaking effects and can, hence, be written as $SO(4)$ multiplets.

5.6.1 Model parameters and $SO(4)$ gauging

It will be illuminating if we calculate some of the propagators, especially $\langle \mathcal{A}_\mu^{\bar{A}}(q)\mathcal{A}_\nu^{\bar{A}}(-q)\rangle$ and $\langle \mathcal{A}_\mu^4(q)\mathcal{A}_\nu^4(-q)\rangle$, and find their behaviour. The transverse and longitudinal parts of the propagators are separated by the projectors, $P_{\mu\nu} = \eta_{\mu\nu} - \frac{q_\mu q_\nu}{q^2}$ and $\frac{q_\mu q_\nu}{q^2}$, pinpointing their dependence on $\bar{M}_2$ and M_2^4 which are gauge-fixing parameters. They are defined in Appendix D and only appear in the longitudinal polarisation:

$$\langle \mathcal{A}_\mu^{\bar{A}}(q)\mathcal{A}_\nu^{\bar{A}}(-q)\rangle = (-i)\lim_{\rho_2\to\infty}\left\{e^{-2A}\left(\bar{D}_2 e^{-2A}q^2 + e^{\chi}\frac{\partial_\rho \mathfrak{v}^{\bar{A}}}{\mathfrak{v}^{\bar{A}}}\right)^{-1}\Bigg|_{\rho=\rho_2} P_{\mu\nu} + e^{-2A}\left(\frac{1}{\bar{M}_2}e^{-2A}q^2 + e^{\chi}\frac{\partial_\rho \mathfrak{v}_L^{\bar{A}}}{\mathfrak{v}_L^{\bar{A}}}\right)^{-1}\Bigg|_{\rho=\rho_2}\frac{q_\mu q_\nu}{q^2}\right\}, \tag{5.6.12}$$

$$\langle \mathcal{A}_\mu^4(q)\mathcal{A}_\nu^4(-q)\rangle = (-i)\lim_{\rho_2\to\infty}\left\{e^{-2A}\left(\hat{D}_2 e^{-2A}q^2 + \frac{g^2}{4}K_5 v_5^2 + \frac{g^2}{4}K_{\mathcal{X},2}\phi^2 + e^{\chi}\frac{\partial_\rho \mathfrak{v}^4}{\mathfrak{v}^4}\right)^{-1}\Bigg|_{\rho=\rho_2} P_{\mu\nu} + e^{-2A}\left(\frac{1}{M_2^4}e^{-2A}q^2 + \frac{g^2}{4}K_5 v_5^2 + \frac{g^2}{4}K_{\mathcal{X},2}\phi^2 + e^{\chi}\frac{\partial_\rho \mathfrak{v}_L^4}{\mathfrak{v}_L^4}\right)^{-1}\Bigg|_{\rho=\rho_2}\frac{q_\mu q_\nu}{q^2}\right\}. \tag{5.6.13}$$

Here, $\mathfrak{v}_L^{4,\bar{A}}$ denotes the longitudinal components (L) of the respective gauge fields. These components manifest in the unphysical longitudinal segments of the two-point functions, which carry gauge-fixing parameters. They are included for completeness, and their detailed equations in the bulk and boundary conditions are provided in Appendix D. An examination of the UV expansions in terms of small $z \equiv e^{-\rho}$ reveals that $A \simeq 4\chi \simeq -\frac{4}{3}\log(z)$ and $\phi \simeq \phi_J z^{\Delta_J}$. The contributions from the second and third terms are relevant for $\langle \mathcal{A}_\mu^4(q)\mathcal{A}_\nu^4(-q)\rangle$, provided we impose the scalings:

$$K_5 = \frac{k_5}{v_5^2}\, z^{8/3}, \tag{5.6.14}$$

$$K_{\mathcal{X},2} = k_{\mathcal{X}}\, z^{8/3-2\Delta_J}, \tag{5.6.15}$$

where k_5 and $k_{\mathcal{X}}$ are introduced as new parameters independent of z.

To determine the fixing of $\bar{D}_2$ and $\hat{D}_2$, we examine the example where $\Delta = \Delta_J = 2$. While

the extension to arbitrary Δ requires an analysis specific to each case, the approach remains straightforward. Referring to the small-z expansions detailed in Appendix E, it becomes apparent that to omit the divergences, one must select:

$$\bar{D}_2 = -z^{-1} + \frac{1}{\bar{\varepsilon}^2}, \quad \hat{D}_2 = -z^{-1} + \frac{1}{\hat{\varepsilon}^2}, \tag{5.6.16}$$

where $\bar{\varepsilon}^2$ and $\hat{\varepsilon}^2$ represent two independent parameters not depending on z. By implementing these substitutions, it becomes feasible to consider the limit $z \to 0$, resulting

$$P^{\mu\sigma}P^{\nu\gamma}\langle \mathcal{A}^{\bar{A}}_\mu(q)\mathcal{A}^{\bar{A}}_\nu(-q)\rangle = -i\left(\frac{q^2}{\bar{\varepsilon}^2} - \frac{3v_3^{\bar{A}}}{v_0^{\bar{A}}}\right)^{-1} P^{\sigma\gamma}\,, \tag{5.6.17}$$

$$P^{\mu\sigma}P^{\nu\gamma}\langle \mathcal{A}^{4}_\mu(q)\mathcal{A}^{4}_\nu(-q)\rangle = -i\left(\frac{q^2}{\hat{\varepsilon}^2} - \frac{3v_3^{4}}{v_0^{4}} + \frac{g^2 k_5}{4} + \frac{g^2 k_{\mathcal{X}}\phi_J^2}{4}\right)^{-1} P^{\sigma\gamma}\,. \tag{5.6.18}$$

Selecting the values of $\bar{\varepsilon}$ and $\hat{\varepsilon}$ leads to a choice for the strength of the weak gauge couplings.[7] Following the rescaling of the field normalisations, setting $\hat{\varepsilon} \to 0$ implies that only the $SO(4)$ subgroup remains gauged in the dual field theory. For small $\bar{\varepsilon}$, the coupling strength associated with this subgroup is approximately $g_4 \equiv \bar{\varepsilon}\, g$.[8] The procedure is valid for small q^2 and $\bar{\varepsilon}$. For a comprehensive treatment across all q^2, the elaborated study on how to refine these results and deriving the physical two-point function is studied in Appendix D of Ref. [6].

Also, to find a non-trivial contribution to the boundary condition in Eq. (5.6.11), coming from $\partial_v^2\mathcal{V}_4$, we impose

$$\partial_v^2\mathcal{V}_4 = m_4^2\, z^{16/3}\,, \tag{5.6.19}$$

for any Δ, that introduces the m_4^2 parameter. This parameter corresponds to the combination $\lambda f^2 \sin^2\theta$, discussed in Eq. (5.4.7).

Here, we summarise the sequence of limits, similar to how it was discussed in Section 5.4. Initially the limit $\lambda_5 \to \infty$ introduces an infinite mass in the action $\mathcal{S}_{P_5}$ (refer to Eq. (5.5.4)), freezing the absolute value of P_5. Second, the limit of $k_5 \to \infty$ is taken. As k_5 becomes very large, the couplings associated with the remaining degrees of freedom in P_5 goes to zero. At this stage, P_5 transitions into a spurion initially introduced as a field transforming under a symmetry but is now reduced to a set of real numbers. Then, $\hat{\varepsilon} \to 0$ gauges the $SO(4)$ subgroup by freezing the gauge bosons along the coset $SO(5)/SO(4)$.[9] We effectively

[7] If we set $\bar{\varepsilon} = \hat{\varepsilon} \equiv \varepsilon$, then in the dual field theory, the entire $SO(5)$ is weakly gauged. When ε is small, the gauge coupling in four dimensions, evaluated at $q^2 \simeq 0$, approximately equals $g_4 \equiv \varepsilon\, g$.

[8] This can also be achieved by setting $\hat{D}_2 = 0$ and allowing $\hat{\varepsilon} \to 0$ depending on $z \to 0$. Both approaches are related to the limit discussed in Section 5.4, where $\tilde{\kappa} \to \infty$.

[9] Importantly, the limits $k_5 \to \infty$ and $\hat{\varepsilon} \to 0$ commute with each other. It also corresponds to setting $\hat{D}_2 = 0$, keeping consistency with the previous limits.

recover an approximate symmetry, which is also spontaneously broken in the dual field theory (as discussed in Section 5.4), while respecting the gauge principle and maintaining unitarity. Fourth limit is $\rho_2 \to \infty$, which removes the UV regulator.

We provide an example of how to establish the UV boundary conditions for the pseudoscalar and vector modes, focusing on the case where $\Delta = 2$. For other values of Δ, a case-by-case calculation is required. Our approach utilises the UV expansions of the fluctuations, as stated in Appendix E. These expansions are substituted into the boundary conditions specified in Eqs. (5.6.6–5.6.11), allowing us to derive relationships between the leading and subleading coefficients that appear in the solution of second-order linearised equations in the bulk. This procedure yields the following relationships:[10]

$$0 = \frac{q^2}{\bar{\varepsilon}^2} v_0^{\bar{A}} - 3\mathfrak{v}_3^{\bar{A}}\,, \tag{5.6.20}$$

$$0 = \cos(v)\mathfrak{v}_0^{\hat{A}} - \sin(v)\mathfrak{v}_0^{\tilde{A}}\,, \tag{5.6.21}$$

$$0 = -3\cos(v)\mathfrak{v}_3^{\tilde{A}} + \sin(v)\left(\frac{g^2}{4}k_{\mathcal{X}}\phi_J^2\mathfrak{v}_0^{\hat{A}} - 3\mathfrak{v}_3^{\hat{A}}\right) + \frac{q^2}{\bar{\varepsilon}^2}\left(\cos(v)\mathfrak{v}_0^{\tilde{A}} + \sin(v)\mathfrak{v}_0^{\hat{A}}\right), \tag{5.6.22}$$

$$0 = \mathfrak{v}_0^4\,, \tag{5.6.23}$$

$$0 = \mathfrak{p}_0^{\hat{A}} - k_{\mathcal{X}}\mathfrak{p}_1^{\hat{A}}\,, \tag{5.6.24}$$

$$0 = \mathfrak{p}_0^4 - \left(k_{\mathcal{X}} + \frac{m_4^2}{q^2\phi_J^2}\right)\mathfrak{p}_1^4\,. \tag{5.6.25}$$

Our numerical investigation, illustrated by the plots in Section 5.7, extensively explores the parameter space of the model. We carefully examine how the entire spectrum of fluctuations varies with the remaining free parameters. Here is a summary.

- The functions of the background are chosen by parameters Δ (related to the dimension of the dual operator inserted to break $SO(5)$) and ϕ_I (controlling the profile for ϕ in the IR expansion, including its departure from 0). We constrain Δ to $\frac{3}{2} \le \Delta \le \frac{7}{2}$ and ϕ_I in the region of the stable branch of solutions identified in Chapter 3, ensuring $\phi_I \le \phi_I(c)$ where $\phi_I(c)$ is the critical value for a first-order phase transition.

- The gauge coupling of the $SO(4)$ in the dual field theory, denoted approximately as $g_4 \equiv \bar{\varepsilon} g$, with g as the bulk coupling, requires $\bar{\varepsilon}$ to be sufficiently small for perturbation theory to apply.

- Adjustments in the vacuum misalignment angle v and the mass m_4^2 of the lightest scalar particle are made to create large separations between parametrically light modes and heavy resonance towers.

[10] In these expressions we reintroduce the dependence on A_U and χ_U via the substitution $q^2 \to e^{2\chi_U - 2A_U} q^2$. Additionally, to maintain consistency, it is necessary to reintroduce A_U and χ_U in Eqs. (5.6.14)–(5.6.16).

- The constant $k_{\mathcal{X}}$ is discussed further in subsection 5.6.2.
- When numerical results are presented, we report the values of $\rho_1 - \rho_o$ and $\rho_2 - \rho_o$ used in the calculation. We confirm that the outcomes are insensitive to these choices within the desired numerical accuracy of our study.

Two important clarifications should be noted in the conclusion. First, only eigenstates with $M^2 = -q^2 \neq 0$ are studied by the bulk equations and boundary conditions discussed herein. For massless modes, the spectrum is already determined by the system symmetries; for instance, the unbroken $SO(3)$ symmetry yields three massless vectors. Another point to mention, the gauging process described occurs in the presence of a bulk profile for ϕ within a D-dimensional asymptotically AdS gravity background, aligning with the discussions in Section 5.4. This process happens if Δ falles within the range $\frac{D-3}{2} \leq \Delta \leq \frac{D+1}{2}$, where the scalar field interpretation in the dual description corresponds to more than one interpretation for the operators inserted in the dual field theory [46]. Notably, in our numerical examples, we adopt $\Delta = 2$ with $D = 6$. This choice will be further explained in the subsequent brief subsection.

5.6.2 More on the gauging of $SO(4)$ and the role of $k_{\mathcal{X}}$

It is beneficial to digress momentarily to discuss the role of the parameter $k_{\mathcal{X}}$. In the context of gravity theory, the action maintains $SO(5)$ gauge invariance, but the background solutions exhibit $\mathcal{X}_\alpha \neq 0$, spontaneously breaking the $SO(5)$ symmetry down to $SO(4)$. The conventional interpretation in field theory involves a combination of explicit and spontaneous breaking of a global $SO(5)$ symmetry, characterised by the parameters ϕ_J and ϕ_V found in the UV expansion of the background solutions.

The asymptotic boundary values of the bulk fields, which act as sources for operators on the dual field theory side, appear as a deformation given by:

$$\int \mathrm{d}^5 x \, \mathcal{X}_\alpha^{(0)} \mathcal{O}^\alpha \,, \qquad \text{where} \qquad \mathcal{X}_\alpha^{(0)} \equiv \lim_{z \to 0} \left(z^{-\Delta_J} \mathcal{X}_\alpha \right) \,, \tag{5.6.26}$$

with $\mathcal{O}^\alpha$ representing the composite operator corresponding to $\mathcal{X}_\alpha$.

The $SO(4)$ symmetry preserved by the deformation described is different from the gauged $SO(4)$. It is not possible to gauge the explicitly broken symmetries due to inherent obstructions. Therefore, to restore the full $SO(5)$ invariance of the field theory, the boundary value $\mathcal{X}_\alpha^{(0)}$ must be transformed into a dynamical field. Then a limit needs to be taken to freeze this spurion. However, for this field (spurion) to be applicable within a unitary field theory framework, its scaling dimension must satisfy:

$$\frac{D-3}{2} \leq \Delta \leq \frac{D+1}{2} \,, \tag{5.6.27}$$

where $D = 6$ in the current context. In simpler terms, $\mathcal{X}_\alpha^{(0)}$ must adhere to these scaling dimension constraints to ensure it can be effectively integrated into the unitary field theory description.

The λ_i terms, which are the boundary-localised potentials for the sigma-model fields, contain mass terms, which are taken to infinity to set up boundary conditions that freeze the magnitude of $\mathcal{X}_\alpha$. This freezing process is analogous to the limit where $\lambda_5 \to +\infty$ for the spurion P_5, and also relates to $\lambda_\Sigma \to +\infty$ limit discussed in Section 5.4. Likewise, the parameter $k_\mathcal{X}$ plays a role analogous to k_5. In Chapter 4, the limit $k_\mathcal{X} \to +\infty$ was implicitly imposed on the boundary conditions, causing the decoupling of the four additional massless degrees of freedom (the PNGBs of the spontaneous breaking of $SO(5)$ to $SO(4)$ due to the $\mathcal{X}_\alpha^{(0)}$ VEV). In this study, however, we retain $k_\mathcal{X}$ as a possibly finite free parameter. Three of the massless scalars are absorbed via the Higgs mechanism, becoming the third polarisation of the massive gauge fields in the $SO(4)/SO(3)$ coset. The last component, which conceptually corresponds to the Higgs boson in a CHM realisation of the model, gets massive as a result of the explicit breaking introduced by $m_4^2 \neq 0$.

5.7 Spectrum

In this section, we show some numerical results illustrating the mass spectrum of fluctuations and its dependence on various model parameters. Throughout this analysis, we fix $\Delta = 2$, $\phi_I = \phi_I(c) \approx 0.3882$, $\rho_2 - \rho_0 = 5$, and $\rho_1 - \rho_0 = 10^{-9}$. Figures 5.3–5.6 depict how the mass spectrum varies with the remaining parameters: $\bar{\varepsilon}$, g, v, m_4^2, and $k_\mathcal{X}$. Note that all spectra, except for Fig. 5.6, are normalized to mass of the lightest spin-2 fluctuation $\mathfrak{e}_{\mu\nu}$.

Let us first focus on Figure 5.3, which specifically shows the dependence of the mass of pseudoscalar fluctuations $\mathfrak{p}^{\hat{A}}$ and $\mathfrak{p}^4$ on the parameter m_4^2, for two distinct choices of $k_\mathcal{X}$. The masses in these sectors are independent of $\bar{\varepsilon}$ or v. Some notable observations from Figure 5.3 are the following. The spectrum of $\mathfrak{p}^{\hat{A}}$ includes three exactly massless states, which vanish when the $SO(4)$ subgroup is gauged as we work in the unitary gauge. These states correspond to the longitudinal polarisation of three vector bosons. There is a tachyonic region in the spectrum of $\mathfrak{p}^4$ for $m_4^2 < 0$, hence this range is physically forbidden. Small positive values of m_4^2 result in a small mass for the state associated with the PNGBs of the spontaneous symmetry breaking of $SO(4)$. In the context of a CHM, this state would analogously be identified with the Higgs boson.

Figures 5.4 and 5.5 provide full depictions of the mass spectra under different parameter choices for g, Δ, ϕ_I, $k_\mathcal{X}$, and m_4^2, as functions of v and $\bar{\varepsilon}^2$, respectively. Upon examining these spectra, several interesting observations can be made despite their apparent complexity. The spectra reveal that only a small subset of states are light, namely the zero modes in the

unbroken, gauged $SO(3)$ sector, which are massless vectors, the lightest $\mathfrak{p}^4$ pseudoscalar and finally, the lightest admixture of vectors in the $SO(4)/SO(3)$ coset. These states stand out as having masses significantly lower than the typical scale of the theory, which is often associated with the mass of the lightest spin-2 state. There is a visible hierarchy between these light states and the rest of the spectrum. As anticipated, the mass of the lightest vector states increases when v or $\bar{\varepsilon}^2$ are small and increasing. Conversely, these masses tend towards zero when either parameter approaches zero. These trends align with expectations for vector bosons linked to the Higgs mechanism in spontaneously broken gauge theories with weak couplings.

Figure 5.6 illustrates three numerical examples of the spectrum, aimed at providing a semi-realistic depiction of how this model could be implemented as a CHM. For illustrative purposes, we overlook the differences with the SM and interpret the lightest state among the $\mathfrak{p}^4$ fluctuations as the Higgs boson. In this case, we denote its mass as m_H and normalise all other masses respective to m_H. To set up these examples, we choose $\Delta = 2$ and $\phi_I = \phi_I(c) \approx 0.3882$. We impose the condition $g_4 = \bar{\varepsilon} g = 0.7$, which is roughly of the order of the $SU(2)_L$ coupling in the SM. We tune the remaining parameters such that the ratio of masses between the lightest vector states ($v^{\hat{A}}$ and $v^{\tilde{A}}$) and the spin-0 sector ($\mathfrak{p}^4$) is approximately $M_Z/m_H \approx 0.73$. Here, M_Z represents the mass of the Z boson in the SM.

It is important to note that this model is not intended to be realistic, and this exercise should be interpreted cautiously. Nonetheless, it serves its purpose by demonstrating that within this framework, it is possible to generate a small difference between the masses of the Higgs boson and the Z boson, alongside the towers of the predicted new bound states in the theory. Furthermore, it is observed that the first states, heavier than the light sector, generally correspond to spin-0 states, with spin-1 and spin-2 states appearing much heavier in comparison.

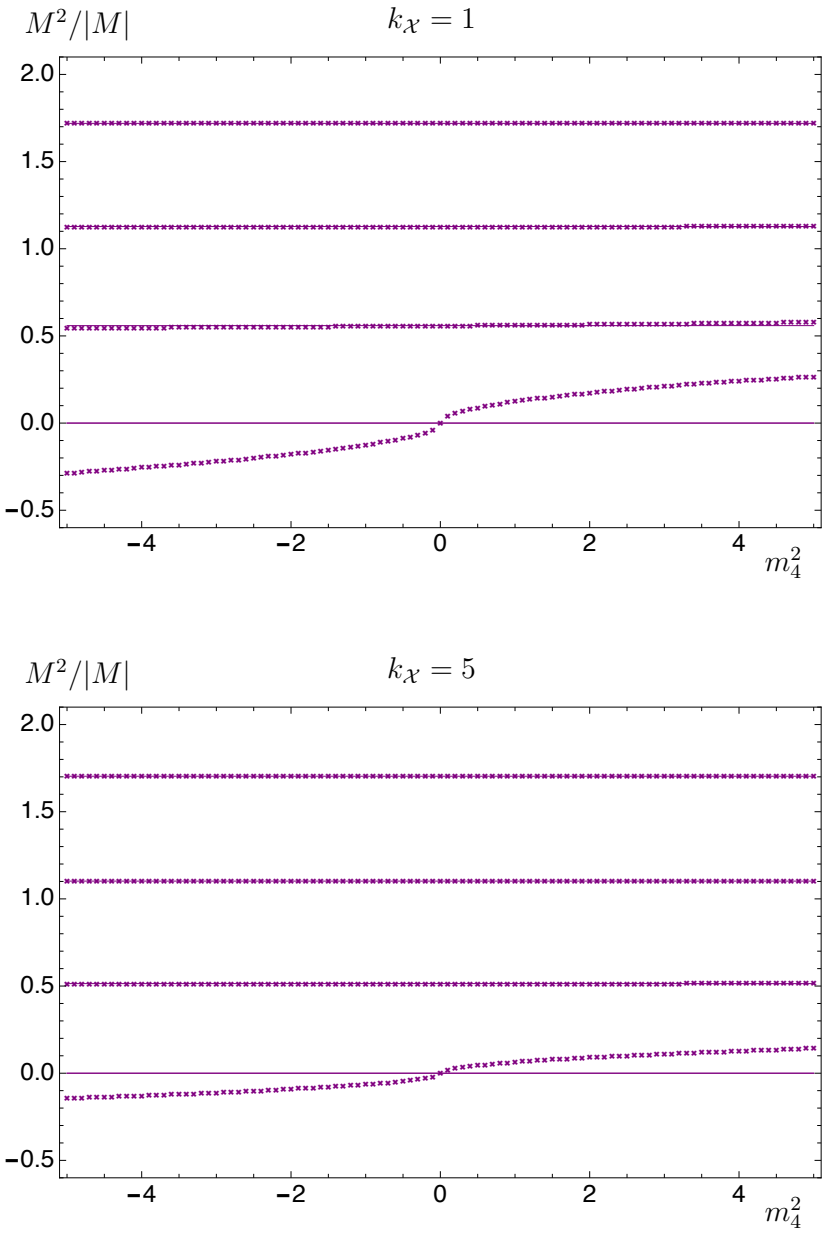

Figure 5.3. The mass spectrum of fluctuations for the pseudoscalar, $\mathfrak{p}^{\hat{A}}$ (lines) and $\mathfrak{p}^4$ (crosses) for two choices of $k_{\mathcal{X}} = 1$ (top panel) and $k_{\mathcal{X}} = 5$ (bottom panel) as a function of m_4^2. The spectrum is before gauging the $SO(4)$; thus, the $\mathfrak{p}^{\hat{A}}$ states contain massless modes, to be higgsed away in the case of gauging. Other parameters are fixed as $\Delta = 2$, $g = 5$, $\phi_I = \phi_I(c) \approx 0.3882$, and the IR and UV cutoffs are, respectively, at $\rho_1 - \rho_o = 10^{-9}$ and $\rho_2 - \rho_o = 5$.

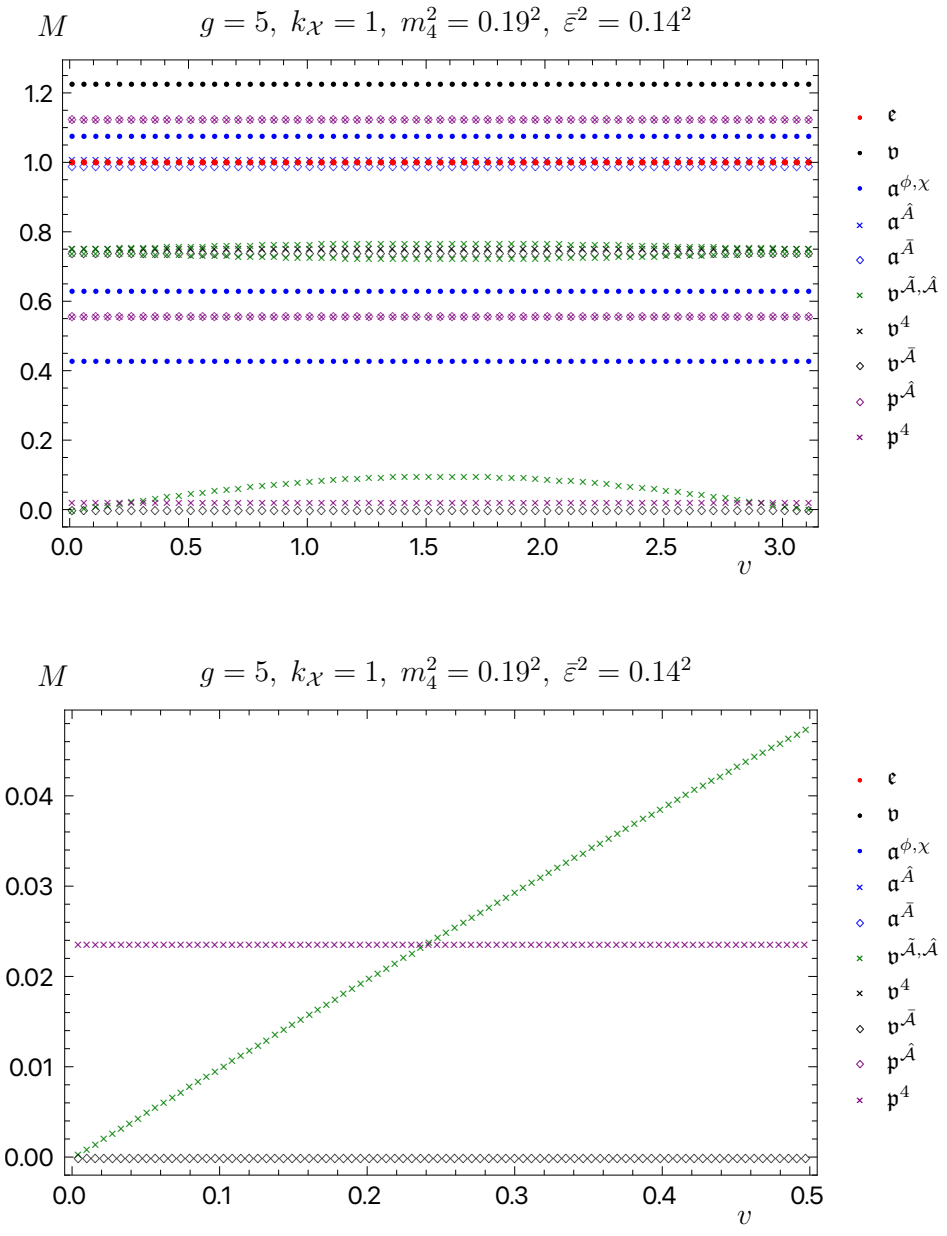

Figure 5.4. Mass spectrumof fluctuations, for spin-2 tensors, $\mathfrak{e}$ (red dots), graviphoton $\mathfrak{v}$ (black dots), active scalars, $\mathfrak{a}^{\phi}, \mathfrak{a}^{\chi}$ (blue dots), pseudoscalars, $\mathfrak{p}^4$ (purple crosses), $\mathfrak{p}^{\hat{A}}$ (purple diamonds), vectors $\mathfrak{v}^{\bar{A}}$ (black diamonds), $\mathfrak{v}^4$ (black crosses), $\mathfrak{v}^{\hat{A}}$ and $\mathfrak{v}^{\tilde{A}}$ (green crosses) and scalars $\mathfrak{a}^{\bar{A}}$ (blue diamond), and $\mathfrak{a}^{\hat{A}}$ (blue crosses), as a function of v, the misalignement angle, for fixed values of parameters $k_{\mathcal{X}}, m_4^2$, and $\bar{\varepsilon}$. The bottom panel is a zoomed version of the top panel. Masses are normalised to the mass of the lightest spin-2 tensor. Plots have $\Delta = 2$, $g = 5$, $\phi_I = \phi_I(c) \approx 0.3882$, and the IR and UV cutoffs are located, respectively, at $\rho_1 - \rho_o = 10^{-9}$ and $\rho_2 - \rho_o = 5$.

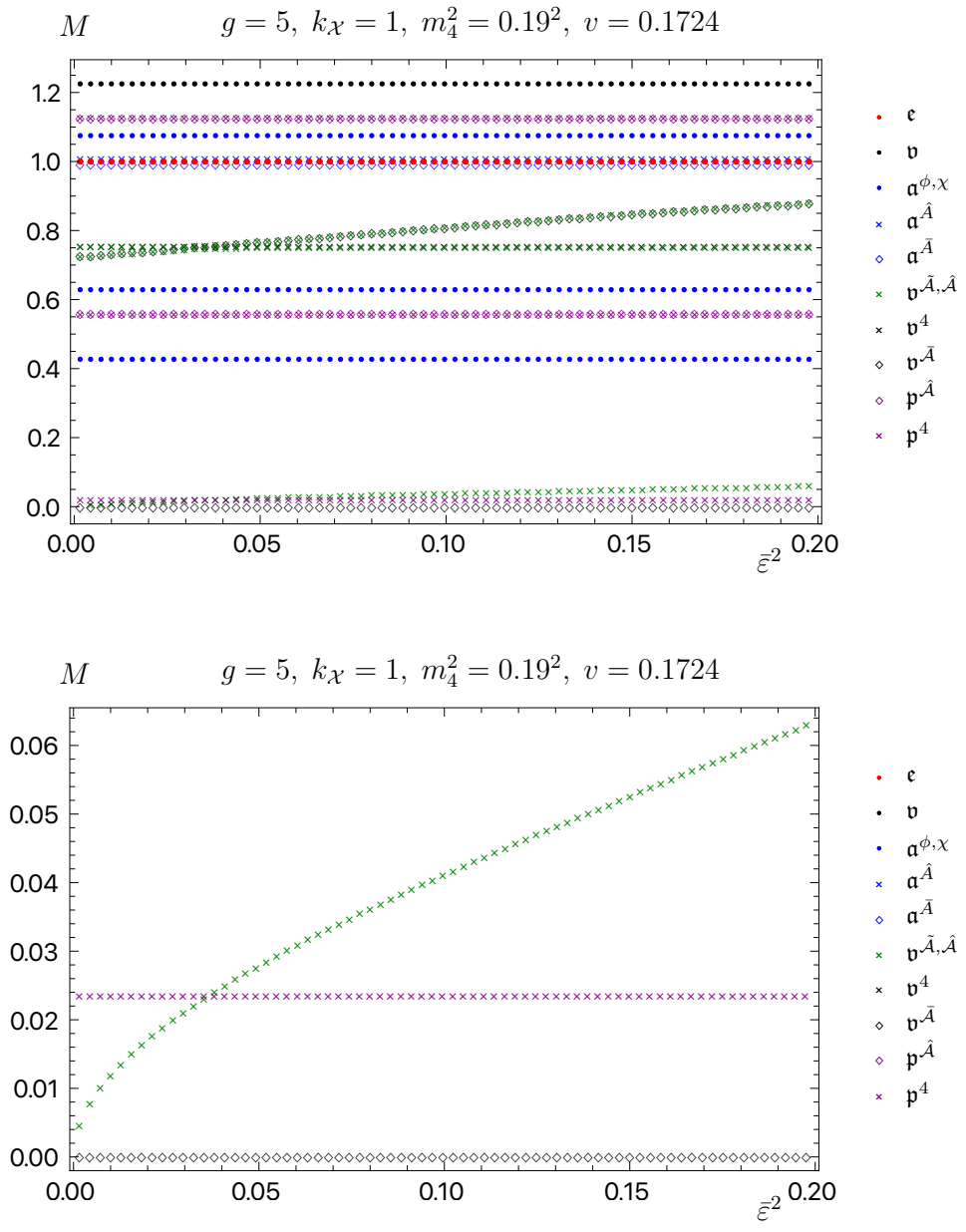

Figure 5.5. Mass spectrumof fluctuations, for spin-2 tensors, $\mathfrak{e}$ (red dots), graviphoton $\mathfrak{v}$ (black dots), active scalars, $\mathfrak{a}^{\phi}, \mathfrak{a}^{\chi}$ (blue dots), pseudoscalars, $\mathfrak{p}^4$ (purple crosses), $\mathfrak{p}^{\hat{A}}$ (purple diamonds), vectors $\mathfrak{v}^{\bar{A}}$ (black diamonds), $\mathfrak{v}^4$ (black crosses), $\mathfrak{v}^{\hat{A}}$ and $\mathfrak{v}^{\tilde{A}}$ (green crosses) and scalars $\mathfrak{a}^{\bar{A}}$ (blue diamond), and $\mathfrak{a}^{\hat{A}}$ (blue crosses), as a function of $\bar{\varepsilon}^2$, for fixed values of parameters $k_{\mathcal{X}}, m_4^2$, and v. The bottom panel is a zoomed version of the top panel. Masses are normalised to the mass of the lightest spin-2 tensor. Plots have $\Delta = 2$, $g = 5$, $\phi_I = \phi_I(c) \approx 0.3882$, and the IR and UV cutoffs are located, respectively, at $\rho_1 - \rho_o = 10^{-9}$ and $\rho_2 - \rho_o = 5$.

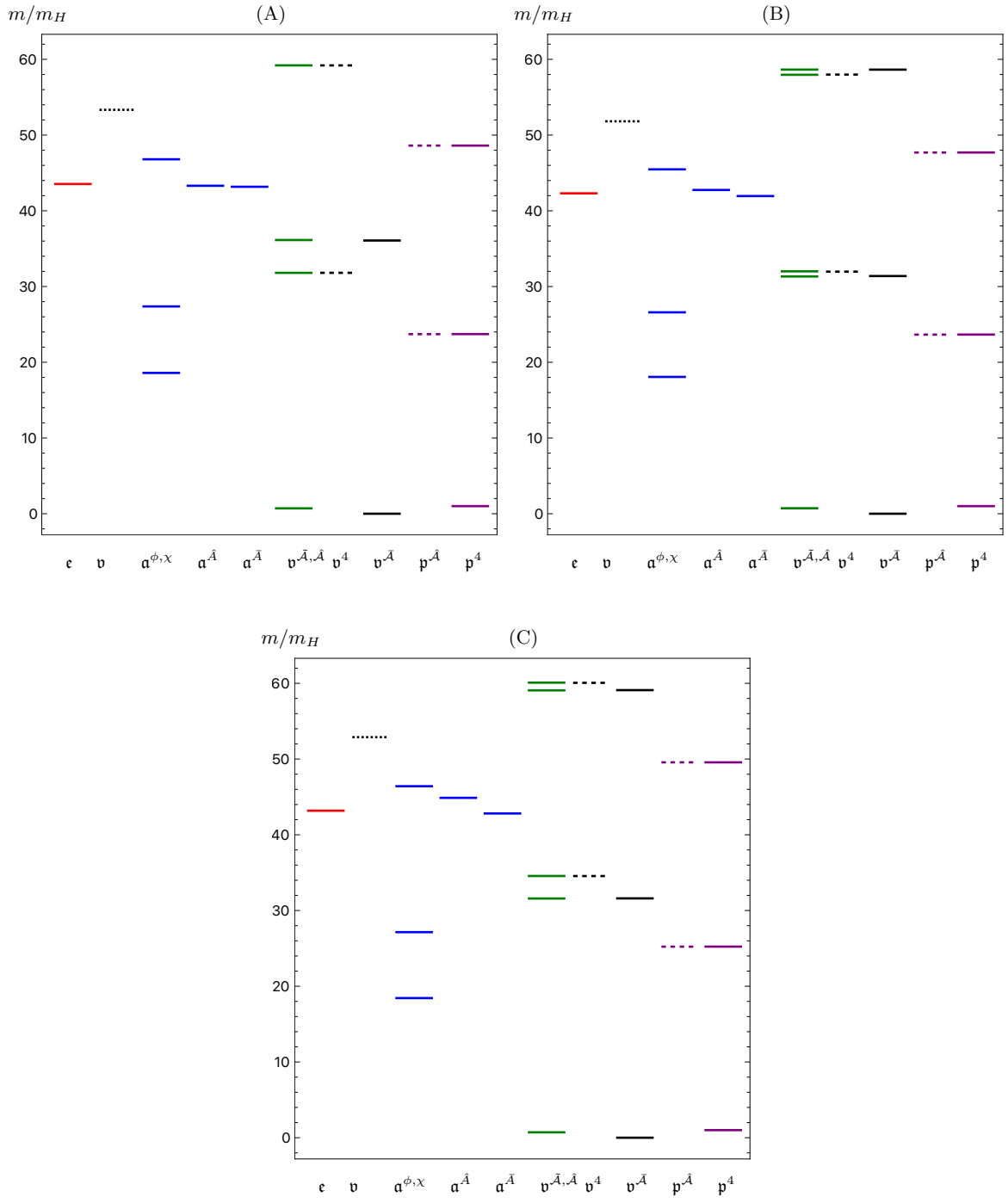

Figure 5.6. Mass spectrum of fluctuations, normalized to the mass of the lightest $\mathfrak{p}^4$ state denoted as m_H, presenting spin-2 tensors, $\mathfrak{e}$ (red), scalars, $\mathfrak{a}^\phi, \mathfrak{a}^\chi, \mathfrak{a}^{\bar{A}}, \mathfrak{a}^{\hat{A}}$ (blue), pseudoscalars, $\mathfrak{p}^{\hat{A}}$ (purple), $\mathfrak{p}^4$ (purple dashed), and vectors, $\mathfrak{v}^{\hat{A}}$ and $\mathfrak{v}^{\bar{A}}$ (green), $\mathfrak{v}^{\bar{A}}$ (black), $\mathfrak{v}^4$ (black dahsed), v (black dotted), for three different choices for the coupling g: (A) $g = 2$, $v = 0.15$, $g_4 = 0.7$, $m_4^2 = 0.185^2$, (B) $g = 5$, $v = 0.1724$, $g_4 = 0.7$, $m_4^2 = 0.19^2$, (C) $g = 8$, $v = 0.17$, $g_4 = 0.7$, $m_4^2 = 0.185^2$. The plots are calculated using $\Delta = 2$, $\phi_I = \phi_I(c) \approx 0.3882$, and $k_{\mathcal{X}} = 1$. The IR and UV cutoffs are chosen, respectively, as $\rho_1 - \rho_o = 10^{-9}$ and $\rho_2 - \rho_o = 5$.

Chapter 6

From conformal to confining field theories using holography

6.1 Motivation and background

From this chapter onwards, we move to a new subject in the context of formal supergravity backgrounds and their holographic interpretation from gauge/gravity duality.

Following the formulation of Maldacena's conjecture and subsequent improvements [2–4], there appeared a compelling initiative to extend these ideas beyond $\mathcal{N} = 4$ Super Yang-Mills to more phenomenologically relevant QFTs. This endeavour focused on exploring concepts such as CFTs and QFTs with minimal or no supersymmetry, aiming to find geometric interpretations of phenomena such as symmetry breaking, confinement, and the presence of condensates.

Pioneering efforts in this direction included early works in Refs. [32, 209, 210], followed by subsequent contributions from [211–213] and others. Notably, advancements were made through the series of papers from [153, 214–218] (summarised in [219]), which provided a comprehensive geometric framework for understanding non-perturbative aspects of a quiver field theory with two-nodes and $\mathcal{N} = 1$ supersymmetry.

Simultaneously, another line of investigation based on wrapped branes, by [32, 154, 220–228] which further developed through works like [229] (reviewed in [230–232]), offered a complementary perspective on the same non-perturbative phenomena. Remarkably, both approaches demonstrated a consistent geometric realisation of strong coupling effects such as confinement and symmetry breaking. The convergence of these two research directions was elegantly demonstrated in the works [233–236], which effectively unified the insights gained from both sides.

An advancement beyond the earlier works, which primarily involved adjoint or bifundamental fields, was the incorporation of fields in the fundamental representation of the gauge group. Initially, this extension was performed in the probe approximation, where "flavour

branes" were introduced to probe the geometry without backreacting, similar to a 'quenched' approximation. For reviews on this approach, see Refs. [112, 156, 159, 160, 237]. Subsequently, efforts were made to refine this probe approximation by the smearing of flavour branes, which allowed for only studying BPS ordinary differential equations instead of more complex BPS partial differential equations. For detailed discussions, refer to works such as [238–246].

However, a recurring issue in these models is that when the high-energy behaviour of the QFT corresponds to a deformed 4-dimensional CFT, the IR region of the holographic dual background often exhibits singularities. This characteristic is observed in earlier models like those discussed in [211], [213], as well as in more recent developments covered in [247–249]. Notably, this IR singularity concern can be mitigated to some extent at finite temperatures. Conversely, models with a smooth IR geometry tend to show a different issue: their UV part typically does not resemble a field theoretical setting because the space is not asymptotically AdS. We will now elaborate on the contents of this chapter, which is a step forward in solving some of these issues.

6.1.1 General structure

To address the previously discussed issues, we focus on a five-dimensional quiver field theory that maintains eight Poincaré supersymmetries and is balanced. At high energies, this theory asymptotes to a strongly coupled CFT. The holographic description of this five-dimensional fixed point is given in works such as [250–252].

Next, we proceed by compactifying this family of 5D Superconformal Field Theories (SCFTs) on a circle, introducing anisotropic VEVs to the stress-energy tensor $T_{\mu\nu}$ and another global symmetry current. This setup initiates an RG flow that culminates in a four-dimensional QFT without supersymmetry. The holographic dual describing this dimensional flow is situated within the framework, albeit with differences, of solutions recently explored by Anabalón and Ross [253]. Related previous backgrounds can be found in [254], with further developments and applications detailed in subsequent works such as [255] through [256]. Our study employs holography to explore various aspects of this family of QFTs. The forthcoming sections of this chapter are organised as follows.

In Section 6.2, we introduce a new family of supergravity backgrounds in Type IIB that form the foundation of our investigation. A notable feature of these backgrounds is their overall smoothness, except at specific locations where localised D7 brane sources, known as flavour branes, are situated. By computing the Page charges, we find that the configuration includes a combination of D5-NS5 and D7 branes, resembling the typical setup described in Hanany-Witten constructions [257] for five-dimensional field theories. The number and type

of present branes, directly correspond to the contents of the balanced dual linear quiver, as elaborated further below.

In Section 6.3, we propose a dual QFT corresponding to this supergravity background. As expected, in the far UV, the theory is described by a family of balanced linear quiver SCFTs in five dimensions. These are compactified on a circle and subjected to deformations involving an anisotropic VEV for $T_{\mu\nu}$ and a global symmetry current, which collectively break supersymmetry. Using holography, we explore various aspects of the low-energy QFT, including a monotonic quantity referred to as the flow-central charge and related to the number of degrees of freedom. This quantity serves as an indicator of the presence of a four-dimensional IR-gapped system that is UV-completed by the underlying five-dimensional SCFT.

We also investigate the behaviour of Wilson loops, observing their initial CFT-like behaviour at small separations of the non-dynamical quarks, followed by a transition to confining behaviour. By constructing an appropriate QCD string configuration, we argue that the presence of localised sources (D7 flavour branes) introduces the possibility of screening effects. Additionally, we compute the Entanglement Entropy on a rectangular strip. This quantity is then related to the free energy of the underlying 5-dimensional SCFT, and we analyse the contributions from the RG flow to this entropy.

Moreover, we propose a method to compute the Holographic Complexity for these dimensional flow scenarios, particularly focusing on transitions away from SCFTs using the CV conjecture [258]. We find that the holographic complexity is connected to the free energy of the 5D SCFT and includes contributions from the RG flow away from the fixed point. At the end, we calculate the masses of spin-2 excitations within the four-dimensional Minkowski theory. Notably, the spectrum reveals positive masses, providing evidence for the stability of our non-supersymmetric QFT.

6.2 The supergravity background

In this section, we introduce a family of new supergravity backgrounds investigated in this chapter and the related brane charges. Appendix F provides detailed derivations and descriptions of the origin of the solutions.

The background solution is written by using the coordinates $(t, x_1, x_2, x_3, r, \phi, \theta, \varphi, \sigma, \eta)$, functions $H(r), f(r)$, seven other functions $f_i(r, \sigma, \eta)$, parameters $(c, \tilde{g}, \mu)$, as well as another

function $V(\sigma,\eta)$. In the convention of $\alpha' = g_s = 1$, one has

$$\begin{aligned} ds_{st}^2 &= f_1\Bigg[\frac{2\tilde{g}^2}{9}H^{1/2}(r)\,r^2\,d\vec{x}_{1,3} + \frac{2\tilde{g}^2}{9}\frac{H^{1/2}(r)}{f(r)}\,dr^2 + \frac{2\tilde{g}^2}{9}H(r)^{-3/2}\,f(r)\,d\phi^2 \\ &\quad + f_2\left(d\theta^2 + \sin\theta^2(d\varphi - A_1^{(3)})^2\right) + f_3\left(d\sigma^2 + d\eta^2\right)\Bigg] \end{aligned} \tag{6.2.1}$$

$$f(r) = -\frac{\mu}{r^3} + \tfrac{2}{9}\tilde{g}^2\,r^2\,H(r)^2\,, \qquad H(r) = 1 - \frac{c^2}{r^3}\,, \quad A_1^{(3)} = A_1^{(3)}(r)d\phi = \frac{\sqrt{2\mu}}{c}\,(1 - \frac{1}{H(r)})\,d\phi\,,$$

$$F_2^{(3)} = dA_1^{(3)} = \frac{\sqrt{2\mu}}{c}\,\frac{H'(r)}{H(r)^2}dr\wedge d\phi, \quad C_0 = f_7, \quad e^{-2\Phi} = f_6, \qquad F_5 = 4(G_5 + *_{10}G_5),$$

$$B_2 = f_4\mathrm{Vol}(\tilde{S}^2) + \frac{2}{9}\eta\cos\theta F_2^{(3)}\,, \quad C_2 = f_5\mathrm{Vol}(\tilde{S}^2) + 4\partial_\sigma(\sigma V)\cos\theta F_2^{(3)}\,.$$

$$\mathrm{Vol}(\tilde{S}^2) = \sin\theta d\theta\wedge\left(d\varphi + A_1^{(3)}(r)d\phi\right).$$

Functions denoted as $f_i(r,\sigma,\eta)$ are written as:

$$\begin{aligned} f_1 &= \frac{3\pi}{2X^2}\left(\sigma^2 + \frac{3X^4\sigma\partial_\sigma V}{\partial_\eta^2 V}\right)^{1/2}, \qquad f_2 = \frac{X^2\partial_\sigma V\partial_\eta^2 V}{3\Lambda}, \qquad f_3 = \frac{X^2\partial_\eta^2 V}{3\sigma\partial_\sigma V}, \\ f_6 &= 12\frac{3X^4(\sigma^2\partial_\sigma V)(\partial_\eta^2 V)}{\left(3X^4\partial_\sigma V + \sigma\partial_\eta^2 V\right)^2}\Lambda, \qquad f_7 = 2\left(\partial_\eta V + \frac{3X^4\sigma\partial_\sigma V\partial^2_{\sigma\eta}V}{3X^4\partial_\sigma V + \sigma\partial_\eta^2 V}\right), \\ f_4 &= \frac{\pi}{2}\left(\eta - \frac{\sigma\partial_\sigma V\partial^2_{\sigma\eta}V}{\Lambda}\right), \qquad f_5 = \frac{\pi}{2}\left(V - \frac{\sigma\partial_\sigma V\left(\partial_\eta V\partial^2_{\sigma\eta}V - 3X^4\partial_\eta^2 V\partial_\sigma V\right)}{\Lambda}\right), \\ \Lambda &= 3X^4\partial_\eta^2 V\partial_\sigma V + \sigma\left[\left(\partial^2_{\eta\sigma}V\right)^2 + \left(\partial_\eta^2 V\right)^2\right], \quad X(r) = \frac{1}{H(r)^{1/4}}, \quad V = V(\sigma,\eta), \end{aligned} \tag{6.2.2}$$

with G_5 representing the differential form

$$G_5 = -\frac{4\tilde{g}^2\sqrt{2\mu}}{27c}r^4H'(r)f_1(r,\sigma,\eta)\;dt\wedge dx_1\wedge dx_2\wedge dx_3\wedge d\left(\cos\theta\sigma^2\partial_\sigma V\right). \tag{6.2.3}$$

Here, $\tilde{S}^2$ sphere is fibered over the ϕ-circle. The metric of the subspace spanned by (θ,φ) coordinates reads

$$ds^2_{\tilde{S}^2} = d\theta^2 + \sin^2\theta\Big(d\varphi - A_1^{(3)}\Big)^2. \tag{6.2.4}$$

If one chooses the periodicity of the circle parametrised by the angle ϕ to be

$$\phi\sim\phi + L_\phi, \quad L_\phi = \frac{8\pi\left(9r^{*5}\right)^2\left(1-\frac{c^2}{r^{*3}}\right)^2}{\left(-8\tilde{g}^2c^4 + 4\tilde{g}^2r^{*6} + 4\tilde{g}^2c^2r^{*3} + 27r^*\mu\right)^2} \equiv 2\pi\left(\frac{2H(r^*)}{f'(r^*)}\right)^2, \tag{6.2.5}$$

this circle shrinks smoothly at $r = r^*$. In this case, the Ricci scalar will be bounded for the range of coordinate $r \in [r^*, \infty)$.

In $r \to \infty$ limit, one has $H(r) \sim 1$, therefore $F_2^{(3)}(r \to \infty) \sim 0$. For regularity of the gauge field, the condition of $A_1^{(3)}(r) = 0$ is imposed at the end of space $r = r^*$ by doing a large gauge transformation as

$$A_1^{(3)} = \frac{\sqrt{2\mu}}{c}\left(1 - \frac{1}{H(r)} - 1 + \frac{1}{H(r^*)}\right) d\phi = \frac{\sqrt{2\mu}}{c}\left(-\frac{1}{H(r)} + \frac{1}{H(r^*)}\right) d\phi. \tag{6.2.6}$$

The gauge field $F_2^{(3)}$ remains unchanged by this transformation. It is noteworthy that the space approaches to $\mathrm{AdS}_6 \times \tilde{S}^2(\theta, \varphi) \times \Sigma_2(\sigma, \eta)$ as $r \to \infty$.

After performing this transformation, if we compute the magnetic flux of the background current, we get

$$\Phi = -\oint A_\phi^{(3)}(r = \infty)\, d\phi = -\frac{1}{2}\int F^{(3)}{}_{\mu\nu} dx^\mu \wedge dx^\nu = \frac{\sqrt{2\mu}}{c}\left(\frac{1}{H(r^*)} - 1\right) L_\phi, \tag{6.2.7}$$

which is related to the holonomy of the background gauge field. Therefore, the solution is characterised by two parameters: μ and c, or equivalently L_ϕ and Φ, which are a more natural parametrisation from the perspective of the dual theory living on boundary.[1]

A two-dimensional Riemann surface Σ is parametrised by the two real coordinates, (σ, η). In order to satisfy the equations of motion of Type IIB supergravity, the so-called "potential function," $V(\sigma, \eta)$, must satisfy a Laplace-like differential equation with suitable boundary conditions. The equation is

$$\partial_\sigma\left(\sigma^2 \partial_\sigma V\right) + \sigma^2 \partial_\eta^2 V = 0\,. \tag{6.2.8}$$

It is convenient to do a redefinition defined as

$$V(\sigma, \eta) = \frac{\hat{V}(\sigma, \eta)}{\sigma} \tag{6.2.9}$$

to obtain the Laplace equation. Using $\hat{V}(\sigma, \eta)$ and introducing a function as a density of charge named as $\mathcal{R}(\eta)$, our Laplace problem is,

$$\begin{aligned}
&\partial_\sigma^2 \hat{V} + \partial_\eta^2 \hat{V} = 0, \\
&\hat{V}(\sigma \to \pm\infty, \eta) = 0, \qquad \hat{V}(\sigma, \eta = 0) = \hat{V}(\sigma, \eta = P) = 0. \\
&\lim_{\epsilon \to 0}\left(\partial_\sigma \hat{V}(\sigma = +\epsilon, \eta) - \partial_\sigma \hat{V}(\sigma = -\epsilon, \eta)\right) = \mathcal{R}(\eta).
\end{aligned} \tag{6.2.10}$$

[1] It is important to note that for a given periodicity L_ϕ and magnetic flux Φ chosen at the boundary, there can be multiple background solutions in bulk. This means that fixing a pair of values for L_ϕ and Φ at the boundary does not uniquely determine the corresponding μ and c values in bulk, leading to different branches or families of background solutions. Our study investigates one such branch.

The fields and warping factors of the background depend on a potential function, $V(\sigma,\eta) = \frac{\hat{V}(\sigma,\eta)}{\sigma}$, defined on the two-dimensional internal space. This potential function satisfies a differential equation (referred to in Eq. (6.2.8)), leading to all equations of motion of the background configuration, as described in Eq. (6.2.1), being satisfied. We have checked that the background does not preserve supersymmetry. The stability of this solution remains a subject for future investigation, with some details given later.

The configuration described by Eq. (6.2.1) provides an infinite family of backgrounds that are asymptotically AdS_6 within Type IIB supergravity. This family is parameterised by the function $V(\sigma,\eta)$, which solves the differential equation in Eq. (6.2.8). As the radial coordinate r tends towards infinity, corresponding to higher energies, the dual field theory approaches a five-dimensional fixed point.

The potential function $V(\sigma,\eta)$, subject to appropriate boundary conditions described in Eq. (6.2.10), can be expressed through a Fourier expansion technique, described further in Ref. [259]

$$V(\sigma,\eta) = \frac{\hat{V}(\sigma,\eta)}{\sigma}, \quad \hat{V}(\sigma,\eta) = \sum_{k=1}^{\infty} a_k \sin\left(\frac{k\pi}{P}\eta\right) e^{-\frac{k\pi}{P}|\sigma|}, \quad a_k = \frac{1}{\pi k}\int_0^P \mathcal{R}(\eta)\sin\left(\frac{k\pi}{P}\eta\right)\, d\eta. \tag{6.2.11}$$

As will be explained below, the Page charges' quantisation conditions force the 'Rank function' or 'density of charge' to be a convex polygonal,

$$\mathcal{R}(\eta) = \begin{cases} N_1\eta & 0 \le \eta \le 1 \\ N_l + (N_{l+1} - N_l)(\eta - l) & l \le \eta \le l+1, \quad l := 1, ..., P-2 \\ N_{P-1}(P-\eta) & (P-1) \le \eta \le P. \end{cases} \tag{6.2.12}$$

The coordinate η is bounded to be in the interval $[0, P]$ while σ has the range $(-\infty, \infty)$.

Now, the behaviour of these solutions is studied near the special points in the internal space.

6.2.1 Behaviour at special points

We examine how the metric and dilaton behave near specific points, focusing on $\eta = 0$, $\eta = P$, and the limits $\sigma \to \pm\infty$, as $r \to \infty$.

We begin by analysing the metric behaviour at the boundary, starting with $\eta = 0$, and note that identical results apply to $\eta = P$. As r approaches infinity, indicating $X(r) \to 1$, we

observe that at this boundary, the functions f_1 and f_3 remain finite,

$$f_1^2(r\to\infty,\sigma,0) = \frac{9\pi^2}{4}\,\frac{\sum_{k=1}^{\infty}\frac{\pi k}{P}a_k\left(\left(\frac{\pi k\sigma}{P}\right)^2+3|\sigma|\frac{\pi k\sigma}{P}+3\right)e^{-\frac{\pi k|\sigma|}{P}}}{\sum_{k=1}^{\infty}a_k\left(\frac{\pi k}{P}\right)^3 e^{-\frac{\pi k|\sigma|}{P}}}\,,$$

$$f_3(r\to\infty,\sigma,0) = \frac{1}{3}\,\frac{\sum_{k=1}^{\infty}a_k\left(\frac{\pi k}{P}\right)^3 e^{-\frac{\pi k|\sigma|}{P}}}{\sum_{k=1}^{\infty}a_k\left(\left(\frac{\pi k}{P}\right)^2|\sigma|+\frac{\pi k}{P}\right)e^{-\frac{\pi k|\sigma|}{P}}}\,,$$

while $f_2\to\eta^2 f_3(+\infty,\sigma,0)$. The metric at these boundaries, using these results, is

$$\begin{aligned}
\eta\to 0 \qquad ds_{10}^2 &= f_1(+\infty,\sigma,0)\left(ds^2(\mathrm{AdS}_6)+f_3(+\infty,\sigma,0)(\eta^2 ds^2(\tilde{S}^2)+d\eta^2+d\sigma^2)\right),\\
\eta\to P \qquad ds_{10}^2 &= f_1(+\infty,\sigma,P)\left(ds^2(\mathrm{AdS}_6)+f_3(+\infty,\sigma,P)((\eta-P)^2 ds^2(\tilde{S}^2)+d\eta^2+d\sigma^2)\right).
\end{aligned} \tag{6.2.13}$$

For $r\to\infty$, $A_1^{(3)}\to\frac{\sqrt{2\mu}}{cH(r^*)}d\phi$, thus the $\tilde{S}^2$ fibration on AdS_6 is trivial.

In these limits, the metric remains regular, structured as a warped product $\mathrm{AdS}_6\times\mathbb{R}^4$ with non-singular warp functions. The fact that the dilaton remains finite further supports the regularity of the entire solution at these boundaries.

Now, turning to the limit where $\sigma\to\pm\infty$ and $r\to\infty$, we utilise the Fourier expansion given in Eq. (6.2.11). Here, the dominant contribution to the potential $\hat{V}=\sigma V$ results from the $k=1$ mode. To study the asymptotic behaviour of space-time, we have the expansion

$$\sigma V(\sigma,\eta)\sim\partial_\eta^2(\sigma V)\sim\sin\left(\frac{\pi}{P}\eta\right)e^{-\frac{\pi}{P}|\sigma|}\,,\quad \sigma^2\partial_\sigma V\sim|\sigma|\sin\left(\frac{\pi}{P}\eta\right)e^{-\frac{\pi}{P}|\sigma|}\,,\quad \Lambda\sim\sigma^{-1}e^{-\frac{2\pi}{P}|\sigma|}\,. \tag{6.2.14}$$

Up to constant factors, the metric reads

$$\sigma\to\pm\infty \qquad ds^2=|\sigma|ds^2(\mathrm{AdS}_6)+\sin^2\left(\frac{\pi}{P}\eta\right)ds^2(S^2)+d\eta^2+d\sigma^2. \tag{6.2.15}$$

While the dilaton is

$$\sigma\to\infty \qquad e^{-\Phi}\sim\frac{e^{-\frac{\pi}{P}|\sigma|}}{\sqrt{|\sigma|}}\,. \tag{6.2.16}$$

By performing a change of coordinates where $|\sigma|\to-\log z$ with z being small and positive, the metric and dilaton can be expressed in the form of a (p,q)-five-brane in the asymptotic regions $\sigma\to\pm\infty$, as detailed in Ref. [250]. Our family of six-dimensional backgrounds show some singularities in the fluxes, dilaton, and metric at $\sigma=0$. To analyse their behaviour, we compute the conserved Page charges. Notably, the constraints imposed on the Rank function $\mathcal{R}(\eta)$, specifically that the charge density forms a convex polygonal shape as defined

in Eq. (6.2.12), gaurantees that the quantisation conditions for charges are satisfied.

6.2.2 Page charges

In this section, we consider the analysis of the quantised Page charges within the background described by Eq. (6.2.1). Specifically, we demonstrate that the constraint imposed on the function $\mathcal{R}(\eta)$, as defined in Eq. (6.2.12), to be a convex, piece-wise linear function leads directly to the quantisation of these charges.

The volume element of the fibered sphere is $\text{Vol}(\tilde{S}^2) = \sin\theta d\theta \wedge d\varphi - \sin\theta A_1^{(3)}(r) d\theta \wedge d\phi$, so the fluxes are

$$H_3 = dB_2 = d\Big[f_4 \text{Vol}(\tilde{S}^2) + \frac{2}{9}\eta\cos\theta F_2^{(3)}\Big] = (\partial_\sigma f_4 d\sigma + \partial_\eta f_4 d\eta) \wedge \text{Vol}(\tilde{S}^2) + \cdots, \tag{6.2.17}$$

$$\hat{F}_1 = F_1 = dC_0 = \partial_\sigma f_7 d\sigma + \partial_\eta f_7 d\eta + \partial_r f_7 dr,$$

$$\hat{F}_3 = F_3 - B_2 \wedge F_1 = d\left(C_2 - C_0 B_2\right) = \left[\partial_\sigma(f_5 - f_7 f_4) + \partial_\eta(f_5 - f_7 f_4)\right] \wedge \text{Vol}(\tilde{S}^2) + \cdots,$$

where the Page fluxes definition $\hat{F} = F \wedge e^{-B_2}$ has been used, and only terms that are relevant for our calculation are kept in the expressions.

By choosing $\alpha' = g_s = 1$ one has,

$$Q_{Dp,Page} = \frac{1}{(2\pi)^{7-p}} \int_{\Sigma_{8-p}} \hat{F}_{8-p}.$$

Implying,

$$Q_{NS5} = \frac{1}{4\pi^2}\int_{M_3} H_3, \quad Q_{D7} = \int_{\Sigma_1} \hat{F}_1, \quad Q_{D5} = \frac{1}{4\pi^2}\int_{\Sigma_3} \hat{F}_3. \tag{6.2.18}$$

We define the cycles M_3, Σ_1, Σ_3 as,

$$M_3 = [\eta, S^2], \text{with } \sigma \to \pm\infty,\ r \to \infty, \qquad \Sigma_1 = [\eta], \text{with } \sigma = 0\ , r \to \infty,$$
$$\Sigma_3 = [\sigma, S^2], \text{with } \eta = \text{fixed},\ r \to \infty.$$

Here, a large gauge transformation $B_2 \to B_2 + \Delta d\Omega_2$ is allowed in the calculations. This does not affect NS5 or the D7 brane charges, but it has an impact on the D5 brane charges.

The field strength $\hat{F}_5 = F_5 - B_2 \wedge F_3 + \frac{1}{2} B_2 \wedge B_2 \wedge F_1$ does not carry any quantised charges of D3 branes since there are no compact five-cycles. Now, we check the possible quantised charges, case by case.

NS-5 branes: By computing the NS-5 brane charges, one has

$$\pi Q_{NS5} = \frac{1}{4\pi}\int_{M_3} H_3 = \int d\eta \partial_\eta f_4(r\to\infty, \sigma\to\pm\infty, \eta) = f_4(\infty,\pm\infty,P) - f_4(\infty,\pm\infty,0). \tag{6.2.19}$$

By making use of relations derived in Appendix C of [8] one can check that the number of NS-5 branes is given by

$$Q_{NS5} = P. \tag{6.2.20}$$

Both contributions from $\sigma = +\infty$ and $\sigma = -\infty$ are included. This indicates that P NS-5 branes are present in the background.

One can also consider another cycle

$$M_3' = [\eta, \theta, \phi], \text{with } r\to\infty,\ \sigma\to\pm\infty, \quad .$$

which gives the NS-5 brane charge as

$$\begin{aligned}\pi Q'_{NS5} = \frac{1}{4\pi}\int_{M_3'} H_3 &= -\int d\eta A_1^{(3)}(r=\infty)\partial_\eta f_4(r\to\infty,\sigma\to\pm\infty,\eta)\\ &= -A_1^{(3)}(r=\infty)\left(f_4(\infty,\pm\infty,P) - f_4(\infty,\pm\infty,0)\right),\\ Q'_{NS5} &= -A_1^{(3)}(r=\infty)P.\end{aligned} \tag{6.2.21}$$

The quantisation of this charge requires the quantisation of the c-parameter in Eq. (6.2.1)—see also Eq. (6.2.6). However, the cycle M_3' is topologically $S^2\times S^1$, not an S^3. Now we move to the D7 brane charge calculation.

D7 branes: The D7 brane cherges reads

$$Q_{D7} = \int_{\Sigma_1}\hat{F}_1 = \int_0^P d\eta\partial_\eta f_7(\infty,0,\eta) = f_7(\infty,0,P) - f_7(\infty,0,0). \tag{6.2.22}$$

After symplifications one has

$$Q_{D7} = \left(\mathcal{R}'(0) - \mathcal{R}'(P)\right). \tag{6.2.23}$$

Because of the integer slopes, one can check that in the interval of $0\le\eta\le 1$ one has $\mathcal{R} = N_1\eta$ and in $P-1\le\eta\le P$ one has $\mathcal{R} = N_{P-1}(P-\eta)$. Thus the final number of D7 branes is

$$Q_{D7} = (N_1 + N_{P-1}). \tag{6.2.24}$$

D5 branes: A large gauge transformation is performed as $B_2\to B_2 + \Delta\text{Vol}(S^2)$. Note that the volume element of the sphere S^2 at $r\to\infty$ of our metric is $\text{Vol}(S^2) = \sin\theta d\theta\wedge d\varphi$

which is well-defined and fibration is trivial in this case. The D5 brane charges are

$$\pi Q_{D5} = \frac{1}{4\pi}\int_{\Sigma_3} F_3 - (B_2 + \Delta \mathrm{Vol}(S^2)) \wedge F_1 = \int_{-\infty}^{\infty} d\sigma \partial_\sigma \left[f_5 - f_7(f_4 + \Delta)\right] = \int_{-\infty}^{-\epsilon} \partial_\sigma [f_5 - f_7(f_4 + \Delta)] + \int_{\epsilon}^{\infty} \partial_\sigma [f_5 - f_7(f_4 + \Delta)]. \tag{6.2.25}$$

The expression $f_5 - f_7(f_4 + \Delta)$ should be evaluated at $\sigma \to \pm\infty$ and $\sigma = \pm\epsilon$ then we need to take $\epsilon \to 0$. The details of calculations are provided in [8]. The function $f_5 - f_7(f_4 + \Delta)$ evaluted at $\sigma \to \pm\infty$ vanishes. Therefore, we only want to calculate

$$\pi Q_{D5} = f_5 - f_7(f_4 + \Delta)\Big]_{\epsilon}^{-\epsilon}, \tag{6.2.26}$$

evaluated at the limit $r \to \infty$ and some fixed value of η. After simplifications, we find

$$Q_{D5} = \mathcal{R}(\eta) - \mathcal{R}'(\eta)\,(\eta - \Delta)\,. \tag{6.2.27}$$

It is important to note that within each interval specified by Eq. (6.2.12), the function $\mathcal{R}(\eta)$ is linear, distinguished by an integer intercept and slope. This gaurantees that the Page charge Q_{D5} associated with D5-branes, as derived in Eq. (6.2.27), is an integer. In particular, by implementing a large gauge transformation $\Delta = k$ specific to each $[k, k+1]$ interval, Eq. (6.2.27) simplifies to:

$$Q_{D5} = N_k. \tag{6.2.28}$$

Here, N_k represents an integer that we interpret as relating the gauge group node $SU(N_k)$ in the quiver theory to the interval $[k, k+1]$ along the η-coordinate axis.

One can also consider another cycle, (similar to the case of the NS-5 calculation)

$$\Sigma_3' = [\sigma, \theta, \phi], \text{with } \eta = \text{fixed},\ r \to \infty\ .$$

with the charge of D5 branes as

$$\pi Q'_{D5} = \frac{1}{4\pi}\int_{\Sigma_3'} F_3 - (B_2 + \Delta \mathrm{Vol}(S^2)) \wedge F_1 = -\int_{-\infty}^{\infty} d\sigma A_1^{(3)}(r=\infty)\partial_\sigma \left[f_5 - f_7(f_4 + \Delta)\right] =$$
$$-A_1^{(3)}(r=\infty)\left(f_5 - f_7(f_4 + \Delta)\right)\Big]_{\epsilon}^{-\epsilon}$$
$$Q'_{D5} = -A_1^{(3)}(r=\infty) N_k \tag{6.2.29}$$

To ensure the quantisation of charges as discussed, a quantisation condition must be imposed on the parameter c in Eq. (6.2.1), as indicated by Eq. (6.2.6). It is noteworthy that the cycle Σ_3' is not topologically S^3, it rather forms $S^2 \times S^1$.

Summarising the total number of branes in this background configuration we have

$$
\begin{aligned}
&Q_{NS5} = P \qquad\qquad (6.2.30)\\
&Q_{D7}[k,k+1] = \mathcal{R}''(k) = (2N_k - N_{k+1} - N_{k-1}),\ Q_{D7,total} = (N_1 + N_{P-1}) = \int_0^P \mathcal{R}''(\eta)d\eta,\\
&Q_{D5}[k,k+1] = \mathcal{R}(\eta) - \mathcal{R}'(\eta)(\eta-\Delta) = N_k\,, \qquad Q_{D5,total} = \int_0^P \mathcal{R}\ d\eta.
\end{aligned}
$$

Moving forward, we will consider the associated QFTs. Given the presence of branes in our configuration, particularly D7 flavour branes, which introduce singularities in the background, it is crucial for the reliability of the background that we consider, to have large values of P. This ensures that the D7 branes are sufficiently separated. In essence, the backgrounds described by Eq. (6.2.1) are dual to field theories in the UV regime that feature long linear quivers with scattered flavour groups.

6.3 Dual field theories and observables

In this section, we explore the field theories that are dual to the family of Type IIB solutions introduced in Section 6.2.

The determination of the holographic dual proceeds as follows: at large radial coordinates where $r \to \infty$, the backgrounds asymptotically approach AdS_6, and $X(r \to \infty) \sim 1$. Additionally, the gauge field, $A_1^{(3)}$, behaves as a pure gauge field with the form given by $A_1^{(3)}(r \to \infty) \approx \frac{2\sqrt{\mu}}{cH(r^*)} d\phi$ (as described in Eq. (6.2.6)), and the field strength $F_2^{(3)}$ tends towards zero. The presence of fluxes and the non-trivial S^2 fibration over the ϕ-coordinate alter the isometries of AdS_6 as one moves deeper into the bulk, towards r^*. This feature has a resemblance to twisted compactifications discussed in [251] and reviewed in broader contexts in [260]. In the cases investigated in [251], there is an infinite family of SCFTs in 5d, selected by the function $V(\sigma,\eta)$ that solves a Laplace-like equation, which is compactified on a curved manifold. Twisted compactifications, originally introduced by Witten, have been explored extensively across various examples and contexts [220, 227, 229, 261, 262]. However, it is important to note that in our case, the compactification on S^1_ϕ does not preserve supersymmetry, as evidenced by the absence of massless spinors in our background (see Appendix A of [8]). Therefore, the solution described in Eq. (6.2.1) does not constitute a twisted compactification. Furthermore, the manifold on which we compactify, S^1_ϕ, remains flat and does not introduce curvature into the compactification.

In the current context, we interpret our backgrounds as providing a holographic description of the compactification of five-dimensional QFTs on a circle, augmented by the inclusion of a Wilson line. This Wilson line is holographically represented by the $A_1^{(3)}$ fibration as given in Eq. (6.2.6). The backgrounds we investigate belong to a class of solutions recently

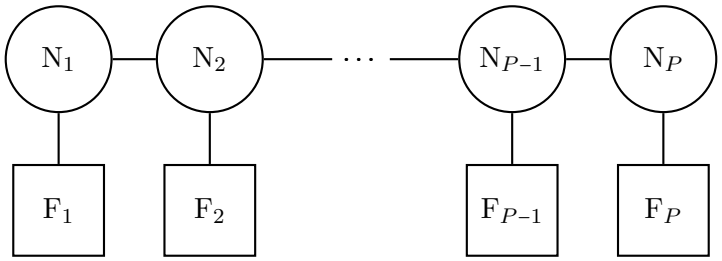

Figure 6.1. Diagram for a linear quiver. The balancing condition is $F_i = 2N_i - N_{i-1} - N_{i+1}$

explored by Anabalón and Ross [253]. These backgrounds build upon earlier work, such as the solutions discussed in [254], and have been further developed and applied in subsequent papers [255, 256].

The 5D linear quivers discussed, approach a conformal fixed point towards high energies. This UV conformal field theory is deformed by the introduction of operators that characterise the compactification process. Moreover, within the holographic framework provided by our geometries described in Eqs. (6.2.1)-(6.2.2), a QFT Wilson line is added and represented by the field $A_1^{(3)}$ as given in Eq. (6.2.6). The key insight from our gravitational backgrounds is that at lower energies compared to the finite size of the compact space S^1_ϕ, the field theories undergo a transition away from the UV conformal behaviour. Instead, they evolve into non-conformal field theories in $(3+1)$ dimensions.

The compactified 5D CFTs described here have the strongly coupled dynamics of linear (balanced) quiver field theories at high energies, as those in Fig. 6.1. The numbers $N_1, N_2, ..., N_P$ and $F_1, ..., F_P$ determine the function $V(\sigma, \eta)$ in a unique fashion. The function $\mathcal{R}(\eta)$, which following Eq. (6.2.11), determines $V(\sigma, \eta)$, is also fixed by these numbers.

In the UV regions of the field theories discussed, relevant operators deform the conformal fixed points. The dimensions of these operators can be extracted from the near AdS_6 boundary expansion of the gauged supergravity metric, as detailed in Appendix F, and further analysed for the near boundary behaviour.

The parameters μ and c in our gravitational backgrounds control the subleading modes of the metric, the scalar field X, and the gauge field in their asymptotic expansions. These parameters correspond to the VEVs of the corresponding dual operators in the field theory. The asymptotic expansions are given in Appendix F.2. The gauge field $A_1^{(3)}$ in the bulk, produces a VEV of a global symmetry current in the dual field theory, which can be interpreted as a background current insertion. The scalar field X induces the VEV for an operator of

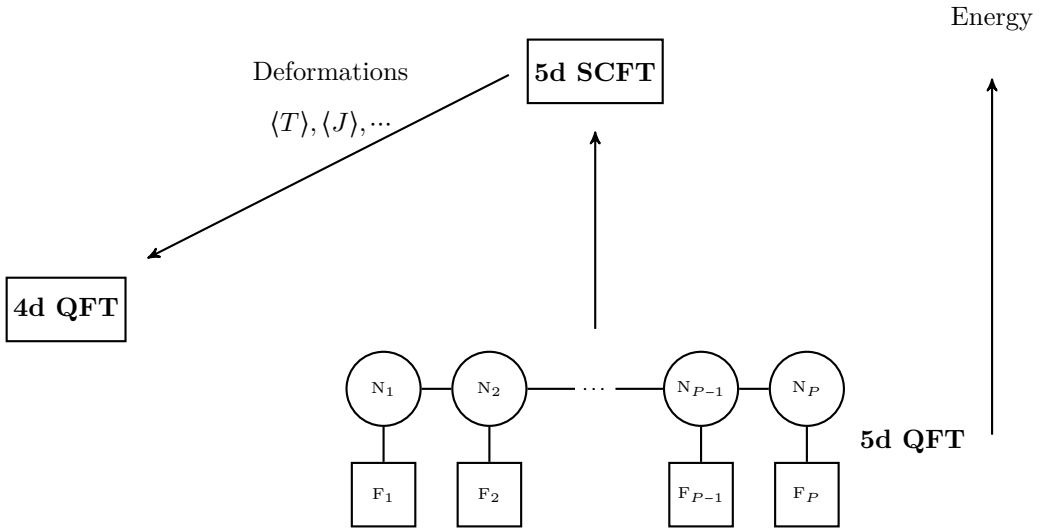

Figure 6.2. RG Flow of the 5d SCFTs under deformations

dimension three. The VEVs are given as, ($\tilde{g} = \sqrt{\frac{9}{2}}$ has been set within this section.)

$$\langle J\rangle = -3c\sqrt{\mu}, \quad \langle \mathcal{O}_X\rangle = \frac{c^2}{4}. \tag{6.3.1}$$

For the components of the boundary stress tensor, the VEVs are as follows:

$$\langle T_{tt}\rangle = -\mu, \quad \langle T_{x_i x_i}\rangle = \mu, \quad \langle T_{\phi\phi}\rangle = 4\mu. \tag{6.3.2}$$

There are some important features. The energy density, represented by $\langle T_{tt}\rangle$, is negative for positive μ. The VEVs in the ϕ-direction and the other flat x_i-directions are different, suggesting an anisotropic insertion of relevant operators in the boundary theory. These relevant operators, initiate an RG flow within the dual field theory. This RG flow culminates in gapped four-dimensional QFTs corresponding to the gravitational backgrounds under consideration. Fig. 6.2 provides a schematic representation of this RG flow, illustrating the field theory evolution under the influence of these deformations and transitions from the UV conformal point to the gapped 4D QFTs.

In the upcoming sections, we compute several observable quantities within the dual QFT. Beginning with the holographic central charge in Section 6.3.1, this quantity serves as a measure of the number of degrees of freedom or, equivalently, the Free Energy of the strongly coupled lower dimensional QFTs. Specifically, we find that it is expressed as a function of the energy scale and involves transcendental functions of the parameters appearing within the quiver structure, capturing the non-perturbative characteristics of these QFTs.

6.3.1 The holographic central charge

In this section, we determine the holographic central charge, which quantifies the number of degrees of freedom throughout the flow. Drawing from Refs. [263] and [264], we initially define this quantity at conformal points and subsequently compute it in specific examples from our type IIB family of geometries.

After analysing the conformal UV regime, we present the central charge along the flow, as originally introduced in [263]. Notably applicable to flow-describing geometries, its key feature is being constant at both ends of the flow.

6.3.1.1 The holographic central charge at fixed points ($r \to \infty$)

In the first stage, we provide a brief summary of the holographic central charge concept. For a $(d+1)$ dimensional QFT, which is dual to a background, with metric and dilaton given by,

$$ds^2 = \alpha(r,\vec{\theta})\Big(dx_{1,d}^2 + \beta(r)dr^2\Big) + g_{ij}(r,\vec{\theta})d\theta^i d\theta^j, \qquad \Phi(r,\vec{\theta}), \tag{6.3.3}$$

we can calculate a weighted internal volume, V_{int}, defined below, and hence, the central charge as

$$\begin{aligned} V_{int} &= \int d\vec{\theta}\sqrt{\det[g_{ij}]e^{-4\Phi}\alpha^d}, \quad \hat{H} = V_{int}^2, \\ c_{hol} &= \frac{d^d}{G_N}\beta^{d/2}\frac{\hat{H}^{\frac{2d+1}{2}}}{(\hat{H}')^d}. \end{aligned} \tag{6.3.4}$$

We apply the aforementioned procedure to the UV fixed point solution of the AdS_6 backgrounds that emerge at $r \to \infty$ and correspond to the far UV limit of our QFTs. We set $d = 4$ in Eqs. (6.3.3) and (6.3.4) and pick Poincaré coordinates for AdS_6. By comparing with Eq. (6.2.1) in the large-r limit and making the necessary coordinate redefinitions, we have

$$\begin{aligned} &ds^2(\mathrm{AdS}_6) = r^2 dx_{1,4}^2 + \frac{dr^2}{r^2}, \quad \alpha = f_1(\sigma,\eta)r^2, \quad \beta = \frac{1}{r^4}, \ d = 4 \\ &g_{ij}d\theta^i d\theta^j = f_1 f_2 d\tilde{S}^2 + f_1 f_3(d\sigma^2 + d\eta^2), \quad V_{int} = \mathcal{N}r^4, \quad \mathcal{N} = \int d\theta\ d\varphi\ d\sigma\ d\eta\ \ \sin\theta\ f_1^4 f_2 f_3 f_6. \end{aligned} \tag{6.3.5}$$

From Eq. (6.3.4) and $X(r \to \infty) = 1$ in Eq. (6.2.2) and the form of the functions $f_i(r \to \infty, \sigma, \eta)$, we get the holographic central charge as

$$c_{hol} = \frac{1}{16G_N}\mathcal{N}, \tag{6.3.6}$$

$$G_N = 8\pi^6, \quad \mathcal{N} = 3^3\pi^5\int_0^P d\eta\int_{-\infty}^{\infty} d\sigma\ \sigma^3\partial_\sigma V\partial_\eta^2 V. \tag{6.3.7}$$

Examples

We now present two examples. For each case, we present the rank function $\mathcal{R}(\eta)$, related Fourier coefficients a_k, and the potential function $\hat{V}(\sigma,\eta)$ from Eq. (6.2.11). We also display the corresponding 5d quiver field theory and compute its holographic central charge.

First, we consider a gauge theory denoted as $\tilde{T}_{N,P}$. The IR behaviour of this gauge theory is characterised by the following quiver diagram:

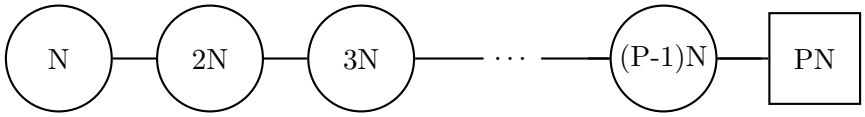

The rank function of this quiver is,

$$\mathcal{R}(\eta) = \begin{cases} N\eta & 0 \le \eta \le (P-1) \\ N(P-1)(P-\eta) & (P-1) \le \eta \le P. \end{cases}$$

The potential function $\hat{V}(\sigma,\eta)$ defined in Eq. (6.2.11) and the coefficients a_k are given as,

$$a_k = (-1)^{k+1}\frac{NP^3}{k^3\pi^3}\sin\left(\frac{k\pi}{P}\right), \tag{6.3.8}$$

$$\hat{V} = \frac{NP^3}{2\pi^3}\mathrm{Re}\left(\mathrm{Li}_3(-e^{-\frac{\pi}{P}(|\sigma|+i+i\eta)}) - \mathrm{Li}_3(-e^{-\frac{\pi}{P}(|\sigma|-i+i\eta)})\right). \tag{6.3.9}$$

Making use of Eq. (6.3.6), the holographic central charge in this case is

$$c_{hol} = \frac{N^2P^6}{8\pi^{10}}\left(2\zeta(5) - \mathrm{Li}_5(e^{\frac{2\pi i}{P}}) - \mathrm{Li}_5(e^{-\frac{2\pi i}{P}})\right). \tag{6.3.10}$$

It is noteworthy that this calculation is reliable for long-quiver limits. Hence, the $P \to \infty$ limit should be taken, and up to the leading order, one has

$$c_{hol} = \frac{N^2P^4}{2\pi^8}\zeta(3) + O\left(\frac{\log P}{P^2}\right). \tag{6.3.11}$$

The appearance of $\zeta(3)$ highlights the fundamentally non-perturbative nature of this quantity and its association with the 5d SCFT. This finding can be verified using a Matrix Model framework, as demonstrated in references [265–268].

Next, we explore another example known as the $+_{P,N}$ theory. The rank function for this

theory is expressed as follows:

$$\mathcal{R}(\eta) = \begin{cases} N\eta & 0 \le \eta \le 1 \\ N & 1 \le \eta \le (P-1) \\ N(P-\eta) & (P-1) \le \eta \le P. \end{cases}$$

This represents a linear balanced quiver field theory given by

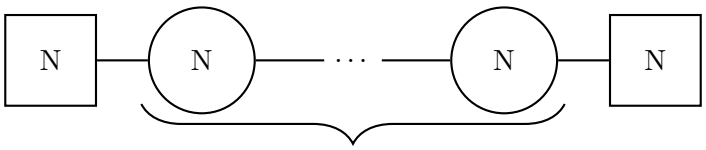

The potential function $\hat{V}(\sigma,\eta)$ defined in Eq. (6.2.11) and the coefficients a_k are given as,

$$a_k = \frac{NP^2}{k^3\pi^3}\sin\left(\frac{k\pi}{P}\right)\left(1+(-1)^{k+1}\right), \tag{6.3.12}$$
$$\hat{V} = \frac{NP^2}{2\pi^3}\mathrm{Re}\Big(\mathrm{Li}_3(e^{-\frac{\pi}{P}(|\sigma|-i\eta+i)}) - \mathrm{Li}_3(-e^{-\frac{\pi}{P}(|\sigma|-i\eta+i)}) + \mathrm{Li}_3(-e^{-\frac{\pi}{P}(|\sigma|-i\eta-i)}) - \mathrm{Li}_3(e^{-\frac{\pi}{P}(|\sigma|-i\eta-i)})\Big).$$

Finally the holographic central charge reads

$$c_{hol} = \frac{N^2P^4}{32\pi^{10}}\left(31\zeta(5) + 8\mathrm{Li}_5(-e^{\frac{2\pi i}{P}}) + 8\mathrm{Li}_5(-e^{-\frac{2\pi i}{P}}) - 8\mathrm{Li}_5(e^{\frac{2\pi i}{P}}) - 8\mathrm{Li}_5(e^{-\frac{2\pi i}{P}})\right).$$
$$c_{hol} \sim \frac{7N^2P^2}{4\pi^8}\zeta(3) + O\left(\frac{\log P}{P^2}\right). \tag{6.3.13}$$

Central Charge Along the Flow

Now, we calculate the central charge for the solution described in Eq. (6.2.1). This is dual to a 5-dimensional CFT, which is compactified on a circle and flows to a QFT with a mass gap.

We substitute $d = 3$ into Eq. (6.3.4). This choice effectively handles the QFT as being in $(3+1)$ dimensions. By comparing Eqs. (6.2.1) and (6.3.3), we derive the following:

$$\alpha(r) = f_1(\sigma,\eta)\frac{2\tilde{g}^2}{9}H^{1/2}(r)r^2, \quad \beta(r) = \frac{1}{r^2 f(r)}, \tag{6.3.14}$$
$$ds^2_{\text{int}} = g_{ij}(r,\vec{\theta})d\theta^i d\theta^j = f_1\left[\frac{2\tilde{g}^2}{9}H^{-3/2}f(r)\,d\phi^2 + f_2\left(d\theta^2 + \sin\theta^2(d\varphi - A_1^{(3)})^2\right) + f_3\left(d\sigma^2 + d\eta^2\right)\right],$$
$$V_{\text{int}} = \mathcal{N}r^3\sqrt{f(r)}, \quad \mathcal{N} = \int d\phi\; d\theta\; d\varphi\; d\sigma\; d\eta\; (\sin\theta\; f_1^4 f_2 f_3 f_6).$$

Calculating $\mathcal{N}$ we find,

$$\mathcal{N} = (\frac{2\tilde{g}^2}{9})^2 3^3 \pi^5 L_\phi \int_0^P d\eta \int_{-\infty}^{\infty} d\sigma \ \sigma^3 \partial_\sigma V \partial_\eta^2 V. \tag{6.3.15}$$

The holographic central charge in this case is,

$$c_{hol} = \frac{\mathcal{N}}{8G_N} \frac{(f(r)^2 r^3)}{(f(r) + r/6 f'(r))^3}, \tag{6.3.16}$$

with $G_N = 8\pi^6$. Fig. 6.3 shows an example plot of the holographic central charge, c_{hol}, respective to the radial coordinate.

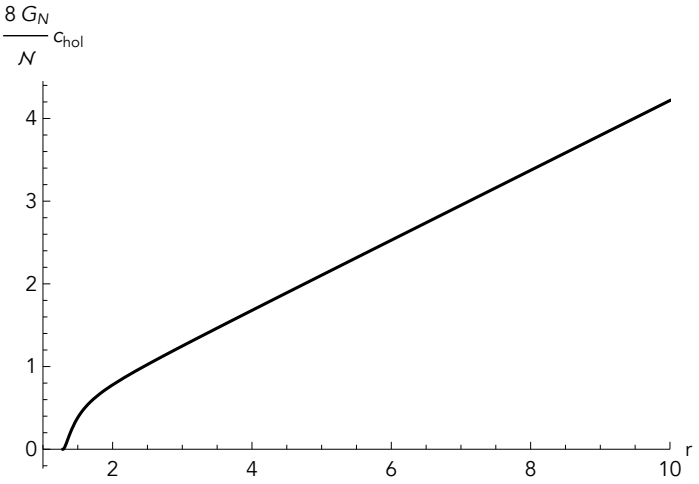

Figure 6.3. The holographic central charge with parameters $c = 1, \mu = 1$

For $r \to \infty$ and $r \to r^*$ limits, we find that Eq. (6.3.16) behaves as

$$\frac{8G_N}{\mathcal{N}} c_{hol} = \begin{cases} \frac{243}{128\tilde{g}^2} r + O(1/r) & r \to \infty \\ \frac{1944 r^{*7} (-12c^2\tilde{g}^2 r^{*2} + 12\tilde{g}^2 r^{*5} - 9\mu)^2}{(4c^4\tilde{g}^2 - 20c^2\tilde{g}^2 r^{*3} + 16\tilde{g}^2 r^{*6} - 27 r^* \mu)^3} (r - r^*)^2 + O(r - r^*)^3 & r \to r^* \end{cases}$$

This quantity diverges at high energies, indicating the need for a UV completion within a 5-dimensional theory. Essentially, it signifies that the infinite tower of Kaluza-Klein modes resulting from the S^1_ϕ compactification of the QFT introduces a divergent count of degrees of freedom as we move to higher energies and are captured by this quantity. Additionally, the central charge described in Eq. (6.3.16) becomes zero when $f(r^*) = 0$, indicating the presence of a gapped system.

It is worth noting that the factor $\mathcal{N}$ defined in Eq. (6.3.15), besides constants, incorporates the same integral found in the totally conformal case (as seen in Eq. (6.3.7)). Physically, this

implies that the degrees of freedom of the 5-dimensional UV, that are proportional to $\mathcal{N}$ in Eq. (6.3.7), are 'weighted' by the volume of the compact manifold. This perspective aligns with the framework discussed in Ref. [262] and is further explored in Ref. [269]. Essentially, the free energy along the flow includes contributions from the evolving nature of the flow itself (the r-dependent part of c_{hol}) and from the UV SCFT (represented by the factor $\mathcal{N}$ in Eq. (6.3.16)).

Because of the compactification on the circle S^1_ϕ, one choses $d = 3$ in Eq. (6.3.16), rather than $d = 4$. This adjustment is necessary as the 4d observable does not fully capture the 5d UV conformal completion.

At the UV limit, the central charge exhibits a linear divergence. This divergence in the free energy towards the UV is anticipated. Massive fields originating from the Kaluza-Klein compactification on the circle S^1_ϕ typically possess masses inversely proportional to the radius of the circle and remain frozen at low energies. As the system flows towards the UV, the massive fields have the possibility to become excited, leading to an increase in the number of these Kaluza-Klein modes with energy, ultimately causing the divergence of the central charge. Similar phenomena have been studied and explained in Refs. [270, 271].

In the upcoming section, we will compute a different quantity known as the 'flow central charge.' This quantity addresses the aforementioned deficiency by being sensitive to both the gapped QFT in the IR and the UV fixed points. Moreover, it is monotonic, making it suitable as a measure of the number of degrees of freedom (density of states) across the flow through different dimensions.

6.3.2 The flow-central charge

In scenarios where the QFT exhibits dimensional flow (QFT with anisotropy in spatial dimensions), we explore a refined definition of the central charge, as presented in [263]. Consider the metric and dilaton taking the following form:

$$\begin{aligned} ds^2 &= -\alpha_0 dt^2 + \alpha_1 dy_1^2 + \alpha_2 dy_2^2 + ... + \alpha_d dy_d^2 + \Pi_{i=1}^d (\alpha_1....\alpha_d)^{\frac{1}{d}} b(r) dr^2 + \\ & g_{ij}(d\theta^i - A_1^i)(d\theta^j - A_1^j), \qquad \Phi(r, \vec{\theta}). \end{aligned} \tag{6.3.17}$$

Here, we consider the case with $d = 4$, addressing a five-dimensional system (t, x_1, x_2, x_3, ϕ) with anisotropy. Our goal is to define a quantity that is monotonic along the flow, identifying the fixed point in the UV limit and distinguishing the gapped nature of the IR phase. Following the approach in [263], we define this quantity for our background as given in Eq. (6.2.1),

$$\begin{aligned} ds^2_{\text{int}} &= \alpha_1 dy_1^2 + \alpha_2 dy_2^2 + ... + \alpha_d dy_d^2 + g_{ij}(d\theta^i - A_1^i)(d\theta^j - A_1^j), \qquad \Phi(r, \vec{\theta}). \\ g_{ij}(d\theta^i - A_1^i)(d\theta^j - A_1^j) &= f_1 \left[f_2 \left(d\theta^2 + \sin\theta^2 (d\varphi - A_1^3)^2 \right) + f_3 \left(d\sigma^2 + d\eta^2 \right) \right]. \end{aligned} \tag{6.3.18}$$

We choose the combination,

$$V_{\rm int} = \int_X \sqrt{\det[g_{\rm int}]e^{-4\Phi}}, \qquad \hat{H} = V_{\rm int}^2. \tag{6.3.19}$$

The integral is over the X manifold, which comprises the internal space g_{ij}. The holographic central charge along the flow, denoted as $c_{\rm flow}$ reads

$$c_{\rm flow} = \frac{d^d}{G_N} b(r)^{d/2} \frac{\hat{H}^{\frac{2d+1}{d}}}{\hat{H}'^d}. \tag{6.3.20}$$

Setting $d = 4$ in the five-dimensional case we have,

$$\begin{aligned}
&\alpha_0 = \alpha_1 = \alpha_2 = \alpha_3 = \frac{2\tilde{g}^2}{9} f_1(\sigma,\eta) H(r)^{1/2} r^2, \quad \alpha_4 = \frac{2\tilde{g}^2}{9} f_1(\sigma,\eta) \frac{f(r)}{H(r)^{3/2}}, \\
&b(r) = \frac{H(r)^{1/2}}{f(r)^{5/4} r^{3/2}}, \quad V_{\rm int} = \mathcal{N} r^3 \sqrt{f(r)}, \quad \hat{H} = \mathcal{N}^2 r^6 f(r). \\
&c_{\rm flow} = \left(\frac{2}{3}\right)^4 \frac{\mathcal{N}}{G_N} \frac{H(r) r^4 f(r)^2}{\left(f(r) + \frac{r f'(r)}{6}\right)^4},
\end{aligned} \tag{6.3.21}$$

with $\mathcal{N}$ given in Eq. (6.3.15). Figure 6.4 shows an example of the flow central charge.

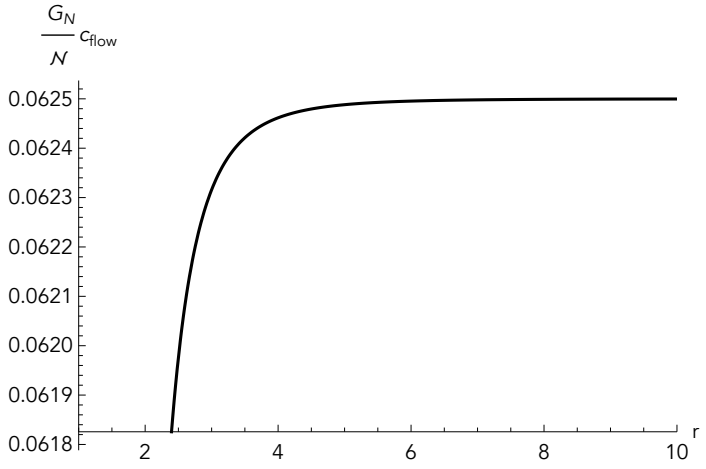

Figure 6.4. The flow central charge with choices $c = 1, \mu = 1$

We observe that the flow central charge $c_{\rm flow}$ is actually monotonic. In previous studies involving SUSY cases [251, 263], it was demonstrated to be monotonic using the BPS equations. In our current non-BPS background, this property still holds. The quantity $c_{\rm flow}$ effectively identifies the UV fixed point and reveals the gapped nature of the theory in the IR phase, indicated by zero degrees of freedom at $r = r^*$.

Now, we proceed to calculate a different observable of the QFT, namely Wilson loops.

6.3.3 Wilson loops

In this section, we compute the Wilson loop expectation values in QFT to examine the proposed mass gap and phenomena like confinement or screening at lower energies. We begin by summarising the general formalism used to compute Wilson loops in holographic QFTs, following the methodologies detailed in references such as [148, 272]. These methods are useful for analysing other probes that can be simplified as an effective action in the background, such as Entanglement Entropy or 't Hooft loops. For further insights, refer also to [273]. For a general background like

$$ds^2 = -g_{tt}dt^2 + g_{xx}d\vec{x}^2 + g_{rr}dr^2 + g_{ij}d\theta^i d\theta^j \tag{6.3.22}$$

where g_{tt}, g_{xx}, and g_{rr} depend only on the r-coordinate, we introduce an embedding for a string, with the Nambu-Goto action as

$$\begin{aligned} &t = \tau, \quad x = x(\gamma), \quad r = r(\gamma), \\ &S_{NG} = T_{F1}\int d\tau d\gamma \sqrt{g_{tt}(r)g_{xx}(r)x'^2 + g_{tt}(r)g_{rr}(r)r'^2}, \end{aligned} \tag{6.3.23}$$

where, (τ, γ) are the worldsheet coordinates that parametrise the embedding of the string. Following the approach outlined in Ref. [148], the equations of motion for the string dynamics in this background are expressed as

$$\frac{dr}{d\gamma} = \pm\frac{dx}{d\gamma}V_{eff}(r)\ . \tag{6.3.24}$$

We define an 'effective potential' as in Ref. [148]

$$V_{eff}(r) = \frac{F(r)}{CG(r)}\sqrt{F^2(r) - C^2}\ , \quad F^2(r) = g_{tt}g_{xx}, \quad G^2(r) = g_{tt}g_{rr}, \tag{6.3.25}$$

with constant $C = \frac{F^2x'}{\sqrt{F^2x'^2+G^2r'^2}}$ obtainable from the equations of motion.

In this formalism, when fixing the coordinate as $x(\gamma) = \gamma$, Eq. (6.3.24) can be derived from the conserved 'Hamiltonian' using the relation $C = F(r_0)$. Here, r_0 is the position where the string embedded in the background turns back, satisfying $r'(\gamma) = 0$. We adopt this gauge throughout and henceforth choose $C = F(r_0)$.

In this setup, we have an open string whose endpoints terminate at a D-brane located at $r \to \infty$. Dirichlet boundary conditions are imposed on the string at $r \to \infty$, ensuring $V_{\text{eff}}|_{r\to\infty} \sim \infty$. The separation between these string endpoints corresponds to the distance between a quark-antiquark pair in the dual gauge theory. The energy between the quark-antiquark

pair is computed using the Nambu-Goto action. A subtraction procedure is implemented to regularise the computation. This subtraction involves subtracting the self-energy of two infinitely massive strings that extend through the entire range of the radial coordinate $[r^*, \infty)$, effectively removing the rest mass contribution of the quark-antiquark pair.

The string forms a U-shape in the bulk. The separation $L_{QQ}(r_0)$ and energy $E_{QQ}(r_0)$ of the quark-antiquark pair can be expressed in terms of the distance from the turning point of the string r_0 as follows:

$$L_{QQ}\left(r_0\right) = 2\int_{r_0}^{+\infty} \frac{dz}{V_{eff}(z)}\,, \tag{6.3.26}$$

$$E_{QQ}\left(r_0\right) = F\left(r_0\right) L_{QQ}\left(r_0\right) + 2\int_{r_0}^{+\infty} dz \frac{G\left(z\right)}{F\left(z\right)} \sqrt{F\left(z\right)^2 - F\left(r_0\right)^2} - 2\int_{r^*}^{+\infty} dz\; G\left(z\right)\,. \tag{6.3.27}$$

The detailed conditions for confinement or screening of the theory are discussed in Ref. [148].

Now, we apply the aforementioned general procedure to the solution described by Eq. (6.2.2). Assuming the embedding of the string in the Σ plane is at a fixed point $(\sigma, \eta) = (\sigma^*, \eta^*)$, we choose coordinates $t = \tau$, $x = \gamma$, and $r = r(\gamma)$. In this setup, we have

$$ds^2_{\text{ind}} = \frac{2\tilde{g}^2}{9} f_1(r, \sigma^*, \eta^*) \left(-H(r)^{1/2} r^2 d\tau^2 + H(r)^{1/2} r^2 \left(1 + \frac{r'(\gamma)^2}{r^2 f(r)}\right) d\gamma^2 \right), \tag{6.3.28}$$

$$S_{NG} = T_{F1} \int d\tau d\gamma \sqrt{\det\left[g_{\alpha\beta}\right]}, = T_{F1} T \frac{2\tilde{g}^2}{9} \int d\gamma \sqrt{F^2 + G^2 r'^2}, \tag{6.3.29}$$

where the definitions

$$F(r) = \sqrt{H(r)} f_1(r, \sigma^*, \eta^*) r^2 \qquad G(r) = \sqrt{\frac{H(r)}{f(r)}} f_1(r, \sigma^*, \eta^*) r, \tag{6.3.30}$$

are used. The effective potential reads

$$V_{eff} = \frac{\sqrt{f(r)} r}{f_1(r_0, \sigma^*, \eta^*) \sqrt{H(r_0)} r_0^2} \sqrt{f_1(r, \sigma^*, \eta^*)^2 H(r) r^4 - f_1(r_0, \sigma^*, \eta^*)^2 H(r_0) r_0^4}. \tag{6.3.31}$$

One can expand the effective potential near to $r_0 = r^*$, $V_{eff} \sim (r - r^*)$, and see that L_{QQ} diverges when r_0 advances towards r^*, see also [148]. This observation could suggest potential confining behaviour in our dual QFT. We will examine this in greater detail below.

To explore the low-energy behaviour of the QFT and examine the possibility of confinement or screening, we investigate the expressions for the length and energy of the quark-antiquark pair. From Eqs. (6.3.26)-(6.3.27), we find that the length L_{QQ} of the quark-antiquark pair and its corresponding energy E_{QQ} are given by

$$L_{QQ}(r_0) = f_1(r_0,\sigma^*,\eta^*)\sqrt{H(r_0)}r_0^2 \times \int_{r_0}^{\infty} \frac{1}{\sqrt{f_1(r,\sigma^*,\eta^*)^2 H(r) r^4 - f_1(r_0,\sigma^*,\eta^*)^2 H(r_0) r_0^4}\sqrt{f(r)}r} dr \ , \tag{6.3.32}$$

$$E_{QQ}(r_0) = F(r_0)L_{QQ}(r_0) + 2\int_{r_0}^{\infty} dr \frac{\sqrt{f_1(r,\sigma^*,\eta^*)^2 H(r) r^4 - f_1(r_0,\sigma^*,\eta^*)^2 H(r_0) r_0^4}}{\sqrt{f(r)}r} - 2\int_{r^*}^{\infty} dr \sqrt{\frac{H(r)}{f(r)}} f_1(r,\sigma^*,\eta^*) r \ . \tag{6.3.33}$$

This integrals are calculated using numerical methods.

Figure 6.5 shows plots for the length of the string connecting the quark-antiquark pair and the corresponding energy as functions of this length, evaluated for specific background parameter values. The configurations for the profile of the string, depicted with $c = 1$ and $\mu =$

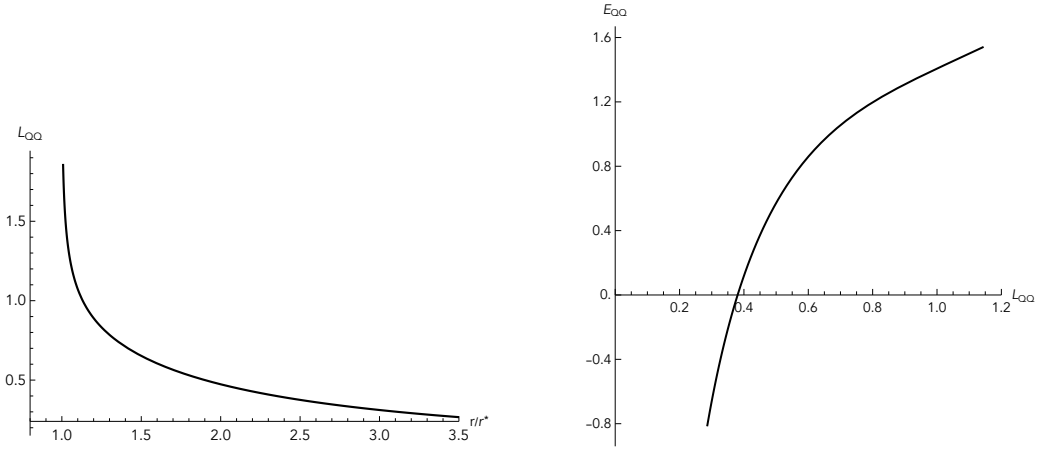

Figure 6.5. The string length between quark anti-quark pair and its energy for $c = 1, \mu = 1$

1, for different separation lengths, are illustrated in Fig. 6.6. These figures exhibit the typical behaviour expected in confining QFTs. We have fixed $\sigma^* = 0$ and kept η^* constant. One can check that the function $f_1(r,\sigma^*,\eta^*)$ does not depend on r, leading to major simplifications in the calculations. The η^* position is directly linked to the gauge node associated with the Wilson loop insertion (see also Ref. [274] and references mentioned there).

It is noteworthy that the energy curve E_{QQ} as a function of L_{QQ} has downward concavity, indicating the stability of the embedded probe string configuration described by Eq. (6.3.23).

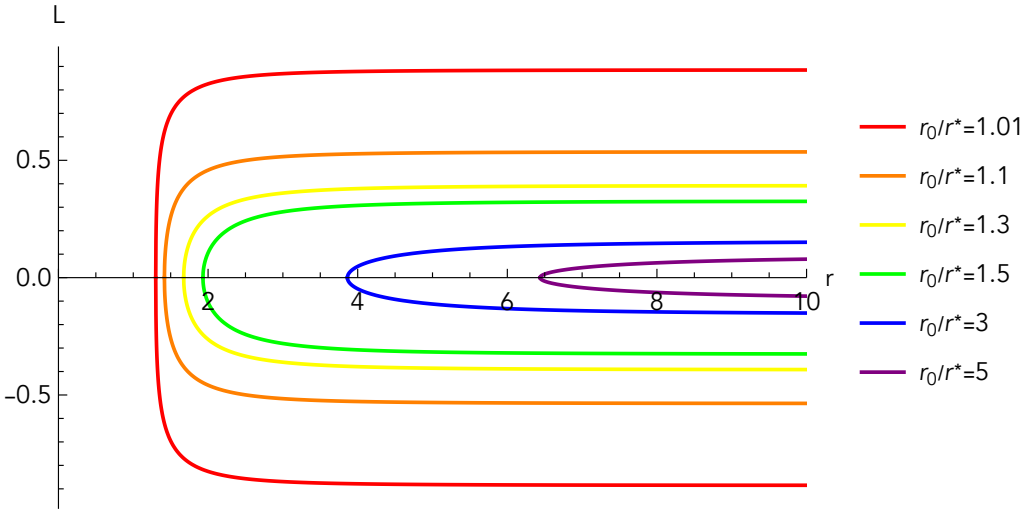

Figure 6.6. String profile related to the Wilson loop calculations for $c = 1, \mu = 1$

Additionally, for large values of L_{QQ}, the energy increases linearly, which is suggestive of confinement.

Below, we discuss a phenomenon that is not fully captured by the embedded strings considered in this section. This new configuration is associated with the presence of flavour branes within this family of background solutions.

6.3.3.1 Screening

In our dual QFT setups, massless flavour quarks are present. Specifically, each kink in the rank function $\mathcal{R}(\eta)$ corresponds to a flavour group, represented by a set of D7 branes localised in the η-direction, as discussed in Eq. (6.2.30). The presence of these flavour groups facilitates the screening phenomenon. This occurs when a pair of flavour quarks is created, which can disrupt the flux tube connecting the heavy probe quark to the anti-quark pair, thereby screening the interaction.

Even in cases where the Wilson loop is attached to a gauge node that does not have flavour quarks directly attached, interactions among the quiver degrees of freedom can eventually excite the flavour quarks. To rigorously investigate this, one would need to insert a probe string into the bulk that could extend not only in the spacelike x_1 and radial r directions but also along the η coordinate, associated to the gauge nodes in the quiver.

Generally, the embedding is parameterised by (τ, γ) variables. The induced metric is

given by

$$
\begin{aligned}
&t=\tau,\quad x=x(\gamma),\quad r=r(\gamma),\quad \eta=\eta(\gamma), \qquad (6.3.34)\\
&ds^2_{ind}=\left(\frac{2\tilde{g}^2}{9}\right)f_1(r,\sigma^*,\eta)\times\\
&\qquad\times\Big[-H(r)^{1/2}r^2d\tau^2+d\gamma^2\left(H(r)^{1/2}r^2x'^2+\frac{H(r)^{1/2}}{f(r)}r'^2+\frac{9f_3(r,\sigma^*,\eta)}{2\tilde{g}^2}\eta'^2\right)\Big].
\end{aligned}
$$

By performing the integration on $0\le\tau\le T$, the Nambu-Goto action takes the form,

$$
\begin{aligned}
&S_{NG}=TT_{F1}\int d\gamma\sqrt{F^2x'^2+G^2r'^2+S^2\eta'^2}, \qquad (6.3.35)\\
&F^2=\left(\frac{2\tilde{g}^2}{9}\right)^2f_1^2(r,\sigma^*,\eta)H(r)r^4,\qquad G^2=\left(\frac{2\tilde{g}^2}{9}\right)^2f_1^2(r,\sigma^*,\eta)\frac{H(r)r^2}{f(r)},\\
&S^2=\left(\frac{2\tilde{g}}{9}\right)f_1^2(r,\sigma^*,\eta)f_3(r,\sigma^*,\eta)H(r)^{1/2}r^2.
\end{aligned}
$$

One should minimise this action to investigate whether a configuration extending in the η-direction can approach the nearest flavour group. This is a cumbersome problem and is deferred for future study. Here, we undertake a simpler procedure that captures the idea of the calculation. Specifically, we introduce a probe string parameterised by $t=\tau$ and $\eta=\gamma$, while keeping other coordinates fixed. We compute the Nambu-Goto action by taking a string that extends from a specified node at $\eta=\eta^*$ to another node that may include flavour degrees of freedom.

If the energy associated with this configuration is lower than the Wilson loop expectation value derived in the previous section, a new stable solution emerges, leading to a phase transition. This transition signals the breakdown of the flux tube when the separation between the probe quark-antiquark pair gains an amount of energy sufficient to produce a dynamical quark pair. Hence, we consider a setup with $x=x_0$, $r=\bar{r}$, and $\sigma^*=0$. For this configuration, we get

$$
\begin{aligned}
&ds^2_{\rm ind}=-\frac{2\tilde{g}^2}{9}f_1(\bar{r},\sigma^*,\eta)H(\bar{r})^{1/2}\bar{r}^2d\tau^2+f_1(\bar{r},\sigma^*,\eta)f_3(\bar{r},\sigma^*,\eta)d\eta^2, \qquad (6.3.36)\\
&S_{NG}=T_{F1}\int d\tau d\gamma\sqrt{\det\big[g_{\alpha\beta}\big]},=T_{F1}T\int d\eta\sqrt{S^2}. \qquad (6.3.37)
\end{aligned}
$$

The $\sigma^*=0$ choice had been made and the simplified results are

$$
\begin{aligned}
&f_1^2(\bar{r},\sigma^*,\eta)=\frac{9\pi^2}{4X^4}\left(\frac{3X^4\sigma\partial_\sigma V+\sigma^2\partial_\eta^2V}{\partial_\eta^2V}\right),\qquad f_3(\bar{r},\sigma^*,\eta)=\frac{X^2\partial_\eta^2V}{3\sigma\partial_\sigma V}. \qquad (6.3.38)\\
&f_1^2f_3=\frac{3\pi^2}{4X^2}\left(\frac{\sigma\partial_\eta^2V}{\partial_\sigma V}+3X^4\right)|_{\sigma^*=0}\simeq\frac{9\pi^2}{4}X^2(\bar{r}),\quad S^2\simeq\frac{\pi^2}{2}\tilde{g}^2\bar{r}^2.
\end{aligned}
$$

Therefore, we obtain

$$S_{NG} = T_{F1} T \frac{\pi \tilde{g}}{\sqrt{2}} \bar{r} \int d\eta, \tag{6.3.39}$$

which is minimized whenever $\bar{r} = r^*$. The integration over η ranges from η^* (corresponding to the gauge group where the Wilson loop is inserted) to the desired position $\eta = \eta_F$ where the flavour branes are located. We observe that, there exist constant-energy configurations that dominate and are preferred over the embedding discussed in the preceding subsection. This phenomenon can be interpreted as screening due to the dynamic fundamental degrees of freedom.

In Appendix D of [8], we investigated a string extending in the η-direction as x increases. We observe a phase transition when the turning point η_0 approaches the position of the flavour brane. Extending this analysis to strings embedded in the r, η directions is a very interesting topic for future investigation.

6.3.4 Entanglement entropy

The entanglement entropy (EE) between two regions of a QFT with a string theory dual is calculable using the prescription given by [275, 276]. This method involves finding an eight-dimensional surface in the gravity dual that minimises a quantity such that the boundary of this surface matches the boundary of the two entangled regions on the dual QFT side. In this approach, we divide the spatial region into two parts: one is a strip of length L_{EE}, and the other is its complement in the space. The entanglement entropy of this system is determined by minimising the following action, as described in Refs. [275–277],

$$S_{EE} = \frac{1}{4G_N} \int_{\Sigma_8} d^8\sigma \sqrt{e^{-4\Phi} \det[g_{ind}]}. \tag{6.3.40}$$

Multiple eight-dimensional surfaces might minimise the entanglement entropy S_{EE} as given by Eq. (6.3.40). Consequently, a phase transition between different minimal surfaces is possible. In Ref. [277], it was suggested that the presence of such phase transitions in entanglement entropy could serve as an indicator of confinement. However, this proposal was scrutinised in Refs. [278, 279], which revealed that phase transitions might be absent in some confining models and that non-confining models could exhibit phase transitions.

Building upon the work of [275, 276] and considering the generalised framework from [277, 278], we compute the EE for a strip-like region in the QFT. This involves calculating the area of the eight-dimensional surface parameterised by $[x_1, x_2, x_3, \phi, \theta, \varphi, \sigma, \eta]$ with $r = r(x_1)$, within the background described in Section 6.2. The induced metric on this eight-dimensional

surface, as well as the resulting entanglement entropy, are given by:

$$ds^2_{st} = f_1 \frac{2\tilde{g}^2}{9}\Big[H(r)^{1/2} r^2\Big((1+\frac{r'^2}{r^2 f(r)})\, dx_1^2 + dx_2^2 + dx_3^2 \Big) + H(r)^{-3/2} f(r)\, d\phi^2\Big] \quad (6.3.41)$$
$$+ f_1 f_2 d\tilde{\Omega}_2 + f_1 f_3 (d\sigma^2 + d\eta^2).$$
$$\sqrt{e^{-4\Phi}\det[g_8]} = \sqrt{f_1^8 f_2^2 f_3^2 f_6^2 \sin^2\theta \frac{2\tilde{g}^2}{9}^4 f(r) r^6 (1+\frac{r'^2}{r^2 f(r)})},$$

$$S_{EE} = \frac{1}{4G_N}\int d^8x \sqrt{e^{-4\Phi}\det[g_8]} = \hat{\mathcal{N}} \int_{-L}^{L} dx \sqrt{r^6 f(r)(1+\frac{r'^2}{r^2 f(r)})}. \quad (6.3.42)$$

Where,

$$\hat{\mathcal{N}} = \frac{3^3\pi^5}{4G_N} L_y L_z L_\phi (\frac{2\tilde{g}^2}{9})^2 \int_0^P d\eta \int_{-\infty}^{\infty} d\sigma\ \sigma^3 \partial_\sigma V \partial_\eta^2 V. \quad (6.3.43)$$

From Eq. (6.3.25), we read

$$F(r) = r^3\sqrt{f(r)}, \qquad G(r) = r^2. \quad (6.3.44)$$

Using the Hamiltonian technique introduced in the Wilson loop calculation section and given in Eqs. (6.3.22)-(6.3.27), one can minimise the S_{EE} quantity. To properly compute S_{EE}, it must be regularised by subtracting the volume contributions of the two eight-dimensional surfaces that extend from infinity to the cutoff, r^*. To determine the entanglement entropy, we first calculate the length of the interval as a function of r_0. We then find the entanglement entropy by evaluating the regulated area of the eight-dimensional surface that has a turning point at r_0,

$$L_{EE}(r_0) = 2r_0^3\sqrt{f(r_0)} \int_{r_0}^{\infty} \frac{dr}{r\sqrt{f(r)}\sqrt{r^6 f(r) - r_0^6 f(r_0)}}, \quad (6.3.45)$$

$$S_{EE}(r_0) = \hat{\mathcal{N}} \int_{r_0}^{\infty} \frac{r^5\sqrt{f(r)}}{\sqrt{r^6 f(r) - r_0^6 f(r_0)}} dr - \hat{\mathcal{N}} \int_{r^*}^{\infty} r^2 dr. \quad (6.3.46)$$

We perform the integrals numerically and an example plot for choices of $c = 1, \mu = 1$ is given in Fig. 6.7.

In the left panel of Fig. 6.7, it becomes evident that L_{EE} does not exhibit a monotonic behaviour. Instead, it starts from a vanishing value at $r_0 = r^*$ and asymptotically approaches zero as $r_0 \to \infty$. This suggests the potential for a phase transition. Indeed, the conditions for a phase transition, as outlined in [278], are met. Specifically, Eqs. (2.26)-(2.29) from [278] indicate that $j = 3$, allowing for the possibility of a phase transition.

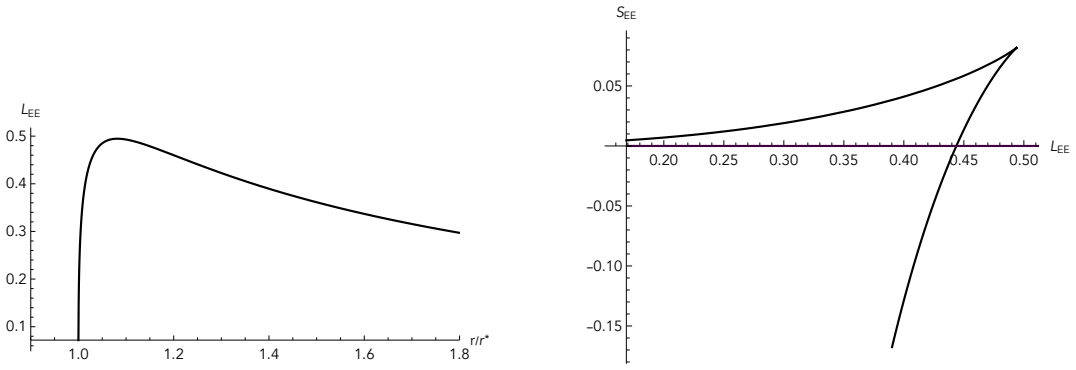

Figure 6.7. L_{EE} and entanglement entropy as a function of L

Furthermore, by setting $c = 0$ and $\mu = 0$, which returns our solution to the AdS_6 configuration, L_{EE} demonstrates a monotonic behavior and the phase transition vanishes. In this scenario, the integrals in Eqs. (6.3.46) can be computed explicitly, yielding $L_{EE} \sim \frac{1}{r_0}$ and $S_{EE} \sim \frac{\hat{\mathcal{N}}}{L_{EE}^3}$.

In the right panel of Fig. 6.7, the plot of $S_{EE}(r_0)$ as a function of L_{EE} exhibits a downward concavity, indicating the stability of the configuration. This graph also presents the disconnected solution, normalised to zero. Following a phase transition, the system favours the disconnected solution over the connected one.

Considering the discussions in Section 6.3.3.1, it becomes apparent that more complex eight-dimensional surfaces may need to be considered than the one discussed below Eq. (6.3.40) to check the stability. For instance, allowing dependencies like $r(x_1, \eta)$ could provide additional insights. However, these considerations are deferred to future research efforts.

6.3.5 Holographic complexity

We begin with a short overview of the complexity in QFTs. Afterwards, following the approach in Ref. [280], we introduce a proposal to calculate this quantity holographically using the backgrounds specified in Eq. (6.2.1). Our primary focus is on exploring the CV conjecture.

Quantum computational complexity is defined as the minimal number of elementary gates required in a quantum circuit to construct a generic state in the Hilbert space, starting from a designated reference state. This concept, initially discussed in Ref. [281], proposes a connection between the bulk geometry and the corresponding boundary state. According to Susskind's conjecture, the complexity of the dual boundary theory correlates with the evolving geometry behind an AdS black hole horizon.

Building upon this idea, the conjecture proposed in Ref. [258] refines the relationship further. It suggests that the complexity of the boundary state at a particular time (on a

spacelike slice of the boundary) is linked to the volume of a maximal spacelike slice within the bulk, terminating on the designated boundary slice. This refined conjecture is commonly referred to as the CV conjecture.

In this context, when we specify a spacelike slice Σ on the boundary of the spacetime of interest, the complexity $\mathcal{C}$ of $|\Psi\rangle$ as a pure state in the holographic field theory is conjectured to be related to the volume of a co-dimension one slice B within the bulk spacetime. This slice B in the bulk is characterised by having a boundary on Σ, and its volume is subject to a maximal condition.

$$\mathcal{C}_{\mathrm{V}} \propto \frac{V(B)}{G_{\mathrm{N}} l_{\mathrm{AdS}}}. \tag{6.3.47}$$

To explore issues concerning divergences encountered in the holographic complexity calculation, refer to Ref. [280].

An illustrative instance involves considering vacuum AdS_6 described in Poincaré coordinates:

$$ds^2 = \frac{\ell^2}{r^2}dr^2 + \frac{r^2}{\ell^2}\left(-dt^2 + d\vec{x}_4^2\right), \tag{6.3.48}$$

which corresponds to a CFT residing in flat spacetime. At fixed time $t = 0$, the maximal volume slice within the bulk with a specific boundary, has its volume as

$$V(B) = \int dr\, d^4x\, \sqrt{h} = \frac{V_{\vec{x}}}{\ell^3}\int_0^{r_M} r^3 dr = \frac{V_{\vec{x}}}{4\ell^3} r_M^4, \tag{6.3.49}$$

with $V_{\vec{x}}$ denoting the volume in the non-compact $\vec{x}_4$ directions, revealing an IR divergence. Consequently, following the CV conjecture, the calculated complexity is given by:

$$\mathcal{C}_{\mathrm{V}} \propto \frac{V_{\vec{x}}}{4G_6\ell^4} r_M^4. \tag{6.3.50}$$

This is directly proportional to the spatial volume of the field theory formulation space and scales with the UV cutoff power, which indicates a UV divergence.

To extend our analysis, we can lift the AdS_6 background to type IIB, as elucidated in Appendix F, as also discussed in Ref. [251] and [282]. The uplifted type IIB background in Eq. (6.2.1) under the conditions $X(r) = 1$, $H(r) = 1$, $A_1^{(3)} = 0$, and with parameters $c = \mu = 0$, contains a time slice with a nine-dimensional line element and a dilaton specified by

$$ds_9^2 = f_1\Big[\left(\frac{2\tilde{g}^2}{9}\right) r^2 d\vec{x}_3^2 + \left(\frac{2\tilde{g}^2}{9}\right)^2 r^2 d\phi^2 + \frac{dr^2}{r^2} + f_2 d\Omega_2 + f_3(d\eta^2 + d\sigma^2)\Big], \quad e^{-4\Phi} = f_6^2.$$

A proposal to calculate the complexity

Here, we propose a method to compute the complexity in this scenario (noting that we are

considering the case of zero temperature). The complexity is defined as the volume of the nine-dimensional manifold, multiplied by factors of the dilaton field and the global conformal factor $\mathcal{A}$ (where in this instance, $\mathcal{A} = f_1$). This is expressed as

$$\mathcal{C}_V \propto \frac{1}{G_{N,10}} \int dx^9 \sqrt{\frac{e^{-4\Phi}\det[g_9]}{\mathcal{A}}}. \tag{6.3.51}$$

Explicitly one has

$$\begin{aligned}
&\int dx^9 \sqrt{\frac{e^{-4\Phi}\det[g_9]}{\mathcal{A}}} = 4\pi V_{\tilde{x}} \left(\frac{2\tilde{g}^2}{9}\right)^{5/2} \left[\int d\sigma d\eta f_1^4 f_2 f_3 f_6\right] \int_0^{r_M} r^3 dr, \\
&\mathcal{C}_V \propto \frac{3^3\pi^5}{G_{N,10}} \left(\frac{2\tilde{g}^2}{9}\right)^{5/2} V_{\tilde{x}} \Big(\int d\sigma d\eta \sigma^3 \partial_\sigma V \partial_\eta^2 V\Big) r_M^4.
\end{aligned} \tag{6.3.52}$$

Now, we examine this relation. Firstly, observe that the factor $\left(\int d\sigma d\eta \sigma^3 \partial_\sigma V \partial_\eta^2 V\right)$ was also present in the expressions for holographic central charges and entanglement entropy (see Eqs. (6.3.7), (6.3.21), and (6.3.43)). This indicates that the complexity is directly proportional to the number of degrees of freedom within the UV CFT and is influenced by the parameters defining the UV quiver structure (as presented in Section 6.3.1.1).

Crucially, when combined with the volume of the two-sphere and the ten-dimensional Newton constant $G_{N,10}$, this factor gives rise to the six-dimensional Newton constant G_6, aligning with Eq. (6.3.50). The divergence with respect to the UV cutoff r_M remains consistent across computations in both the original and lifted backgrounds, as well as the IR divergence associated with $V_{\tilde{x}}$. Note that this outcome relies significantly on the definition outlined in Eq. (6.3.51), which notably includes normalisation by the overall conformal factor $\mathcal{A}$.

We validate our proposal by applying it to the complete background specified in Eq. (6.2.1). In this scenario, incorporating the radial functions $X(r)$, $H(r)$, $A_1^{(3)}$, and the non-zero parameters c and μ, transforms the underlying CFT_5 into a confining four-dimensional QFT at lower energies. By utilising the prescription in Eq. (6.3.51) with the dilaton and metric from Eq. (6.2.1), we reach to

$$\begin{aligned}
e^{-4\Phi}\det[g_9]/\mathcal{A} &= (2\tilde{g}^2/9)^5 f_1^8 f_2^2 f_3^2 f_6^2 r^6 \sqrt{H} \\
\mathcal{C}_V &\propto \frac{1}{G_{N,10}} \int dx^9 \sqrt{e^{-4\Phi}\det[g_9]/\mathcal{A}} \\
&= \frac{3^3\pi^5}{G_{N,10}} (\frac{2\tilde{g}^2}{9})^{5/2}\ \text{Vol}_{R_3}\ L_\phi \Big(\int d\sigma d\eta \sigma^3 \partial_\sigma V \partial_\eta^2 V\Big) \int_{r^*}^{r_M} dr r^3 H^{1/4},
\end{aligned} \tag{6.3.53}$$

with Vol_{R_3} presenting the volume of the three flat directions (x_1, x_2, x_3).

The analysis presented above, which connects complexity with the central charge of the

UV CFT_5, applies directly to this expression. It is important to note that while the UV behaviour in terms of the cutoff r_M resembles that in Eq. (6.3.52), the IR contribution from the background differs from the behaviour observed in the CFT case. If we were to compute the complexity in the six-dimensional solution that uplifts to the background described in Eq. (6.2.1) (see also Appendix F), we would encounter the same factor $\int_{r^*}^{r_M} dr\, r^3 H^{1/4}$.

In Eq. (6.3.53), the complexity exhibits a UV contribution emerging from the upper limit of the integral, which is proportional to r_M^4, consistent with the behaviour observed in the pure AdS_6 case in Eq. (6.3.52). Importantly, there is an additional contribution from the IR region of the geometry, which is in proportion to a Hypergeometric function evaluated at r^*. This introduces a scale related to the mass gap into the complexity calculation, similar to the observations in Ref. [283]. Comparing the complexity calculated in Eq. (6.3.52) with the one in Eq. (6.3.53) provides insights into the complexity of formation, following the approach in [284]. Exploring other definitions of complexity for comparison, as discussed in Ref. [284], would further enrich our understanding.

It is noteworthy that in Refs. [285, 286], an infinite family of observables defined on codimension-one slices of asymptotically AdS spaces were introduced as potential duals of complexity. These observables exhibit desirable features for complexity duality. Further investigation is required to determine whether our proposed approach aligns with this broader framework.

6.3.6 Spin-two glueballs

Regarding the four-dimensional QFT, holographically described by the background in Eq. (6.2.1), we utilise its 6d reduction as given in Eq. (F.1.11) to explore glueball-like fluctuations. These excitations are investigated by examining fluctuations of the background fields within the six-dimensional action. Due to the nonlinear and coupled nature of the equations of motion, any fluctuation in a particular field can induce fluctuations in other fields within the background. This coupling makes the dynamics of small fluctuations governed by a set of linear and coupled second-order differential equations, which pose significant challenges for solutions.

Here, we focus on a specific subset of fluctuations that are more tractable. We briefly outline and summarise the procedure for analysing these special fluctuations, drawing insights from Ref. [287]. For further details, Appendix C of the paper [256] is also referenced, providing additional context and methodology for this analysis.

The metric for the background in the Eq. (F.1.11) is,

$$ds_6^2 = H(r)^{1/2}\left(r^2\, dx_{1,3}^2 + f(r)^{-1}\, dr^2\right) + H(r)^{-3/2} f(r)\, d\phi^2, \tag{6.3.54}$$

where $f(r)$ and $H(r)$ functions are defined in Eq. (6.2.1). We intend to investigate the metric fluctuations as

$$\delta g_{\mu\nu} = e^{2A}\bar{h}_{\mu\nu}, \quad \bar{h}_{\mu\nu} = \begin{pmatrix} h_{ab}(x)\tilde{\psi}(y) & 0 \\ 0 & 0 \end{pmatrix}, \tag{6.3.55}$$

where the fluctuations are transverse to the flat subspace, with x^a representing the coordinates of flat spacetime (t, x_1, x_2, x_3), and y^i corresponding to directions (r, ϕ). We adopt the transverse-traceless gauge:

$$h^a{}_a = 0, \quad \nabla_a h^a{}_b = 0.$$

As presented in Ref. [287], considering vanishing fluctuations for other fields is consistent. Henceforth, we write the background metric as

$$ds^2 = e^{2A(\vec{y})}\left(ds^2(\mathcal{M}_4) + \bar{g}_{ab}(\vec{y})dy^a dy^b\right). \tag{6.3.56}$$

where $\mathcal{M}_4$ denotes a maximally symmetric space with metric $dx^2_{1,3}$, representing four-dimensional Minkowski space. Comparing two equations Eq. (6.3.54) and Eq. (6.3.56), we derive:

$$\begin{aligned} e^{2A(\vec{y})} &= r^2\sqrt{H(r)}, \\ \bar{g}_{ab}dy^a dy^b &= \frac{f(r)}{r^2H^2(r)}d\phi^2 + \frac{1}{r^2 f(r)}dr^2. \end{aligned} \tag{6.3.57}$$

Here, $\sqrt{\det \bar{g}_{ab}} = \frac{1}{r^2H(r)}$.

If we use the variable change $\tilde{\psi}(y) = e^{-2A}\Psi(y)$, similar to Ref. [287], the function $\Psi(y)$ satisfies a Schroedinger-like equation

$$-\bar{\Box}_y\Psi + V(y)\Psi = M^2\Psi, \tag{6.3.58}$$

where the potential is

$$V(y) = e^{-2A}\bar{\Box}_y e^{2A} = \frac{e^{-2A}}{\sqrt{\det \bar{g}_{ab}}}\partial_a\left[\sqrt{\det \bar{g}_{ab}}\bar{g}^{ab}\partial_b e^{2A}\right]. \tag{6.3.59}$$

When this procedure is performed for the background specified in Eq. (6.3.54), we check the glueball excitations depending on the r and ϕ coordinates.

$$\Psi(r,\phi) = e^{i\frac{2\pi}{L_\phi}n\varphi}\Psi(r), \quad n \in \mathbb{Z}, \tag{6.3.60}$$

where the potential from Eq. (6.3.59) reads,

$$V(r) = \sqrt{H(r)}\partial_r\left(\frac{f(r)}{H(r)}\partial_r(r^2\sqrt{H(r)})\right). \tag{6.3.61}$$

Eq. (6.3.58) is,

$$-r^2H(r)\partial_r\left(\frac{f(r)}{H(r)}\partial_r\Psi(r)\right)+\left(V(r)+\frac{n^2r^2H^2(r)}{f(r)}\left(\frac{2\pi}{L_\varphi}\right)^2\right)\Psi(r)=M^2\Psi(r). \tag{6.3.62}$$

Similar to Ref. [256] it is convenient to go to the tortoise coordinate $d\rho = \frac{dr}{r\sqrt{f(r)}}$ and introduce the variable change $\Psi(\rho) = \left(\frac{f(\rho)}{\rho^2H^2(\rho)}\right)^{-1/4}\Theta(\rho)$

$$-\frac{d^2\Theta}{d\rho^2}+\tilde{V}(\rho)\Theta=M^2\Theta, \tag{6.3.63}$$

$$\tilde{V}(\rho)=\left(V(r)+\frac{n^2r^2H^2(r)}{f(r)}\left(\frac{2\pi}{L_\varphi}\right)^2+r^2H(r)\frac{d}{dr}\left[\frac{f(r)}{H(r)}\frac{d}{dr}\left(\frac{f(\rho)}{\rho^2H^2(\rho)}\right)^{-1/4}\right]\right)\Bigg|_{r=r(\rho)}. \tag{6.3.64}$$

which should be evaluated in the ρ coordinate. Our potential after simplifying will be

$$\tilde{V}(\rho)=\left(\frac{-3r^2f'(r)^2+4rf(r)\left(rf''(r)+3f'(r)+4\left(\frac{2\pi n}{L_\varphi}\right)^2r^3H(r)^2\right)+12f(r)^2}{16r^2f(r)^2}\right)\Bigg|_{r=r(\rho)}, \tag{6.3.65}$$

We provide the effective potential plots for some values of n given in Fig. 6.8.

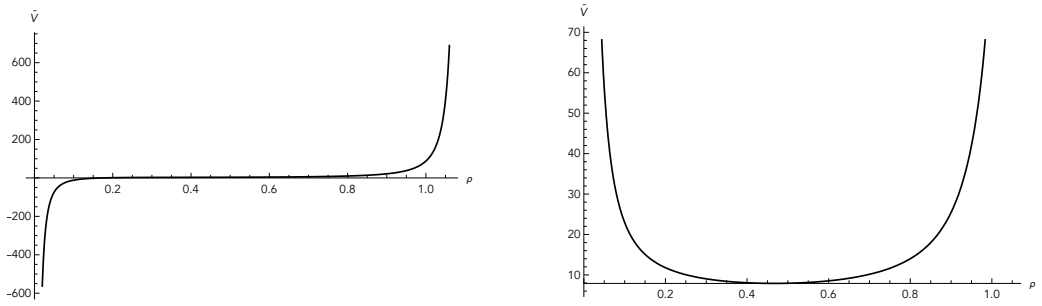

Figure 6.8. $\tilde{V}(\rho)$ potential with for $n = 0$ (left) and $n = 2$ (right) for $c = 1, \mu = 1$.

The fluctuations spectra for various values of n, c, and μ are depicted in Fig. 6.9. These fluctuations exhibit positive mass values, indicating the absence of any tachyonic instability in the background under consideration, when focusing on these specific spin-two fluctuation

modes.

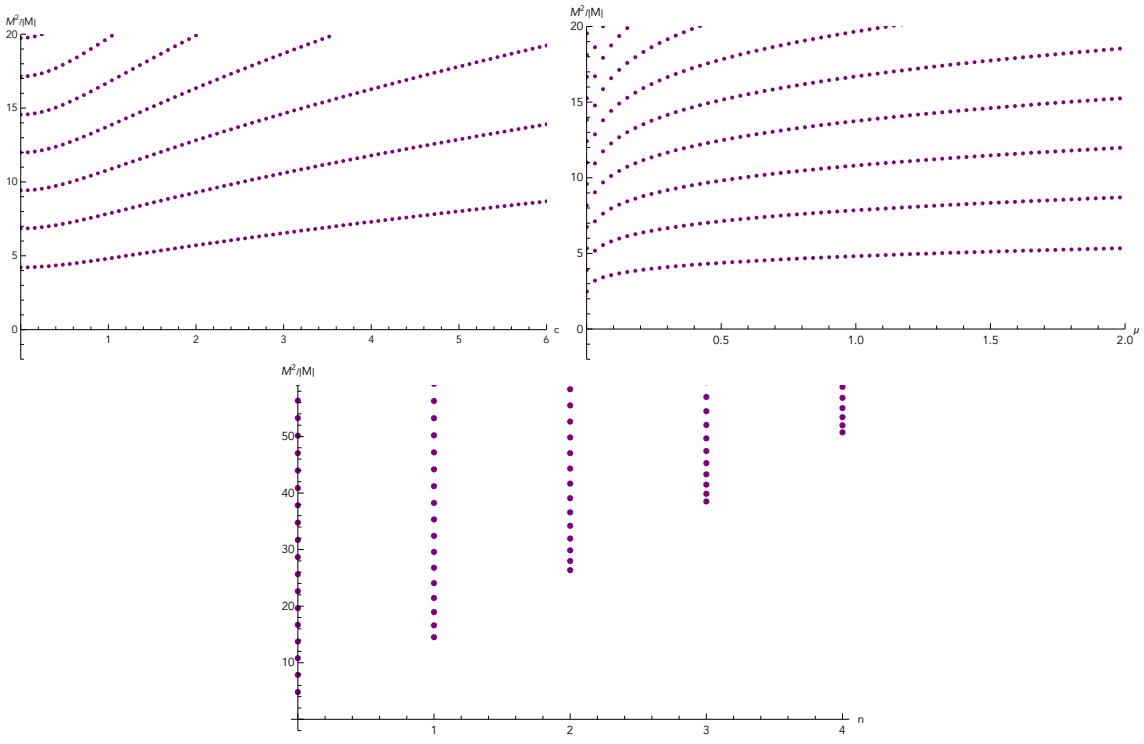

Figure 6.9. Spectrum of spin-2 fluctuations. Top Left: Variation of c for fixed $\mu = 1$. Top Right: Variation of μ for fixed $c = 1$. Bottom: Variation of n for $c = 1, \mu = 1$.

6.3.6.1 A stable background?

While the positive spectrum of masses for spin-two glueballs in the previous section is a step toward showing stability, this alone does not serve as proof of stability for our backgrounds defined by Eqs. (6.2.1)-(6.2.10).

This study does not discuss the detailed stability analysis of our backgrounds, though we will offer some comments on this matter.

A comprehensive analysis of fluctuations in our system is highly complex, involving the fluctuation of all Ramond and NS fields, as well as considering the effects of flavor branes. Restricting the number of fluctuating modes could simplify the analysis. One approach is to reduce the 10-dimensional background to six-dimensional $SU(2)$ gauged supergravity, as described in Appendix F. This reduction focuses on studying fluctuations in six dimensions, thereby involving fewer fields.

In the context of six-dimensional gauged supergravity, we can consider formulating first-order equations as an approach to solving the second-order equations of motion for fluctuations. While these first-order equations may not be conventional BPS equations associated

with supersymmetry, they could provide insights into stability aspects. This method aligns with approaches seen in "fake-supergravity" arguments for stability, as discussed in references such as [142] and related literature.

It is noteworthy to draw on an argument used in a similar context [288]: Our QFT exhibits a mass gap, as demonstrated in Section 6.3.1 where c_{flow} vanishes in the far IR, indicating the presence of a gap. This feature suggests that our deformation from the SUSY background, is not a small deformation. At large r, as the solution is nearly BPS, one can think that it is stable. However, this argument cannot be extrapolated to the region near $r \sim r^*$, where the departure from the CFT_5 dual background is substantial. Conversely, in the smaller r regime where the dual QFT exhibits a gap, one might anticipate that minor fluctuations in the background would not yield negative mass states. In other words, small fluctuations are unlikely to destabilise it significantly.

In conclusion, further rigorous analysis and computations of fluctuations will be crucial to substantiate these insights and ascertain the full stability properties of our backgrounds.

Chapter 7

SCFT deformations via uplifted solitons

7.1 Background and motivation

Following the discussions in Chapter 6, in this chapter, we continue the study of models that provide holographic descriptions of UV CFTs deformed by VEVs of operators, which undergo flows towards gapped and confining systems. This topic is approached from both holographic and field-theoretic perspectives based on works [9, 10]. Our exploration is motivated by several considerations. Initially, we aim to address certain undesirable features existing in the present frameworks and mentioned in Section 6.1. Specifically, we focus on four-dimensional SCFTs that contain an AdS_5 factor in their dual geometries. These SCFTs feature numerous localised flavour branes and are subject to deformation by VEVs of operators, initiating an RG flow that culminates in a state with confinement and a mass gap.

The holographic correspondence produces this field-theoretic evolution, by an asymptotically AdS_5 space that smoothly terminates at a fixed radial coordinate. This setup allows for a consistent exploration of the non-perturbative aspects of the RG flow within the quantum field theory. To implement this idea, we introduce a specific deformation within the holographic framework. Subsequent sections elaborate on this deformation and provide a detailed analysis of its implications and outcomes.

7.1.1 The deformation

The objective of this study is to provide a generic holographic mechanism that transforms known four-dimensional SCFTs into confining, three-dimensional SQFTs. Our inspiration stems from the work by Ref. [253], which introduced a supersymmetry-preserving AdS_5 solitonic solution. This solution, discussed in subsequent works [8, 255, 256, 273, 289–291], represents a compactification of $\mathcal{N} = 4$ Super Yang-Mills theory.

From the AdS_5/CFT_4 perspective, the findings of [253] lead to an $\mathcal{N} = 2$ SYM theory in three dimensions, coupled with massive multiplets. Importantly, this compactification

process preserves some supersymmetry due to mixing between the R-symmetry of $\mathcal{N}=4$ SYM and the isometry associated with the compact circle. This configuration is referred to as a 'twisted' compactification despite small differences with the common examples in the literature. The field-theoretic implications of this construction for $\mathcal{N}=4$ SYM theory are detailed in Ref. [292]. This mechanism is generalised here to different SCFTs with holographic dual backgrounds like

$$\mathrm{AdS}_5 \times M_n, \tag{7.1.1}$$

with $n=5$ and $n=6$ for Type II and 11d supergravity cases, respectively. Specifically, by utilising established embeddings of $d=5$ minimal gauged supergravity solutions into backgrounds of the form of Eq. (7.1.1), we have successfully uplifted the solitonic solution described in Ref. [253]. This effort has led to the discovery of new families of smooth backgrounds structured as

$$\widehat{\mathrm{AdS}_5} \times \widehat{M_n}, \tag{7.1.2}$$

where the hats signify a deformation summarised as follows:

- One AdS_5 direction is compactified into a circle S^1_ϕ of radius $L_\phi/2\pi$.
- The AdS_5 geometry is deformed by introduction of a warping function $f(r)$ that smoothly caps off the S^1_ϕ circle at a finite radius $r=r_\star$, satisfying $f(r_\star)=0$,

$$\frac{r^2}{l^2}(-dt^2+dx_1^2+dx_2^2+d\phi^2)+\frac{l^2}{r^2}dr^2 \quad \rightarrow \quad \frac{r^2}{l^2}(-dt^2+dx_1^2+dx_2^2+f(r)d\phi^2)+\frac{l^2}{r^2}\,\frac{dr^2}{f(r)}, \tag{7.1.3}$$

  where the parameters are chosen such that $L_\phi = \frac{l^2}{r_\star^2}\frac{4\pi}{f'(r_\star)}$ to prevent conical singularities.
- An appropriate $U(1)$ subgroup of the isometry group of the internal manifold M_n is identified and gauged by

$$\mathcal{A} = q\left(\frac{1}{r^2}-\frac{1}{r_\star^2}\right)d\phi, \tag{7.1.4}$$

  with adjustments made to all fluxes to ensure consistency with the equations of motion of ten- or eleven-dimensional supergravity.

The choice $r_\star=(ql)^{1/3}$ is required to preserve four supercharges specific to the $d=5$ gauged supergravity solution being uplifted [253]. Relying on the embedding frameworks established in Refs. [293–295] guarantees the preservation of higher-dimensional supersymmetry. Consequently, all examples presented maintain ten- or eleven-dimensional supersymmetry under this parameter configuration.

Returning to the field theory interpretation of our new solutions, the internal manifold M_n in the undeformed backgrounds Eq. (7.1.1) has essential data of the dual SCFT_4. Our

examples span a range of cases: from $M_5 = S^5$ corresponding to the $\mathcal{N} = 4$ SYM dual, to $M_5 = Y^{p,q}$ describing $\mathcal{N} = 1$ toric quiver field theories, as well as internal manifolds for $\mathcal{N} = 2$ linear quivers and $\mathcal{N} = 1$ SCFTs with non-Lagrangian descriptions.

When we deform each background as described earlier, we effectively implement a specific twisted compactification in the dual field theory. Compactifying on S^1_ϕ requires us to specify boundary conditions for the various fields in the SCFT. Typically, this breaks SUSY, as scalars and gauge fields adopt periodic boundary conditions while fermions become anti-periodic. However, SUSY can be preserved by introducing a background gauge field $\mathcal{A} = \mathcal{A}_\phi\, d\phi$, which mixes a $U(1)$ from the R-symmetry with the $U(1)_\phi$ isometry of the compact circle S^1_ϕ. Importantly, this background gauge field is constant in the boundary field theory but possesses a non-trivial holonomy, and cannot be absorbed by a gauge transformation. This gauge field alters the covariant derivative and, when appropriately adjusted in terms of its charge, allows for the existence of massless fermions that can form supermultiplets.

Introducing the background gauge field $\mathcal{A}_\phi$ and the compactification scale L_ϕ into the field theory indeed breaks conformal symmetry while preserving supersymmetry under suitable parameter choices. At low energies, our holographic approach to this twisted compactification transforms the original SCFT_4 into a strongly coupled SQFT_3, performable due to the shrinking of the circle S^1_ϕ. Utilising a range of holographic observables, we observe signs of confinement in these resulting (2+1)-dimensional IR theories.

This study is divided into two main sections.

In Section 7.3, we explore three new families of backgrounds of the form $\widehat{\text{AdS}}_5 \times M_5$. Here, $\widehat{\text{AdS}}_5$ represents a deformation of AdS_5 (and the dual CFT_4), while M_5 encodes various properties of the CFT_4. The first family originates from D3 branes located at the tip of $Y^{p,q}$ cones [296]. The second family is obtained from systems of D4-D6-NS5 branes, which are UV duals to four-dimensional $\mathcal{N} = 2$ SCFTs presented by Gaiotto and Maldacena [297]. The third family involves configurations of D6-D8-NS5 branes that, upon compactification on a two-manifold, lead to $\mathcal{N} = 1$ SCFTs [298, 299]. These SCFTs are subsequently deformed, as outlined earlier. We provide detailed backgrounds illustrating the deformation away from the conformal point for all three families, noting that our constructions are smooth except at the positions of flavour branes, if present.

In Section 7.4, we employ holographic methods to compute various observables for each dual QFT_3. Our analysis focuses on detecting signs of confinement using Wilson loops and Entanglement Entropy as primary diagnostics. Additionally, we also study the flow central charge that smoothly interpolates between the degrees of freedom of a gapped 3-dimensional system and a 4-dimensional CFT.

These appealing new backgrounds offer a valuable approach to enhance our understanding of the dynamics of QFTs exhibiting strong coupling effects. Importantly, they enable the

holographic investigation of the impacts of fundamental matter, particularly scenarios where the number of flavours, N_f, is comparable to the number of colours, N_c, with an SU(N_f) global symmetry. This introduces a new avenue for future exploration and study.

7.2 Review of the supersymmetric AdS_5 soliton

In this section, we review the original 5-dimensional minimal gauged supergravity solution discussed in Ref. [253], which serves as a template for exploring various uplifts in this study. The details regarding the supersymmetry of this solution can be found in appendix A of [9].

The focus is on the Einstein-Maxwell-AdS system in five dimensions, which has been developed across multiple studies [300–305]. The bosonic sector of the action is

$$S(g,A) = \frac{1}{16\pi G}\int d^5x\sqrt{-g}\left(R+\frac{12}{l^2}-\frac{3}{4}\mathcal{F}_{\mu\nu}\mathcal{F}^{\mu\nu}\right)+\frac{1}{16\pi G}\int \sqrt{-g}\mathcal{F}\wedge\mathcal{F}\wedge\mathcal{A}\,, \tag{7.2.1}$$

with l as the AdS radius. The equations of motion read

$$\begin{aligned} &d\star\mathcal{F}+\mathcal{F}\wedge\mathcal{F}=0\,,\\ &R_{\mu\nu}-\tfrac{1}{2}g_{\mu\nu}R-\tfrac{3}{2}\big[\mathcal{F}_{\mu\rho}\mathcal{F}_{\nu}{}^{\rho}-\tfrac{1}{6}g_{\mu\nu}\mathcal{F}_{\rho\sigma}\mathcal{F}^{\rho\sigma}\big]-\frac{6}{l^2}\,g_{\mu\nu}=0\,. \end{aligned} \tag{7.2.2}$$

We consider cases with $\mathcal{F}\wedge\mathcal{F}=0$ hence the Chern-Simons term will not contribute.

The solution of [253] is derived from the double wick rotation of a black hole solution with an electrical charge having a flat boundary. The resulting solution is

$$\begin{aligned} ds_5^2 &= \frac{r^2}{l^2}(-dt^2+dx_1^2+dx_2^2)+\frac{l^2dr^2}{r^2f(r)}+\frac{r^2}{l^2}f(r)d\phi^2, \qquad f(r)=1-\frac{\mu l^2}{r^4}-\frac{q^2l^2}{r^6},\\ \mathcal{A} &= q\left(\frac{1}{r^2}-\frac{1}{r_\star^2}\right)d\phi, \qquad \mathcal{F}=d\mathcal{A}=-\frac{2q}{r^3}dr\wedge d\phi, \end{aligned} \tag{7.2.3}$$

with $r_\star$ being the largest positive root of $f(r)$, as $f(r_\star)=0$. We have

$$\mu=\frac{(r_\star^6-q^2l^2)}{l^2r_\star^2}. \tag{7.2.4}$$

The ϕ-coordinate represents a circle with a finite radius at $r\to\infty$, but shrinks to zero size at $r=r_\star$. The smoothness of the solution at the end of space requires the periodicity of ϕ to be fixed to

$$L_\phi=\frac{4\pi l^2}{r_\star^2 f'(r_\star)}. \tag{7.2.5}$$

The magnetic flux induced by the gauge field at $r\to\infty$ is $\Phi=-\oint\mathcal{A}=\frac{q}{r_\star^2}L_\phi$.

To gain a deeper understanding of the solution space, it is advantageous to invert the relationships above and express the bulk parameters $r_\star$, q and μ in terms of the boundary parameters L_ϕ and Φ as

$$q = r_\star^2 \frac{\Phi}{L_\phi}, \qquad r_\star = \frac{\pi l^2}{2L_\phi}\left(1 \pm \sqrt{1 - \frac{\Phi^2}{\Phi_{max}^2}}\right), \tag{7.2.6}$$

with $\Phi_{max} = \frac{\pi l}{\sqrt{2}}$.

The parameter μ can be expressed in terms of boundary parameters from Eq. (7.2.4). For $\Phi < \Phi_{max}$, there exist two branches of solutions. For $\Phi \to 0$, the branch denoted as + approaches the AdS soliton, while the other (−) branch to Poincaré-AdS. Our interest lies in the + branch of the solution. These two branches merge at $\Phi = \Phi_{max}$.

As given in [9], supersymmetry preserving solutions need $\mu = 0$. This condition is satisfied when $r_\star^6 = q^2 l^2$, specifically

$$r_\star^2 = \frac{\Phi^2 l^2}{L_\phi^2} \quad \Rightarrow \quad 2 - 3\frac{\Phi^2}{\Phi_{max}^2} \pm 2\sqrt{1 - \frac{\Phi^2}{\Phi_{max}^2}} = 0. \tag{7.2.7}$$

The supersymmetric point is $\Phi_S = \frac{2\pi}{3} l$ on the + branch. We will assume this condition is met when we want to study supersymmetric backgrounds.

It is also useful to have a new parameter Q defined in order to have a simple form for the boundary gauge field as

$$\mathcal{A}(r \to \infty) = Q\, d\phi \tag{7.2.8}$$

for the supersymmetric choice in the parameter space. This can be achieved by defining $q = -Q^3 l^2$. The supersymmetry preserving condition, $\mu = 0$, corresponds to $r_\star^2 = (Ql)^2$. Finally, the solution takes the form of

$$\begin{aligned} ds_5^2 &= \frac{r^2}{l^2}(-dt^2 + dx_1^2 + dx_2^2) + \frac{l^2}{r^2}\frac{dr^2}{f(r)} + \frac{r^2}{l^2} f(r) d\phi^2, \qquad f(r) = 1 - \left(\frac{lQ}{r}\right)^6, \\ \mathcal{A} &= \left(Q - \frac{l^2 Q^3}{r^2}\right) d\phi, \qquad \mathcal{F} = d\mathcal{A} = \frac{2l^2 Q^3}{r^3} dr \wedge d\phi. \end{aligned} \tag{7.2.9}$$

It is noteworthy that the holonomy of the gauge field at the boundary reads

$$\Phi = \oint \mathcal{A} = \frac{2\pi}{3} l. \tag{7.2.10}$$

7.3 Geometry: new families of backgrounds

In this section, we introduce three new infinite families of solutions. Our focus is on highlighting their shared geometric origin across these families from Section 7.2. Despite considerable variations in the dual QFT for each background, there exists a clear continuity from the geometry perspective.

We commence by describing a background within the framework of $\mathrm{AdS}_5 \times S^5$, as previously given in Ref. [253]. Subsequently, we transition to an internal space $\mathrm{T}^{1,1}$ before presenting deformations of general $\mathrm{AdS}_5 \times \mathrm{Y}^{p,q}$ backgrounds. Following this, we introduce additional novel infinite families of backgrounds in Type IIA and massive Type IIA theories, respectively.

7.3.1 Deformed $\mathbf{AdS}_5 \times S^5$ and $\mathbf{AdS}_5 \times \mathrm{Y}^{p,q}$ backgrounds

Consider the deformation of $\mathrm{AdS}_5 \times S^5$ as studied in Ref. [253]. We provide the metric, vielbein basis, and the five-form solving the Type IIB equations of motion. The ten-dimensional metric is given by

$$\begin{aligned} \mathrm{d}s_{10}^2 = \mathrm{d}s_5^2 + l^2 \Big\{ & \mathrm{d}\theta^2 + \sin^2\theta \mathrm{d}\varphi^2 + \sin^2\theta \sin^2\varphi \left(\mathrm{d}\varphi_1 + \frac{\mathcal{A}}{l}\right)^2 \\ & + \sin^2\theta \cos^2\varphi \left(\mathrm{d}\varphi_2 + \frac{\mathcal{A}}{l}\right)^2 + \cos^2\theta \left(\mathrm{d}\varphi_3 + \frac{\mathcal{A}}{l}\right)^2 \Big\}, \end{aligned} \tag{7.3.1}$$

with $\mathrm{d}s_5^2$ representing the line element and $\mathcal{A}$ the one-form from Section 7.2 restated as

$$\mathrm{d}s_5^2 = \frac{r^2}{l^2}(-\mathrm{d}t^2 + \mathrm{d}x_1^2 + \mathrm{d}x_2^2 + f(r)\mathrm{d}\phi^2) + \frac{l^2\,\mathrm{d}r^2}{r^2 f(r)}, \tag{7.3.2}$$

$$f(r) = 1 - \frac{\mu l^2}{r^4} - \frac{q^2 l^2}{r^6}, \quad \mathcal{A} = q\left(\frac{1}{r^2} - \frac{1}{r_*^2}\right)\mathrm{d}\phi\,. \tag{7.3.3}$$

Here $\mathrm{d}\mathcal{A} = \mathcal{F}$, is the field strength of $\mathcal{A}$. We choose $\mu = 0$ throughout this section to preserve supersymmetry. The parameter $r_* = (ql)^{1/3}$ marks the end of the space where $f(r_*) = 0$.

As described previously, to ensure the smoothness of the background, we restrict the angular variable ϕ to vary within the range $\left[0, \frac{2\pi l^2}{3r_*}\right]$. The other angular coordinates vary as follows: $\theta \in [0, \pi/2]$, $\varphi \in [0, \pi/2]$, and $\varphi_1, \varphi_2, \varphi_3 \in [0, 2\pi]$. This choice avoids conical singularities in the metric. Our vielbein read,

$$
\begin{aligned}
&e^1 = \frac{r}{l}\mathrm{d}t\,, \quad e^2 = \frac{r}{l}\mathrm{d}x_1\ ,\ e^3 = \frac{r}{l}\mathrm{d}x_2\ ,\ e^4 = \frac{l\ \mathrm{d}r}{r\sqrt{f(r)}}\ ,\ e^5 = \frac{r}{l}\sqrt{f(r)}\mathrm{d}\phi,\\
&e^6 = l\mathrm{d}\theta\ ,\ e^7 = l\sin\theta\mathrm{d}\varphi\ ,\ e^8 = l\sin\theta\sin\varphi\left(\mathrm{d}\varphi_1 + \frac{\mathcal{A}}{l}\right),\\
&e^9 = l\sin\theta\cos\varphi\left(\mathrm{d}\varphi_2 + \frac{\mathcal{A}}{l}\right)\ ,\ e^{10} = -l\cos\theta\left(\mathrm{d}\varphi_3 + \frac{\mathcal{A}}{l}\right).
\end{aligned}
\tag{7.3.4}
$$

One can introduce the following quantities

$$
\mu_1 = \sin\theta\sin\varphi,\ \ \mu_2 = \sin\theta\cos\varphi,\ \ \mu_3 = \cos\theta. \tag{7.3.5}
$$

In terms of these, we can write

$$
\begin{aligned}
&F_5 = (1+\star_{10})G_5, \qquad G_5 = -\frac{4}{l}e^1\wedge e^2\wedge e^3\wedge e^4\wedge e^5 + J_2\wedge\star_5\mathcal{F},\\
&J_2 = l^2\sum_{i=1}^{3}\mu_i\mathrm{d}\mu_i\wedge\left(\mathrm{d}\varphi_i + \frac{\mathcal{A}}{l}\right), \qquad \mathcal{F} = \frac{2q}{r^3}e^5\wedge e^4, \qquad \star_5\mathcal{F} = -\frac{2q}{r^3}e^1\wedge e^2\wedge e^3,
\end{aligned}
\tag{7.3.6}
$$

where, $\star_5$ is presenting the Hodge star operation restricted to $\mathrm{d}s_5^2$. The quantisation condition for Dp-branes, specifically $D3$-branes in the context of type IIB supergravity, involves the flux of the Ramond-Ramond field C_4 over the compact manifold on which the branes are wrapped. For $D3$-branes, the quantisation condition on the manifold $\Sigma_5[\theta,\varphi,\varphi_1,\varphi_2,\varphi_3]$ is given by:

$$
\begin{aligned}
&\int_{\Sigma_{8-p}} F_{8-p} = (2\pi)^{7-p}g_s\alpha'^{\frac{7-p}{2}}N_{\mathrm{D}p}, \quad \text{which for } p=3 \text{ gives}\\
&N_{\mathrm{D3}} = \frac{l^4}{4\pi g_s\alpha'^2}.
\end{aligned}
\tag{7.3.7}
$$

Now, we proceed to introduce new families of solutions. In these solutions, the five-sphere is substituted with a $\mathrm{Y}^{p,q}$ manifold [306, 307]. The approach mirrors that of the background described by Eqs.(7.3.1)-(7.3.3). Here, we introduce a $\mathrm{U}(1)_R$ isometry that is fibered over the ϕ-direction, compactified with a radius, chosen to prevent singularities. The functions in $\mathrm{d}s_5^2$ are selected similarly to those in Eq. (7.3.3). Analogously, a structure similar to Eq. (7.3.6) emerges for the Ramond forms. As a preliminary example, we study the case of $\mathrm{T}^{1,1}$.

7.3.1.1 Deformed $AdS_5 \times T^{1,1}$ background

The $T^{1,1}$ manifold can be expressed as a fibration of an S^1 over $S^2 \times S^2$, with coordinates $(\theta_1, \phi_1, \theta_2, \phi_2)$,

$$ds^2_{T^{1,1}} = \frac{1}{6}\sum_{i=1}^{2}\left(d\theta_i^2 + \sin^2\theta_i d\phi_i^2\right) + \frac{1}{9}\left(d\psi + \sum_{i=1}^{2}\cos\theta_i d\phi_i\right)^2, \tag{7.3.8}$$

with $\psi \in [0, 4\pi]$. The metric and vielbein for Type IIB theory are,

$$\begin{aligned}
ds^2_{10} &= ds^2_5 + l^2\left[\frac{1}{6}\sum_{i=1}^{2}\left(d\theta_i^2 + \sin^2\theta_i d\phi_i^2\right) + \frac{1}{9}\left(d\psi + \sum_{i=1}^{2}\cos\theta_i d\phi_i + \frac{3}{l}\mathcal{A}\right)^2\right]. \qquad (7.3.9)\\
e^1 &= \frac{r}{l}dt\,, \quad e^2 = \frac{r}{l}dx_1\ ,\ e^3 = \frac{r}{l}dx_2\ ,\ e^4 = \frac{l\ dr}{r\sqrt{f(r)}}\ ,\ e^5 = \frac{r}{l}\sqrt{f(r)}d\phi,\\
e^6 &= \frac{l}{\sqrt{6}}d\theta_1\ ,\ e^7 = \frac{l}{\sqrt{6}}\sin\theta_1 d\phi_1\ ,\ e^8 = \frac{l}{\sqrt{6}}d\theta_2,\\
e^9 &= \frac{l}{\sqrt{6}}\sin\theta_2 d\phi_2\ ,\ e^{10} = \frac{l}{3}\left(d\psi + \cos\theta_1 d\phi_1 + \cos\theta_2 d\phi_2 + \frac{3}{l}\mathcal{A}\right).
\end{aligned}$$

The F_5 field is described using the volume element of the 5d manifold ds^2_5 and the gauge field $\mathcal{A} = q\left(\frac{1}{r^2} - \frac{1}{r_*^2}\right)d\phi$ as

$$\begin{aligned}
&F_5 = G_5 + \star G_5,, \qquad G_5 = \frac{4}{l}\text{vol}_5 - J\wedge\star_5\mathcal{F},\\
&\text{vol}_5 = e^1\wedge e^2\wedge e^3\wedge e^4\wedge e^5, \qquad J = -e^6\wedge e^7 - e^8\wedge e^9.
\end{aligned} \tag{7.3.10}$$

The D3 Page charge quantisation is similar to Eq. (7.3.7) as we integrate over $T^{1,1}$,

$$N_{D3} = \frac{4l^4}{27\pi g_s\alpha'^2}. \tag{7.3.11}$$

7.3.1.2 Deformed $AdS_5 \times Y^{p,q}$ backgrounds

Similar to the previous section, we also provide a metric with $Y^{p,q}$ submanifold, see [307]. One has,

$$\begin{aligned}
ds^2_{10} = ds^2_5 + l^2\Bigg[&\frac{1-y}{6}\left(d\theta^2 + \sin^2\theta d\varphi^2\right) + \frac{1}{w(y)v(y)}dy^2 + \frac{w(y)v(y)}{36}\left(d\beta + \cos\theta d\varphi\right)^2\\
&+\frac{1}{9}\left(d\psi - \cos\theta d\varphi + y\left(d\beta + \cos\theta d\varphi\right) + \frac{3}{l}\mathcal{A}\right)^2\Bigg],
\end{aligned} \tag{7.3.12}$$

where

$$w(y) = \frac{2(a-y^2)}{1-y} \ , \ v(y) = \frac{a+2y^3-3y^2}{a-y^2}, \tag{7.3.13}$$

with a representing a parameter[1]. The vielbein for this background is given as,

$$\begin{aligned}
&e^1 = \frac{r}{l}\mathrm{d}t\,, \quad e^2 = \frac{r}{l}\mathrm{d}x_1 \ , \ e^3 = \frac{r}{l}\mathrm{d}x_2 \ , \ e^4 = \frac{l\ \mathrm{d}r}{r\sqrt{f(r)}} \ , \ e^5 = \frac{r\sqrt{f(r)}}{l}\mathrm{d}\phi,\\
&e^6 = l\sqrt{\frac{1-y}{6}}\mathrm{d}\theta \ , \ e^7 = l\sqrt{\frac{1-y}{6}}\sin\theta\mathrm{d}\varphi \ , \ e^8 = \frac{l}{\sqrt{6}H(y)}\mathrm{d}y,\\
&e^9 = l\frac{H(y)}{\sqrt{6}}(\mathrm{d}\beta+\cos\theta\mathrm{d}\varphi) \ , \ e^{10} = \frac{l}{3}\left(\mathrm{d}\psi-\cos\theta\mathrm{d}\varphi+y(\mathrm{d}\beta+\cos\theta\mathrm{d}\varphi)+\frac{3}{l}\mathcal{A}\right),
\end{aligned} \tag{7.3.14}$$

with $H(y) = \sqrt{\frac{wv}{6}}$. For the four-dimensional base manifold parametrised by $[\theta, \varphi, y, \beta]$, the Kähler form is

$$J = e^6 \wedge e^7 + e^8 \wedge e^9. \tag{7.3.15}$$

Similar to Eq. (7.3.10) the five-form flux is

$$\begin{aligned}
F_5 = &\frac{4}{l}\mathrm{vol}_5 - \frac{4}{l}e^6\wedge e^7\wedge e^8\wedge e^9\wedge e^{10} + \frac{2q}{r^3}e^1\wedge e^2\wedge e^3\wedge J\\
&- \frac{2q}{r^3}e^4\wedge e^5\wedge(e^6\wedge e^7+e^8\wedge e^9)\wedge e^{10},
\end{aligned} \tag{7.3.16}$$

while D3 brane charges are quantised similar to Eq. (7.3.7).

It is worth emphasising that all the backgrounds discussed in this section satisfy the Einstein and Maxwell equations in Type IIB supergravity, along with the corresponding Bianchi identities. Moreover, these solutions preserve four supercharges.

Next, we introduce two distinct families of backgrounds. The first family is based upon solutions in 11-dimensional supergravity described by Gaiotto, and Maldacena [297]. The second family is based on massive Type IIA backgrounds given by Bah, Passias, and Tomasiello (BPT) [308].

7.3.2 Deformed Gaiotto-Maldacena backgrounds

We investigate a new infinite family of backgrounds inspired by the Gaiotto-Maldacena solutions [297]. The goal remains to maintain $\mathcal{N} = 1$ supersymmetry (four supercharges), while modifying the original backgrounds through a fibration involving the R-symmetry, $SU(2)\times U(1)$, and the compactified ϕ-direction within $\mathrm{ds}_5{}^2$.

[1]Specifically, when $0 < a < 1$, the base manifold B can be topologically represented as a product of two-spheres. The coordinate y ranges between the two smallest roots of $a - 3y^2 + 2y^3 = 0$, denoted as y_1 and y_2.

Using the definitions of μ_i from Eq. (7.3.5) and the one-form $\mathcal{A}$ from Eq. (7.3.3), we introduce the differential operators and the volume element for the $\tilde{S}^2$ as follows:

$$D\mu_1 = \mathrm{d}\mu_1 + 2\mu_2\mathcal{A}, \quad D\mu_2 = \mathrm{d}\mu_2 - 2\mu_1\mathcal{A}, \quad D\mu_3 = \mathrm{d}\mu_3,$$
$$\mathrm{Vol}\tilde{S}^2 = \frac{1}{2}\epsilon^{ijk}\mu_i D\mu_j \wedge D\mu_k. \tag{7.3.17}$$

Using these differential forms and a function $V(\sigma,\eta)$ and its derivatives, $\dot{V} \equiv \sigma\partial_\sigma V$ and $V' \equiv \partial_\eta V$, we can construct a configuration within eleven-dimensional supergravity that solves the equations of motion, provided the "potential function" $V(\sigma,\eta)$ solves the Laplace-like equation:

$$\sigma\partial_\sigma\left(\sigma\partial_\sigma V\right) + \sigma^2\partial_\eta^2 V = 0. \tag{7.3.18}$$

The metric and four-form field strength are then given by,

$$\begin{aligned}
&\frac{\mathrm{d}s_{11}^2}{\kappa^{2/3}} = f_1\Big[4\mathrm{d}s_5^2 + f_2 D\mu_i D\mu_i + f_3\left(D\tilde{\chi}\right)^2 + f_4(\mathrm{d}\sigma^2 + \mathrm{d}\eta^2) + f_5\left(\mathrm{d}\tilde{\beta} + f_6 D\tilde{\chi}\right)^2\Big],\\
&\frac{G_4}{4\kappa} = \mathrm{d}\left[f_7 D\tilde{\chi} + f_8\mathrm{d}\tilde{\beta}\right]\wedge \mathrm{vol}\tilde{S}^2 + \mathrm{d}(\mu_3\dot{V})\wedge\star_5\mathcal{F}\\
&+2(f_7 D\tilde{\chi} + f_8\mathrm{d}\tilde{\beta})\wedge\mathrm{d}\mu_3\wedge\mathcal{F} - \left[\mathrm{d}(\mu_3\dot{V})\wedge D\tilde{\chi} + \mathrm{d}(\mu_3\eta)\wedge\mathrm{d}\tilde{\beta}\right]\wedge\mathcal{F}.\\
&f_1 = \left(\frac{\dot{V}\tilde{\Delta}}{2V''}\right)^{\frac{1}{3}}, \quad f_2 = \frac{2V''\dot{V}}{\tilde{\Delta}}, \quad f_3 = \frac{4\sigma^2}{\Lambda}, \quad f_4 = \frac{2V''}{\dot{V}},\\
&f_5 = \frac{2\Lambda V''}{\dot{V}\tilde{\Delta}}, \quad f_6 = \frac{2\dot{V}\dot{V}'}{V''\Lambda}, \quad f_7 = -\frac{\dot{V}^2V''}{\tilde{\Delta}}, \quad f_8 = \frac{1}{2}\left(\frac{\dot{V}\dot{V}'}{\tilde{\Delta}} - \eta\right),\\
&\tilde{\Delta} = \Lambda(V'')^2 + (\dot{V}')^2, \qquad \Lambda = \frac{2\dot{V} - \ddot{V}}{V''}, \qquad D\tilde{\chi} = \mathrm{d}\tilde{\chi} + \mathcal{A}.
\end{aligned} \tag{7.3.19}$$

To ensure the consistency and physical relevance of the configuration described by $V(\sigma,\eta)$, appropriate boundary conditions must be imposed. These boundary conditions carry specific features of the dual linear quiver field theory, through a Rank function similar to the model in Section 6.3. This formalism is comprehensively discussed in Refs. [309] and [310].

In this context, each solution corresponds to an infinite series of backgrounds, with each background associated with a distinct 4-dimensional $\mathcal{N} = 2$ SCFT described by a linear quiver. As we compactify on the ϕ-circle, these UV fixed points evolve into confining quantum field theories.

Upon reducing to Type IIA supergravity along the β-circle to preserve supersymmetry (as explained in Ref. [310]), the resulting ten-dimensional string frame background is given

by,

$$
\begin{aligned}
\mathrm{d}s^2 &= f_1^{\frac{3}{2}} f_5^{\frac{1}{2}} \Big[4\mathrm{d}s_5^2 + f_2 D\mu_i D\mu_i + f_4(\mathrm{d}\sigma^2 + \mathrm{d}\eta^2) + f_3(\mathrm{d}\tilde{\chi} + \mathcal{A})^2 \Big], \\
e^{\frac{4}{3}\Phi} &= f_1 f_5, \qquad H_3 = 4\kappa \ \mathrm{d}\left[f_8 \wedge \mathrm{vol}\tilde{S}^2 - \eta\mu_3 \wedge \mathcal{F} \right], \qquad C_1 = f_6 D\tilde{\chi}, \\
C_3 &= 4\kappa f_7 D\tilde{\chi} \wedge \mathrm{vol}\tilde{S}^2 + 4\kappa \ \mu_3 \dot{V} \left(\star_5 \mathcal{F} - D\chi \wedge \mathcal{F} \right).
\end{aligned}
$$

Here, the relation $\mathrm{d}[\mathrm{vol}\tilde{S}^2] = -2\mathrm{d}[\mu_3] \wedge \mathcal{F}$ has been used. Thus

$$
F_4 = \mathrm{d}C_3 - H_3 \wedge C_1 = 4\kappa \ \mathrm{d}\left[f_7 D\tilde{\chi} \wedge \mathrm{vol}\tilde{S}^2 + \mu_3 \dot{V} \left(\star_5 \mathcal{F} - D\tilde{\chi} \wedge \mathrm{d}\mathcal{A} \right) \right] - H_3 \wedge C_1 .
$$

We have verified that the equations of motion for this background are satisfied when Eq. (7.3.18) is imposed. Following the analysis in Ref. [310], we can proceed to construct the Page fluxes and determine the quantised numbers of D4-branes, D6-branes, and NS5-branes. A thorough discussion of the charge quantisation is given in a more comprehensive study in Ref. [9].

7.3.3 Deformed D6-D8-NS5 AdS$_5$ backgrounds

In this section, we explore another infinite family of solutions as deformed holographic duals corresponding to a family of four-dimensional non-Lagrangian CFTs. These backgrounds are derived through a twisted compactification over a hyperbolic base space involving D6, D8, and NS5 branes [308, 311, 312]. Further compactification of the ϕ-direction of the CFT$_4$ leads to the emergence of a confining 3-dimensional theory.

The metric in the massive Type IIA theory is expressed using a function $\alpha(z)$ that satisfies the following third-order ordinary differential equation:

$$
\dddot{\alpha}(z) = -162\pi^3 F_0, \tag{7.3.20}
$$

where F_0 denotes the RR field, which is the "mass" in massive Type IIA theory. This parameter F_0 is chosen to be piecewise continuous and constant. The solution to this differential equation requires appropriate boundary conditions, with constraints on $\ddot{\alpha}(z)$ reflecting the properties of the dual UV-CFT. For a detailed discussion, refer to Refs. [271, 313]. The background solution for the metric and the dilaton are given by,

$$
\begin{aligned}
\mathrm{d}s_{10}^2 &= 18\pi \sqrt{-\frac{\alpha}{6\ddot{\alpha}}} \left[\mathrm{d}s_5^2 + \frac{1}{3}\mathrm{d}s_\Sigma^2 - \frac{\ddot{\alpha}}{6\alpha}\mathrm{d}z^2 - \frac{\alpha\ddot{\alpha}}{6\dot{\alpha}^2 - 9\alpha\ddot{\alpha}} \left(\mathrm{d}\theta^2 + \sin^2\theta \mathcal{D}\psi^2 \right) \right], \\
e^{-4\Phi} &= \frac{1}{2^5 3^{17} \pi^{10}} \left(-\frac{\ddot{\alpha}}{\alpha} \right)^3 \left(2\dot{\alpha}^2 - 3\alpha\ddot{\alpha} \right)^2, \quad \mathcal{D}\psi = \mathrm{d}\psi - 3\mathcal{A} - A_\Sigma \\
\mathcal{A} &= q \left(\frac{1}{r^2} - \frac{1}{r_*^2} \right) \mathrm{d}\phi, \quad A_\Sigma = \frac{2(v_1 \ \mathrm{d}v_2 - v_2 \ \mathrm{d}v_1)}{1 - v_1^2 - v_2^2}, \quad \mathrm{d}s_\Sigma^2 = 4\frac{(\mathrm{d}v_1^2 + \mathrm{d}v_2^2)}{(1 - v_1^2 - v_2^2)^2}.
\end{aligned} \tag{7.3.21}
$$

Different RR and NS sector fields and field strengths are

$$\begin{aligned} &B_2 = \frac{1}{3}\xi \wedge \mathcal{D}\psi, \qquad C_1 = \frac{\ddot{\alpha}}{162\pi^2}\cos\theta\,\mathcal{D}\psi, \qquad C_3 = \frac{\dot{\alpha}}{162\pi}\mathcal{D}\psi \wedge \mathrm{vol}_\Sigma, \\ &H_3 = \mathrm{d}B_2, \qquad F_2 = F_0 B_2 + \mathrm{d}C_1, \\ &F_4 = \left(\mathrm{d}C_3 + B_2 \wedge F_2 - \frac{1}{2}F_0\, B_2 \wedge B_2\right) - \frac{\ddot{\alpha}}{18\pi}\mathrm{d}z \wedge \left(\star_5\mathcal{F} - \frac{1}{3}\mathcal{F}\wedge\mathcal{D}\psi\right) - \frac{\dot{\alpha}}{54\pi}\mathcal{F}\wedge\mathrm{vol}_\Sigma, \end{aligned} \tag{7.3.22}$$

given in terms of ξ, the $U(1)$ field strength $\mathcal{F} = \mathrm{d}\mathcal{A}$, and the Hodge dual restricted to the five-dimensional submanifold,

$$\xi = 3\pi\left(\cos\theta\mathrm{d}z - \frac{2\alpha\dot{\alpha}}{2\dot{\alpha}^2 - 3\alpha\ddot{\alpha}}\sin\theta\mathrm{d}\theta\right), \quad \mathcal{F} = -\frac{2q}{r^3}\mathrm{d}r\wedge\mathrm{d}\phi, \quad \star_5\mathcal{F} = -2q\ \mathrm{d}t\wedge\mathrm{d}x_1\wedge\mathrm{d}x_2. \tag{7.3.23}$$

We have verified that all equations of motion are satisfied when Eq. (7.3.20) is applied.

To conclude this section, we offer some general comments. Similar to the previous section, all backgrounds presented here share the same $\mathrm{d}s_5^2$ metric as given in Eq. (7.3.3). Each background described by Eqs. (7.3.1), (7.3.9), (7.3.19), (7.3.21) is smooth provided the period of the ϕ-coordinate is appropriately chosen, as explained in Section 7.2. These backgrounds asymptotically approach AdS_5 with a compact ϕ-direction, and exhibit a deformation away from pure AdS_5 characterised by the warping function $f(r)$. A $\mathrm{U}(1)_R$ symmetry within the internal manifold is fibered over the ϕ-direction, and if necessary to preserve supersymmetry, over other compact directions. For the specific case of $\mu = 0$, resulting in $f(r) = 1 - \frac{q^2l^2}{r^6}$, these backgrounds have four Poincaré supercharges.

These shared features across the backgrounds suggest common points in the corresponding deformed 4-dimensional UV-CFTs. Moving forward, we now explore some holographic observables of these QFTs.

7.4 Field theory and observables

In this section, we study some observables of the QFTs using the holographic methods on the backgrounds of Section 7.3. There are particular universal features among all of the families of solutions, showing common properties for their corresponding field theories. Other observables also exist that behave differently among different QFTs. For each family of backgrounds, we provide a brief description of the dual QFT followed by the calculation of the observables.

7.4.1 Comments on the dual QFTs

Following the discussion from Section 7.3, we provide some details about the QFT interpretations.

First we focus on $\mathcal{N}=4$ SYM theory after compactification on a circle of radius $L_\phi = \frac{2\pi l^2}{3r_*}$. The interaction between the R-symmetry and this compactified circle, in holographic terms, corresponds to the form of the $\mathcal{A}$ gauge field introduced in Eq. (7.3.3). This mixing is crucial because, without it, the boundary conditions on the ϕ-circle would break supersymmetry. Notably, as $r \to \infty$, $\mathcal{A}$ becomes a constant one-form with a non zero holonomy $\oint_\phi \mathcal{A} = \frac{q}{r_*^2} L_\phi = \frac{2\pi}{3} l$. This gravitational observation reflects the twisting mechanism described in Section 7.1.

The presence of $\mathcal{A}$ along with the function $f(r)$ in Eq. (7.3.3) introduces a scale through L_ϕ, thereby breaking conformal symmetry. In lower energies, emerges a $(2+1)$ dimensional strongly coupled QFT in the IR. This mechanism is universal across all the examples discussed in this work. The infrared QFT is expected to exhibit confinement, discrete vacua, and should be described by a Chern-Simons topological quantum field theory (TQFT) with level N (corresponding to the number of colour branes) below the energy gap, as discussed in references such as [314] and [292].

The first background presented, described by Eqs. (7.3.1)-(7.3.6), implements the 'twisted compactification' for $\mathcal{N}=4$ SYM on a circle, as discussed before. The solution given in Eqs. (7.3.9)-(7.3.10) is holographically dual to a similar compactification scenario for the Klebanov-Witten CFT. Notably, this CFT lacks a weakly coupled regime, and its holographic description through the background, mirrors the twisted compactification over a Klebanov-Witten geometry. In Eqs.(7.3.12)-(7.3.16), we present a holographic description for the quiver QFTs on D3 branes living on the tip of a cone in a generic Sasaki-Einstein space which the twisted compactification has been performed on them.

Moving to $\mathcal{N}=2$ 4-dimensional linear quiver theories, the twisted compactification procedure becomes more complicated. Here, we twist the ϕ-symmetry with a U(1) subgroup embedded within $\mathrm{SU}(2)_R \times \mathrm{U}(1)_R$. This twisting is represented by the one-form $\mathcal{A}$ as defined in Eq. (7.3.3). Each gauge group in the linear quiver undergoes a similar compactification procedure, presented by a rank function resolving the Laplace-like Eq. (7.3.18), described in. Refs. [309, 310].

The example provided in Eqs. (7.3.20)-(7.3.22) describes the $\mathcal{N}=1$ non-Lagrangian CFTs, twisted compactified, where each distinct function $\alpha(z)$ corresponds to a different CFT. Despite these theories lacking a Lagrangian description, the holographic approach allows us to perform the twisted compactification and investigate the strong infrared dynamics of the resulting $(2+1)$-dimensional, $\mathcal{N}=2$ QFT.

Performing the holographic renormalisation to our backgrounds reveals common features: a current J_ϕ acquires a VEV, specifically $\langle J_\phi \rangle \sim q$. This observation indicates that we are investigating families of 3-dimensional QFTs with four supercharges where a global current obtains a non-zero VEV. If we had set $\mu \neq 0$ in $f(r)$ as defined in Eq. (7.3.3), supersymmetry would be broken due to an (anisotropic) VEV for the stress-energy tensor $T_{\mu\nu}$ as discussed in

Section 6.3. More detailed discussions on this can be found in references such as [8, 253, 255].

Moving forward, we proceed to calculate different observables from these holographic backgrounds. One notable aspect that emerges is that several observable quantities can be decomposed into a contribution arising from the flow dynamics and another stemming from the four-dimensional UV SCFT. This separation is particularly evident in computations involving entanglement entropy or the flow central charge, as discussed below. This phenomenon in QFT aligns with the proposal by Gauntlett and Varela [315], suggesting that by considering fields in the supercurrent multiplet of the SCFT, one can reduce the ten-dimensional supergravity to the minimal gauged AdS_5 supergravity. This gauged supergravity represents the 'universal' part related to the aforementioned flow. Notably, all backgrounds discussed here can be obtained as uplifts of the seed solution within this gauged supergravity framework, discussed in Section 7.2. A comprehensive treatment of this perspective can be found in the work [9].

7.4.2 Observables

In this section, different observables are calculated based on the backgrounds introduced in Section 7.3. We provide brief details of each computation for various backgrounds while pinpointing the universal behaviours. Note that, many details about procedures for holographic calculations are given in the previous chapter.

7.4.2.1 Wilson loops

To begin, we calculate the Wilson loop expectation value across the backgrounds given in Section 7.3 using the standard holographic approach (also used in Section 6.3). This involves embedding a string with fixed endpoints at $x = \pm L/2$ and $r = \infty$ [272]. The worldsheet coordinates are chosen such that $\tau = t$, $\sigma = x_1 \equiv x$, with $r = r(x)$, while all other coordinates remain constant. The induced metric on the worldsheet and the corresponding Nambu-Goto action are given by:

$$\begin{aligned} \mathrm{d}s^2_{\text{ind}} &= -\frac{r^2}{l^2}\mathrm{d}t^2 + \left(\frac{r^2}{l^2} + \frac{l^2}{r^2 f(r)} r'^2\right)\mathrm{d}x^2, \\ S_{\text{NG}} &= \frac{\mathcal{T}}{2\pi\alpha'}\int_{-L/2}^{L/2}\mathrm{d}x\sqrt{\frac{r^4}{l^4} + \frac{r'^2}{f(r)}} = \frac{\mathcal{T}}{2\pi\alpha'}\int_{-L/2}^{L/2}\mathrm{d}x\sqrt{F(r)^2 + G(r)^2 r'^2}, \\ F(r) &= \frac{r^2}{l^2}\ ,\ G(r) = \frac{1}{\sqrt{f(r)}}. \end{aligned} \tag{7.4.1}$$

Notably, these results in Eq. (7.4.1) are *universal* across all backgrounds discussed in Section 7.3. This universality stems from the backgrounds sharing the same five-dimensional metric structure in the directions probed by the string, differing primarily by overall warp

factors that depend on internal coordinates. Therefore, with coordinates t, r, x_1 fixed, the differences among these backgrounds manifest as constant rescalings of the induced metric.

The radial coordinate, r, spans from r_* to ∞, where r_* is determined by the largest root of $f(r_*) = 0$. Specifically, r_* satisfies $r_*^6 = q^2 l^2$, assuming $\mu = 0$ as parameterized in Eq. (7.3.3). The quantity $F(r_*) = \frac{r_*^2}{l^2}$ is important as it relates to the effective tension T_{eff} of the string, as discussed in references such as [145, 278, 316, 317]. This relationship provides insight into the confinement characteristics of these systems. Further detailed analysis is necessary to fully confirm the presence and nature of confinement, noting that for the supersymmetric case of interest, $\mu = 0$.

Regarding the separation of the quark pair, an approximate expression as a function of the turning point, r_0, of the string probe was derived in previous studies [278, 317]. In this case, this approximate separation length is given by:

$$\hat{L}(r_0) = \frac{\pi G(r)}{F'(r)}\bigg|_{r_0} = \frac{\pi l^2 r_0^2}{2\sqrt{r_0^6 - \mu l^2 r_0^2 - q^2 l^2}}. \tag{7.4.2}$$

In the context of the background geometry described here, the behaviour of the effective potential, $V_{\text{eff}}(r)$, plays a crucial role in understanding confinement properties, as suggested in Ref. [318].

The effective potential is defined as:

$$V_{\text{eff}}(r) = \frac{F(r)}{F(r_0)G(r)}\sqrt{F(r)^2 - F(r_0)^2},$$

where

$$F(r) = \frac{\sqrt{r^4 - r_0^4}}{r_0^2 l^2 r}\sqrt{r^6 - l^2(\mu r^2 + q^2)},$$

and $G(r) = \frac{1}{\sqrt{f(r)}}$.

This potential satisfies certain key conditions. As $r \to r_0$, $V_{\text{eff}}(r) \to 0$, indicating that the potential between the quark-anti-quark pair becomes weak, allowing for large separations between them. As $r \to \infty$, $V_{\text{eff}}(r) \sim r^4$, demonstrating a confining behaviour where the potential grows indefinitely with separation.

These features are essential for the proper definition of the Wilson loop and are indicative of confinement. The confining nature of the backgrounds is further evidenced by studying the separation and energy of the quark-anti-quark pair, as detailed in Ref. [318].

In summary, the effective potential provides a clear signature of confinement in these

backgrounds, showing a weakening potential at small separations and a strengthening potential at large separations, aligning with the expected behaviours in confining gauge theories,

$$L_{QQ}(r_0) = 2\int_{r_0}^{\infty} \frac{\mathrm{d}r}{V_{\text{eff}}(r)} = 2l^2 r_0^2 \int_{r_0}^{\infty} \frac{\mathrm{d}r\ r}{\sqrt{\left(r^4 - r_0^4\right)\left[r^6 - l^2(q^2 + r^2\mu)\right]}}, \tag{7.4.3}$$

$$E_{QQ}(r_0) = \frac{r_0^2}{l^2} L_{QQ}(r_0) + \frac{2}{l}\int_{r_0}^{\infty} \mathrm{d}r \frac{\sqrt{r^4 - r_0^4}}{r^2\sqrt{f(r)}} - 2\int_{r_*}^{\infty} \frac{\mathrm{d}r}{\sqrt{f(r)}}. \tag{7.4.4}$$

Although these integrals cannot generally be computed analytically, we can determine $L_{QQ}(r_0)$ and $E_{QQ}(r_0)$ through numerical methods, followed by creating a parametric plot of $E_{QQ}(L_{QQ})$. The outcomes are presented in Fig. 7.1. This plot reveals that the energy scales with the separation of the quark-anti-quark pair in a Coulomb-like manner for small separations, in accordance with conformal behavior. As the separation increases, the scaling transitions to a linear relationship, which signifies confinement.

To ensure the reliability of the string embedding used in these computations, it is essential to examine the stability, as discussed in Ref. [319]. A convenient check is to compute the derivative of the length of the separation respective to the turning point of the string embedding, as given in Ref. [273, 316, 317]. The approximate expression in Eq. (7.4.2) provides:

$$Z(r_0) := \frac{\mathrm{d}\hat{L}(r_0)}{\mathrm{d}r_0} = -\frac{l^4\pi}{4r_0^3\ f^{3/2}(r_0)}\left(\frac{4q^2}{r_0^5} + \frac{2r_0}{l^2} + \frac{2\mu}{r_0^3}\right) < 0. \tag{7.4.5}$$

The negative sign of $Z(r_0)$ indicates the stability of the string embedding.

Two key points stand out. Firstly, the universality of these findings spans across the diverse backgrounds we have examined. This universality is a direct consequence of holography but is not immediately apparent from a QFT standpoint. Indeed, QFT's confining nature can only be definitively understood through holographic analysis. Secondly, the results rely on a specific embedding of the probe string. It would be interesting to explore more generalised embeddings that probe the internal compact manifold. Such investigations could uncover new physical phenomena like screening.

Moving forward, we check the Entanglement Entropy of the QFT on a strip.

7.4.2.2 Entanglement Entropy on the strip

To compute the Entanglement Entropy on a strip-like region, we adopt the standard Ryu-Takayanagi prescription [275], incorporating necessary adjustments for backgrounds having excited NS fields [277, 278]. Initially, we define an eight-dimensional manifold and evaluate the determinant of the induced metric on this manifold, accounting for the dilaton's influence. Below, we provide the construction of the eight-manifold and the metric for each background

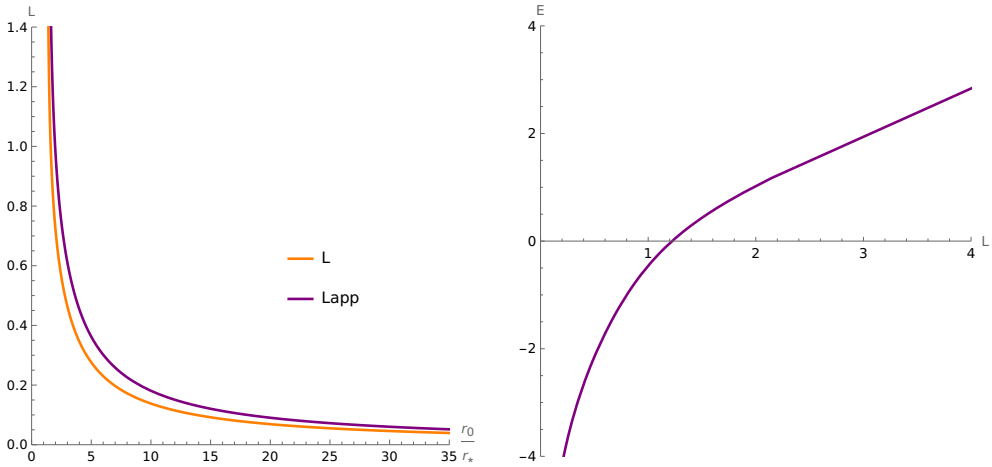

Figure 7.1. The left panel depicts the separation length of the quark-anti-quark pair in Eq. (7.4.3) varying with respect to the string turning point, r_0. Here, we set $l = \mu = q = 1$. The right panel presents the energy in Eq. (7.4.4) relative to the separation length of the pair. This graph demonstrates a transition: initially demonstrating the Coulomb-like behaviour due to conformality and progressing towards linearity for larger L, indicating confinement.

introduced in Section 7.3.

- Deformed $\mathrm{AdS}_5 \times S^5$ from Eq. (7.3.1)

$$\begin{aligned}
&\Sigma_{8,S^5} = [x_1, x_2, \phi, \theta, \varphi, \varphi_1, \varphi_2, \varphi_3], \qquad r(x_1),\\
&\mathrm{d}s^2_{8,S^5} = \frac{r^2}{l^2}\left(\mathrm{d}x_1^2\left(1+\frac{l^4 r'^2}{r^4 f(r)}\right) + \mathrm{d}x_2^2 + f(r)\mathrm{d}\phi^2\right) + l^2\Big\{\mathrm{d}\theta^2 + \sin^2\theta \mathrm{d}\varphi^2 +\\
&\sin^2\theta\sin^2\varphi\left(\mathrm{d}\varphi_1 + \frac{\mathcal{A}}{l}\right)^2 + \sin^2\theta\cos^2\varphi\left(\mathrm{d}\varphi_2 + \frac{\mathcal{A}}{l}\right)^2 + \cos^2\theta\left(\mathrm{d}\varphi_3 + \frac{\mathcal{A}}{l}\right)^2\Big\}.
\end{aligned}$$

- Deformed $\mathrm{AdS}_5 \times \mathrm{Y}^{p,q}$ from Eq. (7.3.12),

$$\begin{aligned}
&\Sigma_{8,\mathrm{Y}^{p,q}} = [x_1, x_2, \phi, \theta, \varphi, y, \beta, \psi], \qquad r(x_1),\\
&\mathrm{d}s^2_{8,\mathrm{Y}^{p,q}} = \frac{r^2}{l^2}\left(\mathrm{d}x_1^2\left(1+\frac{l^4 r'^2}{r^4 f(r)}\right) + \mathrm{d}x_2^2 + f(r)\mathrm{d}\phi^2\right) + l^2\Big\{\frac{1-y}{6}\left(\mathrm{d}\theta^2 + \sin^2\theta\mathrm{d}\varphi^2\right)\\
&+\frac{\mathrm{d}y^2}{w(y)v(y)} + \frac{w(y)v(y)}{36}\left(\mathrm{d}\beta + \cos\theta\mathrm{d}\varphi\right)^2 +\\
&+\frac{1}{9}\left(\mathrm{d}\psi - \cos\theta\mathrm{d}\varphi + y\left(\mathrm{d}\beta + \cos\theta\mathrm{d}\varphi\right) + \frac{3\mathcal{A}}{l}\right)^2\Big\}.
\end{aligned}$$

- Deformed Gaiotto-Maldacena backgrounds from Eq. (7.3.20),

$$\begin{aligned}
&\Sigma_{8,GM} = [x_1, x_2, \phi, \theta, \varphi, \tilde{\chi}, \sigma, \eta], \qquad r(x_1), \\
&ds^2_{8,GM} = \left(f_1^3 f_5\right)^{\frac{1}{2}} \left\{ \frac{4r^2}{l^2} \left(\mathrm{d}x_1^2 \left(1 + \frac{l^4 r'^2}{r^4 f(r)} \right) + \mathrm{d}x_2^2 + f(r)\mathrm{d}\phi^2 \right) + \right. \\
&\left. f_2 D\mu_i D\mu_i + f_4(\mathrm{d}\sigma^2 + \mathrm{d}\eta^2) + f_3(\mathrm{d}\tilde{\chi} + \mathcal{A})^2 \right\}.
\end{aligned}$$

- Deformed Bah-Passias-Tomasiello family of backgrounds,

$$\begin{aligned}
&BPT: \ \Sigma_{8,BPT} = [x_1, x_2, \phi, \theta, \psi, v_1, v_2, z], \qquad r(x_1), \\
&\mathrm{d}s^2_{8,BPT} = 18\pi \sqrt{-\frac{\alpha}{6\ddot{\alpha}}} \left\{ \frac{r^2}{l^2} \left(\mathrm{d}x_1^2 \left(1 + \frac{l^4 r'^2}{r^4 f(r)} \right) + \mathrm{d}x_2^2 + f(r)\mathrm{d}\phi^2 \right) + \frac{1}{3}\mathrm{d}s^2_{\Sigma} - \frac{\ddot{\alpha}}{6\alpha}\mathrm{d}z^2 \right. \\
&\left. - \frac{\alpha\ddot{\alpha}}{6\dot{\alpha}^2 - 9\alpha\ddot{\alpha}} \left(\mathrm{d}\theta^2 + \sin^2\theta \mathcal{D}\psi^2 \right) \right\}.
\end{aligned}$$

To calculate the EE, one has [277, 278]

$$S_{\mathrm{EE}} = \frac{1}{4G_N} \int \mathrm{d}^8 x \sqrt{e^{-4\Phi} \det\left[g_{\Sigma_8}\right]}. \tag{7.4.6}$$

The form of the result will be

$$S_{\mathrm{EE}} = \frac{\mathcal{N}_i}{4G_N} \int_{-L/2}^{L/2} \mathrm{d}x \sqrt{\frac{r^6}{l^6} f(r) \left(1 + \frac{l^4 r'^2}{r^4 f(r)} \right)}, \tag{7.4.7}$$

with the index $i \in \{S^5, \mathrm{Y}^{p,q}, GM, BPT\}$, and

$$\begin{aligned}
&\mathcal{N}_{S^5} = L_{x_2} l^5 \int_0^{\pi/2} \sin^3\theta \cos\theta \ \mathrm{d}\theta \int_0^{\pi/2} \sin\varphi \cos\varphi \ \mathrm{d}\varphi \int_0^{2\pi} \mathrm{d}\varphi_1 \ \mathrm{d}\varphi_2 \ \mathrm{d}\varphi_3 \int_0^{L_\phi} \mathrm{d}\phi = l^5 L_{x_2} \pi^3 L_\phi, \\
&\mathcal{N}_{\mathrm{Y}^{p,q}} = L_{x_2} l^5 \int_{y_1}^{y_2} \mathrm{d}y(1-y) \int_0^{\pi} \sin\theta \mathrm{d}\theta \int_0^{2\pi} \mathrm{d}\varphi \int_0^{2\pi} \mathrm{d}\beta \int_0^{4\pi} \mathrm{d}\psi \int_0^{L_\phi} \mathrm{d}\phi = l^5 L_{x_2} \mathrm{Vol}_{\mathrm{Y}^{p,q}} L_\phi, \\
&\mathcal{N}_{GM} = 256\pi^2 L_{x_2} L_\phi \int_0^{\infty} \mathrm{d}\sigma \int_0^{P} \mathrm{d}\eta \ \sigma \dot{V} V'' \ , \\
&\mathcal{N}_{BPT} = \frac{2}{243} L_{x_2} L_\phi \mathrm{Vol}_\Sigma \int_0^{P} \mathrm{d}z(-\alpha\ddot{\alpha}).
\end{aligned}$$

The contributions to the EE result can be divided into two components. One component arises from the deviation from the CFT, captured by the integral in Eq. (7.4.7). Notably, for $f(r) = 1$, this yields the CFT result. The integral in Eq. (7.4.7) remains universal across our different backgrounds and will be elaborated upon below. The second component, represented by the coefficient $\mathcal{N}_i$, is characteristic of each specific background (or its dual CFT). It contains

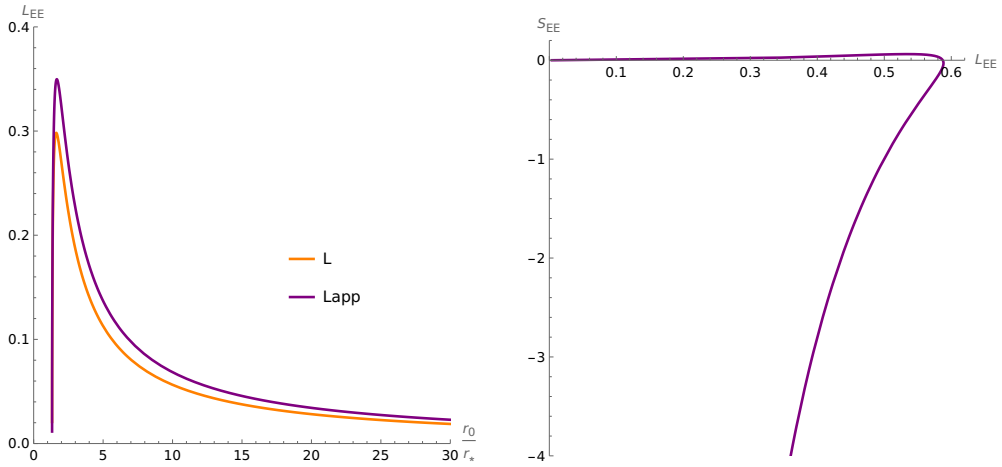

Figure 7.2. The length of the strip and the approximated function as a function of r_0 (left panel). The EE relative to the strip length (right panel).

information on the far UV regime of the QFT, precisely at the conformal point. For instance, $\mathcal{N}_{S^5}$ and $\mathcal{N}_{Y^{p,q}}$ are linked to the volume of the internal space at the UV and provide the central charge for the dual CFT. The quantities $\mathcal{N}_{GM}$ and $\mathcal{N}_{BPT}$ are also related to the central charges of the UV CFT. The results for $\mathcal{N}_{GM}$ and $\mathcal{N}_{BPT}$ are comparable to the Eqs. (2.37) in [309], (2.21) in [320], or (2.14) in [313] to establish these connections. This observable has contributions from a component arising from the deformed AdS_5 and another from the UV-CFT_4 (the coefficient $\mathcal{N}_i$). This explains the notion of how the Gauntlett-Varela proposal [315] manifests itself in this particular QFT observable.

Let us revisit the EE in Eq. (7.4.7), which is computed using

$$\int_{-L/2}^{L/2} \mathrm{d}x \, \sqrt{\frac{r^6}{l^6} f(r) \left(1 + \frac{l^4 r'^2}{r^4 f(r)}\right)} = \int_{-L/2}^{L/2} \mathrm{d}x \, \sqrt{F^2 + G^2 r'^2}.$$

This integral is universal across all the backgrounds examined here. The approach to solve this variational problem is similar to the one described for the Wilson loop. Detailed treatments of these integral expressions can be found in Ref. [278]. Relying on this analysis, we compute $L_{\mathrm{EE}}(r_0)$ and $S_{\mathrm{EE}}(r_0)$ numerically, and then make the final plot for $S_{\mathrm{EE}}(L_{\mathrm{EE}})$. Figure 7.2 presents the results for $L_{\mathrm{EE}}(r_0)$ alongside its approximation, analogous to Eq. (7.4.2). The multi-valued nature of $L_{\mathrm{EE}}(r_0)$ indicates a phase transition in the EE, as proposed in Ref. [277]. Figure 7.2 also illustrates the EE as a function of L_{EE}, highlighting the phase transition more prominently. Similar to the Wilson loop, exploring more generalised embeddings may display additional insights into the system dynamics.

7.4.2.3 Flow central charge

The objective of this section is to calculate the flow central charge, c_{flow}, introduced in Section 6.3.2, as this quantity can detect fixed points along flows across dimensions. To bring it to the form of our desire, consider a background considered to be dual to a $(d+1)$-dimensional QFT. The metric and dilaton are of the form:

$$\begin{aligned} &ds^2 = -\alpha_0 dt^2 + \alpha_1 dx_1^2 + \alpha_2 dx_2^2 + ... + \alpha_d dx_d^2 + (\alpha_1.\alpha_2....\alpha_d)^{\frac{1}{d}}\,\beta(r)dr^2 + g_{ij}(d\theta^i - A^i)(d\theta^j - A^j),\\ &\Phi = \Phi(r,\theta^i). \end{aligned} \tag{7.4.8}$$

Where,

$$\begin{aligned} &G_{ij}d\xi^i d\xi^j = \alpha_1 dx_1^2 + \alpha_2 dx_2^2 + ... + \alpha_d dx_d^2 + g_{ij}(d\theta^i - A^i)(d\theta^j - A^j),\\ &H = \left[\int d\theta^i \sqrt{e^{-4\Phi}\det[G_{ij}]}\right]^2, \qquad c_{flow} = \frac{d^d}{G_N}\beta^{\frac{d}{2}}\frac{H^{\frac{2d+1}{2}}}{(H')^d}. \end{aligned} \tag{7.4.9}$$

For CFT duals, which are isotropic systems where all α_i are equal, the quantity c_{flow} corresponds to the free energy of the CFT. For the theories under consideration here, we are dealing with field theories in $d = 3$ dimensions. The specific values of the parameters α_i, $\beta(r)$, and $H(r)$ are as follows:

$$\underline{\text{case of } \mathbf{S^5}}: \alpha_1 = \alpha_2 = \frac{r^2}{l^2},\ \alpha_3 = \frac{r^2}{l^2}f(r),\quad \beta = \frac{l^4}{r^4 f(r)^{\frac{4}{3}}},\quad H = \frac{\mathcal{N}^2_{S^5}}{L^2_\phi L^2_{x_2}}\frac{r^6}{l^6}f(r), \tag{7.4.10}$$

$$\underline{\text{case of } \mathbf{Y^{p,q}}}: \alpha_1 = \alpha_2 = \frac{r^2}{l^2},\ \alpha_3 = \frac{r^2}{l^2}f(r),\quad \beta = \frac{l^4}{r^4 f(r)^{\frac{4}{3}}},\quad H = \frac{\mathcal{N}^2_{Y^{p,q}}}{L^2_\phi L^2_{x_2}}\frac{r^6}{l^6}f(r).$$

$$\underline{\text{case of } \mathbf{GM}}: \alpha_1 = \alpha_2 = \sqrt{f_1^3 f_5}\frac{4r^2}{l^2},\ \alpha_3 = \alpha_1 f(r),\quad \beta = \frac{l^4}{r^4 f(r)^{\frac{4}{3}}},\quad H = \frac{64\mathcal{N}^2_{GM}}{L^2_\phi L^2_{x_2}}\frac{r^6}{l^6}f(r).$$

$$\underline{\text{case of } \mathbf{BPT}}: \alpha_1 = \alpha_2 = 18\pi\sqrt{-\frac{\alpha}{\ddot{\alpha}}}\frac{r^2}{l^2},\ \alpha_3 = \alpha_1 f(r),\quad \beta = \frac{l^4}{r^4 f(r)^{\frac{4}{3}}},\quad H = \frac{\mathcal{N}^2_{BPT}}{L^2_\phi L^2_{x_2}}\frac{r^6}{l^6}f(r).$$

The quantities $\mathcal{N}_i$ are defined in Eq. (7.4.7), with $i \in \{S^5, Y^{p,q}, GM, BPT\}$. From Eq. (7.4.9) one has

$$c_{flow} = \frac{s_i l^3 \mathcal{N}_i}{8 L_\phi L_{x_2} G_N}\frac{f(r)^{\frac{3}{2}}}{\left(f(r) + \frac{r}{6}f'(r)\right)^3}. \tag{7.4.11}$$

Here, for the GM-case $s_i = 8$, while $s_i = 1$ for other cases.

Similar observations apply to c_{flow} as with the EE. From the results, it is evident that c_{flow} includes a contribution from the UV part, denoted by $\mathcal{N}_i$, which reflects the number of degrees of freedom of each CFT_4. The flow contribution is governed by the r-dependent terms.

Specifically, when $\mu = q = 0$, the function $f(r) = 1$, leading to $c_{flow} = c_{CFT_4}$. Additionally, as $r \to r_*$, we find $c_{flow} \to 0$, indicating the gapped nature of the IR QFT_3.

In summary, we have identified a monotonic quantity that smoothly interpolates between the degrees of freedom of a CFT_4 (UV theory) and a gapped QFT_3 (IR theory).

Chapter 8

Conclusions

The thesis elaborated on two subjects in the context of holography. We will provide conclusory remarks on these subjects separately.

For the CHM project, through Chapters 3-5, we illustrated the construction of a bottom-up holographic model where, at low energies, a sigma model with $SO(5)$ global symmetry breaking to $SO(4)$ is manifest. Within this framework, an $SO(4)$ subgroup is gauged. The introduction of explicit interactions that break the $SO(5)$ symmetry causes vacuum misalignment, leading to the spontaneous breaking of the gauged $SO(4)$ to an $SO(3)$ group. A significant portion of this study focuses on the intricate development of formalism, demonstrating that symmetry breaking can be consistently induced by a bulk scalar field within the gravity theory where $SO(5)$ is gauged. Notably, this mechanism respects the gauge principle despite explicit symmetry breaking present in the dual field theory. Crucially, this consistency hinges on the requirement that the bulk field responsible for symmetry breaking in the dual theory is related to an operator with a scaling dimension in the range $\frac{D-3}{2} \leq \Delta \leq \frac{D+1}{2}$, as elaborated in the main text.

A notable characteristic of this proposal is the complete smoothness of the gravity background, which mimics the confinement of the field theory side and introduces a mass gap. While more advanced holographic descriptions of confinement may require further developments, and while a realistic implementation of the electroweak model has not yet been achieved, our analysis of the spectrum presented here suggests straightforward phenomenology, as anticipated in CHMs in the $SO(5)/SO(4)$ coset. All newly introduced particles are significantly heavier than the bosons fulfilling the roles of the Higgs bosons, Z and W. The incorporation of a (custodial) $SO(4)$ symmetry into the model suggests that a realistic CHM based on this framework would likely have evaded indirect detection, although careful computation of all precision electroweak parameters remains necessary.

To construct a more realistic model that is potentially detectable in direct collider experiments, several other steps are required. Firstly, the model features a gauged $SO(4)$ symmetry, whereas the SM gauge symmetry is $SU(2)_L \times U(1)_Y$. Moreover, ensuring realistic quantum

assignments for SM fermions necessitates identifying an additional $U(1)$ global symmetry linked to baryon and lepton numbers to align with hypercharge assignments. Addressing these challenges remains a subject for future research.

Secondly, the current theory lacks fermions. As outlined in the main text, we proposed two potential ways for their inclusion: either assuming all fermions are localised on the UV boundary or introducing additional bulk fermions that transform under the spinorial representation 4 of $SO(5)$. These components would dictate the mechanism for generating masses for SM fermions and influence their contribution to the effective potential, which, through vacuum misalignment, triggers spontaneous symmetry breaking of the gauge symmetry. Exploring these aspects further will be interesting for later studies.

Lastly, the methodologies demonstrated in this paper are applicable to a broad category of holographic models where bulk scalar fields drive symmetry breaking. Notably, there are significant parallels between the gravitational framework presented here and the one detailed in Ref. [162], which utilises 7d maximal supergravity and contains bulk $SO(5)$ gauge symmetry. As highlighted in the Introduction, a persistent challenge remains in constructing a UV-complete CHM on the $SO(5)/SO(4)$ coset, with embedding the gravity theory within a recognised supergravity framework. The findings of this work represent a substantial step toward addressing this objective.

Concerning the solitonic deformations of the supergravity backgrounds explored in Chapters 6 through 7, we utilised holography to introduce a SUSY-breaking or SUSY-preserving deformation into various dual 5d and 4d SCFTs. This deformation essentially involves a twisted compactification that induces a flow to a gapped 4d or 3d field theory, respectively. Our approach in Chapter 7 is applicable to any SCFT whose holographic dual truncates consistently to the $d = 5$ minimal gauged supergravity. The field theories investigated in Chapter 7 can be categorised into two main groups. First are the field theories that can be described as a weakly coupled theory using Lagrangian and elementary fields. $\mathcal{N} = 4$ SYM and the electrostatic case of $\mathcal{N} = 2$ theories of Gaiotto-Maldacena are some examples. These QFTs, after the deformation, exhibit a dual description represented by the backgrounds in the main text. The second set is the field theories with no weakly coupled description and/or lack of a Lagrangian formulation. Examples of such theories are associated with the BPT and generic Gaiotto-Maldacena backgrounds. These QFTs and their corresponding high energy limit SCFTs are strongly coupled. However, the field theories dual to $T^{1,1}$ and $Y^{p,q}$ backgrounds are inherently strongly coupled due to large anomalous dimensions of elementary fields, yet a superpotential can still be formulated.

In this study, we analysed both categories of examples using holographic observables. Regarding the QFTs in the first category, insights can also be gained from their perturbative descriptions, as discussed for $\mathcal{N} = 4$ SYM in Ref. [292]. Extending such analyses to the

Lagrangian Gaiotto-Maldacena theories would be of interest. For the QFTs of the second type, exploring additional holographic observables or potentially employing algebraic methods could yield further insights.

Here we summarise some of the key conclusions drawn from the final chapter:

- The dual QFT preserves four supercharges when the parameter μ in Eq. (7.2.3) is zero. This preservation of SUSY in the ten- or eleven-dimensional background comes from the four supercharges preserved in the 5d minimal gauged supergravity solution. Additionally, the R-symmetry in the QFT is broken by the VEV of a current, controlled by the parameter q in Eq. (7.2.3).

- The density of degrees of freedom in QFTs is quantified by a monotonic quantity denoted as c_{flow}. This quantity decreases along the energy flow, interpolating between the value of the SCFT at UV and zero.

- Throughout the energy flow, the QFTs remain strongly coupled. In deep IR, the absence of degrees of freedom requires a TQFT description of the system.

- The deformed QFTs exhibit confinement of external non-dynamical quarks, particularly evident when Wilson loops do not probe the internal manifold.

- Certain observables such as EE, c_{flow}, and Complexity exhibit a dual contribution: one factor from the UV SCFT and a second factor from the flow dynamics. The UV contribution can be seen as kinematical in nature, while the flow contribution is dynamically driven. This type of factorisation of observables might be a result of the conjecture in Ref. [315] by Gauntlett and Varela. Specifically, fields within the current multiplet of the SCFT may contribute dynamically, dependent solely on the 5d supergravity solution, which is truncated in Eq. (7.2.3).

Extending the methodology to embed solitonic solutions into supergravity backgrounds featuring other appropriate AdS_d factors represents a straightforward direction for future research. It would be instructive, wherever feasible, to explore this holographic concept of the S^1_ϕ compactification with a Lagrangian analysis of the deformation. It would be particularly interesting to understand how this compactification impacts fields that transform under fundamental representation.

Further investigation into the deep IR regime of the deformed QFTs is also appealing. Drawing from insights in Ref. [314], one anticipates that the 3d IR description may manifest as a Chern-Simons theory with a level determined by the number of colour branes. Understanding how this framework applies specifically to the IR theories discussed here would be valuable.

Lastly, it would be of interest to find observables that do not exhibit a straightforward "factorisation" into contributions from the flow dynamics and the background lower dimentional solution. Utilising probes that are inserted in both the deformed AdS directions and the internal dimensions in more intricate manners could potentially disrupt this observed pattern.

Appendix A

Sigma-model coupled to gravity

A.1 The sigma-model

To establish our conventions, we present the action of the two-derivative sigma-model in D dimensions, which involves n scalars Φ^a (with $a = 1, \cdots, n$), coupled to gravity:

$$\mathcal{S} = \int \mathrm{d}^D x \sqrt{-g} \left[\tfrac{R}{4} - \tfrac{1}{2} g^{MN} G_{ab} \partial_M \Phi^a \partial_N \Phi^b - \mathcal{V}(\Phi^a) \right]. \tag{A.1.1}$$

The D-dimensional space-time indexes are denoted by $M = 0, \cdots, 3, 5, \cdots, D$. Here, g is the determinant of the D-dimensional metric g_{MN}, with signature mostly + and R is the D-dimensional Ricci scalar. The sigma-model metric is written as G_{ab}, with its inverse denoted as G^{ab}. The potential, $\mathcal{V}$, is chosen to be a function of the scalars ,Φ^a.

If we adopt the ansatz that the background solutions take the form of DW solutions and the scalar fields, Φ^a, depend only on the radial coordinate ρ, the action simplifies under these assumptions,

$$\mathrm{d}s_D^2 = \mathrm{d}r^2 + e^{2A(r)} \mathrm{d}x_{1,D-2}^2 \,, \tag{A.1.2}$$

$$\Phi^a = \Phi^a(r) \,, \tag{A.1.3}$$

and the equations of motion are

$$\partial_r^2 \Phi^a + (D-1) \partial_r A \partial_r \Phi^a + \mathcal{G}^a{}_{bc} \partial_r \Phi^b \partial_r \Phi^c - G^{ab} \frac{\partial \mathcal{V}}{\partial \Phi^b} = 0 \,, \tag{A.1.4}$$

$$(D-1) \left(\partial_r A \right)^2 + \partial_r^2 A + \frac{4}{D-2} \mathcal{V} = 0 \,, \tag{A.1.5}$$

$$(D-1)(D-2) \left(\partial_r A \right)^2 - 2 G_{ab} \partial_r \Phi^a \partial_r \Phi^b + 4 \mathcal{V} = 0 \,, \tag{A.1.6}$$

with the sigma-model connection reading

$$\mathcal{G}^d{}_{ab} \equiv \frac{1}{2} G^{dc} \Big(\partial_a G_{cb} + \partial_b G_{ca} - \partial_c G_{ab} \Big) \,. \tag{A.1.7}$$

In case one finds a solution for $\mathcal{W}(\Phi^a)$ solving the partial differential equation

$$\mathcal{V} = \frac{1}{2}G^{ab}\frac{\partial\mathcal{W}}{\partial\Phi^a}\frac{\partial\mathcal{W}}{\partial\Phi^b} - \frac{D-1}{D-2}\mathcal{W}^2\,, \tag{A.1.8}$$

one can conclude that any solution to the following first-order equations

$$\partial_r A = -\frac{2}{D-2}\mathcal{W}\,, \tag{A.1.9}$$

$$\partial_r\Phi^a = G^{ab}\frac{\partial\mathcal{W}}{\partial\Phi^b}\,, \tag{A.1.10}$$

will also be a solution of the second-order classical Eqs. (A.1.4), (A.1.5), and (A.1.6).

A.2 Linearised equations for scalar fluctuations

The linearised equations of motion can be formulated in a gauge-invariant manner, as discussed in Refs. [119–123], where more comprehensive details are provided.

Regarding the scalar fields, the gauge-invariant combination of fluctuations $\mathfrak{a}^a$ satisfy the following equation

$$\left[\mathcal{D}_r^2 + (D-1)\partial_r A\,\mathcal{D}_r - e^{-2A}q^2\right]\mathfrak{a}^a - \mathcal{X}^a{}_c\mathfrak{a}^c = 0\,. \tag{A.2.1}$$

We use the following notations. For a field X^a, the sigma-model covariant derivative is defined as $D_bX^a = \partial_bX^a + \mathcal{G}^a{}_{bc}X^c$ and background-covariant derivatives is $\mathcal{D}_rX^a = \partial_rX^a + \mathcal{G}^a{}_{bc}\partial_r\Phi^bX^c$. These are written in terms of the sigma-model connection $\mathcal{G}^a{}_{bc}$ in Eq. (A.1.7). The Riemann tensor of the sigma-model will be $\mathcal{R}^a{}_{bcd} = \partial_c\mathcal{G}^a{}_{bd} - \partial_d\mathcal{G}^a{}_{bc} + \mathcal{G}^a{}_{ce}\mathcal{G}^e{}_{bd} - \mathcal{G}^a{}_{de}\mathcal{G}^e{}_{bc}$. Hence, the matrix $\mathcal{X}^a_c$ takes the form

$$\begin{aligned}\mathcal{X}^a_c \equiv\ & -\mathcal{R}^a{}_{bcd}\partial_r\Phi^b\partial_r\Phi^d + D_c\left(G^{ab}\frac{\partial\mathcal{V}}{\partial\Phi^b}\right) + \frac{4}{(D-2)\partial_rA}\left[\partial_r\Phi^a\frac{\partial\mathcal{V}}{\partial\Phi^c} + G^{ab}\frac{\mathcal{V}}{\partial\Phi^b}\partial_r\Phi^dG_{dc}\right]\\ & + \frac{16\mathcal{V}}{(D-2)^2(\partial_rA)^2}\partial_r\Phi^a\partial_r\Phi^bG_{bc}\,.\end{aligned} \tag{A.2.2}$$

The boundary-localised masses for all the fluctuations of Φ^a are chosen to be infinite; thus, the Dirichlet boundary conditions are imposed. The boundary conditions emerging for the gauge-invariant variables combination $\mathfrak{a}^a$ will be

$$\partial_r\Phi^c\partial_r\Phi^dG_{db}\mathcal{D}_\rho\mathfrak{a}^b\Big|_{r_i} = \left[\frac{(D-2)\partial_rA}{2}e^{-2A}q^2\delta^c{}_b + \partial_r\Phi^c\left(\frac{4\mathcal{V}}{(D-2)\partial_rA}\partial_r\Phi^dG_{db} + \frac{\partial\mathcal{V}}{\partial\Phi^b}\right)\right]\mathfrak{a}^b\Big|_{r_i}\,. \tag{A.2.3}$$

Appendix B

Probe approximation

In this appendix, we explore further the probe approximation, with additional insights available in Ref. [124]. The fluctuations, $\mathfrak{a}^a = \varphi^a - \frac{\partial_r \Phi^a}{6\partial_r A} h$, arise from the interaction between the scalar fluctuations, $\Phi^a = (\phi, \chi)$, and the fluctuations, h, of the trace of the four-dimensional metric component. The second element couples to the trace of the stress-energy tensor in the boundary theory. When $\mathfrak{a}^a$ is predominantly composed of h, meaning $\mathfrak{a}^a \simeq \frac{\partial_r \Phi^a}{6\partial_r A} h$, the interplay of the states sourced by the boundary operators are effectively described by the dilatonic counterparts.

Conversely, in the probe approximation used for compution, the mixing between the scalar and metric fluctuations is neglected. This approximation remains valid only if $\mathfrak{a}^a \simeq \varphi^a$, allowing the contribution of h in Eq. (A.2.1) to be disregarded.

Hence, the probe approximation is achieved by removing some contributions from the metric, especially h, in Eqs. (A.2.1) and (A.2.3), resulting in [124]

$$0 = \left[\mathcal{D}_r^2 + (D-1)\partial_r A \, \mathcal{D}_r - e^{-2A} q^2 \right] \mathfrak{p}^a - \left[V^a_{\ |c} - \mathcal{R}^a{}_{bcd} \partial_r \Phi^b \partial_r \Phi^d \right] \mathfrak{p}^c \,, \tag{B.0.1}$$

for the bilk. The boundary conditions are reduced to

$$0 = \mathfrak{p}^a \Big|_{r_i} \,. \tag{B.0.2}$$

Here, $\mathfrak{a}^a$ is replaced wth the probe fluctuations denoted by $\mathfrak{p}^a$.

In the main body of the text, we compute the spectra of scalar fluctuations for $\Delta = 5/2$ using two distinct methods. First, we solve the exact equations (A.2.1) with the boundary conditions given by (A.2.3), which allows us to determine the spectrum of masses. Second, we perform the calculation using the probe approximation, solving equations (B.0.1) with boundary conditions (B.0.2) for the same background.

If these two methods yield different spectra, it indicates that the overlap with the dilaton cannot be neglected. Specifically, discrepancies between the spectra obtained from the exact equations and those from the probe approximation suggest significant mixing between the

scalar and metric fluctuations in the system.

Appendix C

Basis of $SO(5)$ generators

Here for the convenience of the reader, we provide a basis of $SO(5)$ generators. They are chosen such that the generators, $t^{\hat{A}}$, with $\hat{A} = 1, \cdots, 4$, span the the coset of $SO(5)/SO(4)$, following the convention in Eq. (4.1.19). The remaining unbroken $SO(4)$ is parametrised by $t^{\bar{A}}$, with $\bar{A} = 5, \cdots, 10$.

$$t^1 = \frac{i}{2}\begin{pmatrix} 0&0&0&0&-1\\ 0&0&0&0&0\\ 0&0&0&0&0\\ 0&0&0&0&0\\ 1&0&0&0&0 \end{pmatrix}, \quad t^2 = \frac{i}{2}\begin{pmatrix} 0&0&0&0&0\\ 0&0&0&0&-1\\ 0&0&0&0&0\\ 0&0&0&0&0\\ 0&1&0&0&0 \end{pmatrix}, \quad t^3 = \frac{i}{2}\begin{pmatrix} 0&0&0&0&0\\ 0&0&0&0&0\\ 0&0&0&0&-1\\ 0&0&0&0&0\\ 0&0&1&0&0 \end{pmatrix}, \quad t^4 = \frac{i}{2}\begin{pmatrix} 0&0&0&0&0\\ 0&0&0&0&0\\ 0&0&0&0&0\\ 0&0&0&0&-1\\ 0&0&0&1&0 \end{pmatrix},$$

$$t^5 = \frac{i}{2}\begin{pmatrix} 0&0&0&-1&0\\ 0&0&0&0&0\\ 0&0&0&0&0\\ 1&0&0&0&0\\ 0&0&0&0&0 \end{pmatrix}, \quad t^6 = \frac{i}{2}\begin{pmatrix} 0&0&0&0&0\\ 0&0&0&-1&0\\ 0&0&0&0&0\\ 0&1&0&0&0\\ 0&0&0&0&0 \end{pmatrix}, \quad t^7 = \frac{i}{2}\begin{pmatrix} 0&0&0&0&0\\ 0&0&0&0&0\\ 0&0&0&-1&0\\ 0&0&1&0&0\\ 0&0&0&0&0 \end{pmatrix},$$

$$t^8 = \frac{i}{2}\begin{pmatrix} 0&0&-1&0&0\\ 0&0&0&0&0\\ 1&0&0&0&0\\ 0&0&0&0&0\\ 0&0&0&0&0 \end{pmatrix}, \quad t^9 = \frac{i}{2}\begin{pmatrix} 0&0&0&0&0\\ 0&0&-1&0&0\\ 0&1&0&0&0\\ 0&0&0&0&0\\ 0&0&0&0&0 \end{pmatrix}, \quad t^{10} = \frac{i}{2}\begin{pmatrix} 0&-1&0&0&0\\ 1&0&0&0&0\\ 0&0&0&0&0\\ 0&0&0&0&0\\ 0&0&0&0&0 \end{pmatrix}. \tag{C.0.1}$$

A basis for $SU(4)$, taken from Ref. [205], is also provided in terms of 4×4 Hermitian matrices. The adjoint of $SU(4)$ in terms of $Sp(4) \sim SO(5)$ representations decomposes as $15 = 5 \oplus 10$, and both are used in the body of the thesis. Γ^A, for $A = 1, \cdots, 5$, cover

the coset $SU(4)/Sp(4)$. This can also represent the 5 of $Sp(4)$. The $Sp(4)$ generators are denoted as T^A, with $A = 1, \cdots, 10$. The normalisation for all $SU(4)$ matrices is chosen as $\mathrm{Tr}\,(T^A T^B) = \frac{1}{4}\delta^{AB} = \mathrm{Tr}\,(\Gamma^A \Gamma^B)$. The Γ^As are

$$\Gamma^1 = \frac{1}{4}\begin{pmatrix} 0&1&0&0\\ 1&0&0&0\\ 0&0&0&1\\ 0&0&1&0 \end{pmatrix}, \qquad \Gamma^2 = \frac{1}{4}\begin{pmatrix} 0&-i&0&0\\ i&0&0&0\\ 0&0&0&i\\ 0&0&-i&0 \end{pmatrix}, \qquad \Gamma^3 = \frac{1}{4}\begin{pmatrix} 0&0&0&-i\\ 0&0&i&0\\ 0&-i&0&0\\ i&0&0&0 \end{pmatrix},$$
$$\Gamma^4 = \frac{1}{4}\begin{pmatrix} 0&0&0&1\\ 0&0&-1&0\\ 0&-1&0&0\\ 1&0&0&0 \end{pmatrix}, \qquad \Gamma^5 = \frac{1}{4}\begin{pmatrix} 1&0&0&0\\ 0&-1&0&0\\ 0&0&1&0\\ 0&0&0&-1 \end{pmatrix}. \tag{C.0.2}$$

The $Sp(4)$ generators, also parametrising 10 of $Sp(4) \sim SO(5)$ are:

$$T^1 = \frac{1}{4}\begin{pmatrix} 0&i&0&0\\ -i&0&0&0\\ 0&0&0&i\\ 0&0&-i&0 \end{pmatrix}, \qquad T^2 = \frac{1}{4}\begin{pmatrix} 0&1&0&0\\ 1&0&0&0\\ 0&0&0&-1\\ 0&0&-1&0 \end{pmatrix}, \qquad T^3 = \frac{1}{4}\begin{pmatrix} 0&0&0&1\\ 0&0&1&0\\ 0&1&0&0\\ 1&0&0&0 \end{pmatrix},$$
$$T^4 = \frac{1}{4}\begin{pmatrix} 0&0&0&i\\ 0&0&i&0\\ 0&-i&0&0\\ -i&0&0&0 \end{pmatrix}, \qquad T^5 = \frac{1}{4}\begin{pmatrix} 0&0&i&0\\ 0&0&0&-i\\ -i&0&0&0\\ 0&i&0&0 \end{pmatrix}, \qquad T^6 = \frac{1}{4}\begin{pmatrix} 0&0&1&0\\ 0&0&0&1\\ 1&0&0&0\\ 0&1&0&0 \end{pmatrix},$$
$$T^7 = \frac{1}{4}\begin{pmatrix} -1&0&0&0\\ 0&-1&0&0\\ 0&0&1&0\\ 0&0&0&1 \end{pmatrix}, \qquad T^8 = \frac{1}{4}\begin{pmatrix} 0&0&1&0\\ 0&0&0&-1\\ 1&0&0&0\\ 0&-1&0&0 \end{pmatrix} \qquad T^9 = \frac{1}{4}\begin{pmatrix} 0&0&-i&0\\ 0&0&0&-i\\ i&0&0&0\\ 0&i&0&0 \end{pmatrix}$$
$$T^{10} = \frac{1}{4}\begin{pmatrix} 1&0&0&0\\ 0&-1&0&0\\ 0&0&-1&0\\ 0&0&0&1 \end{pmatrix}. \tag{C.0.3}$$

These matrices can be presented as commutators of two of the Γ^A matrices, for instance, $T^1 = -2i\left[\Gamma^1, \Gamma^5\right]$.

Appendix D

Gauge fixing formalism

D.1 Vectors, pseudoscalars, and spurions

In this appendix, we present the gauge fixing terms and equations of motion governing the spin-1 and spin-0 fluctuations discussed in Section 5.5. The derived equations for the fields introduced in Eq. (5.5.24) (excluding χ_M), along with other fields that interact with them, are detailed in the subsequent subsections. Section D.1.1 covers the equations of motion and boundary conditions of ${\mathcal{B}_M}^{\tilde{\mathcal{A}}}$ and ${\mathcal{B}_M}^{\hat{\mathcal{A}}}$, including those for the associated spin-0 states. Section D.1.2 focuses on ${\mathcal{A}_M}^4$, while Section D.1.3 considers ${\mathcal{A}_M}^{\bar{\mathcal{A}}}$.

D.1.1 The ${\mathcal{B}_M}^{\hat{\mathcal{A}}}$ and ${\mathcal{B}_M}^{\tilde{\mathcal{A}}}$ sectors

Following the methodology of Ref. [118], we pick the required gauge fixing terms for ${\mathcal{B}_M}^{\hat{\mathcal{A}}}$ and ${\mathcal{B}_M}^{\tilde{\mathcal{A}}}$ as

$$\begin{aligned}\mathcal{S}^{(1)}_{\hat{\xi}} = \int \mathrm{d}^4q\, \mathrm{d}r \\ \left\{-\frac{H^{(1)}_{\hat{\mathcal{A}}\hat{\mathcal{A}}}}{2\hat{\xi}}\left[iq^\mu {\mathcal{B}_\mu}^{\hat{\mathcal{A}}}(-q) - \frac{g\sin(v)}{2v}\frac{\hat{\xi}}{H^{(1)}_{\hat{\mathcal{A}}\hat{\mathcal{A}}}}G^{(1)}_{\hat{\mathcal{A}}\hat{\mathcal{A}}}e^{2A}\pi^{\hat{\mathcal{A}}}(-q) - \frac{\hat{\xi}}{H^{(1)}_{\hat{\mathcal{A}}\hat{\mathcal{A}}}}\partial_r\left(H^{(1)}_{\hat{\mathcal{A}}\hat{\mathcal{A}}}e^{2A}{\mathcal{B}_5}^{\hat{\mathcal{A}}}(-q)\right)\right]\times \right. \\ \left.\times\left[-iq^\nu {\mathcal{B}_\nu}^{\hat{\mathcal{A}}}(q) - \frac{g\sin(v)}{2v}\frac{\hat{\xi}}{H^{(1)}_{\hat{\mathcal{A}}\hat{\mathcal{A}}}}G^{(1)}_{\hat{\mathcal{A}}\hat{\mathcal{A}}}e^{2A}\pi^{\hat{\mathcal{A}}}(q) - \frac{\hat{\xi}}{H^{(1)}_{\hat{\mathcal{A}}\hat{\mathcal{A}}}}\partial_r\left(H^{(1)}_{\hat{\mathcal{A}}\hat{\mathcal{A}}}e^{2A}{\mathcal{B}_5}^{\hat{\mathcal{A}}}(q)\right)\right]\right\}, \end{aligned} \tag{D.1.1}$$

and

$$\begin{aligned}\mathcal{S}^{(1)}_{\tilde{\xi}} = \int \mathrm{d}^4q\, \mathrm{d}r \left\{-\frac{H^{(1)}_{\tilde{\mathcal{A}}\tilde{\mathcal{A}}}}{2\tilde{\xi}}\left[iq^\mu {\mathcal{B}_\mu}^{\tilde{\mathcal{A}}}(-q) - \frac{\tilde{\xi}}{H^{(1)}_{\tilde{\mathcal{A}}\tilde{\mathcal{A}}}}\partial_r\left(H^{(1)}_{\tilde{\mathcal{A}}\tilde{\mathcal{A}}}e^{2A}{\mathcal{B}_5}^{\tilde{\mathcal{A}}}(-q)\right)\right]\times \right. \\ \left.\times\left[-iq^\nu {\mathcal{B}_\nu}^{\tilde{\mathcal{A}}}(q) - \frac{\tilde{\xi}}{H^{(1)}_{\tilde{\mathcal{A}}\tilde{\mathcal{A}}}}\partial_r\left(H^{(1)}_{\tilde{\mathcal{A}}\tilde{\mathcal{A}}}e^{2A}{\mathcal{B}_5}^{\tilde{\mathcal{A}}}(q)\right)\right]\right\}, \end{aligned} \tag{D.1.2}$$

with $\hat{\xi}$ and $\tilde{\xi}$ representing the gauge-fixing parameters. The gauge fixing terms at the $r = r_2$ boundary-localised are

$$\begin{aligned}\mathcal{S}^{(1)}_{\hat{M}} = &\int \mathrm{d}^4q\ \mathrm{d}r\delta\left(r - r_2\right)\\ &\left\{-\frac{1}{2\hat{M}_2}\left[iq^\mu \mathcal{B}_\mu{}^{\hat{\mathcal{A}}}(-q) + \hat{M}_2 H^{(1)}_{\hat{\mathcal{A}}\hat{\mathcal{A}}} e^{2A}\mathcal{B}_5{}^{\hat{\mathcal{A}}}(-q) - \hat{M}_2 K_5 \frac{g v_5}{2} e^{2A}\cos(v) P_5^{\hat{\mathcal{A}}}(-q)\right.\right.\\ &\left.\left. -\frac{g\sin(v)}{2v}\hat{M}_2 C^{(1)}_{2\,\hat{\mathcal{A}}\hat{\mathcal{A}}} e^{2A}\pi^{\hat{\mathcal{A}}}(-q)\right]\times\left[(q\to -q)\right]\right\}\,,\end{aligned} \tag{D.1.3}$$

and

$$\begin{aligned}\mathcal{S}^{(1)}_{\tilde{M}} = &\int \mathrm{d}^4q\ \mathrm{d}r\delta\left(r - r_2\right)\\ &\left\{-\frac{1}{2\tilde{M}_2}\left[iq^\mu \mathcal{B}_\mu{}^{\tilde{\mathcal{A}}}(-q) + \tilde{M}_2 H^{(1)}_{\tilde{\mathcal{A}}\tilde{\mathcal{A}}} e^{2A}\mathcal{B}_5{}^{\tilde{\mathcal{A}}}(-q) + \tilde{M}_2 K_5 \frac{g v_5}{2} e^{2A}\sin(v) P_5^{\tilde{\mathcal{A}}}(-q)\right]\times\right.\\ &\left.\times\left[(q\to -q)\right]\right\}\,.\end{aligned} \tag{D.1.4}$$

The gauge fixing parameters for the boundary theory, $\hat{M}_2$ and $\tilde{M}_2$, do not depend on the dynamics of the bulk. The gauge fixing process at $r = r_1$ is similar. Considering the action Eq. (5.5.17) and all gauge fixing contributions form Eqs. (D.1.1), (D.1.2), (D.1.3), and (D.1.4),

the equations of motion and boundary conditions of $\mathcal{B}_\mu{}^{\hat{\mathcal{A}}}$ and $\mathcal{B}_\mu{}^{\tilde{\mathcal{A}}}$ are the folllowing

$$0 = \left[q^2 H^{(1)}_{\hat{\mathcal{A}}\hat{\mathcal{A}}} - \partial_r\left(H^{(1)}_{\hat{\mathcal{A}}\hat{\mathcal{A}}} e^{2A}\partial_r\right) + \left(\frac{g}{2}\right)^2 G^{(1)}_{\hat{\mathcal{A}}\hat{\mathcal{A}}} e^{2A}\right] P^{\mu\nu}\mathcal{B}_\mu{}^{\hat{\mathcal{A}}}(q,r), \tag{D.1.5}$$

$$\begin{aligned} 0 = &\left[q^2 D^{(1)}_{2\,\hat{\mathcal{A}}\hat{\mathcal{A}}} + H^{(1)}_{\hat{\mathcal{A}}\hat{\mathcal{A}}} e^{2A}\partial_r + e^{2A}\left(\frac{g}{2}\right)^2 C^{(1)}_{2\,\hat{\mathcal{A}}\hat{\mathcal{A}}} + e^{2A}(\frac{gv_5}{2})^2 K_5\cos(v)^2\right] P^{\mu\nu}\mathcal{B}_\nu{}^{\hat{\mathcal{A}}}(q,r)\Big|_{r=r_2} \\ &+ \left[q^2 D^{(1)}_{2\,\hat{\mathcal{A}}\tilde{\mathcal{A}}} - e^{2A}(\frac{gv_5}{2})^2 K_5\cos(v)\sin(v)\right] P^{\mu\nu}\mathcal{B}_\nu{}^{\tilde{\mathcal{A}}}(q,r)\Big|_{r=r_2}, \end{aligned} \tag{D.1.6}$$

$$0 = \left[\frac{q^2}{\hat{\xi}} H^{(1)}_{\hat{\mathcal{A}}\hat{\mathcal{A}}} - \partial_r\left(H^{(1)}_{\hat{\mathcal{A}}\hat{\mathcal{A}}} e^{2A}\partial_r\right) + \left(\frac{g}{2}\right)^2 G^{(1)}_{\hat{\mathcal{A}}\hat{\mathcal{A}}} e^{2A}\right] \frac{q^\mu q^\nu}{q^2}\mathcal{B}_\mu{}^{\hat{\mathcal{A}}}(q,r), \tag{D.1.7}$$

$$\begin{aligned} 0 = &\left[\frac{q^2}{\hat{M}_2} + H^{(1)}_{\hat{\mathcal{A}}\hat{\mathcal{A}}} e^{2A}\partial_r + e^{2A}\left(\frac{g}{2}\right)^2 C^{(1)}_{2\,\hat{\mathcal{A}}\hat{\mathcal{A}}} + e^{2A}(\frac{gv_5}{2})^2 K_5\cos(v)^2\right] \frac{q^\mu q^\nu}{q^2}\mathcal{B}_\nu{}^{\hat{\mathcal{A}}}(q,r)\Big|_{r=r_2} \\ &- \left[e^{2A}(\frac{gv_5}{2})^2 K_5\cos(v)\sin(v)\right] \frac{q^\mu q^\nu}{q^2}\mathcal{B}_\nu{}^{\tilde{\mathcal{A}}}(q,r)\Big|_{r=r_2}, \end{aligned} \tag{D.1.8}$$

$$0 = \left[q^2 H^{(1)}_{\tilde{\mathcal{A}}\tilde{\mathcal{A}}} - \partial_r\left(H^{(1)}_{\tilde{\mathcal{A}}\tilde{\mathcal{A}}} e^{2A}\partial_r\right)\right] P^{\mu\nu}\mathcal{B}_\mu{}^{\tilde{\mathcal{A}}}(q,r), \tag{D.1.9}$$

$$\begin{aligned} 0 = &\left[q^2 D^{(1)}_{2\,\tilde{\mathcal{A}}\tilde{\mathcal{A}}} + H^{(1)}_{\tilde{\mathcal{A}}\tilde{\mathcal{A}}} e^{2A}\partial_r + e^{2A}(\frac{gv_5}{2})^2 K_5\sin(v)^2\right] P^{\mu\nu}\mathcal{B}_\nu{}^{\tilde{\mathcal{A}}}(q,r)\Big|_{r=r_2} \\ &+ \left[q^2 D^{(1)}_{2\,\tilde{\mathcal{A}}\hat{\mathcal{A}}} - e^{2A}(\frac{gv_5}{2})^2 K_5\cos(v)\sin(v)\right] P^{\mu\nu}\mathcal{B}_\nu{}^{\hat{\mathcal{A}}}(q,r)\Big|_{r=r_2}, \end{aligned} \tag{D.1.10}$$

$$0 = \left[\frac{q^2}{\tilde{\xi}} H^{(1)}_{\tilde{\mathcal{A}}\tilde{\mathcal{A}}} - \partial_r\left(H^{(1)}_{\tilde{\mathcal{A}}\tilde{\mathcal{A}}} e^{2A}\partial_r\right)\right] \frac{q^\mu q^\nu}{q^2}\mathcal{B}_\mu{}^{\tilde{\mathcal{A}}}(q,r), \tag{D.1.11}$$

$$\begin{aligned} 0 = &\left[\frac{q^2}{\tilde{M}_2} + H^{(1)}_{\tilde{\mathcal{A}}\tilde{\mathcal{A}}} e^{2A}\partial_r + e^{2A}(\frac{gv_5}{2})^2 K_5\sin(v)^2\right] \frac{q^\mu q^\nu}{q^2}\mathcal{B}_\nu{}^{\tilde{\mathcal{A}}}(q,r)\Big|_{r=r_2} \\ &- \left[e^{2A}(\frac{gv_5}{2})^2 K_5\cos(v)\sin(v)\right] \frac{q^\mu q^\nu}{q^2}\mathcal{B}_\nu{}^{\hat{\mathcal{A}}}(q,r)\Big|_{r=r_2}. \end{aligned} \tag{D.1.12}$$

Equations (D.1.5), (D.1.7), (D.1.9), and (D.1.10) can be compared to Eqs. (5.6.3), (5.6.4), and (5.6.6) in the body of the paper.

The equations for pseudoscalar and spurion fields are derived from the variation of the

action respective to ${\mathcal{B}_5}^{\tilde{\mathcal{A}}}$, ${\mathcal{B}_5}^{\hat{\mathcal{A}}}$, $\pi^{\hat{\mathcal{A}}}$ in the bulk and boundary and $P_5^{\hat{\mathcal{A}}}$ in the boundary:

$$0 = \left[q^2 - \partial_r \left(\frac{\tilde{\xi}}{H^{(1)}_{\tilde{\mathcal{A}}\tilde{\mathcal{A}}}} \partial_r \left(H^{(1)}_{\tilde{\mathcal{A}}\tilde{\mathcal{A}}} e^{2A} \right) \right) \right] {\mathcal{B}_5}^{\tilde{\mathcal{A}}}(q,r)\,, \tag{D.1.13}$$

$$0 = \left[\tilde{\xi} \frac{e^{-2A}}{H^{(1)}_{\tilde{\mathcal{A}}\tilde{\mathcal{A}}}} \partial_r \left(H^{(1)}_{\tilde{\mathcal{A}}\tilde{\mathcal{A}}} e^{2A} \right) + \tilde{M}_2 H^{(1)}_{\tilde{\mathcal{A}}\tilde{\mathcal{A}}} \right] {\mathcal{B}_5}^{\tilde{\mathcal{A}}}(q,r) \Big|_{r=r_2} + \left[\frac{g v_5}{2} \tilde{M}_2 K_5 \sin(v) \right] P_5^{\hat{\mathcal{A}}}(q) \Big|_{r=r_2}\,, \tag{D.1.14}$$

$$\begin{aligned} 0 = & \left[q^2 H^{(1)}_{\hat{\mathcal{A}}\hat{\mathcal{A}}} - H^{(1)}_{\hat{\mathcal{A}}\hat{\mathcal{A}}} \partial_r \left(\frac{\hat{\xi}}{H^{(1)}_{\hat{\mathcal{A}}\hat{\mathcal{A}}}} \partial_r \left(H^{(1)}_{\hat{\mathcal{A}}\hat{\mathcal{A}}} e^{2A} \right) \right) + \frac{g^2}{2} G^{(1)}_{\hat{\mathcal{A}}\hat{\mathcal{A}}} e^{2A} \right] {\mathcal{B}_5}^{\hat{\mathcal{A}}}(q,r) \\ & + \frac{g \sin(v)}{2v} \left[G^{(1)}_{\hat{\mathcal{A}}\hat{\mathcal{A}}} e^{2A} \partial_r - H^{(1)}_{\hat{\mathcal{A}}\hat{\mathcal{A}}} \partial_r \left(\hat{\xi} \frac{G^{(1)}_{\hat{\mathcal{A}}\hat{\mathcal{A}}} e^{2A}}{H^{(1)}_{\hat{\mathcal{A}}\hat{\mathcal{A}}}} \right) \right] \pi^{\hat{\mathcal{A}}}(q,r)\,, \end{aligned} \tag{D.1.15}$$

$$\begin{aligned} 0 = & \left[\frac{e^{-2A}}{H^{(1)}_{\tilde{\mathcal{A}}\tilde{\mathcal{A}}}} \partial_r \left(\hat{\xi} H^{(1)}_{\hat{\mathcal{A}}\hat{\mathcal{A}}} e^{2A} \right) + \hat{M}_2 H^{(1)}_{\hat{\mathcal{A}}\hat{\mathcal{A}}} \right] {\mathcal{B}_5}^{\hat{\mathcal{A}}}(q,r) - \left[\frac{g v_5}{2} \hat{M}_2 \cos(v) K_5 \right] P_5^{\hat{\mathcal{A}}}(q) \Big|_{r=r_2} \\ & + \frac{g \sin(v)}{2v} \left[\hat{\xi} \frac{G^{(1)}_{\hat{\mathcal{A}}\hat{\mathcal{A}}}}{H^{(1)}_{\tilde{\mathcal{A}}\tilde{\mathcal{A}}}} - \hat{M}_2 C^{(1)}_{2\,\hat{\mathcal{A}}\hat{\mathcal{A}}} \right] \pi^{\hat{\mathcal{A}}}(q,r) \Big|_{r=r_2}\,, \end{aligned} \tag{D.1.16}$$

$$\begin{aligned} 0 = & \frac{\sin(v)}{v} \left[\partial_r \left(G^{(1)}_{\hat{\mathcal{A}}\hat{\mathcal{A}}} e^{4A} \partial_r \right) - G^{(1)}_{\hat{\mathcal{A}}\hat{\mathcal{A}}} e^{2A} q^2 - \left(\frac{g}{2} \right)^2 \frac{\hat{\xi}}{H^{(1)}_{\hat{\mathcal{A}}\hat{\mathcal{A}}}} e^{4A} (G^{(1)}_{\hat{\mathcal{A}}\hat{\mathcal{A}}})^2 \right] \pi^{\hat{\mathcal{A}}}(q,r) \\ & + \frac{g}{2} \left[\partial_r \left(G^{(1)}_{\hat{\mathcal{A}}\hat{\mathcal{A}}} e^{4A} \right) - \frac{\hat{\xi}}{H^{(1)}_{\hat{\mathcal{A}}\hat{\mathcal{A}}}} e^{2A} G^{(1)}_{\hat{\mathcal{A}}\hat{\mathcal{A}}} \partial_r \left(H^{(1)}_{\hat{\mathcal{A}}\hat{\mathcal{A}}} e^{2A} \right) \right] {\mathcal{B}_5}^{\hat{\mathcal{A}}}(q,r)\,, \end{aligned} \tag{D.1.17}$$

$$\begin{aligned} 0 = & \frac{\sin(v)}{v} \left[C^{(1)}_{2\,\hat{\mathcal{A}}\hat{\mathcal{A}}} e^{-2A} q^2 + \hat{M}_2 \left(\frac{g}{2} \right)^2 (C^{(1)}_{2\,\hat{\mathcal{A}}\hat{\mathcal{A}}})^2 + G^{(1)}_{\hat{\mathcal{A}}\hat{\mathcal{A}}} \partial_r \right] \pi^{\hat{\mathcal{A}}}(q,r) \Big|_{r=r_2} \\ & + \left[\hat{M}_2 v_5 \left(\frac{g}{2} \right)^2 \cos(v) K_5 C^{(1)}_{2\,\hat{\mathcal{A}}\hat{\mathcal{A}}} \right] P_5^{\hat{\mathcal{A}}}(q) \Big|_{r=r_2} - \left[\frac{g}{2} \hat{M}_2 (C^{(1)}_{2\,\hat{\mathcal{A}}\hat{\mathcal{A}}}) H^{(1)}_{\hat{\mathcal{A}}\hat{\mathcal{A}}} - \frac{g}{2} G^{(1)}_{\hat{\mathcal{A}}\hat{\mathcal{A}}} \right] {\mathcal{B}_5}^{\hat{\mathcal{A}}}(q,r) \Big|_{r=r_2}\,, \end{aligned} \tag{D.1.18}$$

$$\begin{aligned} 0 = & \left[K_5 e^{-2A} q^2 + \left(\frac{g v_5}{2} \right)^2 K_5^2 \left(\cos(v)^2 \hat{M}_2 + \sin(v)^2 \tilde{M}_2 \right) \right] P_5^{\hat{\mathcal{A}}}(q) \Big|_{r=r_2} \\ & + \left[\hat{M}_2 K_5 \left(\frac{g v_5}{2} \right)^2 \frac{\cos(v)\sin(v)}{v} C^{(1)}_{2\,\hat{\mathcal{A}}\hat{\mathcal{A}}} \right] \pi^{\hat{\mathcal{A}}}(q,r) \Big|_{r=r_2} \\ & - \left[K_5 \cos(v) \frac{g v_5}{2} \hat{M}_2 H^{(1)}_{\hat{\mathcal{A}}\hat{\mathcal{A}}} \right] {\mathcal{B}_5}^{\hat{\mathcal{A}}}(q,r) \Big|_{r=r_2} + \left[K_5 \sin(v) \frac{g v_5}{2} \tilde{M}_2 H^{(1)}_{\tilde{\mathcal{A}}\tilde{\mathcal{A}}} \right] {\mathcal{B}_5}^{\tilde{\mathcal{A}}}(q,r) \Big|_{r=r_2}\,. \end{aligned} \tag{D.1.19}$$

Here, after introducing the redefinitions

$$\mathcal{B}_5{}^{\hat{\mathcal{A}}} \equiv \frac{X^{\hat{\mathcal{A}}}}{e^{4A}G^{(1)}_{\hat{\mathcal{A}}\hat{\mathcal{A}}}} - \frac{2}{g}\frac{\sin(v)}{v}\partial_r\pi^{\hat{\mathcal{A}}}\,, \tag{D.1.20}$$

$$\pi^{\hat{\mathcal{A}}} \equiv \frac{v}{\sin(v)}\left(Y^{\hat{\mathcal{A}}} + \frac{(g/2)\partial_r X^{\hat{\mathcal{A}}}}{q^2 e^{2A}G^{(1)}_{\hat{\mathcal{A}}\hat{\mathcal{A}}}}\right), \tag{D.1.21}$$

one can conveniently separate the gauge-invariant combinations from the gauge-dependent ones. The equations for gauge-independent and physical scalar fields, $X^{\hat{\mathcal{A}}}$, as well as gauge dependent, non physical $Y^{\hat{\mathcal{A}}}$ read

$$0 = \left[\partial_r^2 + \left(-2\partial_r A(r) - \frac{\partial_r G^{(1)}_{\hat{\mathcal{A}}\hat{\mathcal{A}}}}{G^{(1)}_{\hat{\mathcal{A}}\hat{\mathcal{A}}}}\right)\partial_r + \left(-q^2e^{-2A(r)} - \frac{g^2G^{(1)}_{\hat{\mathcal{A}}\hat{\mathcal{A}}}}{4H^{(1)}_{\hat{\mathcal{A}}\hat{\mathcal{A}}}}\right)\right]X^{\hat{\mathcal{A}}}(q,r)\,, \tag{D.1.22}$$

$$0 = \left[\partial_r^2 + \left(2\partial_r A(r) + \frac{\partial_r H^{(1)}_{\hat{\mathcal{A}}\hat{\mathcal{A}}}}{H^{(1)}_{\hat{\mathcal{A}}\hat{\mathcal{A}}}}\right)\partial_r + \left(-\frac{q^2e^{-2A(r)}}{\hat{\xi}} - \frac{g^2G^{(1)}_{\hat{\mathcal{A}}\hat{\mathcal{A}}}}{4H^{(1)}_{\hat{\mathcal{A}}\hat{\mathcal{A}}}}\right)\right]Y^{\hat{\mathcal{A}}}(q,r)\,. \tag{D.1.23}$$

The boundary cnditions for $X^{\hat{\mathcal{A}}}$ are:

$$0 = \left[\partial_r + \frac{G^{(1)}_{\hat{\mathcal{A}}\hat{\mathcal{A}}}}{C^{(1)}_{2\,\hat{\mathcal{A}}\hat{\mathcal{A}}}}\right]X^{\hat{\mathcal{A}}}(q,r)\Bigg|_{r=r_2}\,. \tag{D.1.24}$$

Equations (D.1.22) and (D.1.24) are rewritten in Eqs. (5.6.5) and (5.6.10).

D.1.2 The ${\mathcal{A}_M}^4$ sector

The gauge fixing for ${\mathcal{A}_M}^4$ field in bulk can be performed by introducing terms as:

$$\mathcal{S}^{(1)}_{\xi} = \int \mathrm{d}^4q\;\mathrm{d}r\left\{-\frac{H^{(1)}_{44}}{2\xi}\left[iq^\mu{\mathcal{A}_\mu}^4(-q) - \frac{g}{2}\frac{\xi}{H^{(1)}_{44}}G^{(1)}_{44}e^{2A}\Pi^4(-q) - \frac{\xi}{H^{(1)}_{44}}\partial_r\left(H^{(1)}_{44}e^{2A}{\mathcal{A}_5}^4(-q)\right)\right]\times\right.$$
$$\left.\times\left[-iq^\nu{\mathcal{A}_\nu}^4(q) - \frac{g}{2}\frac{\xi}{H^{(1)}_{44}}G^{(1)}_{44}e^{2A}\Pi^4(q) - \frac{\xi}{H^{(1)}_{44}}\partial_r\left(H^{(1)}_{44}e^{2A}{\mathcal{A}_5}^4(q)\right)\right]\right\}, \tag{D.1.25}$$

with ξ being the gauge-fixing parameter. The gauge-fixing terms at $r = r_2$ boundary are

$$\mathcal{S}^{(1)}_{M} = \int \mathrm{d}^4q\;\mathrm{d}r\delta(r-r_2)\left\{-\frac{1}{2M_2}\left[iq^\mu{\mathcal{A}_\mu}^4(-q) + M_2H^{(1)}_{44}e^{2A}{\mathcal{A}_5}^4(-q) - M_2K_5\frac{gv_5}{2}e^{2A}P^4_5(-q)\right.\right.$$
$$\left.\left.-\frac{g}{2}M_2C^{(1)}_{2\,44}e^{2A}\Pi^4(-q)\right]\times[(q\to -q)]\right\}, \tag{D.1.26}$$

where M_2 is our free parameter. The equations of motion and boundary conditions of ${\mathcal{A}_\mu}^4$ are written as

$$0 = \left[q^2 H_{44}^{(1)} - \partial_r \left(H_{44}^{(1)} e^{2A} \partial_r \right) + \left(\frac{g}{2} \right)^2 G_{44}^{(1)} e^{2A} \right] P^{\mu\nu} {\mathcal{A}_\mu}^4(q,r), \tag{D.1.27}$$

$$0 = \left[H_{44}^{(1)} e^{2A} \partial_r + q^2 D_{2\,44}^{(1)} + e^{2A} \left(\frac{g}{2} \right)^2 C_{2\,44}^{(1)} + (\frac{g v_5}{2})^2 K_5 e^{2A} \right] P^{\mu\nu} {\mathcal{A}_\nu}^4(q,r) \Big|_{r=r_2}, \tag{D.1.28}$$

$$0 = \left[\frac{q^2}{\xi} H_{44}^{(1)} - \partial_r \left(H_{44}^{(1)} e^{2A} \partial_r \right) + \left(\frac{g}{2} \right)^2 G_{44}^{(1)} e^{2A} \right] \frac{q^\mu q^\nu}{q^2} {\mathcal{A}_\mu}^4(q,r), \tag{D.1.29}$$

$$0 = \left[H_{44}^{(1)} e^{2A} \partial_r + \frac{q^2}{M_2} + e^{2A} \left(\frac{g}{2} \right)^2 C_{2\,44}^{(1)} + (\frac{g v_5}{2})^2 K_5 e^{2A} \right] \frac{q^\mu q^\nu}{q^2} {\mathcal{A}_\nu}^4(q,r) \Big|_{r=r_2}. \tag{D.1.30}$$

Equations (D.1.27) and (D.1.28) are comparable to Eqs. (5.6.4) and (5.6.9).

The equations are obtained for the pseudoscalars, and the spurion is derived from the variation of the action respective to ${\mathcal{A}_5}^4$ and Π^4 in bulk and boundary and P_5^4 in the boundary.

They are written as follows:

$$0 = \left[q^2 H_{44}^{(1)} - H_{44}^{(1)} \partial_r \left(\frac{\xi}{H_{44}^{(1)}} \partial_r \left(H_{44}^{(1)} e^{2A} \right) \right) + \left(\frac{g}{2} \right)^2 G_{44}^{(1)} e^{2A} \right] \mathcal{A}_5{}^4(q,r) + \frac{g}{2} \left[G_{44}^{(1)} e^{2A} \partial_r - H_{44}^{(1)} \partial_r \left(\frac{\xi G_{44}^{(1)} e^{2A}}{H_{44}^{(1)}} \right) \right] \Pi^4(q,r) \,, \tag{D.1.31}$$

$$0 = \left[\xi \frac{e^{-2A}}{H_{44}^{(1)}} \partial_r \left(H_{44}^{(1)} e^{2A} \right) + M_2 H_{44}^{(1)} \right] \mathcal{A}_5{}^4(q,r) \Big|_{r=r_2} + \frac{g}{2} \left[\frac{\xi}{H_{44}^{(1)}} G_{44}^{(1)} - M_2 C_{2\,44}^{(1)} \right] \Pi^4(q,r) - \left[M_2 \frac{g}{2} K_5 v_5 \right] P_5^4(q) \Big|_{r=r_2} \,, \tag{D.1.32}$$

$$0 = \left[\partial_r \left(G_{44}^{(1)} e^{4A} \partial_r \right) - G_{44}^{(1)} e^{2A} q^2 - \left(\frac{g}{2} \right)^2 \frac{\xi}{H_{44}^{(1)}} e^{4A} (G_{44}^{(1)})^2 \right] \Pi^4(q,r) + \frac{g}{2} \left[\partial_r \left(G_{44}^{(1)} e^{4A} \right) - \frac{\xi}{H_{44}^{(1)}} e^{2A} G_{44}^{(1)} \partial_r \left(H_{44}^{(1)} e^{2A} \right) \right] \mathcal{A}_5{}^4(q,r) \,, \tag{D.1.33}$$

$$0 = \left[C_{2\,44}^{(1)} e^{-2A} q^2 + M_2 \left(\frac{g}{2} \right)^2 (C_{2\,44}^{(1)})^2 + \partial_v^2 \mathcal{V}_4 + G_{44}^{(1)} \partial_r \right] \Pi^4(q,r) \Big|_{r=r_2} + \frac{g}{2} \left[G_{44}^{(1)} - M_2 C_{2\,44}^{(1)} H_{44}^{(1)} \right] \mathcal{A}_5{}^4(q,r) + \left[\frac{g^2 v_5}{4} M_2 K_5 C_{2\,44}^{(1)} - \frac{1}{v_5} \partial_v^2 \mathcal{V}_4 \right] P_5^4(q) \Big|_{r=r_2} \,, \tag{D.1.34}$$

$$0 = \left[K_5 e^{-2A} q^2 + M_2 \left(\frac{g v_5}{2} \right)^2 K_5^2 + \frac{1}{v_5^2} \partial_v^2 \mathcal{V}_4 \right] P_5^4(q) \Big|_{r=r_2} - \left[M_2 \frac{g v_5}{2} K_5 H_{44}^{(1)} \right] \mathcal{A}_5{}^4(q,r) + \left[\frac{g^2 v_5}{4} M_2 K_5 C_{2\,44}^{(1)} - \frac{1}{v_5} \partial_v^2 \mathcal{V}_4 \right] \Pi^4(q,r) \Big|_{r=r_2} \,. \tag{D.1.35}$$

By the introduction of fields

$$\mathcal{A}_5{}^4 \equiv \frac{X^4}{e^{4A} G_{44}^{(1)}} - \frac{2}{g} \partial_r \Pi^4 \,, \tag{D.1.36}$$

we find the equations for gauge-invariant, physical field X^4:

$$0 = \left[\partial_r^2 + \left(-2\partial_r A - \frac{\partial_r G_{44}^{(1)}}{G_{44}^{(1)}} \right) \partial_r + \left(-q^2 e^{-2A} - \frac{g^2 G_{44}^{(1)}}{4 H_{44}^{(1)}} \right) \right] X^4(q,r), \tag{D.1.37}$$

$$0 = \left[\partial_r + G_{44}^{(1)} \left(\frac{\partial_v^2 \mathcal{V}_4 e^{2A(r)} + K_5 v_5^2 q^2}{\partial_v^2 \mathcal{V}_4 K_5 v_5^2 e^{2A(r)} + C_{2\,44}^{(1)} \partial_v^2 \mathcal{V}_4 e^{2A(r)} + K_5 C_{2\,44}^{(1)} v_5^2 q^2} \right) \right] X^4(q,r) \Big|_{r=r_2} \,. \tag{D.1.38}$$

Equations (D.1.37) and (D.1.38) are given in Eqs. (5.6.5) and (5.6.11) in another notation.

D.1.3 The $\mathcal{A}_M{}^{\bar{\mathcal{A}}}$ sector

For $\mathcal{A}_M{}^{\bar{\mathcal{A}}}$ the gauge fixing terms are chosen to be

$$\mathcal{S}^{(1)}_{\bar{\xi}} = \int \mathrm{d}^4q\ \mathrm{d}r \left\{ -\frac{H^{(1)}_{\bar{\mathcal{A}}\bar{\mathcal{A}}}}{2\bar{\xi}} \left[iq^\mu \mathcal{A}_\mu{}^{\bar{\mathcal{A}}}(-q) - \frac{\bar{\xi}}{H^{(1)}_{\bar{\mathcal{A}}\bar{\mathcal{A}}}} \partial_r \left(H^{(1)}_{\bar{\mathcal{A}}\bar{\mathcal{A}}} e^{2A} \mathcal{A}_5{}^{\bar{\mathcal{A}}}(-q) \right) \right] \times \right.$$
$$\left. \left[-iq^\nu \mathcal{A}_\nu{}^{\bar{\mathcal{A}}}(q) - \frac{\bar{\xi}}{H^{(1)}_{\bar{\mathcal{A}}\bar{\mathcal{A}}}} \partial_r \left(H^{(1)}_{\bar{\mathcal{A}}\bar{\mathcal{A}}} e^{2A} \mathcal{A}_5{}^{\bar{\mathcal{A}}}(q) \right) \right] \right\}, \tag{D.1.39}$$

in the bulk, with $\bar{\xi}$ as the gauge fixing parameter. The gauge fixing terms at $r = r_2$ boundary are chosen as

$$\mathcal{S}^{(1)}_{\bar{M}} = \int \mathrm{d}^4q\ \mathrm{d}r \delta(r - r_2)$$
$$\left\{ -\frac{1}{2\bar{M}_2} \left[iq^\mu \mathcal{A}_\mu{}^{\bar{\mathcal{A}}}(-q) + \bar{M}_2 H^{(1)}_{\bar{\mathcal{A}}\bar{\mathcal{A}}} e^{2A} \mathcal{A}_5{}^{\bar{\mathcal{A}}}(-q) \right] \times \left[-iq^\nu \mathcal{A}_\nu{}^{\bar{\mathcal{A}}}(q) + \bar{M}_2 H^{(1)}_{\bar{\mathcal{A}}\bar{\mathcal{A}}} e^{2A} \mathcal{A}_5{}^{\bar{\mathcal{A}}}(q) \right) \right] \right\}, \tag{D.1.40}$$

where $\bar{M}_2$ is the gauge fixing parameter at the boundary.

The equations of motion and boundary conditions for $\mathcal{A}_\mu{}^{\bar{\mathcal{A}}}$ fileds are

$$0 = \left[q^2 H^{(1)}_{\bar{\mathcal{A}}\bar{\mathcal{A}}} - \partial_r \left(H^{(1)}_{\bar{\mathcal{A}}\bar{\mathcal{A}}} e^{2A} \partial_r \right) \right] P^{\mu\nu} \mathcal{A}_\mu{}^{\bar{\mathcal{A}}}(q, r), \tag{D.1.41}$$
$$0 = \left[H^{(1)}_{\bar{\mathcal{A}}\bar{\mathcal{A}}} e^{2A} \partial_r + q^2 D^{(1)}_{2\,\bar{\mathcal{A}}\bar{\mathcal{A}}} \right] P^{\mu\nu} \mathcal{A}_\nu{}^{\bar{\mathcal{A}}}(q, r)\Big|_{r=r_2}, \tag{D.1.42}$$
$$0 = \left[\frac{q^2}{\bar{\xi}} H^{(1)}_{\bar{\mathcal{A}}\bar{\mathcal{A}}} - \partial_r \left(H^{(1)}_{\bar{\mathcal{A}}\bar{\mathcal{A}}} e^{2A} \partial_r \right) \right] \frac{q^\mu q^\nu}{q^2} \mathcal{A}_\mu{}^{\bar{\mathcal{A}}}(q, r), \tag{D.1.43}$$
$$0 = \left[\frac{q^2}{\bar{M}_2} + H^{(1)}_{\bar{\mathcal{A}}\bar{\mathcal{A}}} e^{2A} \partial_r \right] \frac{q^\mu q^\nu}{q^2} \mathcal{A}_\nu{}^{\bar{\mathcal{A}}}(q, r)\Big|_{r=r_2}. \tag{D.1.44}$$

Equations (D.1.41) and (D.1.42) are given in Eqs. (5.6.3), and (5.6.8). In this sector, the fifth component of the gauge field is non-physical and pure gauge; hence, we do not consider them here.

Appendix E

Asymptotic expansions of the fluctuations

In this appendix, some of the asymptotic expansions of the fluctuations used in the text are provided— check also Ref. [6].

E.1 IR expansions

We set $\rho_o = 0$ and $A_I = 0$ in this section,[1] and $\chi_I = 0$ is chosen to avoid the presence of a singularity.

[1] The ρ_o and A_I dependence can be reintroduced by substituting $\rho \to \rho - \rho_o$ and $q^2 \to e^{-2A_I} q^2$ in the provided IR related expressions.

For the scalar fluctuations, one has

$$\begin{aligned}\mathfrak{a}^{\phi} = {}& \mathfrak{a}^{\phi}_{I,0} + \\ & + \mathfrak{a}^{\phi}_{I,l}\log(\rho) + \frac{1}{4}\rho^2\Bigg[-\frac{1}{4}\Delta\left(\mathfrak{a}^{\phi}_{I,0}\left(\Delta\left(15\phi_I^2-4\right)+20\right) + 6\phi_I(\mathfrak{a}^{\chi}_{I,0}-\mathfrak{a}^{\chi}_{I,l})\left(\Delta\left(5\phi_I^2-4\right)+20\right)\right) \\ & + q^2(\mathfrak{a}^{\phi}_{I,0}-\mathfrak{a}^{\phi}_{I,l}) - \frac{1}{48}\mathfrak{a}^{\phi}_{I,l}\left(\Delta\left(25\Delta\phi_I^4+20(10-11\Delta)\phi_I^2+48(\Delta-5)\right)+400\right) \\ & + \log(\rho)\left(\mathfrak{a}^{\phi}_{I,l}\left(-\frac{15\Delta^2\phi_I^2}{4}+(\Delta-5)\Delta+q^2\right) - \frac{3}{2}\mathfrak{a}^{\chi}_{I,l}\Delta\phi_I\left(\Delta\left(5\phi_I^2-4\right)+20\right)\right)\Bigg] + \mathcal{O}\left(\rho^4\right),\end{aligned} \tag{E.1.1}$$

$$\begin{aligned}\mathfrak{a}^{\chi} = {}& \mathfrak{a}^{\chi}_{I,0} + \mathfrak{a}^{\chi}_{I,l}\log(\rho) + \frac{1}{4}\rho^2\Bigg[-\frac{1}{4}\Delta\phi_I(\mathfrak{a}^{\phi}_{I,0}-\mathfrak{a}^{\phi}_{I,l})\left(\Delta\left(5\phi_I^2-4\right)+20\right) + q^2(\mathfrak{a}^{\chi}_{I,0}-\mathfrak{a}^{\chi}_{I,l}) \\ & - \frac{3}{8}\mathfrak{a}^{\chi}_{I,0}\left(\Delta\phi_I^2\left(\Delta\left(5\phi_I^2-8\right)+40\right)+80\right) + \frac{13}{48}\mathfrak{a}^{\chi}_{I,l}\left(\Delta\phi_I^2\left(\Delta\left(5\phi_I^2-8\right)+40\right)+80\right) \\ & + \log(\rho)\left(-\frac{5}{4}\mathfrak{a}^{\phi}_{I,l}\Delta^2\phi_I^3 + \mathfrak{a}^{\phi}_{I,l}(\Delta-5)\Delta\phi_I + \mathfrak{a}^{\chi}_{I,l}\left(-\frac{15}{8}\Delta^2\phi_I^4 + 3(\Delta-5)\Delta\phi_I^2 + q^2 - 30\right)\right)\Bigg] + \\ & + \mathcal{O}\left(\rho^4\right),\end{aligned} \tag{E.1.2}$$

$$\mathfrak{a}^{\bar{A}} = \mathfrak{a}^{\bar{A}}_{I,0} + \rho^2\left(\frac{1}{2}\mathfrak{a}^{\bar{A}}_{I,0}q^2\log(\rho) + \mathfrak{a}^{\bar{A}}_{I,2}\right) + \mathcal{O}\left(\rho^4\right), \tag{E.1.3}$$

$$\mathfrak{a}^{\hat{A}} = \mathfrak{a}^{\hat{A}}_{I,0} + \rho^2\left(\frac{1}{2}\mathfrak{a}^{\hat{A}}_{I,0}\left(q^2+\frac{g^2\phi_I^2}{4}\right)\log(\rho) + \mathfrak{a}^{\hat{A}}_{I,2}\right) + \mathcal{O}\left(\rho^4\right). \tag{E.1.4}$$

While for the pseudoscalar fluctuations, one has

$$\mathfrak{p}^{\hat{A}} = \mathfrak{p}^{\hat{A}}_{I,0} + \rho^2\left[\mathfrak{p}^{\hat{A}}_{I,2} + \frac{1}{2}\mathfrak{p}^{\hat{A}}_{I,0}\left(q^2+\frac{g^2}{4}\phi_I^2\right)\log(\rho)\right] + \mathcal{O}\left(\rho^4\right). \tag{E.1.5}$$

The vector fluctuations follow

$$\begin{aligned}\mathfrak{v} =\ & \mathfrak{v}_{I,-2}\rho^{-2} + \frac{1}{2}q^2\mathfrak{v}_{I,-2}\log(\rho)+\\ & + \mathfrak{v}_{I,0} + \frac{1}{12288}\rho^2\Big[1536q^2\mathfrak{v}_{I,0} + 80\Delta^2\mathfrak{v}_{I,-2}\phi_I^4\left(2\left(8\Delta^2-50\Delta+75\right)-3q^2\right)\\ & + 128(\Delta-5)\Delta\mathfrak{v}_{I,-2}\phi_I^2\left(-3(\Delta-5)\Delta+3q^2-50\right)-64\left(9q^4+60q^2-500\right)\mathfrak{v}_{I,-2}\\ & + 125\Delta^4\mathfrak{v}_{I,-2}\phi_I^8 - 1000(\Delta-2)\Delta^3\mathfrak{v}_{I,-2}\phi_I^6 + 768q^4\mathfrak{v}_{I,-2}\log(\rho)\Big] + \mathcal{O}\left(\rho^4\right), \end{aligned} \tag{E.1.6}$$

$$\begin{aligned}\mathfrak{v}^{\bar{A}} =\ & \mathfrak{v}^{\bar{A}}_{I,0} + \mathfrak{v}^{\bar{A}}_{I,l}\log(\rho) + \frac{1}{96}\rho^2\Big[24q^2(\mathfrak{v}^{\bar{A}}_{I,0}-\mathfrak{v}^{\bar{A}}_{I,l}) + \mathfrak{v}^{\bar{A}}_{I,l}\left(-5\Delta^2\phi_I^4+8(\Delta-5)\Delta\phi_I^2-80\right)\\ & + 24q^2\mathfrak{v}^{\bar{A}}_{I,l}\log(\rho)\Big] + \mathcal{O}\left(\rho^4\right), \end{aligned} \tag{E.1.7}$$

$$\begin{aligned}\mathfrak{v}^{\hat{A}} =\ & \mathfrak{v}^{\hat{A}}_{I,0} + \mathfrak{v}^{\hat{A}}_{I,l}\log(\rho) + \frac{1}{96}\rho^2\Big[\left(24q^2+6g^2\phi_I^2\right)\mathfrak{v}^{\hat{A}}_{I,0}\\ & + \left(-80-24q^2-6g^2\phi_I^2-40\Delta\phi_I^2+\Delta^2\left(8\phi_I^2-5\phi_I^4\right)\right)\mathfrak{v}^{\hat{A}}_{I,l}\\ & + \left(24q^2+6g^2\phi_I^2\right)\log(\rho)\mathfrak{v}^{\hat{A}}_{I,l}\Big] + \mathcal{O}\left(\rho^4\right). \end{aligned} \tag{E.1.8}$$

Finally, for fluctuations of the tensor, we get

$$\begin{aligned}\mathfrak{e} =& \mathfrak{e}_{I,0} + \mathfrak{e}_{I,l}\log(\rho) + \frac{1}{192}\rho^2\Big[48q^2(\mathfrak{e}_{I,0}-\mathfrak{e}_{I,l}) - 25\Delta^2\mathfrak{e}_{I,l}\phi_I^4\\ & + 40(\Delta-5)\Delta\mathfrak{e}_{I,l}\phi_I^2 - 400\mathfrak{e}_{I,l} + 48\mathfrak{e}_{I,l}q^2\log(\rho)\Big] + \mathcal{O}\left(\rho^4\right). \end{aligned} \tag{E.1.9}$$

E.2 UV expansions

In this section, $\Delta = 2$, and $A_U = 0 = \chi_U$ is chosen.[2] The expansions are written in terms of $z \equiv e^{-\rho}$.

For the scalar fluctuations, one has

$$\mathfrak{a}^{\phi} = \mathfrak{a}^{\phi}_2 z^2 + \mathfrak{a}^{\phi}_3 z^3 + \frac{1}{2}\mathfrak{a}^{\phi}_2 q^2 z^4 + \frac{1}{6}\mathfrak{a}^{\phi}_3 q^2 z^5 + \frac{1}{24}\mathfrak{a}^{\phi}_2\left(q^4-12\phi_V^2\right)z^6 + \mathcal{O}\left(z^7\right), \tag{E.2.1}$$

$$\mathfrak{a}^{\chi} = \mathfrak{a}^{\chi}_0 - \frac{1}{6}\mathfrak{a}^{\chi}_0 q^2 z^2 + \frac{1}{24}\mathfrak{a}^{\chi}_0 q^4 z^4 + \mathfrak{a}^{\chi}_5 z^5 + \frac{1}{144}\mathfrak{a}^{\chi}_0 q^2\left(q^4-14\phi_V^2\right)z^6 + \mathcal{O}\left(z^7\right), \tag{E.2.2}$$

$$\mathfrak{a}^{\bar{A}} = \mathfrak{a}^{\bar{A}}_0 - \frac{1}{2}\mathfrak{a}^{\bar{A}}_0 q^2 z^2 + \mathfrak{a}^{\bar{A}}_3 z^3 - \frac{1}{8}\mathfrak{a}^{\bar{A}}_0 q^4 z^4 + \frac{1}{10}\mathfrak{a}^{\bar{A}}_3 q^2 z^5 - \frac{1}{144}\mathfrak{a}^{\bar{A}}_0 q^2\left(q^4+10\phi_V^2\right)z^6 + \mathcal{O}\left(z^7\right), \tag{E.2.3}$$

$$\begin{aligned}\mathfrak{a}^{\hat{A}} =\ & \mathfrak{a}^{\hat{A}}_0 - \frac{1}{2}\mathfrak{a}^{\hat{A}}_0 q^2 z^2 + \mathfrak{a}^{\hat{A}}_3 z^3 + \frac{1}{16}\mathfrak{a}^{\hat{A}}_0\left(g^2\phi_J^2-2q^4\right)z^4 + \frac{1}{20}\left(\mathfrak{a}^{\hat{A}}_0 g^2\phi_J\phi_V + 2\mathfrak{a}^{\hat{A}}_3 q^2\right)z^5\\ & - \frac{1}{288}\mathfrak{a}^{\hat{A}}_0\left(2q^6+(20+g^2)q^2\phi_J^2-4g^2\phi_V^2\right)z^6 + \mathcal{O}\left(z^7\right). \end{aligned} \tag{E.2.4}$$

[2] The χ_U and A_U dependence can be reintroduced by substituting $q^2 \to e^{2\chi_U - 2A_U}q^2$ in the provided UV related expressions.

For the pseudo-scalar fluctuations, one has

$$\mathfrak{p}^{\hat{A}} = \mathfrak{p}_0^{\hat{A}} + \mathfrak{p}_1^{\hat{A}} z + \left(\frac{\mathfrak{p}_0^{\hat{A}} q^2}{2} + \frac{\mathfrak{p}_1^{\hat{A}} \phi_V}{\phi_J} \right) z^2 + \frac{2\mathfrak{p}_0^{\hat{A}} q^2 \phi_J \phi_V + \mathfrak{p}_1^{\hat{A}} q^2 \phi_J^2 + 2\mathfrak{p}_1^{\hat{A}} \phi_V^2}{6\phi_J^2} z^3 + \mathcal{O}\left(z^4\right) . \tag{E.2.5}$$

For the fluctuations of the vectors, we have

$$\begin{aligned} \mathfrak{v} = {} & \mathfrak{v}_0 - \frac{1}{6} q^2 \mathfrak{v}_0 z^2 + \frac{1}{24} q^4 \mathfrak{v}_0 z^4 + \mathfrak{v}_5 z^5 + \frac{1}{144} q^2 \mathfrak{v}_0 \left(q^4 - 14\phi_V^2 \right) z^6 \\ & + \frac{1}{350} q^2 (350 \mathfrak{v}_0 \chi_5 - 38 \mathfrak{v}_0 \phi_V \phi_J + 25 \mathfrak{v}_5) z^7 + \mathcal{O}\left(z^8\right) , \end{aligned} \tag{E.2.6}$$

$$\begin{aligned} \mathfrak{v}^{\bar{A}} = {} & \mathfrak{v}_0^{\bar{A}} - \frac{1}{2} q^2 \mathfrak{v}_0^{\bar{A}} z^2 + \mathfrak{v}_3^{\bar{A}} z^3 - \frac{1}{8} q^4 \mathfrak{v}_0^{\bar{A}} z^4 + \frac{1}{10} q^2 \mathfrak{v}_3^{\bar{A}} z^5 - \frac{1}{144} q^2 \mathfrak{v}_0^{\bar{A}} \left(q^4 + 10\phi_V^2 \right) z^6 \\ & + \frac{1}{280} \left(q^4 \mathfrak{v}_3^{\bar{A}} + 6 q^2 \mathfrak{v}_0^{\bar{A}} (15\chi_5 - \frac{26}{5} \phi_V \phi_J) + 45 \mathfrak{v}_3^{\bar{A}} \phi_V^2 \right) z^7 + \mathcal{O}\left(z^8\right) , \end{aligned} \tag{E.2.7}$$

$$\mathfrak{v}^{\hat{A}} = \mathfrak{v}_0^{\hat{A}} - \frac{1}{2} q^2 \mathfrak{v}_0^{\hat{A}} z^2 + \mathfrak{v}_3^{\hat{A}} z^3 - \frac{1}{8} \mathfrak{v}_0^{\hat{A}} \left(q^4 - \frac{g^2}{2} \phi_J^2 \right) z^4 + \frac{1}{10} \left(q^2 \mathfrak{v}_3^{\hat{A}} + \frac{g^2}{2} \mathfrak{v}_0^{\hat{A}} \phi_J \phi_V \right) z^5 + \mathcal{O}\left(z^6\right) . \tag{E.2.8}$$

The tensor fluctuations obey

$$\mathfrak{e} = \mathfrak{e}_0 - \frac{1}{6} \mathfrak{e}_0 q^2 z^2 + \frac{1}{24} \mathfrak{e}_0 q^4 z^4 + \mathfrak{e}_5 z^5 + \mathcal{O}\left(z^6\right) . \tag{E.2.9}$$

Appendix F

Six Dimensional Background

F.1 The Supergravity Background Origin

In this section, we outline the method for deriving the background described in Eq. (6.2.1). These configurations originate from solutions found within the context of 6-dimensional Romans' gauged supergravity [321], which are subsequently uplifted to Type-IIB theory. Below, we provide a detailed explanation of this process.

F.1.1 Six-dimensional Romans F_4 Supergravity

Here, we summarise the key aspects of six-dimensional Romans' F_4 gauged supergravity [321]. In addition to the vielbein, the bosonic sector includes a real scalar field, X, and a non-Abelian $SU(2)$ gauge field, A^i, where

$$F^i = dA^i + \frac{1}{2}\epsilon^{ijk}A^j \wedge A^k, \tag{F.1.1}$$

with a three-form

$$F_3 = dA_2\,, \tag{F.1.2}$$

and, A_1, an Abelian gauge field with

$$F_2 = dA_1 + \frac{2}{3}\tilde{g}A_2\,. \tag{F.1.3}$$

$\tilde{g}$ is presenting a coupling in the 6d theory.

The bosonic part of the Lagrangian reads

$$\begin{aligned}\mathcal{L} = R *_6 1 + 4\frac{*_6 dX \wedge dX}{X^2} - \tilde{g}^2\left(\frac{2}{9}X^{-6} - \frac{8}{3}X^{-2} - 2X^2\right)*_6 \\ +\frac{1}{2}X^4 *_6 F_3 \wedge F_3 - \frac{1}{2}X^{-2}\left(*_6 F_2 \wedge F_2 + \frac{1}{\tilde{g}^2} *_6 F^i \wedge F^i\right) \\ -\frac{1}{2}\tilde{A}_2 \wedge \left(dA_1 \wedge dA_1 + \frac{2}{3}\tilde{g}dA_1 \wedge A_2 + \frac{4}{27}\tilde{g}^2 A_2 \wedge A_2 + \frac{1}{\tilde{g}^2}F^i \wedge F^i\right).\end{aligned} \tag{F.1.4}$$

While the equations of motion are

$$d(X^4 *_6 F_3) = \frac{1}{2}F_2 \wedge F_2 + \frac{1}{2\tilde{g}^2}F^i \wedge F^i + \frac{2}{3}\tilde{g}X^{-2} *_6 F_2, \tag{F.1.5}$$

$$d(X^{-2} *_6 F_2) = -F_2 \wedge F_3 \tag{F.1.6}$$

$$D(X^{-2} *_6 F^i) = -F_3 \wedge F^i \tag{F.1.7}$$

$$d(X^{-1} *_6 dX) = \frac{1}{4}X^4 *_6 F_3 \wedge F_3 - \frac{X^{-2}}{8}\left(*_6 F_2 \wedge F_2 + \frac{1}{\tilde{g}^2} *_6 F^i \wedge F^i\right) - \tilde{g}^2\left(\frac{1}{6}X^{-6} - \frac{2}{3}X^{-2} + \frac{1}{2}X^2\right) *_6 1, \tag{F.1.8}$$

with D being the $SU(2)$ covariant derivative. The action of the derivative on a generic differential form C^i is given by

$$DC^i = dC^i + \epsilon_{ijk}A^j \wedge C^k\,. \tag{F.1.9}$$

The Einstein's equations of motion are written as

$$R_{\mu\nu} = 4X^{-2}\partial_\mu X\partial_\nu X + \tilde{g}^2\left(\frac{1}{18}X^{-6} - \frac{2}{3}X^{-2} - \frac{1}{2}X^2\right)g_{\mu\nu} + \frac{X^4}{4}\left(F_{3\,\mu}\cdot F_{3\,\nu} - \frac{1}{6}g_{\mu\nu}F_3^2\right) + \frac{X^{-2}}{2}\left(F_{2\,\mu}\cdot F_{2\,\nu} - \frac{1}{8}g_{\mu\nu}F_2^2\right) + \frac{X^{-2}}{2\tilde{g}^2}\left(F^i_{2\,\mu}\cdot F^i_{2\,\nu} - \frac{1}{8}g_{\mu\nu}(F_2^i)^2\right), \tag{F.1.10}$$

Here, $F_\mu = \iota_\mu F$ is representing the contraction with the vector ∂_μ, $F\cdot G = F_{\mu_1\ldots\mu_p}G^{\mu_1\ldots\mu_p}$, where $F^2 = F\cdot F$.

By setting all matter fields to zero as ($A_2 = A_1 = A^i = 0$) and $X = 1$, we obtain a simple solution. In this case, the metric corresponds to AdS_6 with a radius of $R^2 = \frac{2}{9}\tilde{g}^2$ preserving eight Poincaré supercharges.

We will now explain a particular solution within this six-dimensional framework.

F.1.2 The background in 6d Romans Supergravity

We consider a solution that has a non-trivial background metric, equipped with only one of the components of the $SU(2)$ gauge fields, $F_2^{(3)}$, and a dilaton [322],

$$\begin{aligned} ds_6^2 &= -H(r)^{-3/2}f(r)\,dt^2 + H^{1/2}\left(f(r)^{-1}\,dr^2 + r^2\,d\vec{x}_4^2\right), \\ \phi &= \tfrac{1}{\sqrt{2}}\log H(r)\,, \quad A_1^3 = \sqrt{2}(1 - H(r)^{-1})\,\frac{\sqrt{\mu}}{c}\,dt\,, \\ f(r) &= -\frac{\mu}{r^3} + \tfrac{2}{9}g^2\,r^2\,H(r)^2\,, \qquad H(r) = 1 + \frac{c^2}{r^3}\,, \end{aligned}$$

with the dilaton, ϕ, and X field related by $X = e^{-\frac{1}{2\sqrt{2}}\phi}$. Two free parameters, μ and c, appear in the solution.

F.1.3 Double Wick rotation

By applying a double wick rotation for the coordinates $t \to i\phi$, $\phi \to it$ and also analyticly continuing the c parameter we obtain our new solution:

$$\begin{aligned} ds_6^2 &= H^{1/2}\left(f(r)^{-1}\,dr^2 + r^2\left(-dt^2 + dx_1^2 + dx_2^2 + dx_3^2\right)\right) + H(r)^{-3/2}\,f(r)\,d\phi^2\,, \qquad \text{(F.1.11)} \\ \phi &= \tfrac{1}{\sqrt{2}}\log H(r)\,, \quad A_1^3 = \sqrt{2}(1 - H(r)^{-1})\,\frac{\sqrt{\mu}}{c}\,d\phi\,, \\ f(r) &= -\frac{\mu}{r^3} + \tfrac{2}{9}g^2\,r^2\,H(r)^2\,, \qquad H(r) = 1 - \frac{c^2}{r^3}\,. \end{aligned}$$

Because of the presence of the term $H(r)^{-3/2}\,f(r)\,d\phi^2$ in the metric, after compactifying the geometry on the ϕ coordinate, it can shrink to zero radii at the position of the roots of $f(r)$. We take $r^\star$ as the largest positive root of the function $f(r)$ and choose a period for this coordinate to produce a smoothly closing manifold in the (r,ϕ) plane, that is performed in Eq.(6.2.5).

F.1.4 Uplift to Type IIB

Following [259], solutions in 6d Romans supergravity have an uplift to Type IIB supergravity in the form of an infinite family of solutions. Our solution uplifts to a solution in type IIB as,

$$\begin{aligned} ds_{st}^2 &= f_1\left(ds_6^2 + f_2 ds^2(\tilde{S}^2) + f_3 ds^2(R^2)\right) \qquad \text{(F.1.12)} \\ C_0 &= f_7, \quad e^{-2\Phi} = f_6, \qquad F_5 = 4(G_5 + *_{10}G_5), \\ B_2 &= f_4 \mathrm{Vol}(\tilde{S}^2) - \frac{2}{9}\eta y^i F^i\,, \\ C_2 &= f_5 \mathrm{Vol}(\tilde{S}^2) - 4\partial_\sigma(\sigma V) y^i F^i\,. \end{aligned}$$

Where ds_6^2 is given by the six-dimensional gauged supergravity solution as

$$ds_6^2 = \frac{2\tilde{g}^2}{9} ds^2_{\text{gauged sugra.}} \qquad \text{(F.1.13)}$$

The functions f_i are defined as:

$$f_1 = \frac{2}{3X^2}\left(\sigma^2 + \frac{3X^4\sigma\partial_\sigma V}{\partial_\eta^2 V}\right)^{1/2}, \qquad f_2 = \frac{X^2\partial_\sigma V\partial_\eta^2 V}{3\Lambda}, \qquad f_3 = \frac{X^2\partial_\eta^2 V}{3\sigma\partial_\sigma V} \tag{F.1.14}$$
$$f_6 = (18)^2\frac{3X^4(\sigma^2\partial_\sigma V)(\partial_\eta^2 V)}{\left(3X^4\partial_\sigma V + \sigma\partial_\eta^2 V\right)^2}\Lambda, \qquad f_7 = 18\left(\partial_\eta V + \frac{3X^4\sigma\partial_\sigma V\partial_{\sigma\eta}^2 V}{3X^4\partial_\sigma V + \sigma\partial_\eta^2 V}\right),$$
$$f_4 = \frac{2}{9}\left(\eta - \frac{\sigma\partial_\sigma V\partial_{\sigma\eta}^2 V}{\Lambda}\right), \qquad f_5 = 4\left(V - \frac{\sigma\partial_\sigma V\left(\partial_\eta V\partial_{\sigma\eta}^2 V - 3X^4\partial_\eta^2 V\partial_\sigma V\right)}{\Lambda}\right),$$
$$\Lambda = 3X^4\partial_\eta^2 V\partial_\sigma V + \sigma\left[\left(\partial_{\eta\sigma}^2 V\right)^2 + \left(\partial_\eta^2 V\right)^2\right].$$

The sphere $\tilde{S}^2$ has fibrations over the 6d spce,

$$\mathrm{Vol}(\tilde{S}^2) = \epsilon^{ijk}y^i Dy^j \wedge Dy^k, \qquad ds_{\tilde{S}^2}^2 = Dy^i Dy^i, \tag{F.1.15}$$

with y^i chosen as an embedding coordinates for the S^2 sphere. For instance, one choice is

$$y^1 = \sin\theta\sin\varphi_1, \qquad y^2 = \sin\theta\cos\varphi_1, \qquad y^3 = -\cos\theta. \tag{F.1.16}$$

The covariant derivative D is

$$DC^i = dC^i + \epsilon_{ijk}A^j \wedge C^k\,, \tag{F.1.17}$$

with G_5 form given as

$$G_5 = -\frac{2}{3X^2}(*_6 F^i) \wedge D(y^i\sigma^2\partial_\sigma V)\,. \tag{F.1.18}$$

The final form of the 10d metric using the Eq. (F.1.15) is

$$ds_{st}^2 = f_1\left(ds_6^2 + f_2(d\theta^2 + \sin\theta^2(d\varphi_1 - A)^2) + f_3(d\sigma^2 + d\eta^2)\right) \tag{F.1.19}$$

The solution in Eq. (6.2.1) is derivable following this procedure.

F.2 Near Boundary Expansions

In this section, we examine the asymptotic expansion of the fields at the boundary $r \to \infty$, aiming to understand the deformations inserted at the UV fixed point of the dual QFT. This analysis is conducted within the framework of 6-dimensional supergravity discussed in the previous section. The quantum field theory data we require includes the operators inserted by the deformations and their corresponding vacuum expectation values. As the metric at the boundary (or the boundary conformal structure) is coupled to the stress-energy tensor of QFT

at the boundary, the VEV of this tensor can be derived from the asymptotic behaviour of the metric and other associated scalar fields. Following the approach outlined in Refs. [42, 43], near the boundary of an asymptotically AdS background, the bulk metric takes the form

$$ds^2 = \frac{1}{r^2}(dr^2 + g_{ij}(x,r)dx^i dx^j), \tag{F.2.1}$$

in the Fefferman-Graham coordinates with the boundary at $r \to 0$. The tensor $g_{ij}(x,r)$ is given as

$$g_{ij}(x,r) = g_{(0)ij} + r g_{(1)ij} + r^2 g_{(2)ij} + \dots, \tag{F.2.2}$$

The coefficients $g_{(k)ij}, k > 0$ are derivable from Einstein's equations. In a new coordinate $\rho = r^2$ we obtain

$$\begin{aligned} ds^2 = G_{\mu\nu}dx^\mu dx^\nu &= \frac{d\rho^2}{4\rho^2} + \frac{1}{\rho}g_{ij}(x,\rho)dx^i dx^j, \\ g(x,\rho) &= g_{(0)} + \cdots + \rho^{d/2}g_{(d)} + h_{(d)}\rho^{d/2}\ln\rho + \dots. \end{aligned} \tag{F.2.3}$$

The asymptotic expansion of different fields in the background near the boundary, has a form as

$$\mathcal{F}(x,\rho) = \rho^m \left(f_{(0)}(x) + f_{(2)}(x)\rho + \cdots + \rho^n (f_{(2n)}(x) + \log\rho \tilde{f}_{(2n)}(x)) + \dots\right). \tag{F.2.4}$$

In ρ coordinate, the equations of motion are of second-order differential equation form, indicating the presence of two independent solutions. These solutions asymptotically behave as ρ^m and ρ^{m+n}. In the holographic context, the boundary field, $f_{(0)}$, that scales with ρ^m is interpreted as the source for the corresponding operator in the dual field theory. Conversely, the coefficient, $f_{(2n)}$, associated with ρ^{m+n} represents the 1-point function of this operator.

Since our boundary is five-dimensional, we apply the holographic renormalisation procedure outlined in Ref. [42]. This approach enables us to calculate the expectation value of the stress-energy tensor at the boundary, which, after completing holographic renormalisation, is expressed as

$$\langle T_{ij} \rangle = 5l^4 g_{(5)ij}, \tag{F.2.5}$$

with l representing the AdS radius and the cosmological constant given as $\Lambda = -\frac{10}{l^2}$ in terms of l. We choose to set $16\pi G_N \equiv 1$ in this expression.

The metric of Eq. (F.1.11) does not have the Fefferman-Graham form in Eq. (F.2.1). Hence, some coordinate changes follow. Initially, $r \to 1/z$ is performed that takes the boundary

from $r \to \infty$ to $z \to 0$,

$$ds_6^2 = H(z)^{1/2}\left(\frac{1}{f(z)z^4}\,dz^2 + \frac{1}{z^2}\left(-dt^2 + dx_1^2 + dx_2^2 + dx_3^2\right)\right) + H(z)^{-3/2} f(z)\, d\phi^2\,. \tag{F.2.6}$$

Now, using the expansion of the metric near $z \to 0$, we perform a coordinate transformation as $z \to \bar{r}(z)$, which brings the metric to the required form, up to the necessary order in the asymptotic expansion. The coordinate transformation along with its inverse are ($\tilde{g} = \sqrt{\frac{9}{2}}$ is chosen for simplicity)

$$\bar{r}(z) = z + \tfrac{c^2 z^4}{4} + \tfrac{\mu z^6}{10} + O\left(z^7\right), \tag{F.2.7}$$

$$z(\bar{r}) = \bar{r} - \tfrac{c^2 \bar{r}^4}{4} + \tfrac{\mu \bar{r}^6}{10} + O\left(\bar{r}^7\right). \tag{F.2.8}$$

Elements of the metric in the new coordinate system take the asymptotic form as

$$g_{tt}(\bar{r}) = -\tfrac{1}{\bar{r}^2} - \tfrac{\mu \bar{r}^3}{5} + O\left(\bar{r}^4\right), \tag{F.2.9}$$

$$g_{x_i x_i}(\bar{r}) = \tfrac{1}{\bar{r}^2} + \tfrac{\mu \bar{r}^3}{5} + O\left(\bar{r}^4\right), \tag{F.2.10}$$

$$g_{\phi\phi}(\bar{r}) = \tfrac{1}{\bar{r}^2} - \tfrac{4\mu \bar{r}^3}{5} + O\left(\bar{r}^4\right). \tag{F.2.11}$$

Thus, we can find the expectation values of the stress-energy tensor at the boundary from Eq. (F.2.5),

$$\langle T_{tt}\rangle = -\mu, \quad \langle T_{x_i x_i}\rangle = \mu, \quad \langle T_{\phi\phi}\rangle = 4\mu. \tag{F.2.12}$$

The asymptotic expansion for X and $A_1^{(3)}$ reads

$$X(\bar{r}) - 1 = c_2 \bar{r}^2 + c_3 \bar{r}^3 - 11 c_2^2/2 \bar{r}^4 + 1/2(c^2 c_2 - 6 c_2 c_3)\bar{r}^5 + O\left(\bar{r}^6\right), \tag{F.2.13}$$

$$A_1^{(3)}(\bar{r}) = a_0 + a_3 \bar{r}^3 + O\left(\bar{r}^6\right). \tag{F.2.14}$$

Comparison to the expansion for our solution in Eq. (F.1.11)

$$X(\bar{r}) - 1 = \tfrac{c^2}{4}\bar{r}^3 + O\left(\bar{r}^6\right), \tag{F.2.15}$$

$$A_1^{(3)}(\bar{r}) = -3c\sqrt{\mu}\bar{r}^3 + O\left(\bar{r}^6\right), \tag{F.2.16}$$

shows that the subleading terms in the expansions are present in the background, leading to

$$\langle J\rangle = -3c\sqrt{\mu}, \quad \langle \mathcal{O}_X\rangle = \frac{c^2}{4}. \tag{F.2.17}$$

We realise that X corresponds to the presence of a dimension three operator with the given VEV and $A_1^{(3)}$ leads to a global R-symmetry background current inserted to the boundary.

The latter is interpreted as a Wilson loop insertion to the dual QFT.

Bibliography

[1] S. Weinberg, *The Quantum theory of fields. Vol. 1: Foundations*. Cambridge University Press, 6, 2005.

[2] J. M. Maldacena, *The Large N limit of superconformal field theories and supergravity*, *Adv. Theor. Math. Phys.* **2** (1998) 231–252, [hep-th/9711200].

[3] E. Witten, *Anti-de Sitter space and holography*, *Adv. Theor. Math. Phys.* **2** (1998) 253–291, [hep-th/9802150].

[4] S. S. Gubser, I. R. Klebanov, and A. M. Polyakov, *Gauge theory correlators from noncritical string theory*, *Phys. Lett. B* **428** (1998) 105–114, [hep-th/9802109].

[5] D. Elander, A. Fatemiabhari, and M. Piai, *Phase transitions and light scalars in bottom-up holography*, *Phys. Rev. D* **108** (2023), no. 1 015021, [arXiv:2212.07954].

[6] D. Elander, A. Fatemiabhari, and M. Piai, *Toward minimal composite Higgs models from regular geometries in bottom-up holography*, *Phys. Rev. D* **107** (2023), no. 11 115021, [arXiv:2303.00541].

[7] D. Elander, A. Fatemiabhari, and M. Piai, *On Holographic Vacuum Misalignment*, arXiv:2405.08714.

[8] A. Fatemiabhari and C. Nunez, *From conformal to confining field theories using holography*, *JHEP* **03** (2024) 160, [arXiv:2401.04158].

[9] D. Chatzis, A. Fatemiabhari, C. Nunez, and P. Weck, *SCFT deformations via uplifted solitons*, arXiv:2406.01685.

[10] D. Chatzis, A. Fatemiabhari, C. Nunez, and P. Weck, *Conformal to confining SQFTs from holography*, arXiv:2405.05563.

[11] A. A. Migdal and M. A. Shifman, *Dilaton Effective Lagrangian in Gluodynamics*, *Phys. Lett. B* **114** (1982) 445–449.

[12] S. Coleman, *Aspects of Symmetry: Selected Erice Lectures*. Cambridge University Press, Cambridge, U.K., 1985.

[13] **LatKMI** Collaboration, Y. Aoki et al., *Light composite scalar in eight-flavor QCD on the lattice*, *Phys. Rev. D* **89** (2014) 111502, [arXiv:1403.5000].

[14] T. Appelquist et al., *Strongly interacting dynamics and the search for new physics at the LHC*, *Phys. Rev. D* **93** (2016), no. 11 114514, [arXiv:1601.04027].

[15] **LatKMI** Collaboration, Y. Aoki et al., *Light flavor-singlet scalars and walking signals in $N_f = 8$ QCD on the lattice*, *Phys. Rev. D* **96** (2017), no. 1 014508, [arXiv:1610.07011].

[16] A. D. Gasbarro and G. T. Fleming, *Examining the Low Energy Dynamics of Walking Gauge Theory*, *PoS* **LATTICE2016** (2017) 242, [arXiv:1702.00480].

[17] **Lattice Strong Dynamics** Collaboration, T. Appelquist et al., *Nonperturbative investigations of SU(3) gauge theory with eight dynamical flavors*, *Phys. Rev. D* **99** (2019), no. 1 014509, [arXiv:1807.08411].

[18] A. Hasenfratz, *Emergent strongly coupled ultraviolet fixed point in four dimensions with eight Kähler-Dirac fermions*, *Phys. Rev. D* **106** (2022), no. 1 014513, [arXiv:2204.04801].

[19] Z. Fodor, K. Holland, J. Kuti, D. Nogradi, C. Schroeder, and C. H. Wong, *Can the nearly conformal sextet gauge model hide the Higgs impostor?*, *Phys. Lett. B* **718** (2012) 657–666, [arXiv:1209.0391].

[20] Z. Fodor, K. Holland, J. Kuti, S. Mondal, D. Nogradi, and C. H. Wong, *Toward the minimal realization of a light composite Higgs*, *PoS* **LATTICE2014** (2015) 244, [arXiv:1502.00028].

[21] Z. Fodor, K. Holland, J. Kuti, S. Mondal, D. Nogradi, and C. H. Wong, *Status of a minimal composite Higgs theory*, *PoS* **LATTICE2015** (2016) 219, [arXiv:1605.08750].

[22] Z. Fodor, K. Holland, J. Kuti, D. Nogradi, and C. H. Wong, *The twelve-flavor β-function and dilaton tests of the sextet scalar*, *EPJ Web Conf.* **175** (2018) 08015, [arXiv:1712.08594].

[23] Z. Fodor, K. Holland, J. Kuti, and C. H. Wong, *Tantalizing dilaton tests from a near-conformal EFT*, *PoS* **LATTICE2018** (2019) 196, [arXiv:1901.06324].

[24] Z. Fodor, K. Holland, J. Kuti, and C. H. Wong, *Dilaton EFT from p-regime to RMT in the ϵ-regime*, *PoS* **LATTICE2019** (2020) 246, [arXiv:2002.05163].

[25] D. B. Kaplan and H. Georgi, *SU(2) x U(1) Breaking by Vacuum Misalignment*, *Phys. Lett. B* **136** (1984) 183–186.

[26] G. Panico and A. Wulzer, *The Composite Nambu-Goldstone Higgs*, vol. 913. Springer, 2016.

[27] O. Witzel, *Review on Composite Higgs Models*, *PoS* **LATTICE2018** (2019) 006, [arXiv:1901.08216].

[28] G. Cacciapaglia, C. Pica, and F. Sannino, *Fundamental Composite Dynamics: A Review*, *Phys. Rept.* **877** (2020) 1–70, [arXiv:2002.04914].

[29] G. Ferretti and D. Karateev, *Fermionic UV completions of Composite Higgs models*, *JHEP* **03** (2014) 077, [arXiv:1312.5330].

[30] G. Ferretti, *Gauge theories of Partial Compositeness: Scenarios for Run-II of the LHC*, *JHEP* **06** (2016) 107, [arXiv:1604.06467].

[31] G. Cacciapaglia, G. Ferretti, T. Flacke, and H. Serôdio, *Light scalars in composite Higgs models*, *Front. in Phys.* **7** (2019) 22, [arXiv:1902.06890].

[32] E. Witten, *Anti-de Sitter space, thermal phase transition, and confinement in gauge theories*, *Adv. Theor. Math. Phys.* **2** (1998) 505–532, [hep-th/9803131].

[33] J. R. Ronald, *Entanglement and Excitations in Gauge/Gravity Duality*. PhD thesis, Southampton U., 2019. arXiv:1912.09782.

[34] K. Becker, M. Becker, and J. H. Schwarz, *String theory and M-theory: A modern introduction*. Cambridge University Press, 12, 2006.

[35] D. Z. Freedman and A. Van Proeyen, *Supergravity*. Cambridge Univ. Press, Cambridge, UK, 5, 2012.

[36] M. Ammon and J. Erdmenger, *Gauge/gravity duality: Foundations and applications*. Cambridge University Press, Cambridge, 4, 2015.

[37] O. Aharony, S. S. Gubser, J. M. Maldacena, H. Ooguri, and Y. Oz, *Large N field theories, string theory and gravity*, *Phys. Rept.* **323** (2000) 183–386, [hep-th/9905111].

[38] J. Polchinski, *String theory. Vol. 2: Superstring theory and beyond*. Cambridge Monographs on Mathematical Physics. Cambridge University Press, 12, 2007.

[39] E. Witten, *String theory dynamics in various dimensions*, *Nucl. Phys. B* **443** (1995) 85–126, [hep-th/9503124].

[40] M. J. Duff and J. X. Lu, *The Selfdual type IIB superthreebrane*, *Phys. Lett. B* **273** (1991) 409–414.

[41] C. Fefferman and C. R. Graham, *Conformal invariants*, in *Élie Cartan et les mathématiques d'aujourd'hui - Lyon, 25-29 juin 1984*, no. S131 in Astérisque, pp. 95–116. Société mathématique de France, 1985.

[42] S. de Haro, S. N. Solodukhin, and K. Skenderis, *Holographic reconstruction of space-time and renormalization in the AdS / CFT correspondence*, *Commun. Math. Phys.* **217** (2001) 595–622, [hep-th/0002230].

[43] K. Skenderis, *Lecture notes on holographic renormalization*, *Class. Quant. Grav.* **19** (2002) 5849–5876, [hep-th/0209067].

[44] I. Papadimitriou and K. Skenderis, *AdS / CFT correspondence and geometry*, *IRMA Lect. Math. Theor. Phys.* **8** (2005) 73–101, [hep-th/0404176].

[45] I. Papadimitriou and K. Skenderis, *Correlation functions in holographic RG flows*, *JHEP* **10** (2004) 075, [hep-th/0407071].

[46] I. R. Klebanov and E. Witten, *AdS / CFT correspondence and symmetry breaking*, *Nucl. Phys. B* **556** (1999) 89–114, [hep-th/9905104].

[47] P. Breitenlohner and D. Z. Freedman, *Positive Energy in anti-De Sitter Backgrounds and Gauged Extended Supergravity*, *Phys. Lett. B* **115** (1982) 197–201.

[48] P. Breitenlohner and D. Z. Freedman, *Stability in Gauged Extended Supergravity*, *Annals Phys.* **144** (1982) 249.

[49] M. L. Bellac, *Thermal Field Theory*. Cambridge Monographs on Mathematical Physics. Cambridge University Press, 3, 2011.

[50] J. I. Kapusta and C. Gale, *Finite-temperature field theory: Principles and applications*. Cambridge Monographs on Mathematical Physics. Cambridge University Press, 2011.

[51] D. T. Son and A. O. Starinets, *Minkowski space correlators in AdS / CFT correspondence: Recipe and applications*, *JHEP* **09** (2002) 042, [hep-th/0205051].

[52] P. K. Kovtun and A. O. Starinets, *Quasinormal modes and holography*, *Phys. Rev. D* **72** (2005) 086009, [hep-th/0506184].

[53] C. P. Herzog and D. T. Son, *Schwinger-Keldysh propagators from AdS/CFT correspondence*, *JHEP* **03** (2003) 046, [hep-th/0212072].

[54] M. Kaminski, K. Landsteiner, J. Mas, J. P. Shock, and J. Tarrio, *Holographic Operator Mixing and Quasinormal Modes on the Brane*, *JHEP* **02** (2010) 021, [arXiv:0911.3610].

[55] G. 't Hooft, *Naturalness, chiral symmetry, and spontaneous chiral symmetry breaking*, *NATO Sci. Ser. B* **59** (1980) 135–157.

[56] S. Dimopoulos and L. Susskind, *Mass Without Scalars*, *Nucl. Phys. B* **155** (1979) 237–252.

[57] H. Terazawa, Y. Chikashige, and K. Akama, *Unified model of the nambu-jona-lasinio type for all elementary-particle forces*, *Phys. Rev. D* **15** (Jan, 1977) 480–487.

[58] W. D. Goldberger, B. Grinstein, and W. Skiba, *Distinguishing the Higgs boson from the dilaton at the Large Hadron Collider*, *Phys. Rev. Lett.* **100** (2008) 111802, [arXiv:0708.1463].

[59] C. N. Leung, S. T. Love, and W. A. Bardeen, *Spontaneous Symmetry Breaking in Scale Invariant Quantum Electrodynamics*, *Nucl. Phys. B* **273** (1986) 649–662.

[60] W. A. Bardeen, C. N. Leung, and S. T. Love, *The Dilaton and Chiral Symmetry Breaking*, *Phys. Rev. Lett.* **56** (1986) 1230.

[61] K. Yamawaki, M. Bando, and K.-i. Matumoto, *Scale Invariant Technicolor Model and a Technidilaton*, *Phys. Rev. Lett.* **56** (1986) 1335.

[62] D. K. Hong, S. D. H. Hsu, and F. Sannino, *Composite Higgs from higher representations*, *Phys. Lett. B* **597** (2004) 89–93, [hep-ph/0406200].

[63] D. D. Dietrich, F. Sannino, and K. Tuominen, *Light composite Higgs from higher representations versus electroweak precision measurements: Predictions for CERN LHC*, *Phys. Rev. D* **72** (2005) 055001, [hep-ph/0505059].

[64] M. Hashimoto and K. Yamawaki, *Techni-dilaton at Conformal Edge*, *Phys. Rev. D* **83** (2011) 015008, [arXiv:1009.5482].

[65] T. Appelquist and Y. Bai, *A Light Dilaton in Walking Gauge Theories*, *Phys. Rev. D* **82** (2010) 071701, [arXiv:1006.4375].

[66] L. Vecchi, *Phenomenology of a light scalar: the dilaton*, *Phys. Rev. D* **82** (2010) 076009, [arXiv:1002.1721].

[67] Z. Chacko and R. K. Mishra, *Effective Theory of a Light Dilaton*, *Phys. Rev. D* **87** (2013), no. 11 115006, [arXiv:1209.3022].

[68] B. Bellazzini, C. Csaki, J. Hubisz, J. Serra, and J. Terning, *A Higgslike Dilaton*, *Eur. Phys. J. C* **73** (2013), no. 2 2333, [arXiv:1209.3299].

[69] B. Bellazzini, C. Csaki, J. Hubisz, J. Serra, and J. Terning, *A Naturally Light Dilaton and a Small Cosmological Constant*, *Eur. Phys. J. C* **74** (2014) 2790, [arXiv:1305.3919].

[70] T. Abe, R. Kitano, Y. Konishi, K.-y. Oda, J. Sato, and S. Sugiyama, *Minimal Dilaton Model*, *Phys. Rev. D* **86** (2012) 115016, [arXiv:1209.4544].

[71] E. Eichten, K. Lane, and A. Martin, *A Higgs Impostor in Low-Scale Technicolor*, arXiv:1210.5462.

[72] P. Hernandez-Leon and L. Merlo, *Distinguishing A Higgs-Like Dilaton Scenario With A Complete Bosonic Effective Field Theory Basis*, *Phys. Rev. D* **96** (2017), no. 7 075008, [arXiv:1703.02064].

[73] S. Matsuzaki and K. Yamawaki, *Dilaton Chiral Perturbation Theory: Determining the Mass and Decay Constant of the Technidilaton on the Lattice*, *Phys. Rev. Lett.* **113** (2014), no. 8 082002, [arXiv:1311.3784].

[74] M. Golterman and Y. Shamir, *Low-energy effective action for pions and a dilatonic meson*, *Phys. Rev. D* **94** (2016), no. 5 054502, [arXiv:1603.04575].

[75] A. Kasai, K.-i. Okumura, and H. Suzuki, *A dilaton-pion mass relation*, arXiv:1609.02264.

[76] M. Hansen, K. Langæble, and F. Sannino, *Extending Chiral Perturbation Theory with an Isosinglet Scalar*, *Phys. Rev. D* **95** (2017), no. 3 036005, [arXiv:1610.02904].

[77] M. Golterman and Y. Shamir, *Effective pion mass term and the trace anomaly*, *Phys. Rev. D* **95** (2017), no. 1 016003, [arXiv:1611.04275].

[78] T. Appelquist, J. Ingoldby, and M. Piai, *Dilaton EFT Framework For Lattice Data*, *JHEP* **07** (2017) 035, [arXiv:1702.04410].

[79] T. Appelquist, J. Ingoldby, and M. Piai, *Analysis of a Dilaton EFT for Lattice Data*, *JHEP* **03** (2018) 039, [arXiv:1711.00067].

[80] M. Golterman and Y. Shamir, *Large-mass regime of the dilaton-pion low-energy effective theory*, *Phys. Rev. D* **98** (2018), no. 5 056025, [arXiv:1805.00198].

[81] O. Catà and C. Müller, *Chiral effective theories with a light scalar at one loop*, *Nucl. Phys. B* **952** (2020) 114938, [arXiv:1906.01879].

[82] T. Appelquist, J. Ingoldby, and M. Piai, *Dilaton potential and lattice data*, *Phys. Rev. D* **101** (2020), no. 7 075025, [arXiv:1908.00895].

[83] O. Catà, R. J. Crewther, and L. C. Tunstall, *Crawling technicolor*, *Phys. Rev. D* **100** (2019), no. 9 095007, [arXiv:1803.08513].

[84] M. Golterman, E. T. Neil, and Y. Shamir, *Application of dilaton chiral perturbation theory to $N_f = 8$, SU(3) spectral data*, *Phys. Rev. D* **102** (2020), no. 3 034515, [arXiv:2003.00114].

[85] M. Golterman and Y. Shamir, *Explorations beyond dilaton chiral perturbation theory in the eight-flavor SU(3) gauge theory*, *Phys. Rev. D* **102** (2020) 114507, [arXiv:2009.13846].

[86] **Lattice Strong Dynamics (LSD)** Collaboration, T. Appelquist et al., *Goldstone boson scattering with a light composite scalar*, *Phys. Rev. D* **105** (2022), no. 3 034505, [arXiv:2106.13534].

[87] T. Appelquist, J. Ingoldby, and M. Piai, *Nearly Conformal Composite Higgs Model*, *Phys. Rev. Lett.* **126** (2021), no. 19 191804, [arXiv:2012.09698].

[88] T. Appelquist, J. Ingoldby, and M. Piai, *Composite two-Higgs doublet model from dilaton effective field theory*, *Nucl. Phys. B* **983** (2022) 115930, [arXiv:2205.03320].

[89] T. Appelquist, J. Ingoldby, and M. Piai, *Dilaton Effective Field Theory*, *Universe* **9** (2023), no. 1 10, [arXiv:2209.14867].

[90] W. D. Goldberger and M. B. Wise, *Modulus stabilization with bulk fields*, *Phys. Rev. Lett.* **83** (1999) 4922–4925, [hep-ph/9907447].

[91] O. DeWolfe, D. Z. Freedman, S. S. Gubser, and A. Karch, *Modeling the fifth-dimension with scalars and gravity*, *Phys. Rev. D* **62** (2000) 046008, [hep-th/9909134].

[92] W. D. Goldberger and M. B. Wise, *Phenomenology of a stabilized modulus*, *Phys. Lett. B* **475** (2000) 275–279, [hep-ph/9911457].

[93] C. Csaki, M. L. Graesser, and G. D. Kribs, *Radion dynamics and electroweak physics*, *Phys. Rev. D* **63** (2001) 065002, [hep-th/0008151].

[94] N. Arkani-Hamed, M. Porrati, and L. Randall, *Holography and phenomenology*, *JHEP* **08** (2001) 017, [hep-th/0012148].

[95] R. Rattazzi and A. Zaffaroni, *Comments on the holographic picture of the Randall-Sundrum model*, *JHEP* **04** (2001) 021, [hep-th/0012248].

[96] L. Kofman, J. Martin, and M. Peloso, *Exact identification of the radion and its coupling to the observable sector*, *Phys. Rev. D* **70** (2004) 085015, [hep-ph/0401189].

[97] D. Elander and M. Piai, *A composite light scalar, electro-weak symmetry breaking and the recent LHC searches*, *Nucl. Phys. B* **864** (2012) 241–259, [arXiv:1112.2915].

[98] D. Kutasov, J. Lin, and A. Parnachev, *Holographic Walking from Tachyon DBI*, *Nucl. Phys. B* **863** (2012) 361–397, [arXiv:1201.4123].

[99] R. Lawrance and M. Piai, *Holographic Technidilaton and LHC searches*, *Int. J. Mod. Phys. A* **28** (2013) 1350081, [arXiv:1207.0427].

[100] D. Elander and M. Piai, *The decay constant of the holographic techni-dilaton and the 125 GeV boson*, *Nucl. Phys. B* **867** (2013) 779–809, [arXiv:1208.0546].

[101] M. Goykhman and A. Parnachev, *S-parameter, Technimesons, and Phase Transitions in Holographic Tachyon DBI Models*, *Phys. Rev. D* **87** (2013), no. 2 026007, [arXiv:1211.0482].

[102] N. Evans and K. Tuominen, *Holographic modelling of a light technidilaton*, *Phys. Rev. D* **87** (2013), no. 8 086003, [arXiv:1302.4553].

[103] E. Megias and O. Pujolas, *Naturally light dilatons from nearly marginal deformations*, *JHEP* **08** (2014) 081, [arXiv:1401.4998].

[104] D. Elander, R. Lawrance, and M. Piai, *Hyperscaling violation and Electroweak Symmetry Breaking*, *Nucl. Phys. B* **897** (2015) 583–611, [arXiv:1504.07949].

[105] T. Alho, N. Evans, and K. Tuominen, *Dynamic AdS/QCD and the Spectrum of Walking Gauge Theories*, *Phys. Rev. D* **88** (2013) 105016, [arXiv:1307.4896].

[106] N. Evans, P. Jones, and M. Scott, *Soft walls in dynamic AdS/QCD and the technidilaton*, *Phys. Rev. D* **92** (2015), no. 10 106003, [arXiv:1508.06540].

[107] D. Elander, C. Nunez, and M. Piai, *A Light scalar from walking solutions in gauge-string duality*, *Phys. Lett. B* **686** (2010) 64–67, [arXiv:0908.2808].

[108] D. Elander and M. Piai, *On the glueball spectrum of walking backgrounds from wrapped-D5 gravity duals*, *Nucl. Phys. B* **871** (2013) 164–180, [arXiv:1212.2600].

[109] D. Elander, *Light scalar from deformations of the Klebanov-Strassler background*, *Phys. Rev. D* **91** (2015), no. 12 126012, [arXiv:1401.3412].

[110] D. Elander and M. Piai, *Calculable mass hierarchies and a light dilaton from gravity duals*, *Phys. Lett. B* **772** (2017) 110–114, [arXiv:1703.09205].

[111] D. Elander and M. Piai, *Glueballs on the Baryonic Branch of Klebanov-Strassler: dimensional deconstruction and a light scalar particle*, *JHEP* **06** (2017) 003, [arXiv:1703.10158].

[112] T. Sakai and S. Sugimoto, *Low energy hadron physics in holographic QCD*, *Prog. Theor. Phys.* **113** (2005) 843–882, [hep-th/0412141].

[113] T. Sakai and S. Sugimoto, *More on a holographic dual of QCD*, *Prog. Theor. Phys.* **114** (2005) 1083–1118, [hep-th/0507073].

[114] R. C. Brower, S. D. Mathur, and C.-I. Tan, *Glueball spectrum for QCD from AdS supergravity duality*, *Nucl. Phys. B* **587** (2000) 249–276, [hep-th/0003115].

[115] C.-K. Wen and H.-X. Yang, *QCD(4) glueball masses from AdS(6) black hole description*, *Mod. Phys. Lett. A* **20** (2005) 997–1004, [hep-th/0404152].

[116] S. Kuperstein and J. Sonnenschein, *Non-critical, near extremal AdS(6) background as a holographic laboratory of four dimensional YM theory*, *JHEP* **11** (2004) 026, [hep-th/0411009].

[117] D. Elander, A. F. Faedo, C. Hoyos, D. Mateos, and M. Piai, *Multiscale confining dynamics from holographic RG flows*, *JHEP* **05** (2014) 003, [arXiv:1312.7160].

[118] D. Elander, M. Piai, and J. Roughley, *Holographic glueballs from the circle reduction of Romans supergravity*, *JHEP* **02** (2019) 101, [arXiv:1811.01010].

[119] M. Bianchi, M. Prisco, and W. Mueck, *New results on holographic three point functions*, *JHEP* **11** (2003) 052, [hep-th/0310129].

[120] M. Berg, M. Haack, and W. Mueck, *Bulk dynamics in confining gauge theories*, *Nucl. Phys. B* **736** (2006) 82–132, [hep-th/0507285].

[121] M. Berg, M. Haack, and W. Mueck, *Glueballs vs. Gluinoballs: Fluctuation Spectra in Non-AdS/Non-CFT*, *Nucl. Phys. B* **789** (2008) 1–44, [hep-th/0612224].

[122] D. Elander, *Glueball Spectra of SQCD-like Theories*, *JHEP* **03** (2010) 114, [arXiv:0912.1600].

[123] D. Elander and M. Piai, *Light scalars from a compact fifth dimension*, *JHEP* **01** (2011) 026, [arXiv:1010.1964].

[124] D. Elander, M. Piai, and J. Roughley, *Probing the holographic dilaton*, *JHEP* **06** (2020) 177, [arXiv:2004.05656]. [Erratum: JHEP 12, 109 (2020)].

[125] R. Apreda, D. E. Crooks, N. J. Evans, and M. Petrini, *Confinement, glueballs and strings from deformed AdS*, *JHEP* **05** (2004) 065, [hep-th/0308006].

[126] D. B. Kaplan, J.-W. Lee, D. T. Son, and M. A. Stephanov, *Conformality Lost*, *Phys. Rev. D* **80** (2009) 125005, [arXiv:0905.4752].

[127] V. Gorbenko, S. Rychkov, and B. Zan, *Walking, Weak first-order transitions, and Complex CFTs*, *JHEP* **10** (2018) 108, [arXiv:1807.11512].

[128] V. Gorbenko, S. Rychkov, and B. Zan, *Walking, Weak first-order transitions, and Complex CFTs II. Two-dimensional Potts model at $Q > 4$*, *SciPost Phys.* **5** (2018), no. 5 050, [arXiv:1808.04380].

[129] A. Pomarol, O. Pujolas, and L. Salas, *Holographic conformal transition and light scalars*, *JHEP* **10** (2019) 202, [arXiv:1905.02653].

[130] J. Cruz Rojas, D. K. Hong, S. H. Im, and M. Järvinen, *Holographic light dilaton at the conformal edge*, *JHEP* **05** (2023) 204, [arXiv:2302.08112].

[131] D. Elander, M. Piai, and J. Roughley, *Dilatonic states near holographic phase transitions*, *Phys. Rev. D* **103** (2021) 106018, [arXiv:2010.04100].

[132] D. Elander, M. Piai, and J. Roughley, *Light dilaton in a metastable vacuum*, *Phys. Rev. D* **103** (2021), no. 4 046009, [arXiv:2011.07049].

[133] D. Elander, M. Piai, and J. Roughley, *Coulomb branch of N=4 SYM and dilatonic scions in supergravity*, *Phys. Rev. D* **104** (2021), no. 4 046003, [arXiv:2103.06721].

[134] L. Randall and R. Sundrum, *A Large mass hierarchy from a small extra dimension*, *Phys. Rev. Lett.* **83** (1999) 3370–3373, [hep-ph/9905221].

[135] L. Randall and R. Sundrum, *An Alternative to compactification*, *Phys. Rev. Lett.* **83** (1999) 4690–4693, [hep-th/9906064].

[136] M. A. Luty, M. Porrati, and R. Rattazzi, *Strong interactions and stability in the DGP model*, *JHEP* **09** (2003) 029, [hep-th/0303116].

[137] R. C. Brower, A. Hasenfratz, C. Rebbi, E. Weinberg, and O. Witzel, *Composite Higgs model at a conformal fixed point*, *Phys. Rev. D* **93** (2016), no. 7 075028, [arXiv:1512.02576].

[138] F. Coradeschi, P. Lodone, D. Pappadopulo, R. Rattazzi, and L. Vitale, *A naturally light dilaton*, *JHEP* **11** (2013) 057, [arXiv:1306.4601].

[139] R. Zwicky, *QCD with an Infrared Fixed Point and a Dilaton*, arXiv:2312.13761.

[140] R. Zwicky, *QCD with an infrared fixed point: The pion sector*, *Phys. Rev. D* **109** (2024), no. 3 034009, [arXiv:2306.06752].

[141] R. Zwicky, *The Dilaton Improves Goldstones*, arXiv:2306.12914.

[142] D. Z. Freedman, C. Nunez, M. Schnabl, and K. Skenderis, *Fake supergravity and domain wall stability*, *Phys. Rev. D* **69** (2004) 104027, [hep-th/0312055].

[143] S.-J. Rey and J.-T. Yee, *Macroscopic strings as heavy quarks in large N gauge theory and anti-de Sitter supergravity*, *Eur. Phys. J. C* **22** (2001) 379–394, [hep-th/9803001].

[144] J. M. Maldacena, *Wilson loops in large N field theories*, *Phys. Rev. Lett.* **80** (1998) 4859–4862, [hep-th/9803002].

[145] Y. Kinar, E. Schreiber, and J. Sonnenschein, *Q anti-Q potential from strings in curved space-time: Classical results*, *Nucl. Phys. B* **566** (2000) 103–125, [hep-th/9811192].

[146] A. Brandhuber and K. Sfetsos, *Wilson loops from multicenter and rotating branes, mass gaps and phase structure in gauge theories*, *Adv. Theor. Math. Phys.* **3** (1999) 851–887, [hep-th/9906201].

[147] S. D. Avramis, K. Sfetsos, and K. Siampos, *Stability of strings dual to flux tubes between static quarks in $N = 4$ SYM*, *Nucl. Phys. B* **769** (2007) 44–78, [hep-th/0612139].

[148] C. Nunez, M. Piai, and A. Rago, *Wilson Loops in string duals of Walking and Flavored Systems*, *Phys. Rev. D* **81** (2010) 086001, [arXiv:0909.0748].

[149] S. S. Gubser, *Curvature singularities: The Good, the bad, and the naked*, *Adv. Theor. Math. Phys.* **4** (2000) 679–745, [hep-th/0002160].

[150] M. Bianchi, D. Z. Freedman, and K. Skenderis, *Holographic renormalization*, *Nucl. Phys. B* **631** (2002) 159–194, [hep-th/0112119].

[151] C. Csaki, J. Erlich, T. J. Hollowood, and J. Terning, *Holographic RG and cosmology in theories with quasilocalized gravity*, *Phys. Rev. D* **63** (2001) 065019, [hep-th/0003076].

[152] N. Bobev, H. Elvang, D. Z. Freedman, and S. S. Pufu, *Holography for $N = 2^*$ on S^4*, *JHEP* **07** (2014) 001, [arXiv:1311.1508].

[153] I. R. Klebanov and M. J. Strassler, *Supergravity and a confining gauge theory: Duality cascades and chi SB resolution of naked singularities*, *JHEP* **08** (2000) 052, [hep-th/0007191].

[154] J. M. Maldacena and C. Nunez, *Towards the large N limit of pure N=1 superYang-Mills*, *Phys. Rev. Lett.* **86** (2001) 588–591, [hep-th/0008001].

[155] A. Butti, M. Grana, R. Minasian, M. Petrini, and A. Zaffaroni, *The Baryonic branch of Klebanov-Strassler solution: A supersymmetric family of SU(3) structure backgrounds*, *JHEP* **03** (2005) 069, [hep-th/0412187].

[156] M. Kruczenski, D. Mateos, R. C. Myers, and D. J. Winters, *Meson spectroscopy in AdS / CFT with flavor*, *JHEP* **07** (2003) 049, [hep-th/0304032].

[157] C. Nunez, A. Paredes, and A. V. Ramallo, *Flavoring the gravity dual of N=1 Yang-Mills with probes*, *JHEP* **12** (2003) 024, [hep-th/0311201].

[158] J. Erdmenger, N. Evans, I. Kirsch, and E. Threlfall, *Mesons in Gauge/Gravity Duals - A Review*, *Eur. Phys. J. A* **35** (2008) 81–133, [arXiv:0711.4467].

[159] A. Karch and E. Katz, *Adding flavor to AdS / CFT*, *JHEP* **06** (2002) 043, [hep-th/0205236].

[160] J. Babington, J. Erdmenger, N. J. Evans, Z. Guralnik, and I. Kirsch, *Chiral symmetry breaking and pions in nonsupersymmetric gauge / gravity duals*, *Phys. Rev. D* **69** (2004) 066007, [hep-th/0306018].

[161] J. Erdmenger, N. Evans, Y. Liu, and W. Porod, *Holographic Non-Abelian Flavour Symmetry Breaking*, *Universe* **9** (2023), no. 6 289, [arXiv:2304.09190].

[162] D. Elander and M. Piai, *Towards top-down holographic composite Higgs: minimal coset from maximal supergravity*, *JHEP* **03** (2022) 049, [arXiv:2110.02945].

[163] R. Contino, Y. Nomura, and A. Pomarol, *Higgs as a holographic pseudoGoldstone boson*, *Nucl. Phys. B* **671** (2003) 148–174, [hep-ph/0306259].

[164] K. Agashe, R. Contino, and A. Pomarol, *The Minimal composite Higgs model*, *Nucl. Phys. B* **719** (2005) 165–187, [hep-ph/0412089].

[165] K. Agashe and R. Contino, *The Minimal composite Higgs model and electroweak precision tests*, *Nucl. Phys. B* **742** (2006) 59–85, [hep-ph/0510164].

[166] K. Agashe, R. Contino, L. Da Rold, and A. Pomarol, *A Custodial symmetry for $Zb\bar{b}$*, *Phys. Lett. B* **641** (2006) 62–66, [hep-ph/0605341].

[167] R. Contino, L. Da Rold, and A. Pomarol, *Light custodians in natural composite Higgs models*, *Phys. Rev. D* **75** (2007) 055014, [hep-ph/0612048].

[168] A. Falkowski and M. Perez-Victoria, *Electroweak Breaking on a Soft Wall*, *JHEP* **12** (2008) 107, [arXiv:0806.1737].

[169] R. Contino, *The Higgs as a Composite Nambu-Goldstone Boson*, in *Theoretical Advanced Study Institute in Elementary Particle Physics: Physics of the Large and the Small*, pp. 235–306, 2011. arXiv:1005.4269.

[170] R. Contino, D. Marzocca, D. Pappadopulo, and R. Rattazzi, *On the effect of resonances in composite Higgs phenomenology*, *JHEP* **10** (2011) 081, [arXiv:1109.1570].

[171] J. Erdmenger, N. Evans, W. Porod, and K. S. Rigatos, *Gauge/gravity dynamics for composite Higgs models and the top mass*, *Phys. Rev. Lett.* **126** (2021), no. 7 071602, [arXiv:2009.10737].

[172] J. Erdmenger, N. Evans, W. Porod, and K. S. Rigatos, *Gauge/gravity dual dynamics for the strongly coupled sector of composite Higgs models*, *JHEP* **02** (2021) 058, [arXiv:2010.10279].

[173] D. Elander, M. Frigerio, M. Knecht, and J.-L. Kneur, *Holographic models of composite Higgs in the Veneziano limit. Part I. Bosonic sector*, *JHEP* **03** (2021) 182, [arXiv:2011.03003].

[174] D. Elander, M. Frigerio, M. Knecht, and J.-L. Kneur, *Holographic models of composite Higgs in the Veneziano limit. Part II. Fermionic sector*, *JHEP* **05** (2022) 066, [arXiv:2112.14740].

[175] E. Ponton, *TASI 2011: Four Lectures on TeV Scale Extra Dimensions*, in *Theoretical Advanced Study Institute in Elementary Particle Physics: The Dark Secrets of the Terascale*, pp. 283–374, 2013. arXiv:1207.3827.

[176] M. E. Peskin, *The Alignment of the Vacuum in Theories of Technicolor*, *Nucl. Phys. B* **175** (1980) 197–233.

[177] D. B. Kaplan, H. Georgi, and S. Dimopoulos, *Composite Higgs Scalars*, *Phys. Lett. B* **136** (1984) 187–190.

[178] M. J. Dugan, H. Georgi, and D. B. Kaplan, *Anatomy of a Composite Higgs Model*, *Nucl. Phys. B* **254** (1985) 299–326.

[179] D. B. Kaplan, *Flavor at SSC energies: A New mechanism for dynamically generated fermion masses*, *Nucl. Phys. B* **365** (1991) 259–278.

[180] Y. Grossman and M. Neubert, *Neutrino masses and mixings in nonfactorizable geometry*, *Phys. Lett. B* **474** (2000) 361–371, [hep-ph/9912408].

[181] T. Gherghetta and A. Pomarol, *Bulk fields and supersymmetry in a slice of AdS*, *Nucl. Phys. B* **586** (2000) 141–162, [hep-ph/0003129].

[182] P. Lodone, *Vector-like quarks in a 'composite' Higgs model*, *JHEP* **12** (2008) 029, [arXiv:0806.1472].

[183] C. Grojean, O. Matsedonskyi, and G. Panico, *Light top partners and precision physics*, *JHEP* **10** (2013) 160, [arXiv:1306.4655].

[184] J. Roughley, *Non-perturbative aspects of gauge theories from gauge-gravity dualities*. PhD thesis, Swansea U., Swansea U., 2021. arXiv:2109.11949.

[185] E. Pomoni and L. Rastelli, *Large N Field Theory and AdS Tachyons*, *JHEP* **04** (2009) 020, [arXiv:0805.2261].

[186] K. Jensen, A. Karch, D. T. Son, and E. G. Thompson, *Holographic Berezinskii-Kosterlitz-Thouless Transitions*, *Phys. Rev. Lett.* **105** (2010) 041601, [arXiv:1002.3159].

[187] D. Kutasov, J. Lin, and A. Parnachev, *Conformal Phase Transitions at Weak and Strong Coupling*, *Nucl. Phys. B* **858** (2012) 155–195, [arXiv:1107.2324].

[188] A. F. Faedo, C. Hoyos, D. Mateos, and J. G. Subils, *Holographic Complex Conformal Field Theories*, *Phys. Rev. Lett.* **124** (2020), no. 16 161601, [arXiv:1909.04008].

[189] A. F. Faedo, C. Hoyos, D. Mateos, and J. G. Subils, *Multiple mass hierarchies from complex fixed point collisions*, *JHEP* **10** (2021) 246, [arXiv:2106.01802].

[190] A. Pomarol and L. Salas, *Exploring the conformal transition from above and below*, arXiv:2312.08332.

[191] A. Karch, E. Katz, D. T. Son, and M. A. Stephanov, *Linear confinement and AdS/QCD*, *Phys. Rev. D* **74** (2006) 015005, [hep-ph/0602229].

[192] B. Batell, T. Gherghetta, and D. Sword, *The Soft-Wall Standard Model*, *Phys. Rev. D* **78** (2008) 116011, [arXiv:0808.3977].

[193] J. C. Collins and J. A. M. Vermaseren, *Axodraw Version 2*, arXiv:1606.01177.

[194] S. Weinberg, *Implications of Dynamical Symmetry Breaking*, *Phys. Rev. D* **13** (1976) 974–996. [Addendum: Phys.Rev.D 19, 1277–1280 (1979)].

[195] L. Susskind, *Dynamics of Spontaneous Symmetry Breaking in the Weinberg-Salam Theory*, *Phys. Rev. D* **20** (1979) 2619–2625.

[196] E. Eichten and K. D. Lane, *Dynamical Breaking of Weak Interaction Symmetries*, *Phys. Lett. B* **90** (1980) 125–130.

[197] B. Holdom, *Techniodor*, *Phys. Lett. B* **150** (1985) 301–305.

[198] T. W. Appelquist, D. Karabali, and L. C. R. Wijewardhana, *Chiral Hierarchies and the Flavor Changing Neutral Current Problem in Technicolor*, *Phys. Rev. Lett.* **57** (1986) 957.

[199] R. S. Chivukula, *Lectures on technicolor and compositeness*, in *Theoretical Advanced Study Institute in Elementary Particle Physics (TASI 2000): Flavor Physics for the Millennium*, pp. 731–772, 6, 2000. hep-ph/0011264.

[200] K. Lane, *Two Lectures on Technicolor*, hep-ph/0202255.

[201] C. T. Hill and E. H. Simmons, *Strong Dynamics and Electroweak Symmetry Breaking*, *Phys. Rept.* **381** (2003) 235–402, [hep-ph/0203079]. [Erratum: Phys.Rept. 390, 553–554 (2004)].

[202] F. Sannino, *Conformal Dynamics for TeV Physics and Cosmology*, *Acta Phys. Polon. B* **40** (2009) 3533–3743, [arXiv:0911.0931].

[203] M. Piai, *Lectures on walking technicolor, holography and gauge/gravity dualities*, *Adv. High Energy Phys.* **2010** (2010) 464302, [arXiv:1004.0176].

[204] A. Banerjee and G. Ferretti, *Vacuum misalignment in presence of four-Fermi operators*, *Phys. Rev. D* **107** (2023), no. 9 095006, [arXiv:2302.11598].

[205] E. Bennett, D. K. Hong, J.-W. Lee, C. J. D. Lin, B. Lucini, M. Piai, and D. Vadacchino, *Sp(4)*

gauge theory on the lattice: towards SU(4)/Sp(4) composite Higgs (and beyond), *JHEP* **03** (2018) 185, [arXiv:1712.04220].

[206] E. Bennett, D. K. Hong, J.-W. Lee, C.-J. D. Lin, B. Lucini, M. Mesiti, M. Piai, J. Rantaharju, and D. Vadacchino, *$Sp(4)$ gauge theories on the lattice: quenched fundamental and antisymmetric fermions*, *Phys. Rev. D* **101** (2020), no. 7 074516, [arXiv:1912.06505].

[207] S. R. Coleman and E. J. Weinberg, *Radiative Corrections as the Origin of Spontaneous Symmetry Breaking*, *Phys. Rev. D* **7** (1973) 1888–1910.

[208] R. L. Arnowitt, S. Deser, and C. W. Misner, *The Dynamics of general relativity*, *Gen. Rel. Grav.* **40** (2008) 1997–2027, [gr-qc/0405109].

[209] N. Itzhaki, J. M. Maldacena, J. Sonnenschein, and S. Yankielowicz, *Supergravity and the large N limit of theories with sixteen supercharges*, *Phys. Rev. D* **58** (1998) 046004, [hep-th/9802042].

[210] H. J. Boonstra, K. Skenderis, and P. K. Townsend, *The domain wall / QFT correspondence*, *JHEP* **01** (1999) 003, [hep-th/9807137].

[211] L. Girardello, M. Petrini, M. Porrati, and A. Zaffaroni, *Confinement and condensates without fine tuning in supergravity duals of gauge theories*, *JHEP* **05** (1999) 026, [hep-th/9903026].

[212] L. Girardello, M. Petrini, M. Porrati, and A. Zaffaroni, *The Supergravity dual of N=1 superYang-Mills theory*, *Nucl. Phys. B* **569** (2000) 451–469, [hep-th/9909047].

[213] J. Polchinski and M. J. Strassler, *The String dual of a confining four-dimensional gauge theory*, hep-th/0003136.

[214] I. R. Klebanov and E. Witten, *Superconformal field theory on three-branes at a Calabi-Yau singularity*, *Nucl. Phys. B* **536** (1998) 199–218, [hep-th/9807080].

[215] S. S. Gubser and I. R. Klebanov, *Baryons and domain walls in an N=1 superconformal gauge theory*, *Phys. Rev. D* **58** (1998) 125025, [hep-th/9808075].

[216] I. R. Klebanov and A. A. Tseytlin, *Gravity duals of supersymmetric SU(N) x SU(N+M) gauge theories*, *Nucl. Phys. B* **578** (2000) 123–138, [hep-th/0002159].

[217] S. S. Gubser, C. P. Herzog, and I. R. Klebanov, *Symmetry breaking and axionic strings in the warped deformed conifold*, *JHEP* **09** (2004) 036, [hep-th/0405282].

[218] A. Dymarsky, I. R. Klebanov, and N. Seiberg, *On the moduli space of the cascading SU(M+p) x SU(p) gauge theory*, *JHEP* **01** (2006) 155, [hep-th/0511254].

[219] S. S. Gubser, C. P. Herzog, and I. R. Klebanov, *Variations on the warped deformed conifold*, *Comptes Rendus Physique* **5** (2004) 1031–1038, [hep-th/0409186].

[220] B. S. Acharya, J. P. Gauntlett, and N. Kim, *Five-branes wrapped on associative three cycles*, *Phys. Rev. D* **63** (2001) 106003, [hep-th/0011190].

[221] M. Naka, *Various wrapped branes from gauged supergravities*, hep-th/0206141.

[222] H. Nieder and Y. Oz, *Supergravity and D-branes wrapping special Lagrangian cycles*, *JHEP* **03** (2001) 008, [hep-th/0011288].

[223] J. P. Gauntlett, N. Kim, and D. Waldram, *M Five-branes wrapped on supersymmetric cycles*, *Phys. Rev. D* **63** (2001) 126001, [hep-th/0012195].

[224] J. D. Edelstein and C. Nunez, *D6-branes and M theory geometrical transitions from gauged supergravity*, *JHEP* **04** (2001) 028, [hep-th/0103167].

[225] J. Gomis, *D-branes, holonomy and M theory*, *Nucl. Phys. B* **606** (2001) 3–17, [hep-th/0103115].

[226] I. Bah, C. Beem, N. Bobev, and B. Wecht, *Four-Dimensional SCFTs from M5-Branes*, *JHEP* **06** (2012) 005, [arXiv:1203.0303].

[227] N. Kim and M. Shim, *Wrapped Brane Solutions in Romans $F(4)$ Gauged Supergravity*, *Nucl. Phys. B* **951** (2020) 114882, [arXiv:1909.01534].

[228] P. Karndumri, *Holographic RG flows in six dimensional F(4) gauged supergravity*, *JHEP* **01** (2013) 134, [arXiv:1210.8064]. [Erratum: JHEP 06, 165 (2015)].

[229] C. Nunez, I. Y. Park, M. Schvellinger, and T. A. Tran, *Supergravity duals of gauge theories from F(4) gauged supergravity in six-dimensions*, *JHEP* **04** (2001) 025, [hep-th/0103080].

[230] O. Aharony, *The NonAdS / nonCFT correspondence, or three different paths to QCD*, in *NATO Advanced Study Institute and EC Summer School on Progress in String, Field and Particle Theory*, pp. 3–24, 12, 2002. hep-th/0212193.

[231] F. Bigazzi, A. L. Cotrone, M. Petrini, and A. Zaffaroni, *Supergravity duals of supersymmetric four-dimensional gauge theories*, *Riv. Nuovo Cim.* **25N12** (2002) 1–70, [hep-th/0303191].

[232] M. Bertolini, *Four lectures on the gauge / gravity correspondence*, *Int. J. Mod. Phys. A* **18** (2003) 5647–5712, [hep-th/0303160].

[233] J. Maldacena and D. Martelli, *The Unwarped, resolved, deformed conifold: Fivebranes and the baryonic branch of the Klebanov-Strassler theory*, *JHEP* **01** (2010) 104, [arXiv:0906.0591].

[234] J. Gaillard, D. Martelli, C. Nunez, and I. Papadimitriou, *The warped, resolved, deformed conifold gets flavoured*, *Nucl. Phys. B* **843** (2011) 1–45, [arXiv:1004.4638].

[235] E. Caceres, C. Nunez, and L. A. Pando-Zayas, *Heating up the Baryonic Branch with U-duality: A Unified picture of conifold black holes*, *JHEP* **03** (2011) 054, [arXiv:1101.4123].

[236] D. Elander, J. Gaillard, C. Nunez, and M. Piai, *Towards multi-scale dynamics on the baryonic branch of Klebanov-Strassler*, *JHEP* **07** (2011) 056, [arXiv:1104.3963].

[237] M. Kruczenski, D. Mateos, R. C. Myers, and D. J. Winters, *Towards a holographic dual of large N(c) QCD*, *JHEP* **05** (2004) 041, [hep-th/0311270].

[238] R. Casero, C. Nunez, and A. Paredes, *Towards the string dual of N=1 SQCD-like theories*, *Phys. Rev. D* **73** (2006) 086005, [hep-th/0602027].

[239] R. Casero, C. Nunez, and A. Paredes, *Elaborations on the String Dual to N=1 SQCD*, *Phys. Rev. D* **77** (2008) 046003, [arXiv:0709.3421].

[240] C. Hoyos-Badajoz, C. Nunez, and I. Papadimitriou, *Comments on the String dual to N=1 SQCD*, *Phys. Rev. D* **78** (2008) 086005, [arXiv:0807.3039].

[241] F. Benini, F. Canoura, S. Cremonesi, C. Nunez, and A. V. Ramallo, *Unquenched flavors in the Klebanov-Witten model*, *JHEP* **02** (2007) 090, [hep-th/0612118].

[242] F. Benini, F. Canoura, S. Cremonesi, C. Nunez, and A. V. Ramallo, *Backreacting flavors in the Klebanov-Strassler background*, *JHEP* **09** (2007) 109, [arXiv:0706.1238].

[243] F. Bigazzi, A. L. Cotrone, J. Mas, A. Paredes, A. V. Ramallo, and J. Tarrio, *D3-D7 Quark-Gluon Plasmas*, *JHEP* **11** (2009) 117, [arXiv:0909.2865].

[244] F. Bigazzi, A. L. Cotrone, A. Paredes, and A. V. Ramallo, *The Klebanov-Strassler model with massive dynamical flavors*, *JHEP* **03** (2009) 153, [arXiv:0812.3399].

[245] F. Bigazzi, A. L. Cotrone, A. Paredes, and A. Ramallo, *Non chiral dynamical flavors and screening on the conifold*, *Fortsch. Phys.* **57** (2009) 514–520, [arXiv:0810.5220].

[246] C. Nunez, A. Paredes, and A. V. Ramallo, *Unquenched Flavor in the Gauge/Gravity Correspondence*, *Adv. High Energy Phys.* **2010** (2010) 196714, [arXiv:1002.1088].

[247] N. Bobev, F. F. Gautason, B. E. Niehoff, and J. van Muiden, *Uplifting GPPZ: a ten-dimensional dual of* $\mathcal{N} = 1^*$, *JHEP* **10** (2018) 058, [arXiv:1805.03623].

[248] M. Petrini, H. Samtleben, S. Schmidt, and K. Skenderis, *The 10d Uplift of the GPPZ Solution*, *JHEP* **07** (2018) 026, [arXiv:1805.01919].

[249] J. Armas, G. Batzios, and J. P. van der Schaar, *Holographic duals of the* $\mathcal{N} = 1^*$ *gauge theory*, *JHEP* **04** (2023) 021, [arXiv:2212.02777].

[250] E. D'Hoker, M. Gutperle, A. Karch, and C. F. Uhlemann, *Warped* $AdS_6 \times S^2$ *in Type IIB supergravity I: Local solutions*, *JHEP* **08** (2016) 046, [arXiv:1606.01254].

[251] A. Legramandi and C. Nunez, *Holographic description of* $SCFT_5$ *compactifications*, *JHEP* **02** (2022) 010, [arXiv:2109.11554].

[252] F. Apruzzi, J. C. Geipel, A. Legramandi, N. T. Macpherson, and M. Zagermann, *Minkowski*$_4$ $\times$ S^2 *solutions of IIB supergravity*, *Fortsch. Phys.* **66** (2018), no. 3 1800006, [arXiv:1801.00800].

[253] A. Anabalon and S. F. Ross, *Supersymmetric solitons and a degeneracy of solutions in AdS/CFT*, *JHEP* **07** (2021) 015, [arXiv:2104.14572].

[254] N. Bobev, A. M. Charles, and V. S. Min, *Euclidean black saddles and* AdS_4 *black holes*, *JHEP* **10** (2020) 073, [arXiv:2006.01148].

[255] A. Anabalón, A. Gallerati, S. Ross, and M. Trigiante, *Supersymmetric solitons in gauged* $\mathcal{N} = 8$ *supergravity*, *JHEP* **02** (2023) 055, [arXiv:2210.06319].

[256] C. Nunez, M. Oyarzo, and R. Stuardo, *Confinement and D5-branes*, *JHEP* **03** (2024) 080, [arXiv:2311.17998].

[257] A. Hanany and E. Witten, *Type IIB superstrings, BPS monopoles, and three-dimensional gauge dynamics*, *Nucl. Phys. B* **492** (1997) 152–190, [hep-th/9611230].

[258] D. Stanford and L. Susskind, *Complexity and Shock Wave Geometries*, *Phys. Rev. D* **90** (2014), no. 12 126007, [arXiv:1406.2678].

[259] A. Legramandi and C. Nunez, *Electrostatic description of five-dimensional SCFTs*, *Nucl. Phys. B* **974** (2022) 115630, [arXiv:2104.11240].

[260] E. Witten, *Supersymmetric Yang-Mills theory on a four manifold*, *J. Math. Phys.* **35** (1994) 5101–5135, [hep-th/9403195].

[261] J. M. Maldacena and C. Nunez, *Supergravity description of field theories on curved manifolds and a no go theorem*, *Int. J. Mod. Phys. A* **16** (2001) 822–855, [hep-th/0007018].

[262] N. Bobev and P. M. Crichigno, *Universal RG Flows Across Dimensions and Holography*, *JHEP* **12** (2017) 065, [arXiv:1708.05052].

[263] Y. Bea, J. D. Edelstein, G. Itsios, K. S. Kooner, C. Nunez, D. Schofield, and J. A. Sierra-Garcia, *Compactifications of the Klebanov-Witten CFT and new AdS_3 backgrounds*, *JHEP* **05** (2015) 062, [arXiv:1503.07527].

[264] N. T. Macpherson, C. Núñez, L. A. Pando Zayas, V. G. J. Rodgers, and C. A. Whiting, *Type IIB supergravity solutions with AdS_5 from Abelian and non-Abelian T dualities*, *JHEP* **02** (2015) 040, [arXiv:1410.2650].

[265] C. F. Uhlemann, *Exact results for 5d SCFTs of long quiver type*, *JHEP* **11** (2019) 072, [arXiv:1909.01369].

[266] M. Akhond, A. Legramandi, C. Nunez, L. Santilli, and L. Schepers, *Massive flows in AdS6/CFT5*, *Phys. Lett. B* **840** (2023) 137899, [arXiv:2211.09824].

[267] M. Akhond, A. Legramandi, C. Nunez, L. Santilli, and L. Schepers, *Matrix models and holography: Mass deformations of long quiver theories in 5d and 3d*, *SciPost Phys.* **15** (2023), no. 3 086, [arXiv:2211.13240].

[268] C. Nunez, L. Santilli, and K. Zarembo, *Linear Quivers at Large-N*, arXiv:2311.00024.

[269] A. F. Faedo, C. Nunez, and C. Rosen, *Consistent truncations of supergravity and $\frac{1}{2}$-BPS RG flows in 4d SCFTs*, *JHEP* **03** (2020) 080, [arXiv:1912.13516].

[270] A. González Lezcano, J. Hong, J. T. Liu, L. A. Pando Zayas, and C. F. Uhlemann, *c-functions in flows across dimensions*, *JHEP* **10** (2022) 083, [arXiv:2207.09360].

[271] P. Merrikin, C. Nunez, and R. Stuardo, *Compactification of 6d N=(1,0) quivers, 4d SCFTs and their holographic dual Massive IIA backgrounds*, *Nucl. Phys. B* **996** (2023) 116356, [arXiv:2210.02458].

[272] J. Sonnenschein, *What does the string / gauge correspondence teach us about Wilson loops?*, in

Advanced School on Supersymmetry in the Theories of Fields, Strings and Branes, pp. 219–269, 7, 1999. hep-th/0003032.

[273] C. Nunez, M. Oyarzo, and R. Stuardo, *Confinement in (1 + 1) dimensions: a holographic perspective from I-branes*, *JHEP* **09** (2023) 201, [arXiv:2307.04783].

[274] A. Fatemiabhari and C. Nunez, *Wilson loops for 5d and 3d conformal linear quivers*, *Nucl. Phys. B* **989** (2023) 116125, [arXiv:2209.07536].

[275] S. Ryu and T. Takayanagi, *Holographic derivation of entanglement entropy from AdS/CFT*, *Phys. Rev. Lett.* **96** (2006) 181602, [hep-th/0603001].

[276] S. Ryu and T. Takayanagi, *Aspects of Holographic Entanglement Entropy*, *JHEP* **08** (2006) 045, [hep-th/0605073].

[277] I. R. Klebanov, D. Kutasov, and A. Murugan, *Entanglement as a probe of confinement*, *Nucl. Phys. B* **796** (2008) 274–293, [arXiv:0709.2140].

[278] U. Kol, C. Nunez, D. Schofield, J. Sonnenschein, and M. Warschawski, *Confinement, Phase Transitions and non-Locality in the Entanglement Entropy*, *JHEP* **06** (2014) 005, [arXiv:1403.2721].

[279] N. Jokela and J. G. Subils, *Is entanglement a probe of confinement?*, *JHEP* **02** (2021) 147, [arXiv:2010.09392].

[280] A. Reynolds and S. F. Ross, *Complexity in de Sitter Space*, *Class. Quant. Grav.* **34** (2017), no. 17 175013, [arXiv:1706.03788].

[281] L. Susskind, *Computational Complexity and Black Hole Horizons*, *Fortsch. Phys.* **64** (2016) 24–43, [arXiv:1403.5695]. [Addendum: Fortsch.Phys. 64, 44–48 (2016)].

[282] J. Hong, J. T. Liu, and D. R. Mayerson, *Gauged Six-Dimensional Supergravity from Warped IIB Reductions*, *JHEP* **09** (2018) 140, [arXiv:1808.04301].

[283] A. R. Frey, M. P. Grehan, and P. Singh, *Holographic complexity of the Klebanov-Strassler background*, arXiv:2311.18804.

[284] J. Yang and A. R. Frey, *Complexity, scaling, and a phase transition*, *JHEP* **09** (2023) 029, [arXiv:2307.08229].

[285] A. Belin, R. C. Myers, S.-M. Ruan, G. Sárosi, and A. J. Speranza, *Does Complexity Equal Anything?*, *Phys. Rev. Lett.* **128** (2022), no. 8 081602, [arXiv:2111.02429].

[286] A. Belin, R. C. Myers, S.-M. Ruan, G. Sárosi, and A. J. Speranza, *Complexity equals anything II*, *JHEP* **01** (2023) 154, [arXiv:2210.09647].

[287] C. Bachas and J. Estes, *Spin-2 spectrum of defect theories*, *JHEP* **06** (2011) 005, [arXiv:1103.2800].

[288] O. Aharony, E. Schreiber, and J. Sonnenschein, *Stable nonsupersymmetric supergravity solutions from deformations of the Maldacena-Nunez background*, *JHEP* **04** (2002) 011, [hep-th/0201224].

[289] A. Anabalón, H. Nastase, and M. Oyarzo, *Supersymmetric AdS Solitons and the interconnection of different vacua of $\mathcal{N}$ = 4 Super Yang-Mills*, arXiv:2402.18482.

[290] A. Anabalón, D. Astefanesei, A. Gallerati, and J. Oliva, *Supersymmetric smooth distributions of M2-branes as AdS solitons*, arXiv:2402.00880.

[291] A. Anabalón and H. Nastase, *Universal IR holography, scalar fluctuations, and glueball spectra*, *Phys. Rev. D* **109** (2024), no. 6 066011, [arXiv:2310.07823].

[292] S. P. Kumar and R. Stuardo, *Twisted circle compactification of $\mathcal{N}$ = 4 SYM and its Holographic Dual*, arXiv:2405.03739.

[293] A. Buchel and J. T. Liu, *Gauged supergravity from type IIB string theory on Y**p,q manifolds*, *Nucl. Phys. B* **771** (2007) 93–112, [hep-th/0608002].

[294] J. P. Gauntlett and O. Varela, *D=5 SU(2) x U(1) Gauged Supergravity from D=11 Supergravity*, *JHEP* **02** (2008) 083, [arXiv:0712.3560].

[295] C. Couzens, N. T. Macpherson, and A. Passias, *A plethora of Type IIA embeddings for d = 5 minimal supergravity*, *JHEP* **01** (2023) 047, [arXiv:2209.15540].

[296] S. Benvenuti, S. Franco, A. Hanany, D. Martelli, and J. Sparks, *An Infinite family of superconformal quiver gauge theories with Sasaki-Einstein duals*, *JHEP* **06** (2005) 064, [hep-th/0411264].

[297] D. Gaiotto and J. Maldacena, *The Gravity duals of N=2 superconformal field theories*, *JHEP* **10** (2012) 189, [arXiv:0904.4466].

[298] F. Apruzzi, M. Fazzi, A. Passias, and A. Tomasiello, *Supersymmetric AdS_5 solutions of massive IIA supergravity*, *Journal of High Energy Physics* **2015** (June, 2015) 195, [arXiv:1502.06620].

[299] S. Cremonesi and A. Tomasiello, *6d holographic anomaly match as a continuum limit*, *JHEP* **05** (2016) 031, [arXiv:1512.02225].

[300] J. H. Schwarz, *Covariant Field Equations of Chiral N=2 D=10 Supergravity*, *Nucl. Phys. B* **226** (1983) 269.

[301] P. S. Howe and P. C. West, *The Complete N=2, D=10 Supergravity*, *Nucl. Phys. B* **238** (1984) 181–220.

[302] M. Gunaydin and N. Marcus, *The Spectrum of the s**5 Compactification of the Chiral N=2, D=10 Supergravity and the Unitary Supermultiplets of U(2, 2/4)*, *Class. Quant. Grav.* **2** (1985) L11.

[303] M. Pernici, K. Pilch, and P. van Nieuwenhuizen, *Gauged N=8 D=5 Supergravity*, *Nucl. Phys. B* **259** (1985) 460.

[304] M. Gunaydin, L. J. Romans, and N. P. Warner, *Gauged N=8 Supergravity in Five-Dimensions*, *Phys. Lett. B* **154** (1985) 268–274.

[305] M. Cvetic, M. J. Duff, P. Hoxha, J. T. Liu, H. Lu, J. X. Lu, R. Martinez-Acosta, C. N. Pope,

H. Sati, and T. A. Tran, *Embedding AdS black holes in ten-dimensions and eleven-dimensions*, *Nucl. Phys. B* **558** (1999) 96–126, [hep-th/9903214].

[306] J. P. Gauntlett, D. Martelli, J. Sparks, and D. Waldram, *Sasaki-Einstein metrics on S**2 x S**3*, *Adv. Theor. Math. Phys.* **8** (2004), no. 4 711–734, [hep-th/0403002].

[307] D. Martelli and J. Sparks, *Toric geometry, sasakieinstein manifolds and a new infinite class of ads/cft duals*, *Communications in Mathematical Physics* **262** (Nov., 2005).

[308] I. Bah, A. Passias, and A. Tomasiello, *AdS_5 compactifications with punctures in massive IIA supergravity*, *Journal of High Energy Physics* **2017** (Nov., 2017) 50, [arXiv:1704.07389].

[309] C. Nunez, D. Roychowdhury, S. Speziali, and S. Zacarias, *Holographic aspects of four dimensional $\mathcal{N} = 2$ SCFTs and their marginal deformations*, *Nucl. Phys. B* **943** (2019) 114617, [arXiv:1901.02888].

[310] N. T. Macpherson, P. Merrikin, and C. Nunez, *Marginally deformed AdS_5/CFT_4 and spindle-like orbifolds*, arXiv:2403.02380.

[311] F. Apruzzi, M. Fazzi, A. Passias, A. Rota, and A. Tomasiello, *Six-Dimensional Superconformal Theories and their Compactifications from Type IIA Supergravity*, *Phys. Rev. Lett.* **115** (2015), no. 6 061601, [arXiv:1502.06616].

[312] F. Apruzzi, M. Fazzi, A. Passias, and A. Tomasiello, *Supersymmetric AdS_5 solutions of massive IIA supergravity*, *JHEP* **06** (2015) 195, [arXiv:1502.06620].

[313] C. Nunez, J. M. Penin, D. Roychowdhury, and J. Van Gorsel, *The non-Integrability of Strings in Massive Type IIA and their Holographic duals*, *JHEP* **06** (2018) 078, [arXiv:1802.04269].

[314] D. Cassani and Z. Komargodski, *EFT and the SUSY Index on the 2nd Sheet*, *SciPost Phys.* **11** (2021) 004, [arXiv:2104.01464].

[315] J. P. Gauntlett and O. Varela, *Consistent Kaluza-Klein reductions for general supersymmetric AdS solutions*, *Phys. Rev. D* **76** (2007) 126007, [arXiv:0707.2315].

[316] A. F. Faedo, M. Piai, and D. Schofield, *On the stability of multiscale models of dynamical symmetry breaking from holography*, *Nucl. Phys. B* **880** (2014) 504–527, [arXiv:1312.2793].

[317] A. F. Faedo, M. Piai, and D. Schofield, *Gauge/gravity dualities and bulk phase transitions*, *Phys. Rev. D* **89** (2014), no. 10 106001, [arXiv:1402.4141].

[318] C. Nunez, M. Piai, and A. Rago, *Wilson Loops in string duals of Walking and Flavored Systems*, *Phys. Rev. D* **81** (2010) 086001, [arXiv:0909.0748].

[319] D. Chatzis, *Stability of Wilson loops and other observables in various type IIB backgrounds*, *Nucl. Phys. B* **1004** (2024) 116560, [arXiv:2401.13637].

[320] K. Filippas, C. Núñez, and J. Van Gorsel, *Integrability and holographic aspects of six-dimensional $\mathcal{N} = (1, 0)$ superconformal field theories*, *JHEP* **06** (2019) 069, [arXiv:1901.08598].

[321] L. J. Romans, *The F(4) Gauged Supergravity in Six-dimensions*, *Nucl. Phys. B* **269** (1986) 691.

[322] M. Cvetic, H. Lu, and C. N. Pope, *Gauged six-dimensional supergravity from massive type IIA*, *Phys. Rev. Lett.* **83** (1999) 5226–5229, [hep-th/9906221].